Erosion-Corrosion of Marine Alloys

Hang Meng

Submitted in accordance with the requirements for the degree of
Doctor of Philosophy

The University of Leeds
School of Mechanical Engineering

July, 2009

The candidate confirms that the work submitted is his own and that appropriate credit has been given where reference has been made to the work of others.

Acknowledgements

I would like to give special thanks to my supervisor Professor Anne Neville and co-supervisor Dr. Xinming Hu for their support, invaluable advice, encouragement and enthusiasm throughout this project, also many thanks to Weir Materials & Foundies, Weir Engineering Services, Weir Pumps, Noel Village Ltd, Lloyds Register, Sea Technology Group, Defence Science and Technology Laboratory, and Langley Alloys Meighs Ltd for financial support.

I would like to thank all the staff of School of Mechanical Engineering for their assistance. Special thanks to my group mates Valdir, Fasail and Inga who help me during this study with valuable suggestions, assistance and discussions. Thanks to all my group mates for spending enjoyable time together.

I would sincerely like to thank my wife Li Lu for infinite love, support and encouragement during the years of my study. To my parents and parents in-law Yumei Zhang, Guangyou Meng, Yu Pang and Xiupin Lu for their love, motivation and encouragement.

Abstract

Marine alloys such as stainless steels, copper-base alloys and cast iron have a long history of applications over a wide range of industries. They always are exposed to aggressive erosion-corrosion environments to support or transmit forces during the service, where more than millions of pounds are involved to repair the material degradation every year. In order to minimize this cost, lots of money and research have been put into practice, from which more and more erosion-corrosion behaviour and mechanisms of marine alloys were understood, however, downtime of marine systems still happens, moreover it is still a fact that it is quite difficult to choose the optimum material for the specific working environment.

In this project, erosion-corrosion performance of eight marine alloys which include three different grade stainless steels, four copper-base alloys and one Ni-resist cast iron has been assessed under liquid-solid jet impingement over eight sets of test conditions in 3.5% sodium chloride solution. Firstly, the weight loss of different marine alloys ranks the priority of their corrosion, erosion and erosion-corrosion resistance over the range of the test conditions, furthermore the total weight loss test, in conjunction with *in-situ* electrochemistry measurements, enable the relative contribution of the different mechanisms interacting in the degradation to be quantified, meanwhile the aspects of erosion-corrosion mechanisms of different marine alloys have been detailed. Even erosion-corrosion is a complex process, but microhardness has been found to be the controlling factor in severe erosion-dominated conditions. More importantly, primary concerns have been brought on the factorial contributions of individual environmental parameters and their interactions to the overall material degradations. A full two-level factorial experimental design method combined with following analysis of variance was applied to qualify these factorial contributions, which shows effects of the individual environmental parameters and their interactions on the weight loss during the erosion-corrosion processes, and the prominent factors are velocity, sand loading and their interaction. Fluid temperature has the smallest effect compared with other environmental parameters.

The purpose of any research is to build the interaction of theory and practice as close as possible. The correlations between this study and the practice are not only contributed to the further academic understandings of materials' erosion-corrosion behaviour and environmental parameters effects on the components of total weight loss, but the ultimate objective is to develop a prediction model for future material selection for erosion-corrosion marine applications. Since there are few successful predictions model to refer, mathematical and experimental design modelling have been adopted to develop this prediction model. The further comparison needs to make to find which model is more reliable to the practice.

Content

Figures

Tables

Nomenclature

G	energy
ΔG	free energy
n	numbers of electrons being transferred
F	Faraday's constant of 96,494 Coulombs/mole
E	potential
E_0	equilibrium electrode potential
E_{cell}	cell potential
E_{anode}	electrode potential for the anodic reaction
$E_{cathode}$	electrode potential for the cathodic reaction
E_{corr}	free corrosion potential
E_b	breakdown potential
β	Tafel constant
i_{corr}	corrosion current density
i_L	limiting current density
i_0	exchange current density
i_{rev}	reversal current density
i_{max}	maximum current density
i_s	stabilised current density
D	diffusion coefficient
C_B	concentration of the reacting molecules or ions in the bulk solution (*mol/l*)
x	thickness of the diffusion layer (*mm*)
CR	corrosion rate (g)
Q	overall charge (*C*)
W	atomic weight (*g/mol*)
A	area (cm^2)
$PREn$	pitting resistance equivalent number

TWL total weight loss

E weight loss due to pure erosion

C weight loss due to pure corrosion

S weight loss due to synergistic effect

dE_C enhancement of erosion due to corrosion

dC_E enhancement of corrosion due to erosion

W weight of material removed by a number of grains

α angle between the particle velocity vector and the surface

K ratio of vertical to horizontal force components on particle

p horizontal component of the stress on the particle face

V velocity (ms^{-1})

S sand loading (mgl^{-1})

ρ particle density (g/cm^3)

M total mass of a number of particles

ψ ratio of the length of contact between particle and surface to the vertical coordinate of particle tip

E_w erosion rate (g)

d particle size (mm)

C solid concentration (gml^{-1})

W_{lv} average effect corresponding to the velocity at low level

W_{hv} average effect corresponding to the velocity at high level

W_G average total weight loss for eight trial conditions

SS sum of square

Chapter 1 Introduction

1.1 Introduction

Corrosion was often considered as a calamity, a necessary evil, an unavoidable pestilence to which we had to submit without being able to control or even understand it [1]. Massive costs are related with corrosion maintenance and corrosion repair every year. The recent surveys (Table 1.1, Table 1.2) stated the astronomical costs spent in the oil, gas and offshore industries. It is widely recognised within these industries that effective management of corrosion must be developed to achieve benefits including increased plant availability, reduction in unplanned maintenance and reduction in deferment costs. The rate of plant degradation due to corrosion carries an element of uncertainty. This uncertainty can be reduced by both proactive and reactive corrosion measurements. The effect of implementing an appropriate corrosion management system is a reduction/elimination of corrosion related damage/deterioration of assets. This not only assists in compliance with regulatory requirements but also has a direct effect on the overall economic performance of the assets [2]. The objective of these efforts is to enable the facilities serving in severe environments to run in a safe and cost-effective condition.

It is especially true that erosion-corrosion damage to pumps, impellers, valves, heat exchanger tubes and other hydraulic equipment and also to components used in offshore, marine technologies, oil and gas production *etc* is prevalent. It is well known that industries which transport slurries and other particle-laden liquids in pipes for sectors such as offshore and marine technologies spend millions of pounds every year to repair material damage. In a recent survey erosion-corrosion was rated in the top five most prevalent forms of corrosion damage in the oil and gas industry [3]. Laboratory research work is therefore vital to minimise the possibility of this expensive cost.

Corrosion Expense	Cost ($ x thousand)
Inspection, Monitoring, Staff costs	9,625
Repairs	1,350
Corrosion inhibitor (chemical alone)	7,200
TOTAL	18.175 million

Table 1.1: Costs of various corrosion expenses for a large oil field [4]

Type of ships	Num.	Average corrosion repair cost per ship ($)	Yearly repair cost (million $)	Average corrosion downtime cost per ship ($)	Yearly downtime cost (million $)
Oil	6,920	200,000	1,384	140,000	969
Chemical	2,417	300,000	741	140,000	346
Bulk Dry	6,252	50,000	313	56,000	350
Cargo	18,611	50,000	931	73,000	1,303
Fishing	23,711	25,000	593	20,000	474
Supply	12,954	50,000	648	50,000	648
Refrigerated	1,441	50,000	72	50,000	72
Cruise	337	200,000	67	1,000,000	337
Passenger	5,386	50,000	269	56,000	302
Others	7,724	50,000	386	56,000	433
		World Total	5,404	*World Total*	5,234

Table 1.2: Estimated average corrosion cost per year due to maintenance, repairs, and downtime for each of the major types of ships [5]

Because more and more costs are invested in repairing material degradation due to erosion-corrosion, the topic has attracted much interest over recent decades. Many low cost and flexible simulation test methods have been developed, which make it considerably more reliable for laboratory research into the mechanisms of erosion-corrosion and assessing the influence of operating variables on erosion-corrosion rates. Many basic investigations have provided a tremendous input into corrosion protection technologies for oil and gas production and thermal and marine technologies *etc.* It has been shown that there is hardly any area in science and technology that demonstrates the close interaction of theory and practice better than erosion-corrosion as suggested by Heitz [6]. Hence, simulated erosion-corrosion tests build reliable and close interaction between the research and the practice.

Up to the present, many materials for marine applications (Figure 1.1) have been developed such as carbon steel, austenitic stainless steel, copper-base alloys, duplex and super duplex stainless steels, super austenitic stainless steel, titanium, nickel-base alloys, glass reinforced epoxy *etc*, and most commonly used materials are carbon steel, 316L stainless steel, 22%*Cr* and 25%*Cr* duplex stainless steels, copper-nickel, some monel/nickel based alloys and titanium. Tremendous material research and design modification have been carried out to reduce the operating costs and to improve their running life; even efforts have been made in achieving this in a low cost manner. However, there is not a systematic analysis about the effects of environmental parameters on mass loss in erosion-corrosion conditions, and also there is still not a universal criterion for material selection, including considering the material inherent properties such as hardness, toughness and strength *etc*, but also taking into account of the erosion-corrosion rate based on empirical data from experiments and experience.

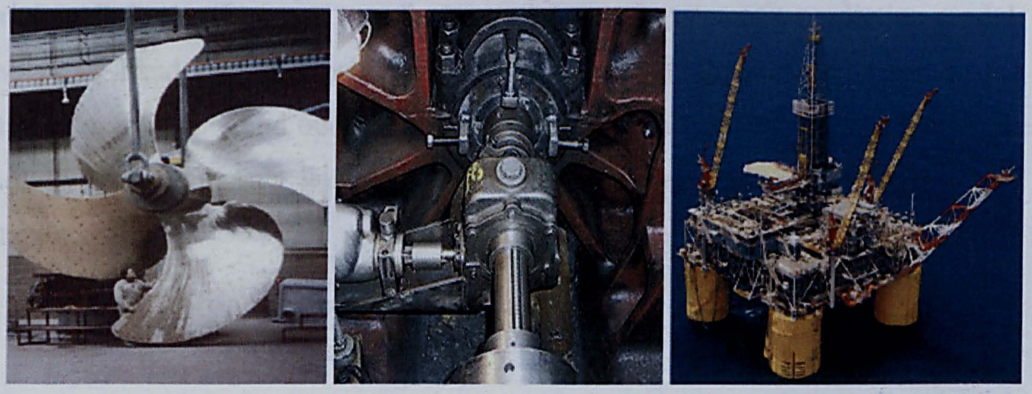

(a) (b) (c)

Figure 1.1: The example application of marine alloys: (a)Propellers ~ Cast nickel aluminium bronze (b) Portable line boring of compressor saddle and caps ~ Cast iron (c) Oil platform ~ 316 stainless steel housing, stainless steel bolts/nuts, flange in super duplex

1.2 Background

Corrosion can be defined as the reaction of a metallic material with its environments. The products of this reaction may be solid, liquid or gaseous. Both

the physical and chemical properties of the products are important since they may both influence the subsequent rate of reaction [7]. Erosion is the mechanical removal of a protective film and a substrate by a complicated impacting, cracking and cutting action, which produces fresh reactive corrosion site and erosion-enhanced corrosion. Erosion-corrosion is a combined process of corrosion and erosion which is classified to tribocorrosion processes. Many researchers have proved the existence of the synergy, the interactions between erosion and corrosion, and also they have defined and qualified this variance [3, 8-10].

One prerequisite in preventing erosion-corrosion failures is to predict the occurrence of such phenomenon; however, all the predictions are based on characterisation of erosion-corrosion in numerous environments, affected by factors such as velocity, temperature, sand loading, pH and so on. In this study, extensive laboratory work and analysis was undertaken to characterise and quantify how individual factors and their interactions affect the erosion-corrosion on different materials. All these efforts are transferred to develop a systematic prediction model; on the other hand the information from this work can then be fed back to the material manufacturers and operators in industries, and also respond to optimize the technology in materials' design, construction, selection, installation and maintenance.

1.3 Objectives

The objectives of this study are:

- To investigate the erosion-corrosion behaviour of eight marine alloys.
- To improve the understanding of material corrosion and erosion-corrosion degradation mechanisms in erosion-corrosion conditions.
- To optimise the erosion-corrosion experiments using an experimental design method.
- To analyse the factorial contributions of individual environmental parameters and their interactions to total weight loss, pure erosion, pure corrosion and synergy

over the range of test conditions.

- To correlate the material mechanical properties with the erosion and erosion-corrosion resistance.

- To develop a reliable prediction model for future material selection across a range of conditions.

1.4 Outline of this thesis

The layout of this thesis is summarized as following:

Chapter 2 presents some basic corrosion theory relating to this study involving thermodynamics and electrochemistry. Chapter 3 is mainly focus on the literature review from the extensive studies related to this project such as erosion-corrosion of marine alloys, their development and some discovering of erosion-corrosion regime and mechanisms. Some quantitive analyse of effects of environmental parameters on erosion-corrosion resistance are also reviewed, as well as some existing erosion-corrosion prediction model. Chapter 4 provides the detailed information about the materials in this study, experimental facilities and procedures.

Chapter 5 is composed by all the data collected from the experiments, which is related to erosion-corrosion behaviour and mechanism studies. Eight materials are classified into three groups, and then analyze the data in total weight loss, surface analysis, cathodic protection, anodic polarisation and synergy.

Chapter 6 is analysis of variance and prediction model, in which the contributions of environmental parameters to the components of total weight loss in simulated erosion-corrosion environments, and also the initialisation of the prediction model with model validation.

Chapter 7 is discussion, which includes erosion-corrosion behaviour analysis of eight materials over the range of test condition, the correlation of the mechanical

properties of the materials with their erosion-corrosion resistance and the dependence of erosion-corrosion resistance of copper-base alloys on the adhesion ability of their protective films. The applications of prediction model for future material selection based on the experimental design are addressed in the chapter. Conclusion and future work of this project are presented in the final two chapters.

Chapter 2 Theory

2.1 Electrochemical reactions

Naturally electrochemical reactions involve two or more electrode reactions: anodic partial reaction (oxidation of the metal and loss of electrons simultaneously) and the cathodic partial reaction (reduction of the oxidising substance and absorption of electrons simultaneously)

The most common anodic reaction is the dissolution of metal into the corrosive environments, and at the same time the metal loses electron. For a typical example when copper is exposed to corrosive environment, it reacts with the environment to form the oxide; firstly, *Cu* is oxidized to Cu^+.

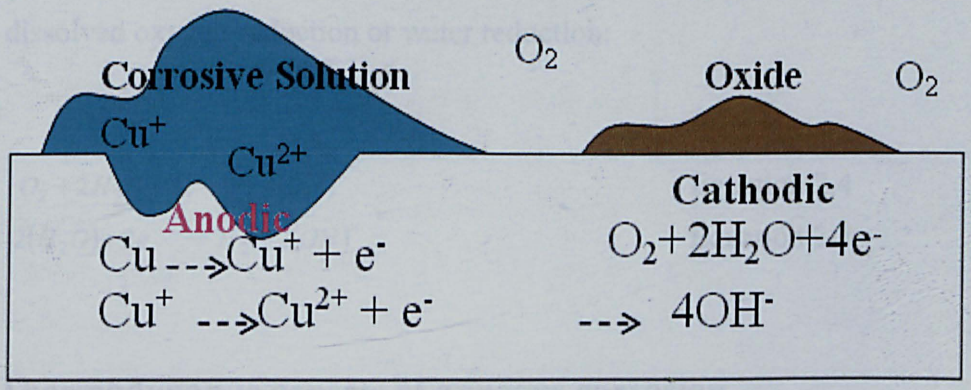

Figure 2.1: Schematic of the corrosion mechanisms for metal in the corrosive solution

In fact *Cu* is oxidized to Cu^+ in the corrosive environment and the transfer of electrons e^- from one substance to another occurs simultaneously.

$$Cu \rightarrow Cu^{+} + e^{-}$$ Equation 2.1

In turn, Cu^{+} can be oxidized to Cu^{2+} during which Cu^{+} loses a further electron and becomes Cu^{2+}

$$Cu^{+} \rightarrow Cu^{2+} + e^{-}$$ Equation 2.2

In nature everything should follow the principle of the conservation of energy; the corrosion process is not exceptional. When anodic reactions happen, cathodic activities occur at the same time, namely that the electrons released from the anode are consumed by the cathodic reaction. The cathodic reaction depends on the *pH* of the environment. In acidic environments, the cathodic reaction is normally hydrogen evolution or hydrogen ion consumption which can be written as:

$$2H^{+} + 2e^{-} \rightarrow H_2$$ Equation 2.3

While in the neutral or alkaline conditions, the cathodic reaction is quantified as the dissolved oxygen-reduction or water reduction:

$$O_2 + 2H_2O + 4e^{-} \rightarrow 4(OH)^{-}$$ Equation 2.4

$$2(H_2O) + 2e^{-} \rightarrow H_2 + 2(OH)^{-}$$ Equation 2.5

2.2 Thermodynamic aspects of aqueous corrosion

2.2.1 Free energy

When a metal oxidizes there is a change in the free energy, *G*, of the system which is equal to the work done or absorbed during the process. It is a maximum when the process takes place reversibly. It is the change in the free energy of the

system that is the "driving force" of the reaction and it represents the maximum fraction of the energy that can be converted into work. The performance of this work must be accompanied by a decrease in the free energy of the system ($-\Delta G$), otherwise the reaction cannot take place [7].

Free energy determined by the electrochemical work can be calculated by the following equation:

$$\Delta G = -nFE \qquad \text{Equation 2.6}$$

Where;

n is the numbers of electrons being transferred

F is the Faraday constant (96485 $C\ mol\ (e^-)^{-1}$)

E is the cell potential (V)

The transition state theory is an important concept to explain the rates of corrosion reaction, which can be quantified as the following equation:

$$A + B \rightarrow C + D \qquad \text{Equation 2.7}$$

This equation can be understood that two reactants, A and B, interact together to form two new products, C and D. In order to produce the new species it is essential that A and B do not just come into contact with each other, but physically join together, forming an intermediate species AB. In reality, this may happen for only the briefest instant, and then only when the reactants process sufficient energy and the correct orientation for the joining to occur. AB is called transition state, and it is re-organisation of the transition state which leads to the products, C and D.

A schematic diagram can be used to describe the free energy changes which occur during the reaction. The y-axis is present as the energy; while x-axis is present as the extent to which the reaction process has progressed. The transition state is always of higher energy that the sum of the energies of the individual reactants. After interacting together, the energies of products C and D must be less than the

sum of the energies of the individual reactant, by an amount of ΔG. By changing into the products, the transition state is able to reach a lower free energy situation so this is the favoured of the two possibilities.

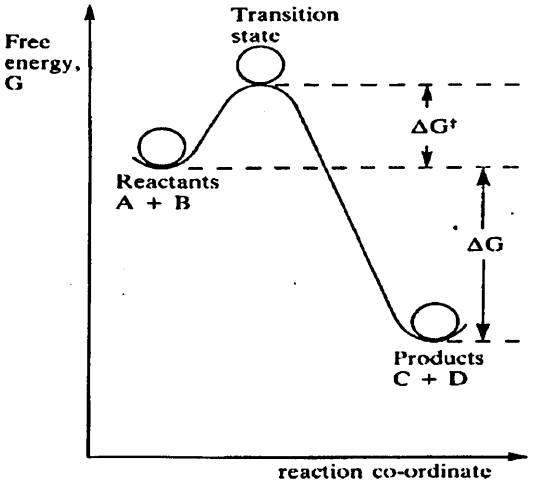

Figure 2.2: Energy profile for the reaction which converts $A+B$ to $C+D$ via the transition state [7]

According to the equation 2.6, the standard free energy of the cell reaction ΔG_0 can be correlated with the standard potential difference across the cell, E_0

$$\Delta G_0 = -nFE_0 \qquad \text{Equation 2.8}$$

Meanwhile the cell voltage in corrosive environment will be obtained

$$E_{cell} = E_{cathode} - E_{anode} \qquad \text{Equation 2.9}$$

Comparing the measured E_{cell} with E_0, it is possible to determine whether the electrochemical reaction is towards anodic or cathodic direction. This rule can be schematically shown in the following figure. With an increasing noble potential, at potentials more positive that E_0, anodic oxidation reactions are possible; at potentials more negative that E_0, cathodic reduction-reactions can occur [11].

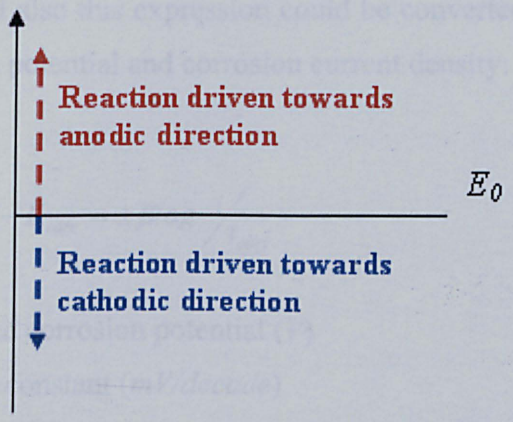

Figure 2.3: Trends in reaction compared with E_0

2.2.2 Activation polarisation

On a corroding metal, oxidation reactions occur in an electrochemical cell at anodic sites. In this case, the potential of the anodic site will no longer be at equilibrium. This deviation from equilibrium potential is known as polarisation. Polarisation is extremely important because it enables useful statements to be made about the rates of corrosion processes. Electrochemical polarisation is divided into three main types: (*i*) activation polarisation, (*ii*) concentration polarisation and (*iii*) resistance polarisation [7].

Activation polarisation refers to the situation where an electrochemical reaction is controlled by a slow step in the reaction sequence and activation reaction energy effects are the controlling factor [11]. It is well known that corrosion leads to a non-equilibrium state during the material degradation. The Tafel equation describes the relationship between reaction rate and overvoltage (E-E_0 measured in volts):

$$E - E_0 = \pm \beta log \, {}^{i}/_{i_0} \qquad \text{Equation 2.10}$$

And also this expression could be converted to relationship responding to free corrosion potential and corrosion current density:

$$E - E_{corr} = \pm \beta log \, {}^{i}/_{i_{corr}} \qquad \text{Equation 2.11}$$

Where;

E_{corr} is free corrosion potential (V)

β is Tafel constant ($mV/decade$)

i_0 is the rate of oxidation or reduction in terms of current density (A/cm^2)

i_{corr} is corrosion current density (A/cm^2)

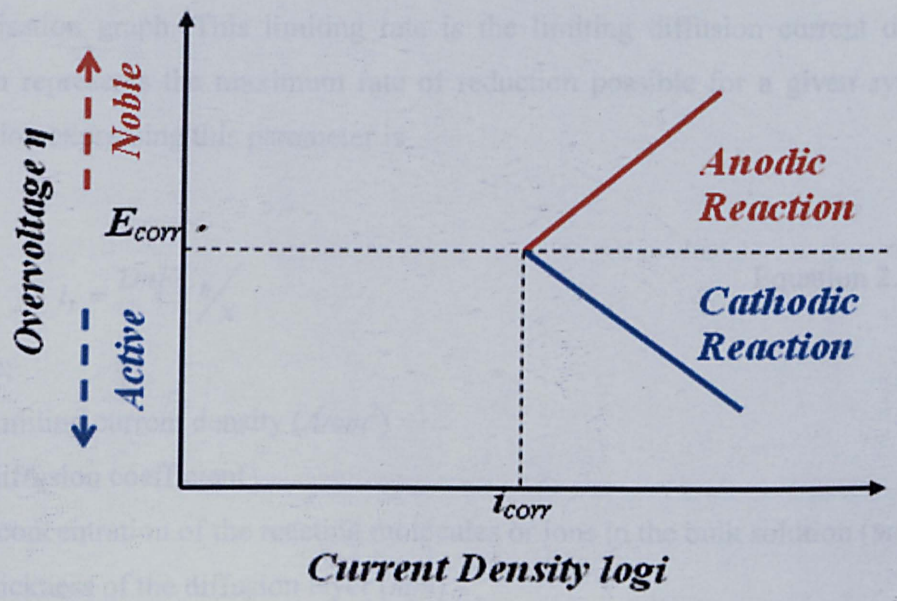

Figure 2.4: Tafel plot for activation polarization curve

As there is a linear relationship between overvoltage and the logarithmic current density, the Tafel constant for both anodic and cathodic direction can be determined as shown in Figure 2.4. Also it is obvious that the absolute values of the potentials are 50 mV greater than the reversible potential (free corrosion potential), where the oxidation and reduction are equal. The material shows more noble behaviour at higher potential, but more positive at lower potential. On a free corrosion surface, the zero voltage potential is also referred to as free corrosion potential. The current density i_{corr} is the corrosion current density at the free corrosion potential.

2.2.3 Concentration polarisation

Concentration polarisation refers to the situation where a reaction is controlled by the supply of reactants or the removal of products form a surface. One reaction which is commonly affected by concentration polarisation effect is the oxygen-reduction reaction in aqueous corrosion. At low reduction rates the distribution of oxygen molecules in the solution adjacent to the electrode surface is relatively even. At very high reduction rates the region adjacent to the electrode surface will become depleted of oxygen molecules. If the reduction rate is increased further, a limiting rate will be reached that is determined by the diffusion rate of oxygen molecules to the electrode surface. These processes can be shown schematically in the cathodic polarisation graph. This limiting rate is the limiting diffusion current density i_L, which represents the maximum rate of reduction possible for a given system; the equation expressing this parameter is

$$i_L = DnFC_B / x \qquad \text{Equation 2.12}$$

where;

i_L is limiting current density (A/cm^2)

D is diffusion coefficient

C_B is concentration of the reacting molecules or ions in the bulk solution (mol/l)

x is thickness of the diffusion layer (mm)

The diffusion layer thickness is influenced by the shape of the particular electrode, the geometry of the system and by agitation. Agitation tends to decrease the diffusion layer thickness because of convection current and consequently increases the limiting diffusion current density, which also is positively affected by the environmental parameters such as velocity, temperature and concentration.

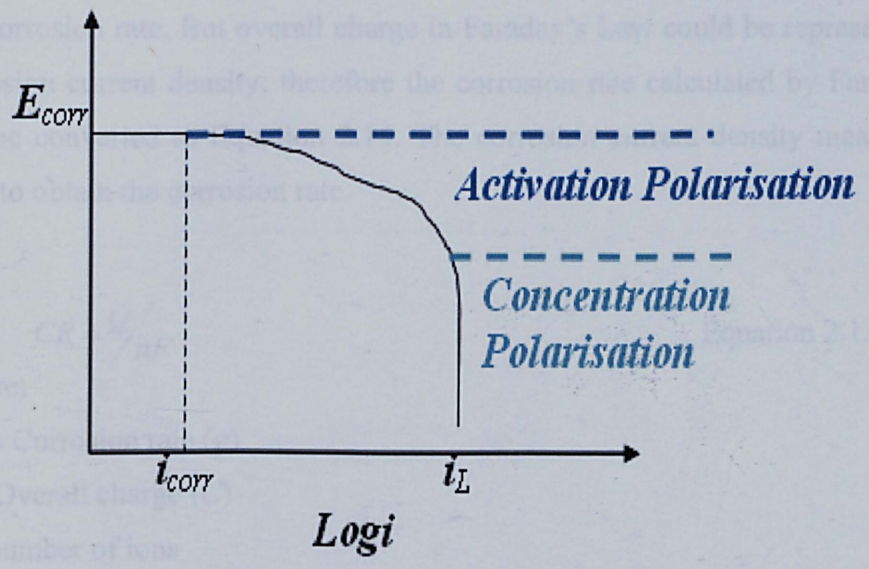

Figure 2.5: Schematic polarisation curve – activation and concentration polarisation

It has been demonstrated that the limiting current density depends on the environmental parameters *e.g.* the solution velocity, concentration, or temperature. Higher current density will be achieved at more severe environments (Figure 2.6).

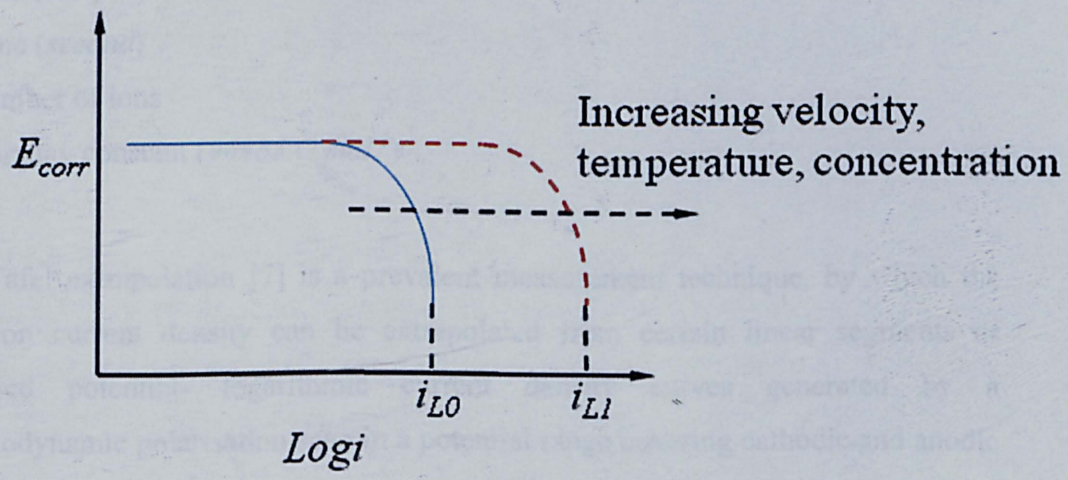

Figure 2.6: The effects of environmental parameters on the concentration curve

2.2.4 Electrochemical corrosion rate measurement

The established Faraday's Law (Equation 2.13) is acknowledged to calculate

the corrosion rate. But overall charge in Faraday's Law could be represented by the corrosion current density; therefore the corrosion rate calculated by Faraday's Law can be converted to Equation 2.14. The corrosion current density measurement is vital to obtain the corrosion rate.

$$CR = Q/nF \qquad \text{Equation 2.13}$$

Where;

CR is Corrosion rate (g)

Q is Overall charge (C)

n is number of ions

F is Faraday constant ($96485\ C\ mol^{-1}$)

$$CR = i_{corr}WAT/nF \qquad \text{Equation 2.14}$$

Where;

CR is corrosion rate (g)

i_{corr} is corrosion current density (A/cm^2)

W is atomic weight (g/mol)

A is area (cm^2)

T is time ($second$)

n is number of ions

F is Faraday constant ($96485\ C\ mol^{-1}$)

Tafel extrapolation [7] is a prevalent measurement technique, by which the corrosion current density can be extrapolated from certain linear segments of measured potential- logarithmic current density curves generated by a potentiodynamic polarisation scan in a potential range covering cathodic and anodic reactions. The typical measurement theory is schematically shown in Figure 2.7.

By this way, at values of potential positive and negative from E_{corr} by 50 mV a linear *E-Logi* relationship is observed. At potentials closer to E_{corr} of both sides of the polarisation curve, there is still a contribution to the total measured current of the cathodic and anodic reactions, so linear relationship between potential and logarithmic current density is not established in that area. The current density

responding to the intersection by extrapolating the activation polarisation back to free corrosion potential is corrosion current density.

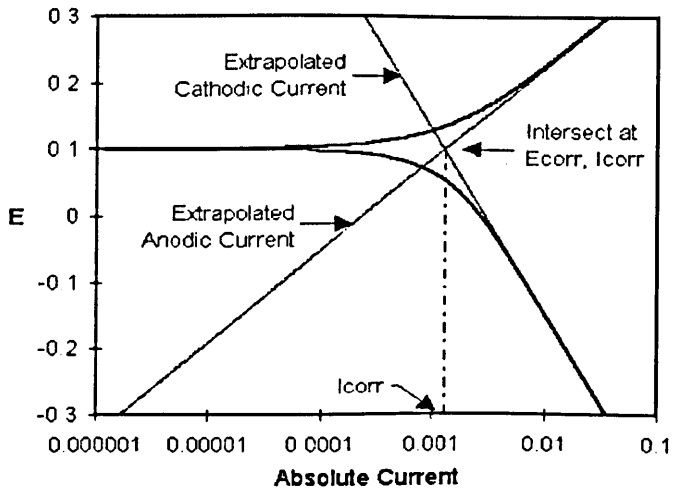

Figure 2.7: Schematic Tafel extrapolation for corrosion current density measurement

2.2.5 Cathodic protection

The first reported practical use of cathodic protection is generally credited to Sir Humphrey Davy in the 1820s [12]. Davy's advice was sought by the Royal Navy in investigating the corrosion of copper sheeting used for cladding the hulls of naval vessels. Davy found that he could preserve copper in seawater by the attachment of small quantities of iron, zinc or tin. The copper became, as Davy put it, "cathodically protected". It was quickly abandoned because by protecting the copper its antifouling properties became retarded, hence reducing the streamline of the ships, as they began to collect marine growths.

The principle of cathodic protection is in connecting an external anode to the metal to be protected and the passing of an electrical DC current so that all areas of the metal surface become cathodic and therefore do not corrode. The external anode may be a galvanic anode, where the current is a result of the potential difference between two metals, or it may be an impressed current anode, where the current is impressed from an external DC power source. In electro-chemical terms, the

electrochemical potential between the metal and the electrolyte and the electrolyte solution with which it is in contact is made more negative, by the supply of negative charged electrons, to a value at which the corroding (anodic) reactions are stifled and only cathodic reactions can take place [13-16].

2.2.5.1 Sacrificial anode protection

When a metal in contact with a different type of metal, and also both metals are in an electrolyte, the ion migration occurs due to their different electrode potentials (Figure 2.8); whereby metallic ions can move from the anode to the cathode. These results in the anodic metal corroding more quickly than it otherwise would; the corrosion of the cathodic metal is retarded or prevented.

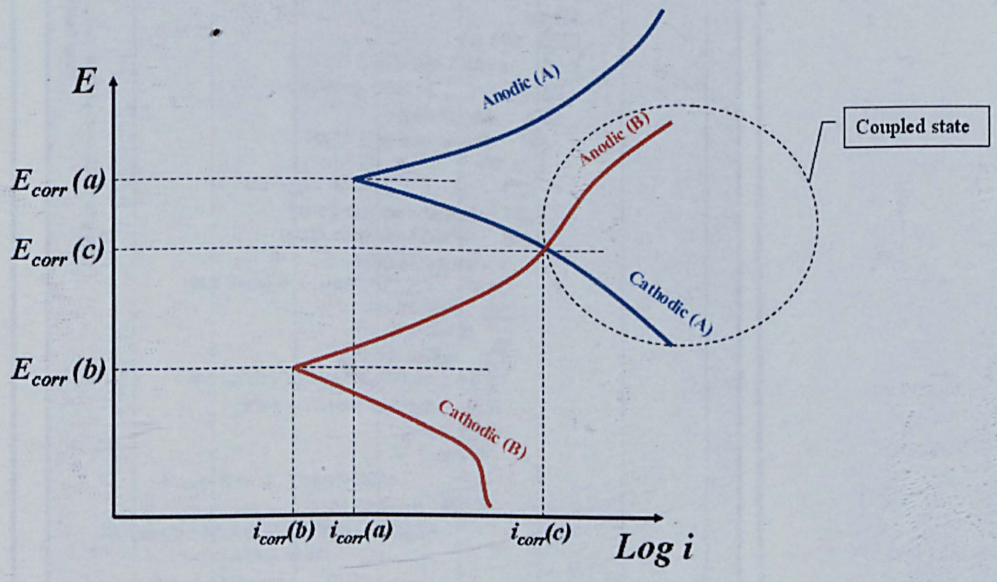

Figure 2.8: Schematic of the anodic and cathodic reactions of two metals in isolated and coupled states

Another essential feature of sacrificial anode cathodic protection to the metal is the electrolyte and a conducting path between the contacted metals which presence cause corrosion where otherwise neither metal alone would have corroded. The electrolyte provides the conducting path, but also to produce the driving force for ion migrations. Figure 2.9 shows the galvanic series of the relative corrosion activity

of the different metals in the certain electrolyte. The lower free potential the metal has, the metal shows more active corrosion action. Furthermore the more difference between the two metals' free potentials, higher driving force ion migrations will be produced. However, the galvanic series of dissimilar metals shown in Figure 2.9 just represents the corresponding corrosion behaviour in the specific environment, namely that the valuable free potentials of dissimilar metals change as the environments change.

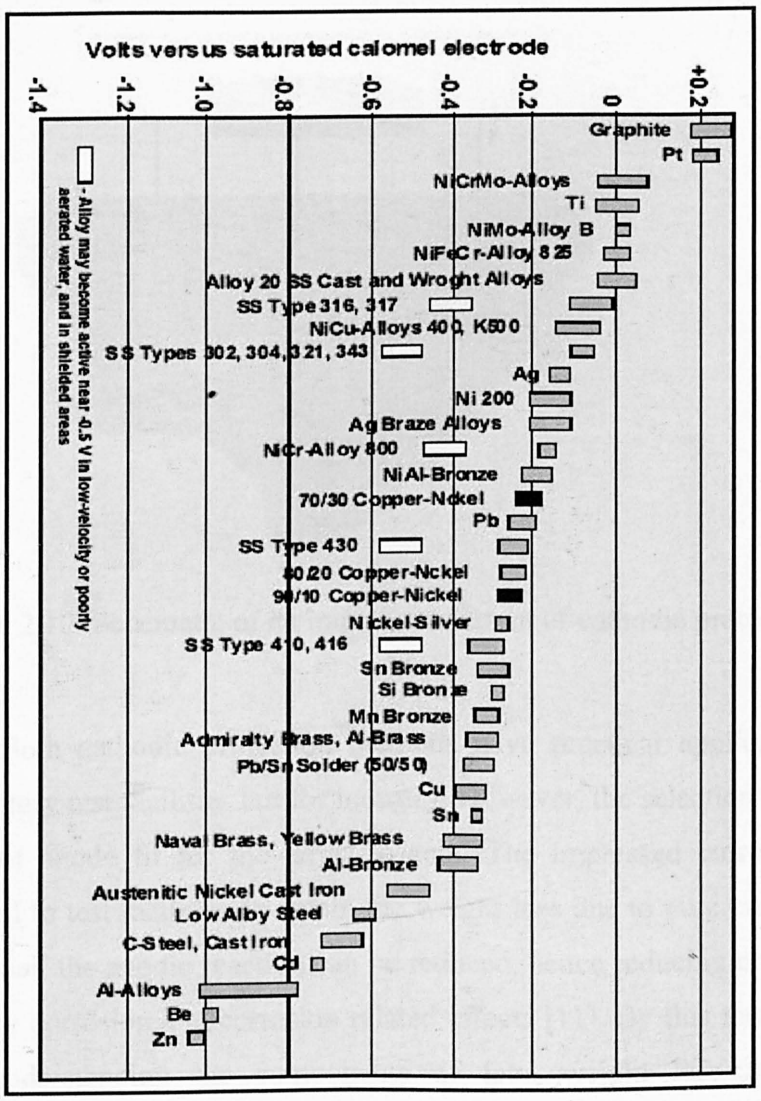

Figure 2.9: Galvanic series of dissimilar metals

2.2.5.2 Impressed current

Impressed current is another practical way for cathodic protection. Generally the basic requirements for an impressed current cathodic protection system are (Figure 2.10):

a) Inert anodes, b) a DC power supply source, c) electrically well insulated, minimum resistance and secure conductors between anodes and power source.

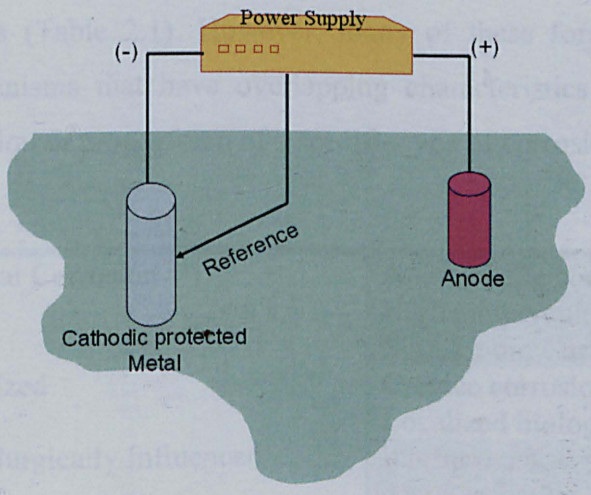

Figure 2.10: Schematic of an impressed current of cathodic protection system

Both cathodic protection methods have practical applications not only for laboratory test facilities but for industry. However, the selection of the most suitable type of anode fit for the target system. The impressed current method is often applied to test facilities to obtain the weight loss due to pure erosion. At a cathodic potential, the anodic reaction can be reduced, hence reducing or minimizing weight loss by corrosion and corrosion related effects [11]. By this means, it will improve the understanding the components of total weight loss in erosion-corrosion environments and classifying the dominant processes in erosion-corrosion [17].

2.3 Corrosion classification

One knows at present that there is a science of corrosion, which is not more difficult than most other sciences, but it is a complex one. It necessitates full knowledge in electrochemistry, in chemistry, in metallurgy and in the physical chemistry of interfaces [18]. Forms of corrosion have been well understood based on the extensive studies, which are helpful to adopt the efficient and predictive methods to reduce the cost caused by corrosion in the industries. Corrosion manifests itself in forms that have certain similarities and therefore can be categorised into specific groups (Table 2.1). However, many of these forms are not unique but involve mechanisms that have overlapping characteristics that may influence or control initiation or propagation of a specific type of corrosion.

General Corrosion	Atmospheric corrosion; Galvanic corrosion; High temperature corrosion; Oxidation; Sulfidation; Carburization; Hot corrosion
Localized	Crevice corrosion; Pitting corrosion; Localized biological corrosion
Metallurgically Influenced	Intergranular corrosion; Dealloying corrosion
Mechanically degradation	Erosion-corrosion; Fretting corrosion; Cavitation corrosion; Fatigue corrosion
Enironmentally Induced cracking	Stress-corrosion cracking; Hydrogen damage; Liquid metal embrittlement; Solid metal induced embrittlement

Table 2.1: Corrosion classifications

Wide range of corrosion has been defined and studied, which is based on the gradually furthered understanding of corrosion occurring in the practical industry. The current corrosion classification will be generally explained in the next paragraph.

2.3.1 General corrosion

General corrosion is defined as corrosive attack dominated by uniform thinning, which is characterized by corrosion attack proceeding evenly over the entire surface area, or a large fraction of the total area. Comparing with the other corrosion forms, general corrosion is easily measured and predicted, and also the general corrosion can be practically controlled by cathodic protection. The common failure of the metal in general corrosion is shown in

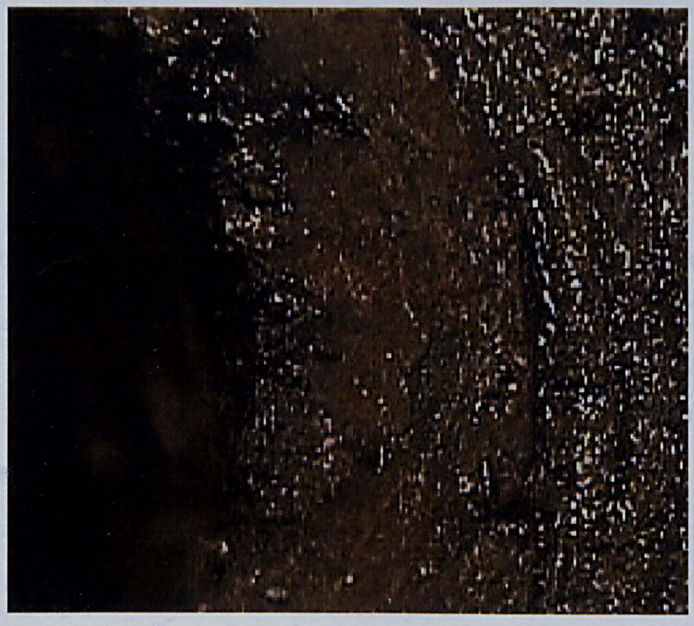

Figure 2.11: The common form of the general corrosion which leads to a surface with bumps and valleys indicating areas of greater and less attacks (Image source: http://www.argentumsolutions.com/wiki/en/General_Corrosion)

2.3.1.1 Galvanic corrosion

Galvanic corrosion occurs when a metal or alloy is electrically connected with another metal or conductive non-metal in the same electrolyte (Figure 2.12), generally galvanic corrosion is determined by the following three parameters:

1. Materials processing different open circuit potential
2. A common electrolyte
3. A common electrical path

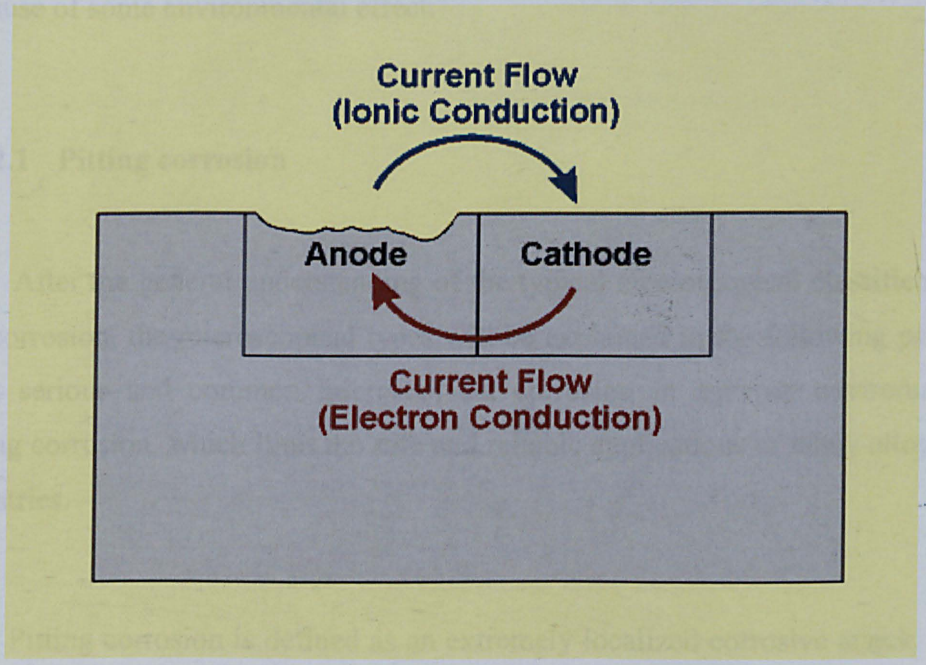

Figure 2.12: Schematic diagram of galvanic corrosion (Image source: http://www.corrosion-club.com/images/corrosioncell.gif)

Galvanic corrosion could be avoided by the electrical isolation. Once the different materials are coupled, corrosion of the less corrosion-resistant metal increases and the surface becomes anodic, while corrosion of the more corrosion-resistant metal reduces and the surface becomes cathodic. The driving force for corrosion or current flow is the potential difference developed by the dissimilar metals. The extent of galvanic corrosion is affected by the potential difference of the materials, the environment severity and the geometric relationship of the component materials.

2.3.2 Localised corrosion

Localized corrosion can be defined as unpredictable removal of metal by corrosion at small areas or zones on a metal surface in contact with an aggressive environment, such as in liquid and atmosphere. It usually occurs when small local sites are attacked at a much higher rate than the rest of the original surface, either because of an inherent property of the materials, such as the microstructure of the

materials and the formation of a protective oxide film on the material surface, or because of some environmental effect.

2.3.2.1 Pitting corrosion

After the general understanding of the typical macroscopical classifications of the corrosion, the microscopical types will be explained in the following parts. The most serious and common microscopical corrosion in aqueous environments is pitting corrosion, which limit the safe and reliable applications of many alloys in the industries.

Pitting corrosion is defined as an extremely localized corrosive attack. Simply stated, pitting is the type of localized corrosion that produces pits, that is, sites of corrosive attack that are relatively small compared to the overall exposed surface [19]. If appreciable attack is confined to a relatively small fixed area of metal acting as an anode, the resultant pits are described as deep. If the area of attack is relatively larger and not so deep, the pits are called shallow. Depth of pitting is sometimes expressed by the term pitting factor [20]. This is the ratio of deepest metal penetration to average metal penetration as determined by the weight loss of the specimen.

The pits start by the breakdown of the passivity at selective areas on the metal surface. The breakdown is followed by the formation of a minute area of an electrolytic cell, which forms an anode, while the cathode is a considerable area of passive metal. The large potential difference characteristic of the anodic-cathodic part results in considerable flow of current with rapid corrosion at the tiny anodic area. The corrosion resistant passive metal surrounding the anode and the activating corrosion products within the pits leads to the tendency of corrosion to penetrate the metal rather than spread all over the surface (Figure 2.13)

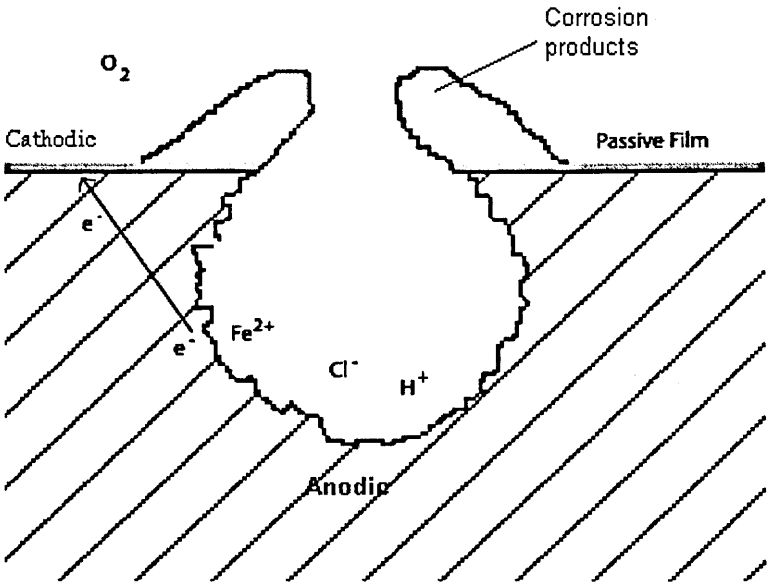

Figure 2.13: Schematic diagram of pitting corrosion (image source: http://octane.nmt.edu/waterquality/corrosion/image/pit.gif)

Once pits are initiated, they may continue to propagate or suspend due to their self-sustaining or self-repairing ability. Pit growth is controlled by rate of depolarization at the cathode areas. In the common aggressive environments, the growth is controlled by the amount and availability of dissolved oxygen and ferric chloride [21].

The propagation of pits is thought to involve the dissolution of metal and the maintenance of a high degree of acidity at the bottom of the pit by the hydrolysis of the dissolved metal ions. Since pitting corrosion is relatively unpredictable, so it attracts more and more research, which concludes some reasonable factors that control pit initiation. For example, the kinetic theories explain the breakdown of passivity in terms of the competitive absorption between chloride ions and oxygen, and also the thermodynamic theories prove the pitting potential at which the chloride ion is in equilibrium with the oxide film [19], *etc.*

Combined with the laboratory efforts, some practical approaches have been take to minimize the possibility of pitting corrosion incurrence.

- Reduce the aggressivity of the environment (chloride concentration, acidity and oxidizing medias *etc*)

- Modify the microstructure of the materials and alloying elements to resist pitting corrosion
- Optimize the design of the system with good drainage to avoid crevice, circulate/stir to eliminate stagnant solutions

2.3.2.2 Crevice corrosion

Crevice corrosion is quite common for the connection parts such as gasket, washers, fastener heads in the marine environments, which always provide the opening gap to deposit the stagnant solution between metal-to-metal and non-metal to metal (Figure 2.14).

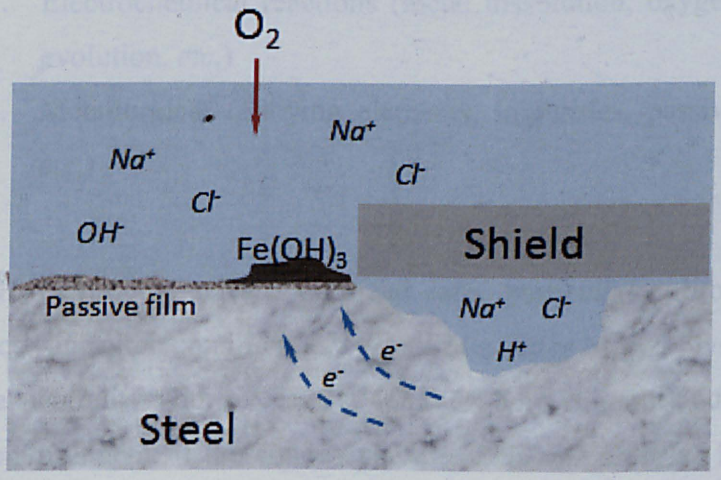

Figure 2.14: The typical schematic crevice corrosion

Regardless of the materials, the environments where crevice corrosion incurs possibly differ from the bulk environment. In its simplest form, crevice corrosion may result from the establishment of oxygen differential cells. This can occur when oxygen within the crevice electrolyte is consumed, while the boldly exposed surface has ready access to oxygen and becomes cathodic relative to the crevice area. Crevice corrosion, for example, can be encountered by stainless-type alloys in some concentrations of sulphuric acid. Although the passivity of the exposed surface is maintained by dissolved oxygen in the acid, the presence of a crevice excludes oxygen and corrosion ensues in the active state.

Crevice corrosion in neutral chloride containing environments, such as natural waters and acid-chloride media, is more complex than the preceding example given for acid. It does, however, begin with the de-oxygenation stage.

For stainless steels, numerous interrelated metallurgical, geometrical, and environmental factors affect both crevice corrosion initiation and propagation [22]. A number of these factors are:

1. Geometrical (type of crevice, tightness, depth, exterior to interior surface area ratio, *etc*)
2. Environmental (oxygen content, pH, chloride level, mass transport and migration, diffusion and convection, hydrolysis equilibria, *etc*)
3. Electrochemical reactions (metal dissolution, oxygen reduction, hydrogen evolution, *etc.*)
4. Metallurgical (alloying elements, impurities, passive film characteristics, *etc.*)

However, the release of metal ions, particularly chromium, in the crevice produces an acidic condition as a result of a series of hydrolysis reactions. To affect charge neutrality with excess H^+ ions, Cl^- ions migrate and concentrate from the bulk environment. If the concentration of acid and chloride in the crevice solution becomes sufficiently aggressive to cause breakdown of the passive film, crevice corrosion initiation occurs.

Crevice corrosion of copper-base alloys is frequently identified as metal ion concentration cell corrosion. A number of years ago, it was proposed that the concentration of metal ions in the crevice electrolyte rendered the crevice area cathodic to the area immediately outside the mouth of the crevice. Corrosion outside of the crevice (anode) progressed because the bulk environment contained a much lower concentration of metal ions. In some cases, this has been supported by the observation of plated-out copper within the crevice. Other researchers have refuted this premise, suggesting that the mode of attack is merely a variation on the oxygen

differential cell mechanism [23]. In any event, the morphology of crevice-related attack for copper alloys is distinctly different from that for stainless steels and can be recognized accordingly.

Crevice corrosion becomes one of the main degradation for the materials served in industrial systems. Some methods have been applied to eliminate the possibility of crevice corrosion. Most importantly, crevice corrosion should be avoided during the design. Otherwise, the system should be kept as open and shallow as possible to allow continued entry of the bulk environment, or some remedial could be taken to minimize the crevice corrosion such as weld sealing, cathodic protection, coating and greases *etc.*

2.3.3 Metallurgically influenced corrosion

Metallurgically influenced corrosion is classified as a result of the significant role that metallurgy plays in these forms of attack. It is well understood that metallurgy is important in all forms of corrosion, but this classification is meant to emphasize its role in these specific forms of attack.

2.3.3.1 Intergranular corrosion

In order to obtain the improved control for the integrity of the facilities in the industry, some relevant data including metallurgical factors should be supplied for the erosion-corrosion management.

The most common form of metallurgically influenced corrosion is intergranular corrosion, that is, grain boundaries are relatively susceptible to be corroded, and then this will result in the dislodgement of individual grains and a roughening of the affected areas (Figure 2.15). The occurrence of the intergranular corrosion is determined by the difference in corrosion rate between the grain boundaries and grain interiors.

The differences in corrosion rate may be caused by a number of reactions. A phase may precipitate at a grain boundary and deplete the matrix of an element that affects its corrosion resistance and also erosion-corrosion resistance. A grain-boundary phase may be more reactive than the matrix. Various solute atoms may segregate to the grain boundaries and locally accelerate corrosion [19]. That is, intergranular corrosion normally is due to active grain boundaries and a passive matrix.

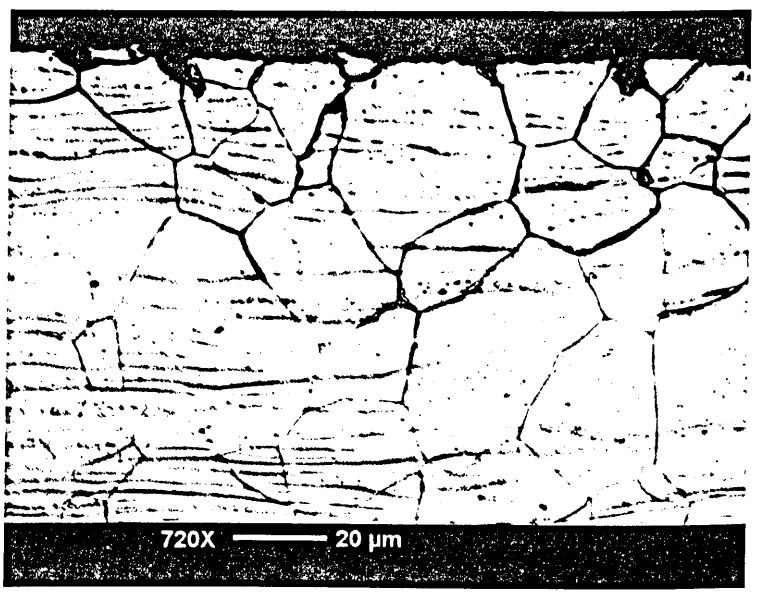

Figure 2.15: The typical intergranular corrosion in austenitic stainless steel(Image source: http://www.easypedia.gr/el/images/shared/2/28/Intergranular_corrosion)

Intergranular corrosion can occur in a wide range of alloys. For stainless steels, the distribution of carbon is probably the most important variable influencing the susceptibility to intergranular corrosion.

Carbon in austenitic stainless steel has affinity to chromium which results in the depletion of chromium in the grain boundaries and chromium carbide precipitation simultaneously, but it depends on the metallurgical processing technology. Phase other than carbides can also influence the corrosion behaviour of austenitic stainless steels. Ferrite, which is the result of an unbalanced composition,

appears to reduce the pitting resistance of the steels. The presence of martensite may render the steels susceptible to hydrogen embrittlement under some conditions. The martensite can be produced by the deformation of unstable austenite. Although this phenomenon can occur in a number of commercial stainless steels, it is most common in the lower-nickel steels, in which the transformation is used to increase formability [19].

2.3.4 Mechanically assisted degradation

Mechanically assisted degradation classifies those forms of corrosion that contain a mechanical mechanism, such as abrasion and hydrodynamics, which has a significant effect on the corrosion behaviour.

2.3.4.1 Erosion-corrosion

Erosion-corrosion falls into a broad category of tribocorrosion processes which include abrasion-corrosion and cavitation-corrosion as examples. These are not specific forms of corrosion but are degradation processes, which involve the action of a mechanical process (*e.g.* an impact of a solid particle) in conjunction with an electrochemical corrosion process [8]. The combined mechanical and electrochemical reactions in aggressive aqueous environments with solid particles are known as erosion-corrosion to cause the horrible failures of the components in the industry (Figure 2.16). While erosion-corrosion arises from a combination of electrochemical attack and the physical abrasion as a consequence of the fluid motion, but it could not simply be considered as accumulative effects due to erosion and corrosion. However, erosion-corrosion is composed by the erosion and corrosion respectively and the interactive effects which erosion-corrosion also consists of the acceleration in the rate of corrosion attack due to the relative motion of a corrosive fluid and a metal surface and the acceleration of erosion due to corrosion in metal.

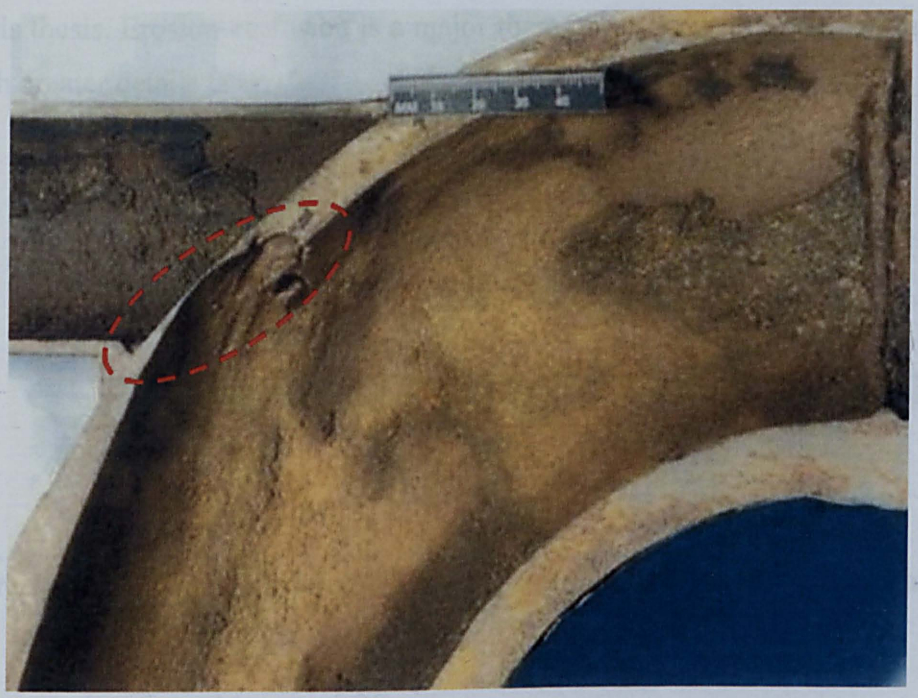

Figure 2.16: The failure at a pipe elbow due to erosion-corrosion

The erosion-corrosion resistance depends not only on the materials themselves, but also the environmental severity. Practically as the environment becomes more and more severe, for example higher velocities, higher temperature, higher sand loading and lower pH *etc*, the materials show more severe erosion-corrosion degradation (Figure 2.17). Theoretically the mechanical properties and corrosion resistance of the materials are always most popularly concerned factors which are used to assess the material erosion-corrosion resistance. For the materials with the protective films, the erosion-corrosion resistance usually is associated with:

- The mechanical properties of the protective films
- The self-repairing ability of the protective films
- The adhesion ability of protective films the substrate
- The mechanical properties of the materials
- The corrosion resistance of the materials

For materials without a protective film, the erosion-corrosion resistance is always associated with the mechanical properties of the materials and the corrosion resistance of the material. A detailed review of these aspects will be addressed later

in this thesis. Erosion-corrosion is a major theme of this thesis which is dealt with a much greater details later.

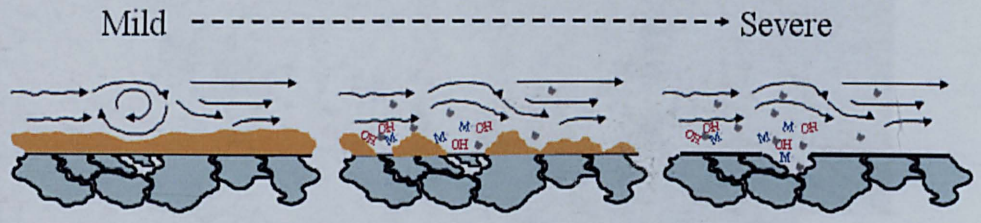

Figure 2.17: The schematic environment-dependent erosion-corrosion resistance

2.3.5 Environmentally induced cracking

The environmentally induced cracking follows the current trend in the literature of combining those forms of cracking that are produced by corrosion in the presence of stress. As the introduction to this article explains, there are many differences as well as similarities among these forms of cracking. However, the distinction between each form is not always apparent; it is therefore easier to combine these different forms into one all-encompassing form.

2.3.5.1 Stress corrosion cracking (*SCC*)

Stress Corrosion Cracking (*SCC*) is a term used to describe the result of stress concentration at corrosion generated surface flaws which result in the crack initiation and further propagation (Figure 2.18). The observed crack propagation is the result of the combined and synergistic interaction of mechanical stress and the environments.

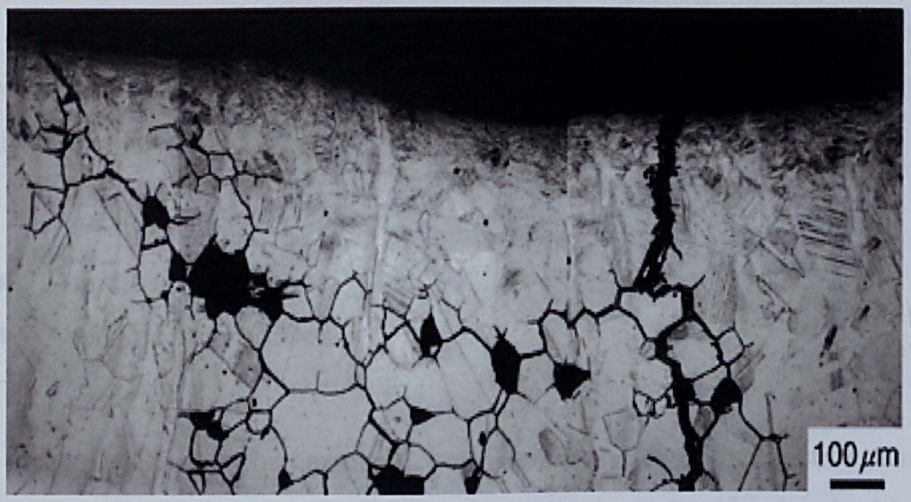

Figure 2.18: The branched stress corrosion cracking in pipe cross section (image source: http://jolisfukyu.tokai-sc.jaea.go.jp)

SCC always occurs when aggressive environmental exposure and application of stress are applied simultaneously, and stress concentration does happen around the flaws which are caused by the environmental corrosion; furthermore the stress concentration will cause time-dependent crack initiation and propagation. The process could be described as the combined simultaneous interaction of mechanical and chemical forces results in crack propagation where neither of factors acting independently or alternately would results in the same effect.

The stresses required to cause *SCC* are very small, usually below the macroscopic yield stress, and are tensile in nature. The stresses can be externally applied, but residual stresses often cause *SCC* failures. However, compressive residual stresses can be used to prevent this phenomenon. Static loading is usually considered to be responsible for *SCC*. Stress corrosion cracking is usually used to describe failure in metallic alloys. However, other classes of materials also exhibit delayed failure by environmentally induced crack propagation. Ceramics exhibit environmentally induced crack propagation [24] and polymeric materials exhibit craze cracking as a result of the interaction of applied stress and environmental reaction [25], these two materials are very popular for the coating applications.

Two mechanisms have been proposed to explain the synergistic stress-corrosion interaction that occurs at the crack tip. The supposed mechanisms can be classified into two basic types:

- Anodic mechanisms
- Cathodic mechanisms

Obviously during the corrosion, both anodic and cathodic reactions must occur, and the phenomena that result in crack propagation may be associated with either of reactions. The anodic mechanism could be expressed as the active dissolution and removal of the materials for the crack initiation and propagation. Simultaneously, the cathodic mechanism is hydrogen evolution, absorption, diffusion and further material embrittlement, which will result in the materials is susceptible to the crack propagation.

Chapter 3 Literature review

3.1 General review of erosion-corrosion problems

As marine and offshore technologies have been developed for several decades, the marine alloys have evolved to resist corrosion. It is common that marine technologies spend millions of pounds to repair material degradation resulting in the failure of the structural components. Even though a huge amount of cost has been invested, unplanned shutting of the systems still happens on offshore structure and marine transport systems. Especially in a recent survey erosion-corrosion was rated as one of the top five most prevalent corrosion damage type in the marine and offshore industries [26]. One of the practical significance for this project is to provide as much laboratory data as possible to enable prediction of erosion-corrosion and hence minimize material loss in the industry.

As large numbers of incidents that occur in marine industries are related to erosion-corrosion, it is therefore essential to maintain the integrity of facilities in the industry. Due to more requirements for improved productivity and increasing efficiency, combined with the increased attention to safety and environmental issues, the activities related to erosion-corrosion management play an increasingly important role.

To obtain an improved control of the integrity, the relevant data need to be applied, such as process and production data, erosion-corrosion monitoring data, inspection and maintenance data. The key to success is thereby related to the management of future mass loss prediction, future material selection and erosion-corrosion prevention methods.

3.2 General review of marine alloys

Materials are chosen largely for a combination of suitable mechanical properties and corrosion resistance for the marine application. The highest mechanical properties seldom go with the best corrosion resistance and the choice of material usually involves a compromise [27]. The marine environment is a very aggressive natural environment, and so many alloys have been developed to combat the environment such as cast iron, copper-base alloys, aluminium, stainless steels, titanium *etc.* They are used in the different applications due to their resistance to the different forms of corrosion. Typical applications include pumps, valves, drilling equipments, propeller shafts, exhaust systems, piping systems, heat exchangers, fasteners and desalination equipments *etc.*

In all fields of engineering, but nowhere more than marine and offshore service, designer, fabrication and end users are concerned about the applicability, maintenance and improvement of marine alloys. Today, with millions of tons of marine alloys in offshore and marine service, old- and false- notions about cost, applicability and fabrication are less and less likely due to the improved understanding of erosion-corrosion. Marine alloys should be selected that are functionally compatible, can operate safely during the service time, and can be obtained and fabricated at a reasonable cost, combined with consideration of the corrosion resistance. Interacting with marine environments marine alloys can exhibit various modes of corrosion (uniform corrosion, localized corrosion, galvanic corrosion, intergranular corrosion, erosion-corrosion and microbiologically influenced corrosion *etc.*). Table 3.1 summarises the corrosion performance of marine alloys in seawater, which generally is considered as the basic guideline for the future material selections. More and more technologies have been developed not only on material modifications, but also other technologies such as cathodic protection and coatings *etc.* to minimise costs associated with modern marine equipment which handle fluids demands increasing flow rates with the inherent risk of flow-dependent corrosion [28].

Type of Corrosion	Cast Iron	Copper Alloys	Stainless Steel
General corrosion	Susceptible	Resistant/Susceptible	Resistant
Crevice corrosion	Susceptible	Susceptible	Susceptible
Pitting corrosion	Susceptible	Susceptible	Resistant/Susceptible
Erosion-corrosion	Susceptible	Resistant/Susceptible	Resistant

Table 3.1: The review of corrosion performance of marine alloys in marine environments

3.2.1 *Ni*-resist cast iron

Each alloy element influences the mechanical properties in the same cast in a different way. Appropriate balance of the alloying elements and heat treatment are two prevalent methods to improve the properties of the materials [29]. In the same manner, the erosion-corrosion resistance of marine alloys could be enhanced to some degree due to their alloying compositions.

Ductile cast iron has been widely used as a structural material in the machine, the automobile industry, the mining industry especially as the parts of the slurry pumps [19]. Because the ductile iron has an appropriate combination of impact fatigue resistance and abrasive wear resistance through the control of its microstructures [30]. The mechanical properties are improved by high nickel compositions for example tensile strength and hardness [31]. Chromium has a much stronger tendency to increases corrosion resistance by the formation of protective oxide films on the surface of the materials. Combined with chromium, nickel can improve both strength and corrosion resistance for cast irons [19]. The hardness of cast iron is directly related to the chemical composition. The amount of copper contributes to the hardness [32]. Silicon not only affects the corrosion resistance of cast iron, but also the hardness. Corrosion resistance is enhanced dramatically when silicon content is over 14%. However, the cast iron turns brittle when silicon content is over 16% [33]. The corrosion mechanism of *Ni*-resist cast iron has been well studied by Xu [34]. *Ni*-resist cast iron is covered by Fe_2O_3 and Fe_3O_4 when it is applied in corrosive environment. The corrosion products (Fe_2O_3 and Fe_3O_4) cannot stop ferrous ions dissolving into the solution, namely that the material is corroded continuously (Figure 3.1).

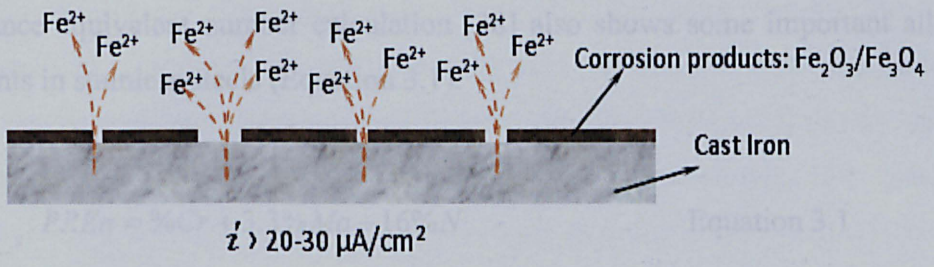

Figure 3.1: Schematic corrosion mechanism of *Ni*-resist cast iron [34]

3.2.2 Stainless steel alloys

Stainless steels are known to have ability to form a protective passive film on their surface when exposed to a corrosive media [35]. Stainless steels derive their corrosion resistance from that thin and invisible oxide layers, which have formed during a reaction between the metal and oxygen present in the ambient environment. This protective film consists mainly of chromium oxide and it forms spontaneously in environments containing enough oxidant [36]. This film acts as a barrier between the oxygen and the underlying metal to drastically decrease the corrosion rate of stainless steel (Figure 3.2).

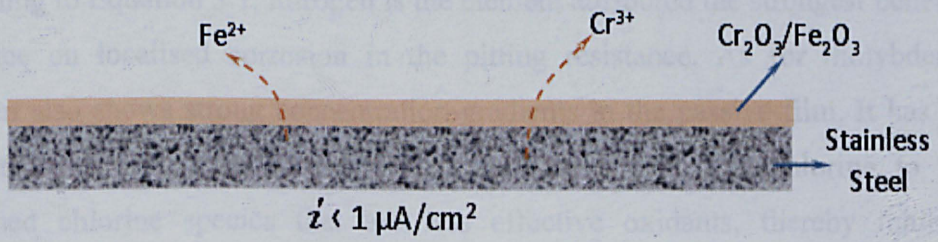

Figure 3.2: Schematic corrosion mechanism of stainless steel [11]

From a corrosion point of view, seawater may be looked upon as a neutral chloride solution, *i.e.* an environment promoting localized corrosion in stainless steels [37]. A common factor of stainless steels is a high content of the alloying elements chromium, molybdenum and nitrogen. Attempts have been made to establish a measure of the pitting and crevice corrosion resistance by calculating the sum of the most important alloying elements in a weighed form. This sum is called pitting resistance equivalent number (*PREn*) [36]. The empirical equation of pitting

resistance equivalent number calculation [38] also shows some important alloying elements in stainless steels (Equation 3.1).

$$PREn = \%Cr + 3.3\%Mo + 16\%N \qquad \text{Equation 3.1}$$

Molybdenum stabilizes the passive film. It has a favourable effect on the pitting resistance of stainless steels, either molybdenum enhances the stability of the passive film from the solution side, or enhances the presence of molybdenum in the metal phase near the oxide/metal interface limits the dissolution rate of iron and chromium [39]. When molybdenum is added in stainless steels, it is incorporated into the passive film, showing complex oxide chemistry with different states of oxidation, that is, hexavalent *Mo* is found to be enriched at the surface, whereas tetravalent states show a more homogeneous distribution through the film [40]. Nitrogen additions improve the resistance to pitting and crevice corrosion of stainless steels in solutions containing chloride ions [41]. Recent research on the effect of nitrogen in austenitic stainless steels have been focused on the improvement of mechanical and corrosion properties [42]. Nitrogen frequently in combination with manganese, is used for stabilising the austenitic structure, for strengthening and most recently for retarding formation of intermetallic phases [43]. According to Equation 3.1, nitrogen is the element attributed the strongest beneficial influence on localised corrosion in the pitting resistance. As for molybdenum, nitrogen also shows strong concentration gradients in the passive film. It has been suggested that ammonia or ammonium ions react with free chlorine to form combined chlorine species that are less effective oxidants, thereby inhibiting chlorination enhanced localised corrosion [44]. Another possibility is the formation of a nitride at the metal/film interface which brings down the dissolution rates for the individual elements in the alloy. Nitride has also been put forward as a possible mechanism for synergy between nitrogen and molybdenum [45].

Low alloyed austenitic stainless steels, types 304 and 316, are being used for a large number of components. These alloys are far less prone to sulphide stress cracking than ferritic and martensitic alloys as long as they are in the annealed condition [46]. High alloyed austenitic stainless steels can provide excellent trouble-

free service in seawater for marine equipment [47]. Austenitic stainless steel series are chosen for conditions where a better corrosion resistance is needed, even though their mechanical strength is less. Usually, the control of little changes in microstructure or in the environmental conditions is crucial, since the synergistic effects are sensitive to microscopic features such as second phase precipitates, grain boundaries and surface texture of the components [48, 49]. The low-carbon austenitic stainless steel has been employed extensively for a couple of decades in the construction of marine pumping systems and plants. Especially under flowing conditions, austenitic stainless steel is favoured over the aluminium brass and copper-nickel alloys because of its much superior resistance to erosion-corrosion [48]. Since austenitic stainless steels have a wide scope range of applications in different industries, it isn't avoidable to confront some problems. The extensive applications of this kind of stainless steels in industries are due to their good erosion-corrosion resistance. Quraishi *et al.* concluded that this type of stainless steel is covered with a protective film rich in chromium that imparts corrosion resistance to its surface. However, chloride-containing acidic solutions are aggressive to this film layer and results in severe pitting formation. Several organic molecules contain sulphur and nitrogen hetero-atoms were suggested as inhibitors for steel in acidic medium [50], and also austenitic stainless steel, for example AISI 316, undergo less pitting at increased velocities and an approximate velocity of greater than 1.5 ms^{-1} is recommended to avoid pitting, which is the so-called critical velocity [51].

The high strength of duplex stainless steels together with their high resistance to chloride induced localized corrosion are important reasons for their popularity in oil and gas production [52]. Duplex stainless steel became available in the 1930s. Generally duplex stainless steels have very good localised corrosion resistance because of their high chromium and molybdenum contents. Duplex stainless steels are also considered for the use as heavy section tube sheets that would be compatible in strength and corrosion resistance with the highly alloyed austenitic stainless and ferritic stainless steels [43]. Over the last few decades, several new duplex stainless steels have been developed which can be produced in a much wide range of applications. One important difference between early and modern duplex stainless steels is the nitrogen alloying of the newer grades, which is beneficial to both

structural stability and corrosion resistance [53]. Definitely, super duplex belongs to the newer generation of duplex stainless steels. Super duplex grades have enhanced pitting and crevice corrosion resistance compared with the ordinary austenitic or duplex types. This is due to the further additions of chromium, molybdenum and nitrogen to these grades. The second generation duplex stainless steels use nitrogen as an austenite stabilizer. The addition of nitrogen has been claimed to improve tensile properties, pitting and crevice corrosion resistance after welding by reducing the detrimental influence of heat-affected zones by stabilizing the austenitic phase at higher temperature [54]. Much recent research has focused on the development of high-grade alloys. It has involved refinement of the alloy composition to contain optimum amounts of the crucial alloying elements *Cr*, *Mo* and *N* which have been shown in previous investigations to increase the resistance to localised attack particularly in saline conditions [9].

3.2.3 Copper-base alloys

Copper base alloys are widely used in marine engineering and on-board ships for pipe work systems that carry seawater supplies, typically for cooling purposes. These materials offer a good combination of strength, toughness, antifouling properties and corrosion resistance at reasonable cost for many applications. Their overall suitability has since been confirmed by continuing use in the industrial applications [55].

Nickel is the primary alloying element for all copper-base alloys. Besides, different grades of copper-base alloys have some specific additions of alloying elements to improve their corrosion resistance and mechanical properties. All the copper-nickel alloys contain small but important additions of iron and manganese which have been chosen to provide the best combinations of resistance to flowing seawater and overall resistance [55]. It has been well known that small addition of iron to copper-nickel alloys can improve their resistance to erosion-corrosion [56, 57]. However, Pearson reported that iron addition increases erosion-corrosion resistance of copper-nickel alloys in flowing seawater, only if iron remains in solid solution, and also concluded that increasing iron concentration increases the

resistance to impingement attack but decreases the resistance to localized attack [58]. North and Pryor hypothesized that nickel and iron were incorporated into the Cu_2O film, occupied cations vacancies, and thus, reduced the cations vacancy concentration, which increases the resistance [59].

It was demonstrated that there is a synergistic effect between nickel and iron in copper-based alloys with nickel content from 0 to 30% and iron content from 0.05 to 2%. Nickel improves the corrosion resistance of copper, but its effect is greatly enhanced by the presence of iron in the alloy. Nickel is incorporated into a continuous cuprous oxide film, which is formed as one of the anodic reaction products. It has been reported that nickel has a positive effect on the electrochemical behaviour of these alloys, and also as if nickel content was up to 30%, the passive film thickness of copper-nickel alloys would increase. Furthermore, the increase of nickel content shifts the breakdown potential towards more positive values [60].

It has been manifested that the addition of chromium to copper-nickel alloys increases their resistance to erosion-corrosion. For example, the copper-nickel alloys modified by chromium have lower erosion-corrosion rates than the chromium-free copper-nickel alloys [61]. Chromium increases strength of the materials, and has a surprisingly favourable effect on resistance to erosion-corrosion in fast flowing seawater and to erosion by solids.

The addition of tin increases the tensile strength, tarnish resistance and wear resistance of copper-nickel alloys. While the addition of niobium increases tensile strength and proof strength and weldability, the addition of titanium promotes the formation of pore-free welds because it can tie up oxygen, hydrogen and nitrogen. The addition of manganese and silicon act as deoxidant. Aluminium increases strength, seawater and scaling resistance [62].

Copper and nickel are adjacent to one another in the periodic system of elements, with atomic number 29 and 28 and atomic weight 63.54 and 68.71. The two elements are closely related and are completely miscible in both the liquid and

solid state. Copper nickel alloys were first developed during *World War II* as a replacement to copper in Royal Navy seawater pipe work [63]. The most common copper nickel alloys used in marine service are 90/10 (C71500) and 70/30 (C70600). The 70/30 copper nickel alloy is quite strong to withstand higher seawater velocities, but as for 90/10 copper nickel alloy, it provides good service at a lower cost. They are both superior to coppers and to other copper-base alloys in resisting and solutions and are highly resistant to *SCC* and impingement corrosion [64].

North *et al.* showed that cuprous oxide films formed on the surface of copper-nickel alloy, and the nickel content in copper nickel alloys improved the resistance of the film by the incorporation of nickel into the vacant lattice sites and as a substitute for copper ions [59].The corrosion resistance from the copper nickel alloys is contributed by the formation of a thin, adherent, protective surface film. The film is complex and predominantly comprises of cuprous oxide, often containing nickel and iron oxide, cuprous hydroxyl-chloride and cupric oxide [65]. That is, the protective films formed on copper nickel alloys' surface somehow depends on the alloying elements and the significant agent concentration of the solutions. For example, in significant chloride concentration solution, Kato *et al.* discovered the thin layer next to the metal surface is copper chloride, which provides the high level of cathodic polarisation. The high resistance to corrosion of 90/10 copper-nickel is achieved primarily by inhibition of the cathodic process, the reduction of dissolved oxygen. Reversely, the outer layer of cuprous oxide enriched in nickel and iron contributes only a small amount of anodic polarisation. [66]. *Fe* in copper-nickel alloys attributes to the improvements of their corrosion resistance. Stewart and LaQue suggested that *Fe* in copper-nickel forms a hydrated *Fe* oxide in the corrosion product thereby improve their protective ability [67]. As for the films formed on the surface of 70/30 copper-nickel alloys, obviously they are enriched in nickel, but the nature of the films are quite similar to 90/10 copper-nickel alloys , which results in the films on 70/30 copper-nickel alloys show higher corrosion resistance than 90/10 copper-nickel alloys.

The corrosion behaviour of 90/10 copper nickel alloys has been extensively studied due to their widespread applications in seawater and saline environments. It

is reported that 90/10 copper-nickel passive oxide in quiescent *NaCl* solutions was a duplex oxide with a reddish Cu_2O inner layer and a greenish trihydroxy copper (II) monochloride ($Cu_2[OH]_3Cl$) outer layer. The outer $Cu_2(OH)Cl$ layer was believed to be deposited from the solution. Its mechanical removal had little effect on the corrosion resistance of the sample. This inner Cu_2O layer was identified as the barrier layer. It is noted that this barrier layer could dissolve up to 30% *Ni* and 10% *Fe* with no apparent change in structure. Nickel and iron incorporate into the Cu_2O lattice and reduce the cation vacancies, thereby increasing the ionic and electronic resistance [37, 38]. The higher the valency of the alloying element has, the greater number of cation vacancies and positive holes neutralized [68]. 90/10 copper-nickel alloy is resistant to chloride, ammonia and sulphide stress corrosion cracking [69], and also good resistance to biofouling due to the release of copper ions [70]. G. Kear *et al.* reviewed the electrochemical literature on 90/10 copper-nickel alloy either in seawater or sodium chloride electrolytes, and they reported that the corrosion mechanism of 90/10 copper nickel alloy is very similar to that of unalloyed copper. The mass transfer is assumed to be the rate of movement of a cuprous chloride complex away from the electrode surface to the bulk of the electrolyte [68].

As for 70/30 copper alloy, it has better corrosion resistance than 90/10 copper-nickel alloy. Some results showed that 70/30 copper-nickel has good resistance to general and localized corrosion in natural and unpolluted seawater, which are mainly attributed by the film on the surface formed by copper oxides with nickel and iron compounds. The presence of nickel or iron atoms in copper compound lattice decrease its defect number thus increasing the passivating power of the corrosion layer [71, 72].

Since understandings of corrosion mechanism were gradually obtained, marine alloys have been modified continuously. High strength copper nickel alloys are examples of a relatively new generation of corrosion-resistant materials specifically designed for use on offshore structures [73]. The principle high strength copper nickel alloys result from the fact that the addition of aluminium to a copper-nickel binary alloy increases the strength through the formation of age-hardening precipitates. This effect has been known since the 1930's, and a number of alloys

have been produced based on the copper nickel system. The first commercial aluminium containing copper nickel alloys was HIDURAX SPECIAL developed in the 1940's to meet the requirement for a high strength corrosion resistant alloy in naval applications [74].

High strength copper nickel alloys, Marinel grade, have developed with excellent corrosion resistance, immunity to hydrogen embrittlement, high impingement resistance, good resistance to stress corrosion cracking and good mechanical properties [74]. Due to the excellent qualities high strength copper nickel alloys have been extensively used in oil and gas industries, aerospace and automotive *etc.* It is well known that high strength copper nickel alloys have high resistance to erosion-corrosion. Jet impingement tests have been carried out on high strength *Cu-Ni-Al* alloys in aerated seawater flowing at 9.3 ms^{-1} for 28 days and show that these materials have resistance to impingement attack. Their corrosion properties in this case are similar to cast nickel aluminium bronze and superior to wrought iron containing 70/30 and 90/10 copper nickel alloys [74].

Nickel aluminium bronze (*NAB*) is a family of copper-based alloys with a combination of mechanical and chemical properties. Both cast and wrought nickel aluminium bronze offer a good combination of mechanical properties and corrosion resistance. Consequently, aluminium bronzes have been widely used for decades in a variety of marine applications, including valves and fittings, ship propellers, pump castings, pump shafts, valve stems and heat exchanger waterboxes [75]. The qualities often make nickel aluminium bronze the only logical choice, which are attributed by its excellent strength, excellent corrosion resistance, favourable high temperature properties, good resistance to fatigue and good resistance to creep *etc.* Consequently, they have been used for decades in a wide variety of marine applications including valves, fittings, ship propellers *etc* [75]. However, nickel aluminium bronze isn't ideal for all conditions, as reported by Meigh [76].

Nickel aluminium bronze alloys are generally two-phase, duplex alloys containing 5% to 11% aluminium as well as additions of iron and nickel for strength. More aluminium contents result in higher strength, which is attributed to a hard

body-centred-cubic phase [77]. Nickel improves corrosion resistance and yield strength. Iron acts as a grain refiner and increases tensile strength. It is well known that nickel aluminium bronze alloys are metallurgical complex alloys in which small variations in composition can result in the development of markedly different microstructure [78, 79]. The corrosion resistance of nickel aluminium bronze has been attributed to a protective layer, perhaps 900 to 1000 nm thick, containing both aluminium and copper oxides (Figure 3.3). Additions of nickel and iron enable greater amounts of aluminium to be present in the alloy before chemically and mechanically detrimental Cu_9Al_4 phases are produced [80]. The oxide layer is aluminium – rich adjacent to the base metal and richer in copper in the outer regions. There are also oxides of nickel and iron, together with trace amounts of copper salts and copper hydroxychlorides, *e.g.*, $Cu_2(OH)_3Cl$ and $Cu(OH)Cl$, which form after longer exposure times to seawater. The oxide layer adheres firmly to the base metal and consequently provides corrosion protection reducing the corrosion rate by a factor of 20-30 [81]. The passivation of nickel aluminium bronze is based upon the common system of oxidation resistant materials, where solute *Al* has a greater affinity for oxygen than solute *Cu*. Under standard conditions, Al_2O_3 is almost eleven times more stable than Cu_2O relative to their metals in the zero oxidation state. For *Cu*- 10%, thermal oxidation is based on a rapid initial production of Cu_2O from which $N_{Al_2O_3}$ is achieved at the alloy/oxide interface due to the depletion of *Cu*. Alumina subsequently forms as a protective oxide which is highly impermeable to the passage of cuprous cations which can no longer enter what is the outermost layer of cuprous oxide. The higher the aluminium content of the alloy, therefore, the greater the corrosion resistance due to the protective Al_2O_3 since the limiting mole fraction is achieved over a shorter exposure time and is maintained at lower copper dissolution rates [82].

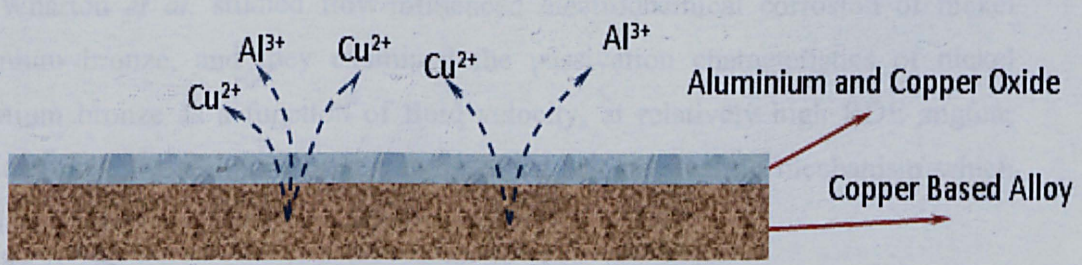

Figure 3.3: Schematic corrosion mechanism of nickel aluminium bronze [80]

Ault *et al.* reported that nickel aluminium bronze is the most resistant of copper-base alloys under conditions of service such as high velocity seawater and high degree of turbulence, and the attacks always occur locally in the protective layers, and then expose the unprotective metal, and also vary logarithmically with velocity [83].

The open circuit potential of nickel aluminium bronze becomes more negative as the rotation speed increases; moreover it is lower than the copper nickel alloys in response to the specific rotation speed. Nickel aluminium bronze is the most resistant of the readily available copper-base alloys to flow induced corrosion. Under conditions of service involving exposure to seawater flowing at high speed, or with a high degree of turbulence, damage can occur to the protective oxide layer, locally exposing the unprotected bare metal [82]. Nickel aluminium bronze is vulnerable to such attacks in unpolluted seawater at fluid velocity in excess of 4.3 ms^{-1} and this degree of attack is reported to vary logarithmically with velocity: from 0.5 mmy^{-1} at 7.6 ms^{-1} to 0.76 mmy^{-1} at 30.5 ms^{-1}, and even at 7.6 ms^{-1} corrosion rates could rise locally to 2 mmy^{-1} [83]. The velocity effects on erosion-corrosion behaviour have been studied, and it is concluded that the total mass loss due to erosion-corrosion increases as the kinetic energy increases. Jet impingement velocities between 3 and 5 ms^{-1} have demonstrated the superior corrosion performance of nickel aluminium bronze in contrast with non-passivating carbon steel. The erosion and erosion-corrosion performance of nickel aluminium bronze was consistent with a ductile metal undergoing plastic deformation processes during sand impacts [82].

Wharton *et al.* studied flow-influenced electrochemical corrosion of nickel aluminium bronze, and they examined the passivation characteristics of nickel aluminium bronze as a function of fluid velocity, at relatively high RDE angular velocities nickel aluminium bronze exhibited a self-passivating mechanism which significantly improved to dissolution resistance [82].

3.3 Erosion-corrosion

It is very common that materials come into contact with sand-bearing liquids in offshore well systems. This requires the material selection to minimize erosion-corrosion damage, which is a common cause of failure in oilfield equipment. Erosion-corrosion is associated with a flow-induced mechanical removal of the protective surface film that results in a subsequent corrosion rate increase via either electrochemical or chemical processes. The mechanical damage by the impacting fluid imposes disruptive shear stresses or pressure variations on the material surface and/or the protective surface film. The morphology of surfaces affected by erosion-corrosion may be in the form of shallow pits or horseshoes or other local phenomena related to the flow direction [84].

3.3.1 Components of erosion-corrosion

Erosion-corrosion is literally related with dynamic liquid corrosion and erosion. Comparing with static corrosion, dynamic liquid corrosion is often used to describe the accentuation in corrosion rates when mass transfer of reactants and products is enhanced due to the flow inducements. With flow-induced corrosion in neutral environments, materials are susceptible to general corrosion, and also the materials suffer accelerated corrosion due to the enhanced transport of aggressive agents and/or the removal of corrosion products [85]. In addition, liquid erosion occurs when the solution repeatedly impacts the metal surface. The liquid erosion may be attributed to removal of the materials, the adherent film, and/or the protective corrosion scales [86].

In practice, when the materials are exposed to an impinging jet of solution containing solid particles, they suffer the weight loss due to the combination of the flow induced corrosion and erosion. That is, mechanical processes and electrochemical processes are interacting and forming a complex degradation mechanism, which results in the material loss as a key problem in many industrial applications such as hydraulic turbines, slurry pumps, valves, pipelines conveying

solid particles, *etc* [87]. So the total material degradation isn't simply composed by the material degradations due to pure corrosion and pure erosion, but also the interactions between pure corrosion and pure erosion which is known as synergistic effect in erosion-corrosion. The synergistic effect in erosion-corrosion is defined as the difference between erosion-corrosion and the sum of its two parts [88-90]. This synergistic effect has been widely observed in abrasion [91, 92], erosion [93-96] and sliding wear [97-99]. It can be expressed as Equation 3.2 [17, 100-102]:

$$T = E + C + S \qquad \text{Equation 3.2}$$

Where;

T is Total weight loss in erosion-corrosion process

E is Weight loss due to pure erosion in erosion-corrosion process

C is Weight loss due to pure corrosion in erosion-corrosion process

S is Weight loss due to synergistic effect in erosion-corrosion process

They are all gravimetric terms relating to the erosion-corrosion processes. But the understanding is not consistent in the use and meaning of the synergistic effect in aqueous erosion-corrosion. Some describe it as the sum of the enhancement of erosion due to corrosion and *vice versa* (dE_C and dC_E) [10]. But some describe the term to refer to an erosion enhancement due to corrosion (S or dE_C), in this case the mass loss due to corrosion in the erosion-corrosion processes consists of the pure corrosion in the absence of erosion (C') and the corrosion enhancement due to erosion (dC_E), so the equation of total weight loss (Equation 3.2) could be converted to Equation 3.3:

$$T = E + C' + dC_E + dE_C \qquad \text{Equation 3.3}$$

In order to identify the synergistic effect, a lot of tests will be studied independently under controlled conditions. Therefore, the total weight loss tests are performed to get the total weight loss (T); anodic polarisation tests are performed to get the weight loss due to corrosion (C); and cathodic protection tests are performed to get the weight loss due to erosion (E), and then the synergistic effect could be determined:

$$S = T - C - E \qquad \text{Equation 3.4}$$

The study proved that the contributions to overall erosion-corrosion material weight loss from direct corrosive attack and from indirect mechanisms (synergy) can be substantial in liquid-impingement situations under liquid and solid/liquid conditions [100]. Neville *et al.* conducted electrochemical tests under liquid-solid erosion jet impingement on cast iron and austenitic stainless steel in liquid of varying salinity and temperature. The erosion, corrosion and synergy were identified for both materials at 3.5% and 0.5% *NaCl* and for 30 °C and 50 °C. It was also found that the exposure "history" of the materials under the changing conditions, which have effects on their erosion-corrosion behaviours. The total damage, erosion rate, corrosion rate and their synergy were determined for various conditions, showing that corrosion and related effects represent a significant part of the total weight loss [103].

Neville *et al.* concluded that the erosion significantly enhances the corrosion rate of tested materials, and has an effect of shifting the passive regime into an active corrosion regime. However, in terms of the magnitude of the material loss components, the synergy is a much more prominent feature for tested materials [8].

Neville *et al.* reported that corrosion plays an important role in the erosion-corrosion process of even high grade stainless steels due to depassivation-repassivation events corresponding to solid impacts in the corrosive medium. Although the pure corrosion process constitutes only a small part of the total material loss, there is an important synergistic factor defined as the effect of corrosion on erosion which means that corrosion related processes can be significant in erosion-corrosion [104].

Wood *et al.* proposed a way of presenting the synergistic results in the form of *S/C vs. E/C* ratios to standardise the presentation of results but this approach has not

been followed by many researchers. The synergy degradation mechanisms can be divided in two categories (Table 3.2)

Erosion-enhanced corrosion	Corrosion-enhanced erosion
Local acidification in the erosion pits, accelerating corrosion rates and prohibiting film formation	The removal of work hardening by corrosion, exposing the softer metal
Increase ion transportation by high turbulence levels caused by surface roughening	Preferential corrosive attack at grain boundaries, resulting in grain loosening
Lowering of the fatigue strength of the metal	The increase in the number of stress concentrating defects from corrosion micro-pitting
*When the passive film is continually removed by the impacting particle	*Micro-structural modification of the surface *When a thick and adherent oxide film forms with different properties than the substrate material

Table 3.2: Mechanisms of erosion corrosion synergy [105]

3.3.2 Erosion-corrosion regimes and mechanisms

In the past several decades the importance of erosion-corrosion problems has continued to grow in several industrial areas. A recent survey reported that erosion-corrosion was rated in the top five most prevalent forms of corrosion damage in the oil and gas industry [106]. The significance of the understanding of the erosion-corrosion regimes under specific environments not only contributes to the erosion-corrosion protection methods, but also to the future material selections.

Even though there are a lot of complexities in predicting erosion-corrosion behaviours of different materials under specific application environments, still extensive efforts have been made to describe the regimes of erosion-corrosion, which is quite useful to tell the material is corrosion dominant, erosion-dominant or erosion-corrosion dominant under specific conditions. All this information combining with the materials properties will do a great favour for future material selections.

So far several erosion-corrosion regime models have been built up based on an amount of experiments, but there is still not a systematic analysis for the erosion-corrosion regimes. Stack *et al.* presented the wet erosion-corrosion at ambient temperature [107], and oxidising gaseous environments at elevated temperatures [108]. The regimes correspond to conditions where erosion of the base material, or erosion of the corrosion product layer, is the predominant wastage mechanism. That erosion-corrosion regime includes four parts (Figure 3.4):

(I) Erosion-dominated behaviour which occurs at low temperature, so erosion of metal is the dominant process and wastage.

(II) Erosion-corrosion-dominated behaviour (above the transition temperature T_a), as the temperature increases, the rate of oxidation increases. The wastage is mainly consisted of the loss of oxide scale and the loss of the metal.

(III) Corrosion-dominated behaviour I (above the transition temperature T_b). As the temperature increases up to a critical value, the scale which forms between successive erosion events becomes sufficiently thick and cohesive not to be removed to the scale-metal interface. Above the critical temperature, the total mass loss decreases as the temperature increases.

(IV) Corrosion-dominated behaviour II. This behaviour occurs when the overall weight loss tend to zero at higher temperatures. Such a pattern has been observed for erosion-corrosion in "dry" oxidising environments and for erosion-corrosion of steam turbines in pressurised aqueous environments.

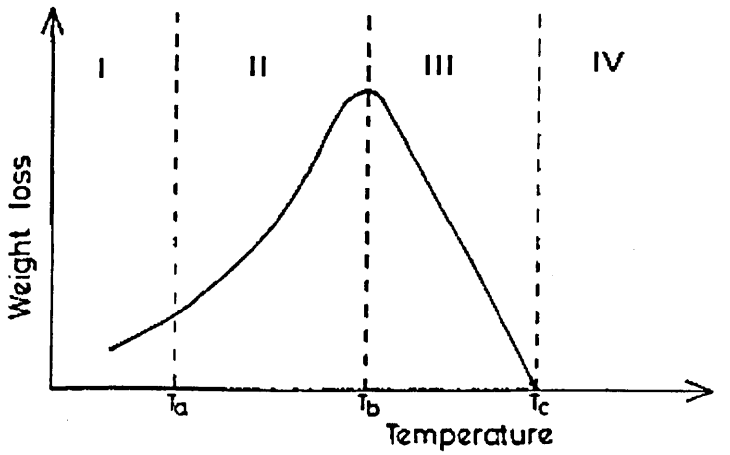

Figure 3.4: Schematic diagram for the erosion corrosion regime: (I) Erosion dominated behaviour; (II) Erosion-corrosion dominated behaviour; (III) Corrosion dominated I behaviour; (IV) Corrosion dominated II behaviour [107]

Regimes in aqueous erosion-corrosion environments have been identified using a rotating cylinder electrode. It has been shown that an increase in velocity (0 to 8 ms^{-1}) increases the passive current density [108]. Experiments were carried out for one hour using mild steel (BS6323) in 0.5 M $NaHCO_3$ + 0.5 M Na_2CO_3, containing 300 gl^{-1} of alumina (100 μm). The presence of solid particles indicated a transition from purely passive behaviour to a situation where erosion enhances the average passive current. An increase in the erosion parameter and the corrosion parameter changed the degradation behaviour of the material (Figure 3.5). In fact there is still limitation of this kind of erosion-corrosion regime model, because it limits the specific materials over the range of specific test conditions, but this idea could be spread as a necessary input to build up the predictive model for future material selection.

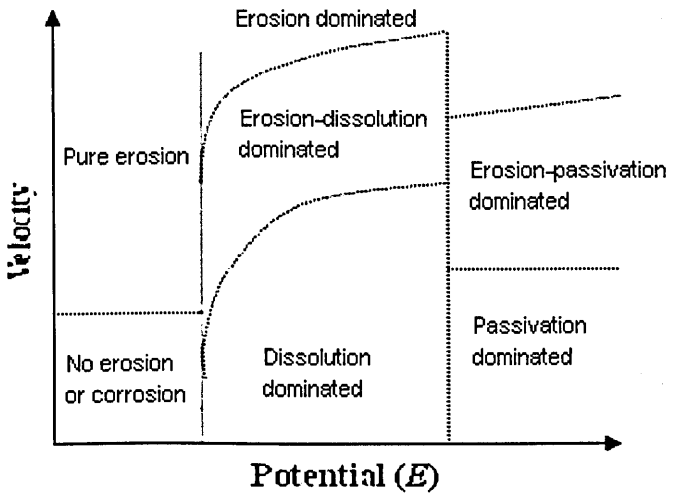

Figure 3.5: Schematic diagram of an aqueous erosion corrosion map [108]

From the macroscopical view, erosion-corrosion is the general term encompassing a spectrum of mechanisms from accelerated corrosion to purely mechanical damages:

- Dissolution dominant
- Flow thins protective film to equilibrium thickness which is a function of both mass transfer rate and growth kinetics. Erosion-corrosion rate is controlled by the dissolution of the protective films.
- Film is locally removed by dissolution, fluid induced stress or particle/bubble impact, but it can repassivate. Erosion-corrosion rate is a function of the frequency of film removal, bare metal dissolution rate and subsequent repassivation rate.
- Film is removed and does not reform. Erosion-corrosion is the rate the bare metal can dissolve.
- Film is removed and underlying metal surface is mechanically damaged which contributes to overall metal loss, i.e., erosion-corrosion rate is equal to bare metal dissolution rate plus possibly synergistic effect of mechanical damage.
- Film is removed and mechanical damage to underlying metal is the dominant damage mechanism
- Mechanical damage dominant

But from the microscopical view, there are still some detailed erosion-corrosion mechanisms, which depend on specific materials and applied specific environments.

3.3.3 Erosion-corrosion models

Building models of physicochemical processes has many purposes. They are of help to an engineer in industry as much as to a researcher in a laboratory. Models (should) reflect a way of thinking, a way of making sense of all the accumulated information, a way of seeing how it all fits together (or does not), and last but not least are a tool to predict what may happen in the future. Models are tools that can assist engineers in making decisions related to design, operations and control [109].

The significance of the laboratory simulation experiments not only contributes to the detailed analysis for the specific cases, but it intangibly has built up a huge database to develop the prediction models. If any physical or chemical phenomenon and processes can be explained, the rest of the modelling process is usually a mathematical exercise or numerical mapping.

Therefore, Bryan reviewed some approaches used to predict erosion-corrosion, and he concluded that whichever approach is used, the relationship between mass transfer coefficient and erosion-corrosion rate is not always the expected linear (Figure 3.6). This prediction model is critically dependent on materials, environmental and hydrodynamic factors, especially combined with the possible effects of surface roughness.

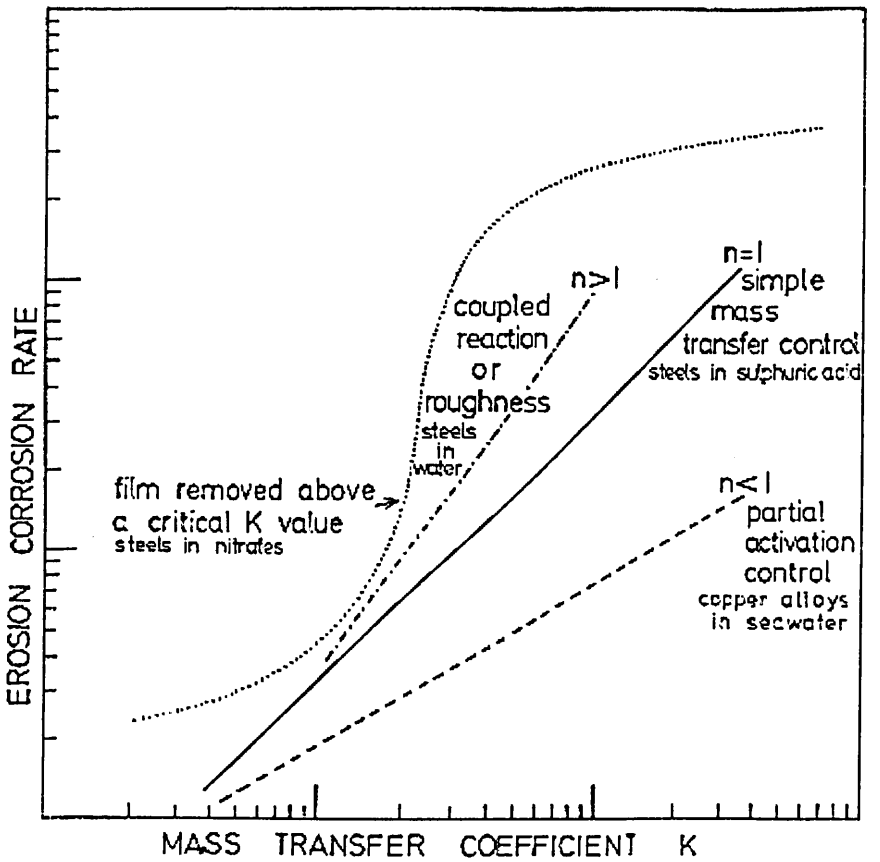

Figure 3.6: Possible relationships between erosion-corrosion and mass transfer [110]

Srdian [109] reviewed many different mathematical models for CO_2 corrosion used by engineers in the oil and gas industry. The CO_2 corrosion models have been classified into three broad categories based on how firmly they are grounded in theory.

- Mechanistic models: these models describe the mechanisms of the underlying reactions and have a strong theoretical background.
  1. Mechanistic model
  2. Electrochemical model
  3. Transport based electrochemical model
- Semi-empirical models
- Empirical models

Apart from corrosion, some erosion models have been developed. For example, Finnie studied the erosion of ductile metals, based on which the prediction model of the volume of material removed has been developed according to the particle trajectory (Equation 3.5) [111].

$$W = \frac{\rho}{p\psi}\frac{MV^2}{K}\left[\sin 2\alpha - \frac{6}{K}\sin^2\alpha\right]\left(\tan\alpha \le K/6\right)$$
$$W = \frac{\rho}{p\psi}\frac{MV^2}{K}\left[\frac{K\cos^2\alpha}{6}\right]\left(\tan\alpha \ge K/6\right) \qquad \text{Equation 3.5}$$

Where;

W is the weight of material removed by a number of grains

α is the angle between the particle velocity vector and the surface

K is the ratio of vertical to horizontal force components on particle

p is horizontal component of the stress on the particle face

V is the particle velocity

ρ is the particle density

M is the total mass of a number of particles

ψ is the ratio of the length of contact between particle and surface to the vertical coordinate of particle tip

After modifying the original analysis by reassessing the fraction of particles cutting in an idealised manner, the above model has been updated in the following expressions (Equation 3.6)

$$W \approx \frac{MV^2}{8p}\left[\sin 2\alpha - 3\sin^2\alpha\right]\left(\alpha \le 18.5^\circ\right)$$
$$W \approx \frac{MV^2}{24p}\cos^2\alpha\left(\alpha \le 18.5^\circ\right) \qquad \text{Equation 3.6}$$

At the same time, the other efforts have been made to develop the erosion prediction model. There is something in common. That is, the total mass loss in erosion process is proportional to the solid particle mass involved in the erosion process and the impact velocity of the flow (Equation 3.7). Hu [11] reviewed the

erosion prediction models and summarised that the exponents of velocity vary from 2 to 3 [112-114].

$$W \propto MV^n \qquad \text{Equation 3.7}$$

Many investigators [115-118] have proposed empirical correlations for estimation of slurry erosion wear based on a large number of experimental data developed through laboratory test rigs (Equation 3.8). All these developed models show the dependence of erosion and erosion-corrosion rates on the velocity and solid particles.

$$E_w = KV^{\beta} d^{\gamma} C^{\varphi} f(\alpha) \qquad \text{Equation 3.8}$$

Where;

E_w is erosion rate (g)

V is velocity (ms^{-1})

d is the particle size (mm)

C is solid concentration (gml^{-1})

K is constant

β is constant

γ is constant

φ is constant

3.4 Environmental factors related with erosion-corrosion

As mentioned in many works, the environmental conditions differ significantly and this can have a strong effect upon the erosion-corrosion behaviours of the materials, such as velocity, sand loading, temperature, pH value, the contents of the aggressive ions in the solution *etc.* Clark [119] summarised a number of factors affecting the slurry erosion (Figure 3.7). Incorporating the effect of corrosion in slurry erosion-corrosion further complicates degradation process [8].

Liquid	*Particles*
Viscosity	Size, size range
Density	Density
Surface activity–lubricity	Shape–angularity
	Hardness–friability
Target	*Flow-field*
Ductility–brittleness	Target–particle velocity
Melting point	Angle of impact
Metallographic structure	Boundary layer properties
Work hardening	Particle–particle interactions
Toughness–resilience	Particle rebound
Residual stress levels	Reynolds number
	Size and shape of target

Figure 3.7: Factors affecting slurry erosion rates [119]

Likewise, the inherent properties of the materials also have a great effect on the erosion-corrosion resistance. As we all know, the erosion-corrosion is a mechanical and electrochemical combined process. Many works have proved that the various mechanical properties of the materials have more or less effects on the erosion-corrosion resistance under the specific working conditions, and also this point depends on what kind of mechanical change occurs during the erosion-corrosion processes. In this project the main factors considered are sand loading, velocity, temperature and their interactions on the erosion-corrosion behaviour of the marine alloys. Apart from that, whether there is a correlation between the components of the total weight loss and the material hardness or other mechanical property is also of concern.

3.4.1 Environmental factors relating with erosion-corrosion

The purpose of the studies of erosion-corrosion is to help engineers to choose the right material for a specific application. Hence it is always necessary to correlate the material selection with the environmental parameters. That is, the erosion-corrosion rate is strongly dependent upon the change of severity of erosion-corrosion conditions [120]. The prevalent concerns about the environmental effects

on erosion-corrosion behaviour concentrate on hydrodynamic, thermodynamic and the contents of the aggressive solutions.

3.4.1.1 Temperature effect on erosion-corrosion

Generally speaking, when temperature increases, although the passive film is probably thickened [121], the higher corrosion current is due to the higher thermodynamic driving force making corrosion occur at a higher rate during the depassivation period, so more mass loss due to high corrosion current will occur at higher temperature [122]. The temperature is becoming an important factor to be considered in wear and corrosion applications, not only because of its effect on the growth of the protective film on the surface, but also its effect on the transitions of ductile-brittle behaviour of the material in aqueous erosion-corrosion environments. Since ductile-to-brittle transitions in mechanical behaviour can affect the mechanisms of mass removal from the surface. At low temperatures, the wear mechanisms are associated to formation of micro-cracks at the surface, which grow leading to material loss in the form of flakes. When temperature is increased, ductile mechanisms like cutting and plastic deformation are favoured and the corrosion processes at the surface are intensified [123]. Moreover, the temperature plays an important role on the growth of the protective film with duplex structure on the surface of stainless steels [121]. An increase of temperature magnifies the thickness of the protective film on stainless steels. Mesa [124] *et al.* found increasing the testing temperature led to a reduction in both slurry wear and electrochemical corrosion resistance of all the studied materials. The effect of temperature on erosion-corrosion in impingement jet saline environments has been valued for a range of materials [9, 34, 85, 95, 100]. The results showed that temperature increment accelerates the corrosive and erosive-corrosive damages of the materials as expected.

For copper nickel alloys, the temperature increment has been shown to cause little change [125], a decrease [126] or an increase [57] on corrosion rate. The apparent disagreement in the effect of temperature on corrosion is partly due to the variations in the oxygen content in the solution. In addition the character of the

surface film may change as the temperature increases, which will affect the corrosion resistance contributed by the surface films. The kinetics of repassivation is a function not only of temperature, but also of alloy composition, velocity, and chloride content of the solution [57]. It also has been proved that as the temperature increases [72]:

1. the corrosion rate of the copper nickel alloy increases
2. selective copper dissolution takes place
3. the nickel amount in the corrosion rate of the alloy increases owing to the formation of a copper-nickel oxide

3.4.1.2 Velocity effect on erosion-corrosion

A considerable body of empirical information has been developed on the effect of seawater velocity on corrosion rates of various metals [127-129]. Various hydrodynamic parameters have been suggested as controlling the occurrence and extent of flow-assisted corrosion, one of which is velocity. For both practical and mechanistic reasons there is a need to identify the hydrodynamic parameter which controls the occurrence and rate of erosion-corrosion. In general, velocity has two effects on corrosion, which are the mass loss transfer effect and mechanical effect; moreover these effects during erosion-corrosion processes will become greater in the presence of the solid particles in the erosive-corrosive environments.

It is reviewed by Webber in 1992 [130] who defined the effects of flow velocity in three categories:

1) At low flow velocities and in the absence of induced convection, natural convection is responsible for mass transfer and can affect corrosion rate.

2) When induced convection leads to increased mass transfer at moderate flow velocities, the corrosion rate can increase but in this regime there are no mechanical effects.

3) At high velocities mechanical flow effects can result and in this case the

damage mechanisms become increasingly complex.

In terms of mechanical effect, low impact velocities will bring a more regular surface with a lower amount of peaks in the roughness profile and smaller peak amplitudes [131].

The erosion-corrosion behaviour of the metals is sensitive to the velocity. One material classification method has been developed according to the various responses from different materials over a range of test velocities [132]. Fifty three alloys are exposed including stainless steels, titanium, nickel, copper *etc* to seawater flowing at velocities over the range from 0 to 36.6 ms^{-1}. All the tested alloys were classified into three groups, which supplies a foremost way to select the right material at the specific velocity.

1. First group ~ Alloys could form very tenacious and protective surface oxide films, and have excellent corrosion resistance at all velocities. Titanium alloys and *Ni-Cr-Mo* alloy belonged to this group.

2. Second group ~ Alloys form very tenacious and protective surface films and exhibit excellent corrosion resistance at high and intermediate velocities. However, at low velocities, where the settling of sand and other deposits are possible, pitting or crevice corrosion is often a problem. Most stainless steels and nickel based alloys were in this group.

3. Third group ~ Alloys exhibit excellent corrosion resistance at low velocities but are subject to degradation by erosion-corrosion in the high and intermediate ranges, where the protective films are stripped from the metal surface. Copper-base alloys were defined in this group.

It is plain to understand that higher impingement velocities bring more kinetic energy of the fluid with solid particles, which definitely result in more severe degradations of the materials. From a hydrodynamic point of view, on increasing the velocity, more particles impact onto the specimen surface close to the stagnation

point rather than slip away in the flowing fluid. The increase in velocity can also result in the enhancement of corrosion rate in erosion-corrosion conditions. It is found that the increase in velocity caused the anodic polarisation for austenitic stainless steel to shift to higher current value. With the increase in velocity of slurry, particles abraded the metal at an increase rate, thus removing the protective oxide film at a faster rate [90]. Zheng *et al.* concluded that the increase in total weight loss of materials in erosion-corrosion conditions at a higher impinging velocity is due to not only the enhancement of mechanical and electrochemical effects, but also the synergistic effect [133]. Various studies correlated the velocity with the criteria to corrosion, erosion and erosion-corrosion resistance. All proved that velocity has negative effects on the erosion-corrosion behaviours of the materials.

Wharton *et al.* [128] reviewed the effect of fluid velocity on the corrosion of stainless steels. That is, fluid velocity is one of the most important parameters to be considered when determining suitability for use in chloride environments, in which pitting corrosion at low velocities is a problem. Austenitic stainless steels, such as AISI 304 and 316, undergo less pitting at increased velocities and an approximately velocity of greater than 1.5 ms^{-1} is recommended to avoid pitting – the so called critical velocity [51, 57, 127, 129, 134]. For copper-base alloys, corrosion rates remain low due to the resilience of the protective films with increasing seawater flow rate [55]. Comparing with stainless steels, copper-base alloys are more sensitive to the velocity. If the velocity of the medium is increased beyond a critical point, however, the protective film will be damaged by erosion-corrosion impingement attack and the active underlying metal will be exposed. For pipe diameter >100 *mm*, seawater flow velocities are limited to 3.0 ms^{-1} for aluminium brass, 3.5 ms^{-1} for 90-10 copper nickel and 4.0 ms^{-1} for 70-30 copper nickel [68].

3.4.1.3 Sand loading effect on erosion-corrosion

Sand loading acts as an important role in erosion-corrosion processes. When the solid particles impact on the surface of the materials, the protective films formed on the surface of the material will be partly damaged or fully removed under the impingement jet. At low sand loading concentration, the total weight loss will be

affected very little. As the sand loading increases, the protective film on the surface of the material will be gradually stripped off, and then more and more naked metal will be exposed to the severe erosion-corrosion environment, which will lead to severe erosion-corrosion. Moreover, in saline solutions containing liquid-solid, high solid loading enables more solid particles to impact on the specimen surface, and the removal of the passive film and naked metal occur in a higher metal dissolution rate. At the same time the continuous impacts prevent repassivation from occurring. Hu [122] *et al.* studied the correlations between sand loading and the current density and total weight loss under impingement jet, which proved approximately exponential curve (Figure 3.8). The effects of sand loading on corrosion current density could be extrapolated in the same manner (Figure 3.9). This analysis also supplies a way to compare corrosion, erosion and erosion-corrosion resistance of the different materials under the different sand loading.

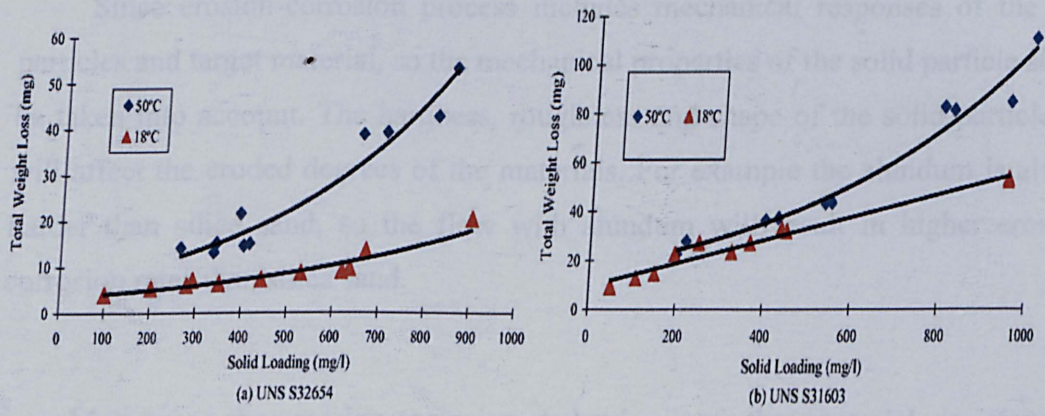

Figure 3.8: The correlations between sand loading and total weight loss of two stainless steels (weight loss tests on materials in erosion-corrosion after 8 *h*, 17 ms^{-1}, at 18 and 50 °C in 3.5% *NaCl*) [122]

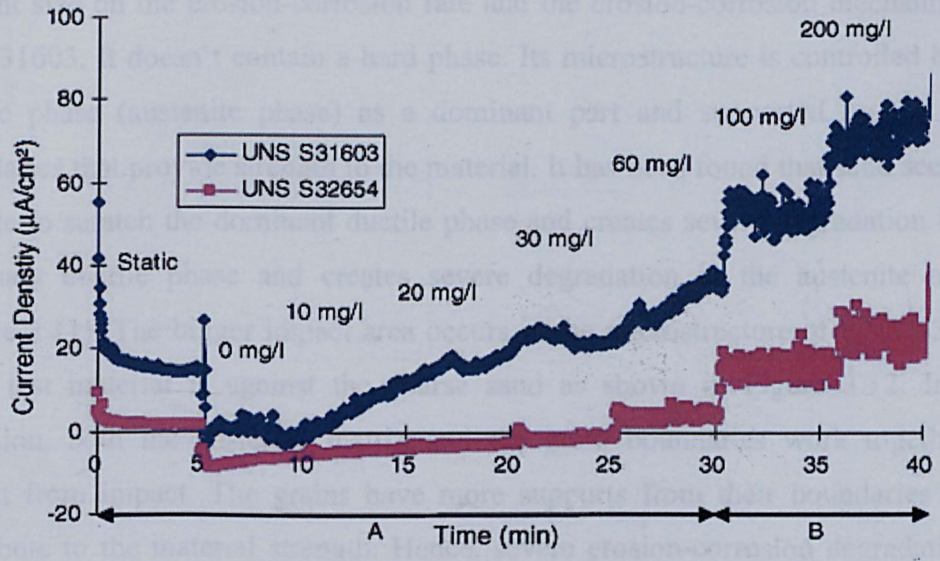

Figure 3.9: Correlations between corrosion current density and sand loading of two different stainless steels (test at 50°C, 17 ms^{-1} in 3.5% *NaCl* solution) [122]

Since erosion-corrosion process includes mechanical responses of the solid particles and target material, so the mechanical properties of the solid particle should be taken into account. The hardness, roughness and shape of the solid particle *etc.* will affect the eroded degrees of the materials. For example the alundum is always harder than silica sand, so the flow with alundum will result in higher erosion-corrosion rates than silica sand.

Moreover, the erosion-corrosion behaviour of the material is strongly dependent on the erodent size [120]. Anand [135] *et al.* stated that if the damage zone by one single impact was appreciably larger than the microstructure size, the erosion behaviour is more likely to be similar to that of ductile materials with a maximum erosion rate occurring at oblique impact angles and these angles tend to increase with the volume fraction of brittle phase. If the damage zone was smaller than the microstructure size, then the erosion behaviour would tend to be similar to that of the brittle materials with a maximum impact angle closer to 90°.

It was found that there is an inherent effect of particle size in erosion since both for steels and Pyrex glass the specific energy to produce volume loss increases with decreasing particle size [136]. Neville [120] *et al.* well studied the effects of

erodent size on the erosion-corrosion rate and the erosion-corrosion mechanism of UNS 31603. It doesn't contain a hard phase. Its microstructure is controlled by the ductile phase (austenite phase) as a dominant part and supported by the grain boundaries that provide strength to the material. It has been found that sand seems to be able to scratch the dominant ductile phase and creates severe degradation in the dominant ductile phase and creates severe degradation in the austenite matrix (Figure 3.11). The bigger impact area occurs in the microstructure of UNS S31603 when test material is against the coarse sand as shown in Figure 3.12. In this condition, both the austenite matrix and the grain boundaries work together to protect from impact. The grains have more supports from their boundaries more contribute to the material strength. Hence, severe erosion-corrosion degradation is avoided.

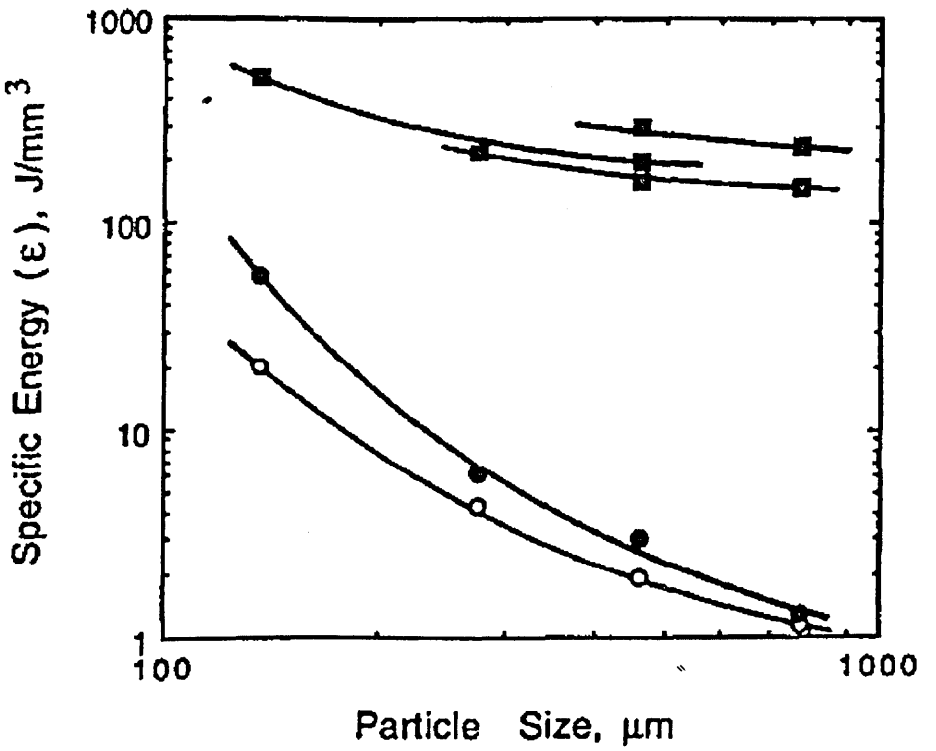

Figure 3.10: Variation of specific energy for deformation wear as a function of *SiC* particle size [136].

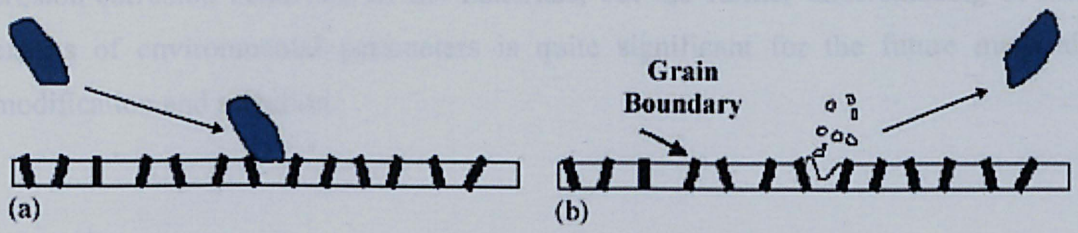

Figure 3.11: (a) The coarse sand (AFS 50/70 Ottawa silica sand) striking a UNS S31603 and (b) schematic of crushing the matrix ductile austenite phase [120].

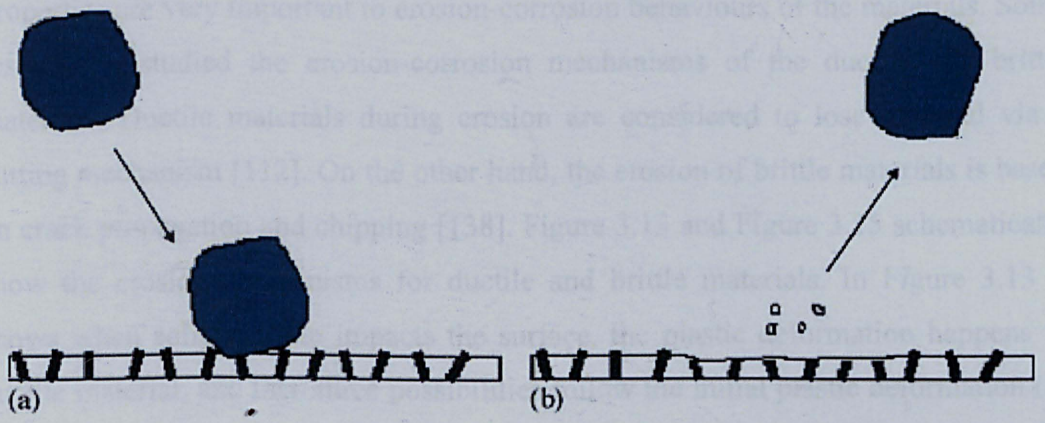

Figure 3.12: (a) The coarse sand (ASTM 20/30 Ottawa silica sand) striking a UNS S31603 and (b) schematic of material removal [120]

3.4.1.4 Interactive effect on erosion-corrosion

The corrosion resistance of metals covered with a protective passive layer can be markedly diminished by the mechanical deterioration of their surface by solid particles. Erosion-corrosion is a process influenced by many factors. Some interactions among them have not been fully described yet [137]. It has been proved when erosion and corrosion act together; the total material degradation must be greater than the sum of mass loss from the erosion and corrosion separately. This reason is due to the interactive effects between erosion and corrosion, which latterly has been defined as synergy. In the similar manner, when the environmental parameters are mixed together to simulate the real condition, besides the individual effects of environmental parameters on erosion-corrosion there are supposed to be the interactive effects between the environmental parameters. Little work concentrated on the interactive effects between the environmental parameters on

erosion-corrosion behaviour of the materials, but the further understanding of the effects of environmental parameters is quite significant for the future material modification and selection.

3.4.1.5 Mechanical properties related with erosion-corrosion

Erosion-corrosion process involves mechanical process, so the mechanical properties are very important to erosion-corrosion behaviours of the materials. Some researchers studied the erosion-corrosion mechanisms of the ductile and brittle materials. Ductile materials during erosion are considered to lose material via a cutting mechanism [112]. On the other hand, the erosion of brittle materials is based on crack propagation and chipping [138]. Figure 3.13 and Figure 3.15 schematically show the erosion mechanisms for ductile and brittle materials. In Figure 3.13 it shows when solid particle impacts the surface, the plastic deformation happens to ductile material, and then three possibilities follow the initial plastic deformation (c_1) the fracture of the solid particle due to work hardening of the material, (c_2) the further plastic deformation and (c_3) the cutting of the material. During this process, the hardness and tensile strength need to be taken into account, especially tensile strength is crucial to determine the work hardening under the solid particle impacts (Figure 3.14). In Figure 3.15 it shows when solid particle impacts the surface, the following initial crack formed due to the impact fracture, but another possibility is the initial crack formed in the grain boundary due to corrosion. Finally the part of the material is chipped off due to the loss of the adhesion to the grain or the further crack propagation of the grain. In this case, hardness, ultimate stress and toughness of the brittle material are foremost. The area (Figure 3.16) up to the yield point is termed the modulus of resilience, and the total area up to fracture is termed the modulus of toughness. The term "resilience" alludes to the concept that up to the point of yielding, the material is unaffected by the applied stress and upon unloading the material will return to its original shape. But when the strain exceeds the yield point, the material is deformed irreversibly, so that some residual strain will persist even after unloading. The modulus of resilience is then the quantity of energy the material can absorb without suffering damage. Similarly, the modulus of toughness is the energy needed to completely fracture the material. So the materials showing

good impact resistance are generally those with high modulus of toughness. The magnitudes vary from the different materials. Under erosion-corrosion impingement jet, the materials experience the impact of solid particles. The materials with higher modulus of toughness can have higher resistance to plastic deformation under impacts (Figure 3.16).

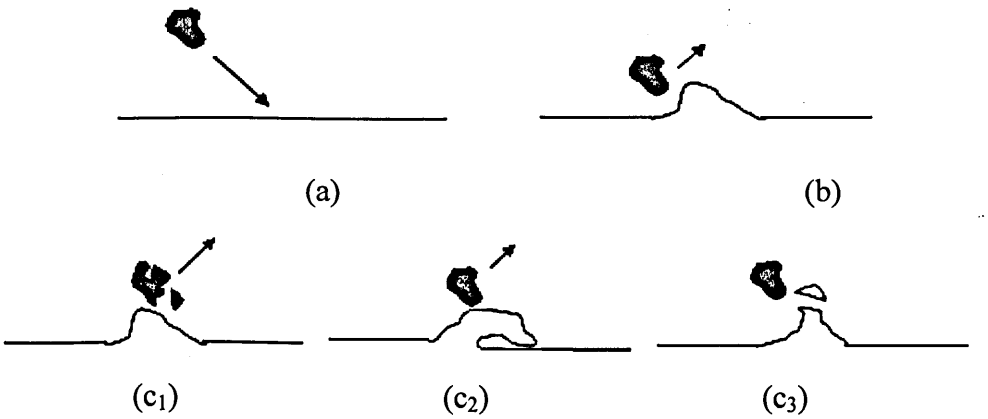

Figure 3.13: The schematic erosion mechanism of ductile material (a) the beginning of solid particle impact (b) the initial plastic deformation (c_1) the fracture of the solid particle (c_2) further plastic deformation (c_3) cutting of the material

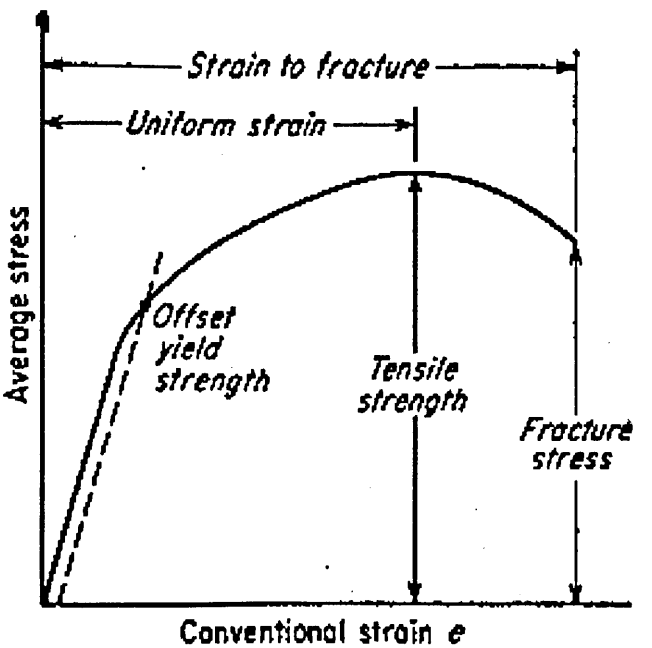

Figure 3.14: The engineering *Stress-Strain* curve [139]

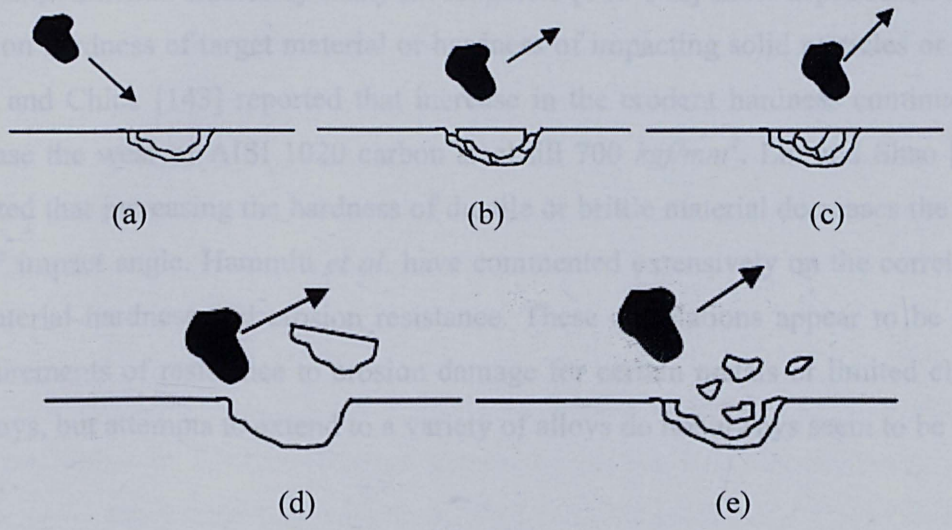

Figure 3.15: The schematic erosion mechanism of brittle material (a) the beginning of solid particle impact (b) the initial crack at grain boundary (c) the initial crack at grain (d) the chipping due to the loss of adhesion of grain boundary to grain (e) the chipping of the grain due to brittle fracture

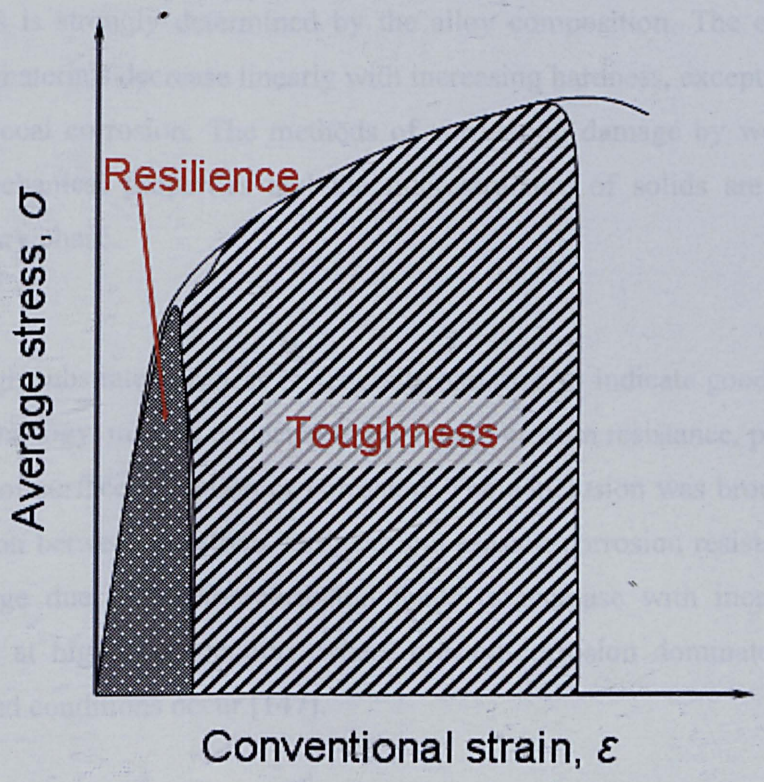

Figure 3.16: Modulus of resilience and toughness from Stress-Strain curve [139]

Experimental studies by many investigators [140-142] show dependence of the wear on hardness of target material or hardness of impacting solid particles or both. Levy and Chick [143] reported that increase in the erodent hardness continuously increase the wear of AISI 1020 carbon steel till 700 kgf/mm^2. Lin and Shao [144] reported that increasing the hardness of ductile or brittle material decreases the wear at 90° impact angle. Hammitt *et al.* have commented extensively on the correlation of material hardness and erosion resistance. These correlations appear to be good measurements of resistance to erosion damage for certain metals or limited classes of alloys, but attempts to extend to a variety of alloys do not always seem to be valid [145].

Hardness is usually a good index of abrasion resistance when the same alloy or very similar alloys are considered at different hardness levels as shown by Barker *et al.* [146] with martensitic experimental alloys. Heitz [85] correlated erosion-corrosion with the hardness of materials, and found that the behaviour of ferrous materials is strongly determined by the alloy composition. The erosion-corrosion rates of materials decrease linearly with increasing hardness, except in materials that exhibit local corrosion. The methods of correlating damage by wear or cavitation with mechanical properties and the microstructure of solids are still on a very elementary phase.

High substrate hardness is generally assumed to indicate good wear resistance and, by analogy, may be expected to give good erosion resistance, particularly in the absence of surface oxidation or corrosion. The conclusion was brought forward the correlation between substrate hardness and erosion-corrosion resistance. The extent of damage due to erosion-corrosion tends to increase with increasing substrate hardness at higher temperature where erosion-corrosion dominated or corrosion-dominated conditions occur [147].

However, bulk hardness is not a good indicator of abrasion-corrosion resistance for different types of alloys since the same hardness levels may see variations of as much as an order of magnitude in abrasion-corrosion resistance. As an example metastable austenitic stainless steels were shown to have outstanding

abrasion-corrosion resistance in comparison with dual phase stainless steel or carbon steel with similar Vickers hardness. Preece [148] reported that neither hardness nor strain energy to fracture give a satisfactory measure of erosion resistance for the whole range of engineering materials, or even for ductile materials. Moreover, it has been concluded that the hardness of the materials is not the controlling factor in the materials' resistance to erosion-corrosion [104].

For toughness, erosion wear of more brittle materials is predominantly governed either by flow or fracture depending on the impact conditions. If the impact of an erosive particle leads to brittle fracture, material is removed from the surface by nucleation and intersection of cracks. In this case, the most relevant material property which determines the erosion resistance is fracture toughness [149]. Also the erosion wear in *WC-Co-Cr* thermally sprayed coating was studied, and researchers [91] found that subsurface cracks produced by erosion were similar to those produced by indentation testing. Therefore, the fracture toughness determined by the indentation method is an appropriate parameter to assess the erosion resistance of the materials.

Finnie [138] is the first person to classify the materials into brittle and ductile types, and then developed two models to predict the erosion rate as a function of the impact angle. According to this prediction model, the angle of maximum erosion rate for ductile material occurs approximately between 20° and 30°. Conversely, the angle of maximum erosion rate for brittle material is close to nominal (Figure 3.17).

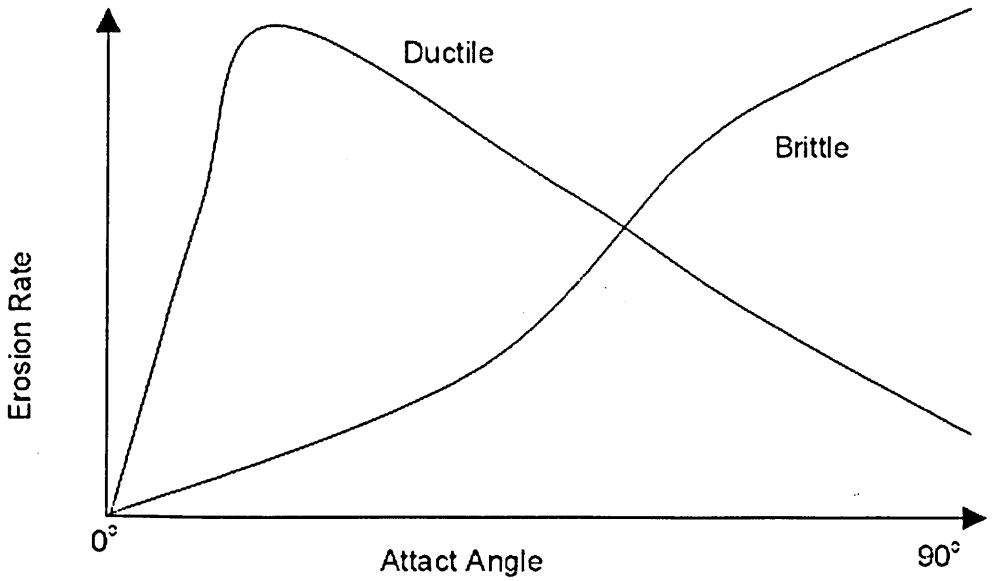

Figure 3.17: Schematic representation of erosion rate as a function of impact angle for ductile and brittle materials [138]

3.5 Experimental design

A wide variety of approaches, methods and analysis techniques, known collectively as experimental design, has been around for many decades and is well documented in books like Box, Hunter, and Hunter (1978) or Montgomery (1997). One of the principle goals of experimental design is to estimate how changes in input factors affect the results, or responses, of the experiment [150].

The last 20 years of the last millennium are characterized by complex automatization of industrial plants. Complex automatization of industrial means as witch to factories, automatons, robots and self-adaptive optimization systems. The above-mentioned processes can be intensified by introducing mathematical methods into all physical and chemical processes. By being acquainted with the mathematical model of a process it is possible to control it, maintain it at an optimal level, provide maximal yield of the product, and obtain the product at a minimal cost. Statistical methods in mathematical modelling of a process should not be opposed to traditional theoretical methods of complete theoretical studies of a phenomenon. The higher the

theoretical level of knowledge the more efficient is the application of statistical methods like design of experiment (*DOE*) [151, 152].

Experimental design methods are widely used in research as well as in an industrial setting, however, sometimes for very different purposes. The primary goal in scientific research is usually to show the statistical significance of the effect that a particular factor exerts on the dependent variable of interests. Experimental design is the well defined plan for data collection, analysis and interpretation. The process can help to answer the questions about the hypotheses and about how different factors influence a response variable [153].

Experimental design methods have also been carried out for quality control. For industrial engineering, they are used for

a) Exploration: gathering data to learn more about a process or product characteristic. More and more explorations are helpful for further improvements.
b) Estimation: use data to estimate the effects of certain variables on other variables.
c) Confirmation: gather data to verify a hypothesis about a relationship among variables.

As a basic example of such techniques, suppose that we can identify just two values, or levels, of each of input factors. There is no general prescription on how to set test levels, but we should set them to be opposite in nature but not so extreme that they are unrealistic. If we have n input factors, there are thus 2^n different combinations of the input factors, each defining a different configuration of the model; this is called a 2^n factorial design. Referring to the two levels of each factors as the "-" and "+" level, we can form what is called a design matrix describing exactly what each of the 2^n different model configurations are in terms of their input factor levels. For instance, if there are $n = 3$ factors, we would have $2^3 = 8$

configurations, and the design matrix would be as in Table 3.2, with R_i denoting the simulation response from the ith configuration.

Run (i)	Factor 1	Factor 2	Factor 3	Response
1	–	–	–	R_1
2	+	–	–	R_2
3	–	+	–	R_3
4	+	+	–	R_4
5	–	–	+	R_5
6	+	–	+	R_6
7	–	+	+	R_7
8	+	+	+	R_8

Figure 3.18: Design matrix for a 2^3 factorial experiment

If the number of factors is even moderately large, the number of possible factor-level combinations simply explodes far beyond anything remotely practical. It is unlikely, though, that all input factors are really important in terms of having a major impact on the outputs. As the very least, there will be big differences among your factors in terms of their impact on your responses.

Since it is the number of factors that causes the explosion in the number of combinations, it would be most helpful to identify early in the course of experimentation which factors are important and which are not. The unimportant factors can then be fixed at some reasonable value and dropped from consideration, and further investigation can be done on the important factors, which will be fewer in number.

Selecting the appropriate forecasting model and then establishing suitable modelling setting is a challenging task even for the most experienced decision-makers. Among the numerous experimental design methods, the Taguchi experimental design methods made much successful statistical analysis for many applications. For example, the Taguchi experimental design method reduces cost, improves quality, and provides robust design solutions. Khoei *et al.* employed this

method to determine the optimal configuration of performance, quality and cost design parameters in the aluminium recycling process. It is proved that the Taguchi method is capable of establishing an optimal design configuration, even when significant interactions exist between and among the control variables. The Taguchi method can also be applied to design factorial experiments and analyzing their outcomes [154].

3.6 Summary of literature of review

Marine alloys are widely used in many industrial applications. They are optimally chosen combined their varied erosion-corrosion resistances with diverse products and maintenance costs. The literature has demonstrated clearly the environmental parameters have more or less effects on erosion-corrosion behaviours of the materials, but ambiguously showed there supposed to be the interactive effects between and among the environmental parameters. Moreover there is no systematic analysis, which quantitatively shows how the environmental parameters affect the erosion-corrosion behaviours of the materials, even their interactive effects. Naturally it has been difficult to predict quantitatively how the damage will be affected by factors and their interactions, which will extend an attempt to understand of how factors affect the extent of damage in erosion-corrosion and constitution of that damage (*i.e.* corrosion, erosion and synergy).

It has been reviewed that experimental design method has been widely used in scientific research to show the statistical significance of the effect that a particular factor exerts on the dependent variable of interest, and also experimental design method provides a well-defined framework for data collection, analysis and interpretation. In virtual of this experimental design method, it exploits an attempt to integrate the erosion-corrosion behaviour analysis with statistical analysis of environmental parameters and future material prediction model together.

Chapter 4 Materials and experimental procedures

4.1 Material under study

As described in the literature review, cast iron, stainless steels and copper-base alloys have been applied in marine services for a long time. Eight materials are involved in this study:

1.	Ni-resist cast iron	*BS 3468 S2W*
2.	Austenitic stainless steel	*UNS S31603*
3.	Super duplex stainless steel	*UNS S32760*
4.	Super austenitic stainless steel	*Vistar*
5.	High strength copper nickel	*Marinel 220*
6.	High strength copper nickel	*Marinel 230*
7.	Nickel aluminium bronze	*747*
8.	Copper nickel chromium	*824*

The eight materials used in this study are all manufactured from a casting process which provides the alloys with uniform physical and mechanical properties throughout compared with other formation methods. The measured compositions and microhardness values of the eight materials for testing are shown in Table 4.1 and Table 4.2.

	BS 3468 S2W	UNS S31603	UNS S32760	Vistar
C	2.64%	0.048%	0.026%	0.025%
Cr	1.79%	18.5%	24.93%	24.5%
B		0.005%		
Si	2.17%	0.96%	0.87%	0.3%
Mn	1.16%	1.18%	0.84%	8.5%
P	0.015%	0.03%	0.024%	0.02%
S	‹0.01%	0.014%	0.003%	0.005%
Ni	19.2%	17.5%	8.4%	10.3%
N			0.21%	0.72%
Nb	0.17%			
Mo		2.2%	3.65%	4.5%
Cu	0.02%		0.85%	
Mg	0.03%			
Fe	Bal.	Bal.	Bal.	Bal.
Micro-hardness	231.4 HB	182.7 HB	295.6 HB	281.6 HB

Table 4.1: Measured compositions and microhardness values of cast iron and stainless steels in this project

	Marinel 220	Marinel 230	824	747
C	0.006%	0.02%	0.001%	
Cr	0.43%	1.1%	1.76%	0.008%
Co			0.001%	
Si	0.053%	0.003%	0.37%	0.001%
Mn	5%	3.07%	0.72%	0.82%
P	0.007%	0.001%	0.005%	
S	0.004%	0.006%	0.005%	
Ni	20.93%	24.78%	31.24%	4.57%
Nb	0.58%	2.2%		
Al	1.97%	2.62%		9.32%
Zn	0.009%	0.01%		0.03%
Mg	0.03%	‹0.02%		0.001%
Sn	0.007%	‹0.01%		0.001%
Pb	0.01%	0.019%	0.003%	0.01%
Zr			0.12%	
Ti			0.09%	
Fe	0.78%	0.64%	0.63%	4.26%
Cu	Bal.70.18%	Bal. 65.5%	Bal.	Bal.
Micro-hardness	308.3 HB	325.6 HB	177.7 HB	192.7 HB

Table 4.2: Measured compositions and microhardness values of copper based alloys in this project

In general the corrosion and oxidation resistance of stainless steels improves as the chromium content increases. The addition of nickel to create the austenitic

stainless steel grades strengthens the oxide film and raises their performance in more aggressive conditions. The addition of molybdenum to either the ferritic or austenitic stainless steels improves their pitting corrosion resistance. In practice the austenitic stainless steels are resistant to a wide range of industrial atmospheres encountered. Their resistance to attack by acids, alkalis and other chemicals has led to a wide use in the chemical and industrial plant. In respect to duplex stainless steels, they are designed to have improved localised corrosion resistance, especially to stress corrosion cracking, crevice and pitting corrosion.

"Super" grades have enhanced pitting and crevice corrosion resistance compared with the ordinary types. This is due to the further additions of chromium, molybdenum and nitrogen as alloying elements. The main reason of nitrogen alloying is to increase the mechanical strength of the steels and to replace some of the expensive alloying elements such as nickel. In addition, increased nitrogen content can also increase the resistance to localised corrosion and retard the precipitation of carbide and inter-metallic phases. For super austenitic stainless steel, chromium and molybdenum have a positive effect on pitting resistance properties of stainless steels. Pitting resistance of Vistar is further enhanced by balanced additions of nitrogen and boron, and interstitial element locates in the face centred cubic lattice, which becomes part of a dense, closely packed system. Hence, it is inherently strong and resistant to both alkaline and acidic attack.

For various types of copper-nickel alloys, nickel has a significant effect on the physical and mechanical properties of copper nickel alloys [62]. As the nickel content increases, the tensile strength, proof strength, hot strength and corrosion resistance increase (Figure 4.1). Copper-nickel alloys contain small but important elements. In principle iron and manganese have been chosen to provide the best combination of resistance to flowing seawater and overall corrosion resistance [55]. Furthermore manganese is also known to increase strength and softening temperature (Figure 4.2). Iron increases the corrosion resistance of copper-nickel alloys, and also promotes the formation of an adherent, uniform protective coating in water, resulting in improved corrosion resistance, primarily in fast flowing seawater. The solubility of iron depends on the nickel content of the alloys. There is an

increase in the iron solubility with increasing nickel content until 30% after which the solubility of iron decreases as nickel content continues to increase. Tin, as an addition element, improves the tensile strength, tarnish resistance and wear resistance of copper-nickel alloys. Silicon improves the castability of casting alloys and also acts as deoxidant. Niobium increases tensile strength and proof strength but drop the elongation. The most important role of niobium is to improve the weldability of cast alloys. Chromium increases strength and shows a favourable effect on resistance to erosion-corrosion in fast flowing seawater and to erosion by solids. Aluminium increases strength, seawater corrosion and scaling resistance. Beryllium has the strongest effect on mechanical properties after age – hardening [55]. Since phosphorus, carbon, sulphur and bismuth have negative effect on mechanical and anti-corrosion properties of cupper-nickel alloys, the quantities of these elements should be present as low as possible in practical applications [62].

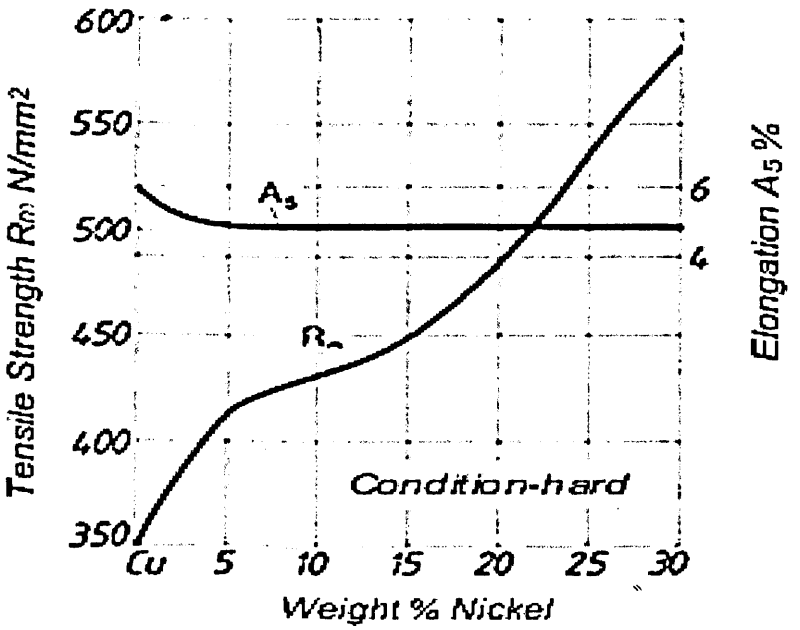

Figure 4.1: Tensile strength and elongation of *Cu-Ni* alloys as a function of nickel content [62]

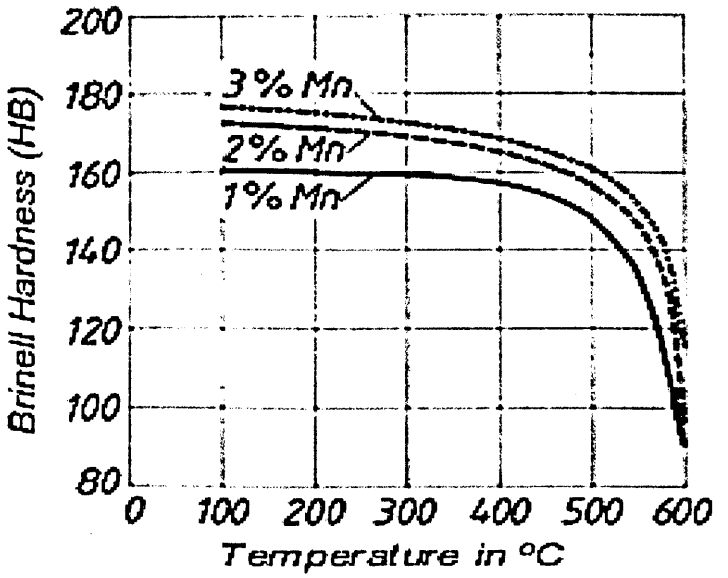

Figure 4.2: Softening characteristics of a *Cu-Ni* alloy containing 20% Ni with different manganese additions [55]

Nickel aluminium bronzes are generally two-phase, duplex alloys containing 5% to 11% aluminium as well as additions of iron and nickel for improved strength. Increase of the aluminium content results in higher strength due to the formation of the hard body-centred-cubic phase. The alloying elements also improve properties and alter microstructure. It has also been reported that nickel improves corrosion resistance and yield strength, while iron acts as a grain refiner and increases tensile strength. Both nickel and manganese can also act as a microstructure stabilizer [155].

4.2 Sample preparation

Samples for conducting experiments in this study are disks with 25 *mm* diameter and 5 *mm* thickness for super austenitic stainless steel, all copper based alloys and BS 3468 S2W. Square samples with area of 2.89 cm^2 and 5 *mm* thickness were made for austenitic and super duplex stainless steels from as-received casted bars. In this study, the effect of difference in sample sizes on corrosion and erosion-corrosion results is considered to be negligible as relative areas are used to calculate corrosion rate of materials. Some preliminary erosion-corrosion tests using different sizes of stainless steel UNS S31603 have also confirmed the least effect of surface

area on the results (<0.01 mg in total material loss after four hours tests). The specimens used in static electrochemical tests were ground to 1200 grit with *SiC* paper and polished up to 3 μm with diamond suspension to a surface finish of *Ra* less than 1 μm. The specimens used for erosion-corrosion testing were polished up to 1200 grit. The specimens were washed with distilled water and degreased with acetone after polishing. To enhance a protective film to form on the surface of the copper based alloys, all the specimens were immersed in 3.5% *NaCl* solution for twenty four hours. The surfaces were then washed with distilled water, then degreased with acetone, and dried with cold compressed air. A glass container with desiccant was used for storage of the samples. A precision balance with a range of 200 *g* and accuracy of ± 0.01 *mg* was used for gravimetric analysis. After erosion-corrosion tests the same cleaning procedure was applied to the specimens, in addition to which, the copper based alloys followed the cleaning procedure prescribed in the ASTM standard [156]. The copper based alloys were immersed in 10% sulphuric acid for 1 ~ 3 minutes to remove corrosion products without significant removal of base metal. This allows an accurate determination of the mass loss of the metal or alloy that occurred during the exposure to the corrosive environments.

4.3 Experimental design method

To build a predictive capability for future material selection for erosion-corrosion applications, a large amount of data is required from tests developed in this study. A systematic approach using two-level factorial experimental design method was chosen to focus on the eight materials and three environmental parameters for primary study: velocity, sand loading and temperature which were considerably relevant to marine industry.

Alloys to be tested

1.BS 3468 S2W

2.UNS S31603

3.UNS S32760

4.Vistar

5.Marinel 220

6.Marinel 230

7.747

8.824

Three parameters and their levels concerned in this project

1.***T*** (*temperature*): 18 °C and 50 °C

2.***S*** (*sand loading*): 50 mgl^{-1} and 500 mgl^{-1}

3.***V*** (*velocity*): 7 ms^{-1} and 20 ms^{-1}

Each parameter was set at two levels as described in the above section, and there are 2×2×2=8 trials for each material. For each test the duration is kept at four hours, and the angle of impingement is 90°. By choosing three factors at two levels, the programme is manageable and the variable tendency of the total weight loss and its components (*E, C, and S*) can be determined from the eight matrix experiments. The change in weight loss between high and low levels represents the level of the parameters effects on the material erosion-corrosion performance over the range of test conditions. These tests will produce an initial database to build a model for predicting material degradation rate in erosion-corrosion environments. In this study for each material, three duplicate tests are conducted to make an assessment of variability. A specific example will be given to explain this experimental design method as follows in Table 4.3:

Trail	Variables			Outputs			
	T	S	V	Total weight loss	Corrosion	Erosion	Synergy
1	1	1	1	T_1	C_1	E_1	S_1
2	1	1	2	T_2	C_2	E_2	S_2
3	1	2	1	T_3	C_3	E_3	S_3
4	1	2	2	T_4	C_4	E_4	S_4
5	2	1	1	T_5	C_5	E_5	S_5
6	2	1	2	T_6	C_6	E_6	S_6
7	2	2	1	T_7	C_7	E_7	S_7
8	2	2	2	T_8	C_8	E_8	S_8

Table 4.3: Design matrix for a three-parameter, eight-run experiments for one material

Example:

T (temperature): high level 50 °C (which is represented as 2); low level 18 °C (which is represented as 1)

S (sand loading): high level 500 mgl^{-1} (which is represented as 2); low level 50 mgl^{-1} (which is represented as 1)

V (velocity): high level 20 ms^{-1} (which is represented as 2); low level 7 ms^{-1} (which is represented as 1)

The results matrix can then be used as an instruction to determine:

a. How total weight loss, corrosion rate, erosion rate and synergy under erosion-corrosion conditions are affected by temperature, sand loading, velocity and their interactions.

b. How the data collected from experimental design method can be used to identify the key factors and interactions, and also to quantify their effects as an input into modelling erosion-corrosion.

c. How a reliable basis on which to build the next experimental programme steps can be given according to the data analysis.

4.4 Experimental procedure

4.4.1 Anodic polarisation

The primary focus of this study is the erosion-corrosion behaviour of the materials in dynamic conditions. In order to have a good understanding of the electrochemical mechanisms in dynamic conditions, a standard three-electrode electrochemical cell was set up as shown in Figure 4.3.

The anodic polarisation tests are conducted by the computer-controlled potentiostat. Anodic polarisation is an accelerated technique to study the corrosion behaviour of materials, and this technique has been widely used to determine the resistance to the breakdown of the passive films due to pitting or crevice corrosion for passive materials [85].This test involves shifting the potential of the working electrode from the free corrosion potential (E_{corr}) in the positive direction, and the scan rate is kept at 15 *mV/min*. The current value between the working electrode and the counter electrode in the electrochemical cell can be recorded.

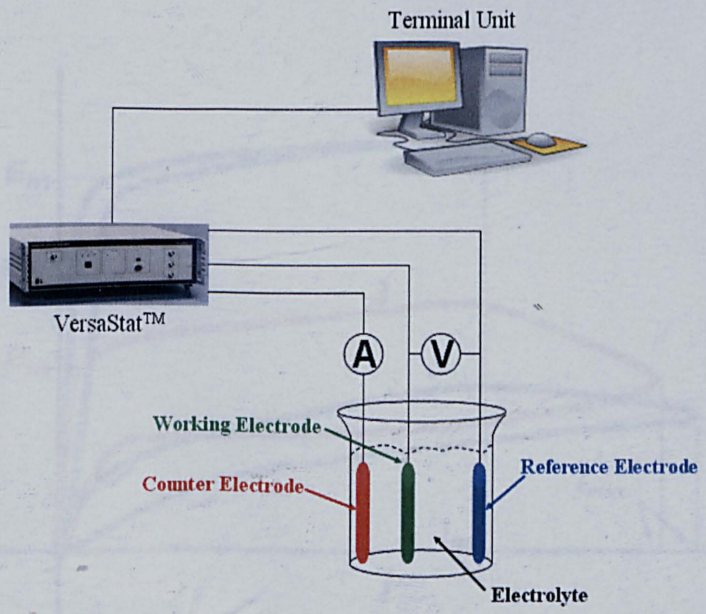

Figure 4.3: Experimental measurements setup for static electrochemical test: three-electrode electrochemical cell

Schematic plots showing different anodic polarisation behaviour are shown in Figure 4.4. For a passive material, as the potential is scanned towards the positive direction from the free corrosion potential (E_{corr}). The current density remains very small until the potential reaches the breakdown potential (E_b), the current density shows a sudden increase. With the absence of the crevice corrosion, this potential is also referred to pitting potential, where metastable pit nuclei may be transformed into stable pits [157]. In principle the breakdown potential of the material shows the resistance of materials to passivity breakdown due to not only pitting corrosion but also crevice corrosion. As the potential reverses at i_{rev} (500 mA/cm^2), the current density for some materials often increase indicating the occurrence of corrosion propagation. An indication of the extent of the propagation is therefore obtained by consideration of maximum current density (i_{max}). The pitting or crevice corrosion propagation resistance is determined by a maximum current density value (i_{max}). Free corrosion potential, breakdown potential and maximum current density are commonly used to assess the localised corrosion resistance of the materials. For active material current density increases rapidly as the potential increases and the electrochemical dissolution is considered to be the corrosion mechanism. The anodic polarisation curves are also used to determine the corrosion rate of the material by Tafel extrapolation, the detail of which will be demonstrated in the following chapter.

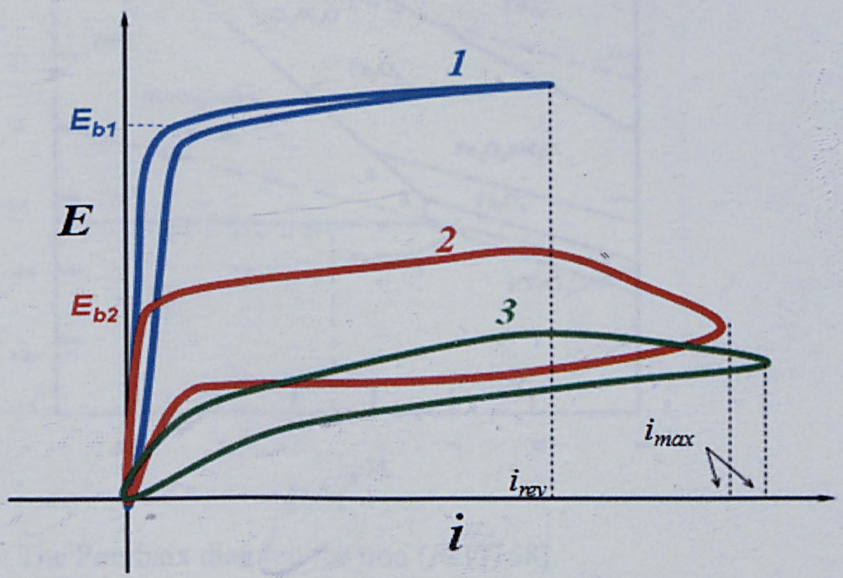

Figure 4.4: Typical anodic polarisation curves: (1) passive material; (2) passive material; (3) active material

4.4.2 DC cathodic protection

The aim of the cathodic protection test is to eliminate electrochemical corrosion processes on the material surface when submerged to a corrosive environment. The weight loss of material can then be considered to be due to pure mechanical erosion under liquid-solid impingement conditions. In this study, cathodic protection (*CP*) potential was applied on the specimens for the duration of the test period under liquid-solid impingement. The protective potential at which materials are immune to corrosion was determined to be -0.8 *V* versus *Ag/AgCl* with saturated *KCl* (-0.603 *V* versus *SHE*) according to the Pourbaix diagrams for *Fe*, *Cr*, *Cu* and *Ni* (Figure 4.5 - Figure 4.8). Applying a constant potential in the cathodic region has ensured the residual anodic activity on the sample to be minimised, and the electrochemical processes cannot significantly affect the material degradation. The cathodic protection current was recorded in the period before the jet was directed onto the specimen, and for a few minutes after the rig was switched off.

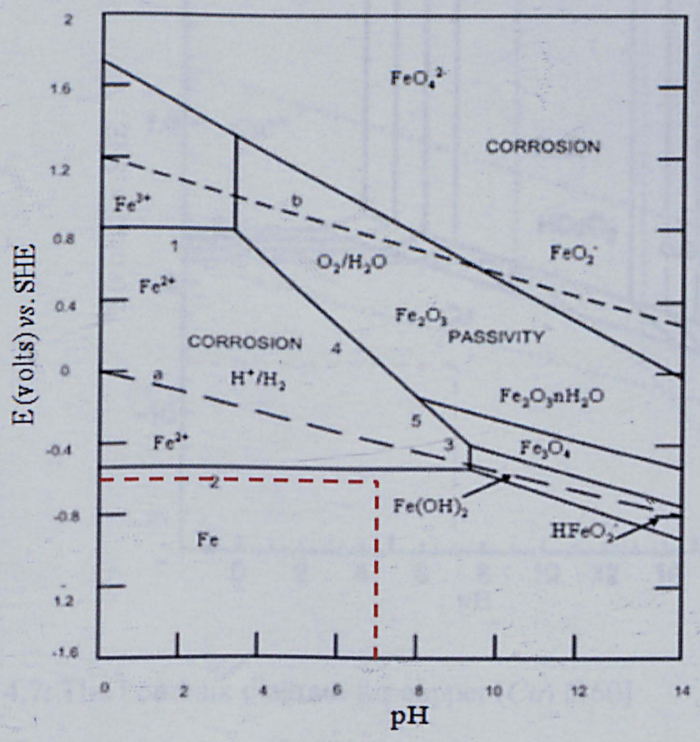

Figure 4.5: The Pourbaix diagram for iron (*Fe*) [158]

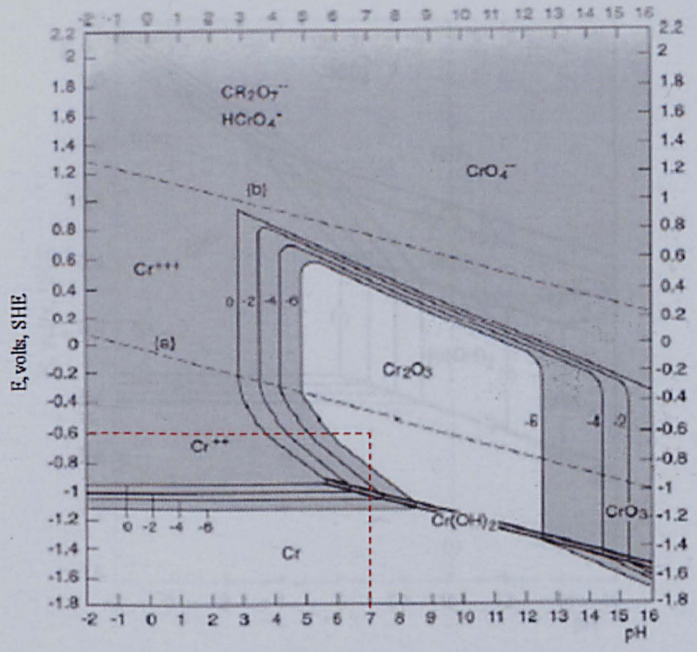

Figure 4.6: The Pourbaix diagram for Chromium (*Cr*) [159]

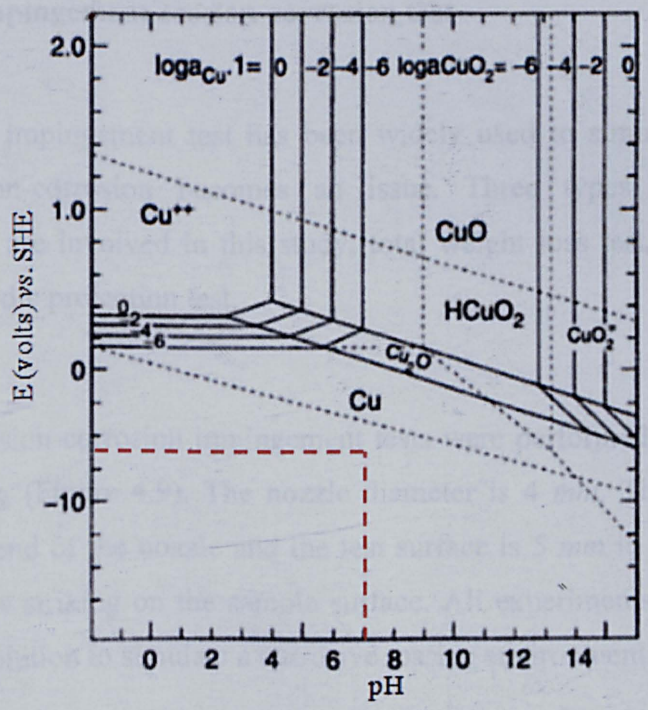

Figure 4.7: The Pourbaix diagram for copper (*Cu*) [160]

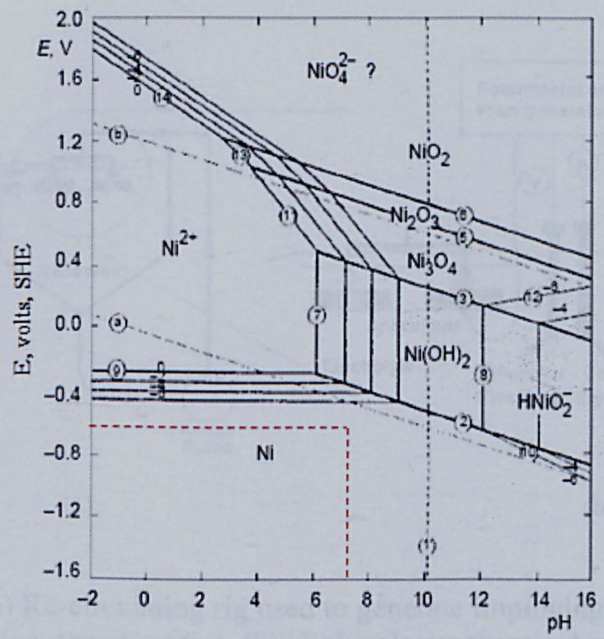

Figure 4.8: The Pourbaix diagram for nickel (*Ni*) [161]

4.4.3 Jet impingement erosion-corrosion test

The jet impingement test has been widely used to simulate field conditions where erosion-corrosion becomes an issue. Three types of tests under jet impingement are involved in this study, total weight loss test, anodic polarisation test and cathodic protection test.

The erosion-corrosion impingement tests were performed in a closed loop re-circulating rig (Figure 4.9). The nozzle diameter is 4 *mm*. The stand-off distance between the end of the nozzle and the test surface is 5 *mm* in order to guarantee a turbulent flow striking on the sample surface. All experiments were carried out in 3.5% *NaCl* solution to simulate a corrosive marine environment.

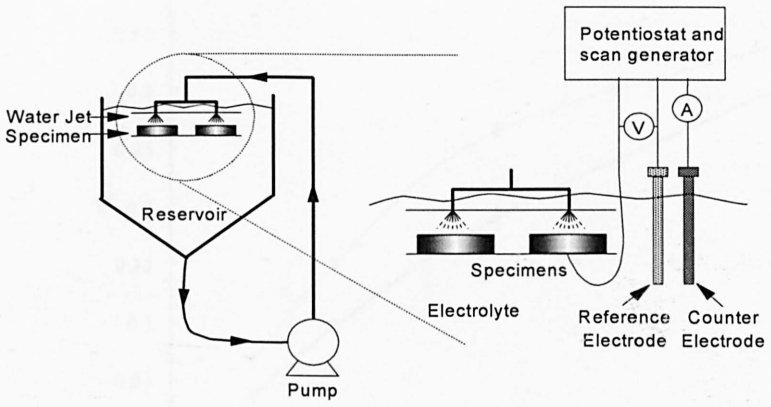

Figure 4.9: (a) Re-circulating rig used to generate impinging jet of liquid-solid slurry for erosion-corrosion test, (b) in-situ electrochemical monitoring apparatus.

The sand abrasivity as a function of time in the closed loop system is taken into consideration in this study. Analyses were carried out on the silica sand size distribution before and after impinging on stainless specimens [86] (Figure 4.10). It is clear that there is a decrease in the sand size after 4 hours tests. From reported results [11] (Figure 4.11), the change in sand size shows very small effects on the total weight loss for the first four hours. However, the weight loss rate decreases after eight hours and this is considered to result from reduction in sand abrasivity due to degradation of sand particles. Therefore the duration of all the tests in this study has been decided to be four hours to avoid the sand degradation effect.

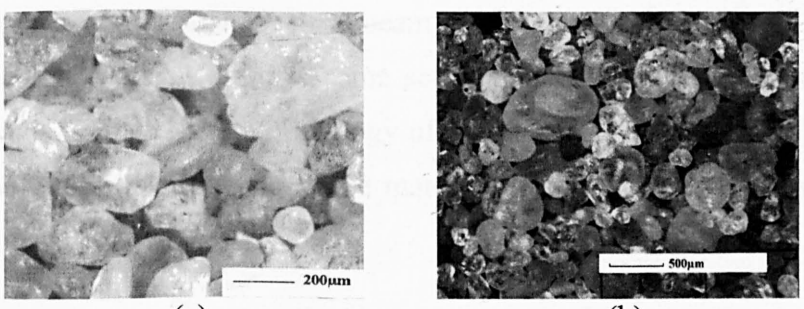

Figure 4.10: Silica sand particles used in this study, (a) original sand, (b) after 4-hour tests [11]

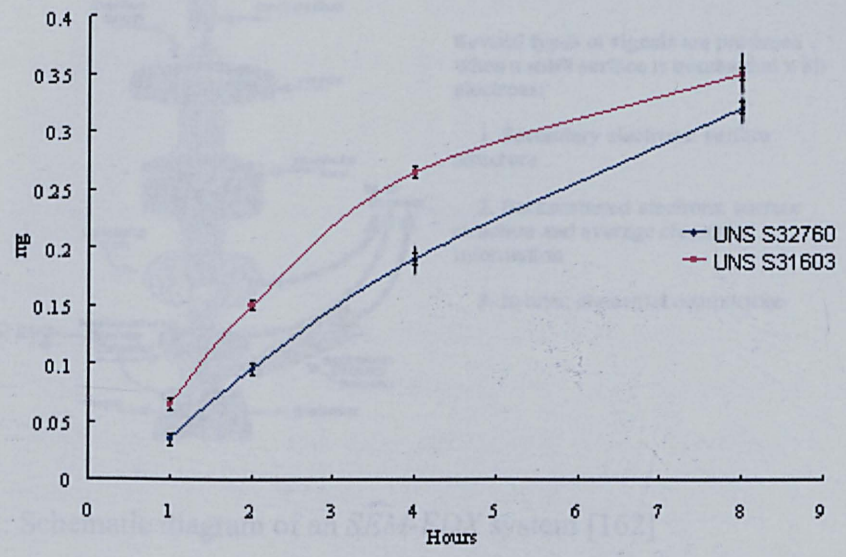

Figure 4.11: The duration for the experiment at 18 °C, $20ms^{-1}$ and $500mgl^{-1}$ [11]

4.4.4 Pre and post- surface characterisation

The initial surface and post-test microstructure of materials under investigation was examined using scanning electron microscopy (*SEM*). Energy dispersive X-ray analysis (*EDX*) enables the elemental composition of the surface to be determined.

Scanning electron microscopy has been widely considered as an extremely useful investigation tool for microstructure and morphology analysis of the material. Before the material is scanned, the material should be well prepared; moreover the specimen to be examined must be electrically conductive. In principle, the surface of a specimen is scanned with an electron beam, and the reflected beam of electron is obtained, and then displayed at the same scanning rate on a cathode ray tube as illustrated in Figure 4.12. The morphology of the materials obtained by *SEM* could be used to study the mechanisms of the material degradations during the erosion-corrosion processes.

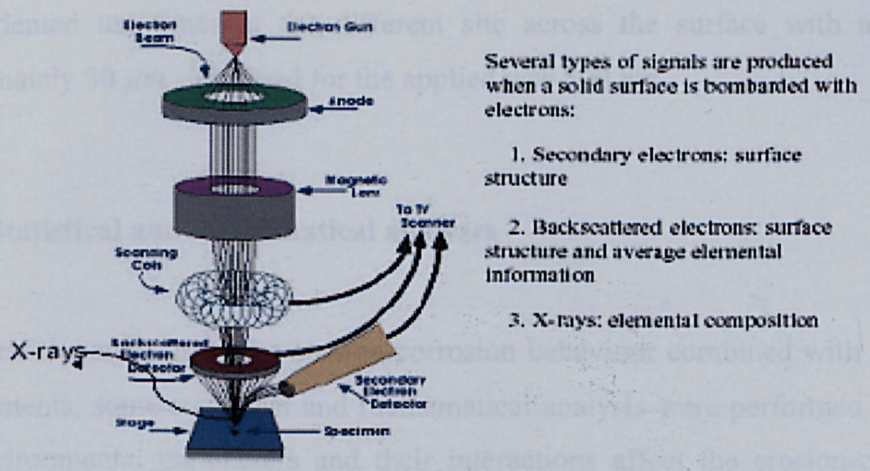

Figure 4.12: Schematic diagram of an *SEM-EDX* system [162]

Additionally, the low energy secondary electrons, backscattered electrons and X – rays are also generated by primary electron bombardment. The intensity of backscattered electrons can be responded to the atomic number of the element within the sampling volume, which will analyze the elemental volume of the specific area in the microstructure.

4.4.5 Hardness measurements

As reviewed in the literature review section, hardness is considered to be an important criteria correlated to the material erosion resistance. As high microhardness value of the material can result in the decrease of other mechanical properties such as toughness, it is often optimised when considering to improve the material erosion resistance. In order to determine the correlation between the erosion-corrosion resistance and the microhardness, the microhardness was measured cross the surface after erosion-corrosion test. The microhardness data in this work was measured by using a *Mitutoyo – MVK – H1* microhardness testing machine. Indent diagonal length measurements were performed automatically from the machine. Before the indentation of the initial microhardness measurements, all specimens were ground with *SiC* papers up to 1200 grit, then rinsed with distilled water and acetone and air dried. The specimens after the preparation procedures

were indented ten times at the different site across the surface with a gap of approximately 50 μm.. The load for the applied was 500 mg.

4.4.6 Statistical and mathematical analyses

After the analysis of the erosion-corrosion behaviour combined with post-test measurements, some statistical and mathematical analysis were performed to study how environmental parameters and their interactions affect the erosion-corrosion behaviours followed by developing a prediction model

Analysis Of VAriance (*ANOVA*) was adopted for the statistical analysis, which is defined as a collection of statistical models, and their associated procedures, in which the observed variance is partitioned into components due to different explanatory variables. The initial techniques of the analysis of variance were developed by the statistician and geneticist R. A. Fisher, which is sometimes known as Fisher's *ANOVA* or Fisher's analysis of variance [163].

MATLAB was used to visualise the prediction model for future material selection in this work. MATLAB is the language of technical computing, and high-level interactive environment that enable us to perform computationally intensive tasks faster than with the traditional programming languages such as C, C++ and Fortran [164].

Chapter 5 Results

When the materials are impacted by the flow containing solid particles, the surface will experience catastrophic damage due to the simultaneous mechanical and electrochemical processes. The degradation mechanisms occurring in erosion-corrosion have been explained in the literature review with emphasis on the synergisms due to the interactions between erosion and corrosion. Due to such effects a greater mass loss than the sum of the separate processes (erosion and corrosion) can often be observed. In this chapter, the components of the total weight loss and erosion-corrosion mechanisms will be reported for the materials used in this study and effects of the environmental parameters on the components of the total weight loss will be analysed.

In this study, the materials have been categorised into three groups: stainless steels (often referred to as corrosion resistant alloys), Copper-Nickel alloys and cast iron. Danek's work [132] manifested that most alloys can been divided into three groups according to their corrosion responses correlating to the velocity from 0 to 36.6 ms^{-1} as followed:

1. First group: Alloys could form very tenacious and protective surface oxide films and have excellent corrosion resistance at all velocities. Titanium alloys and *Ni-Cr-Mo* alloy belong to this group.

2. Second group: Alloys form very tenacious and protective surface films and exhibit excellent corrosion resistance at high and intermediate velocities. However, at low velocities, where the settling of sand and other deposits are possible, pitting or crevice corrosion is often a problem. Most stainless steels and nickel based alloys were in this group.

3. Third group: Alloys exhibit excellent corrosion resistance at low velocities but are subject to degradation by erosion-corrosion in the high and intermediate ranges, where the protective films are stripped from the metal surface. Copper-base alloys were defined in this group.

For Ni-resist cast irons there is no protective film on the surface. Corrosion resistance is the lowest compared with the materials in the above three groups. However, relatively high erosion-corrosion resistance has been found due to improved mechanical properties by the addition of alloying element nickel [34].

The material loss and erosion-corrosion mechanisms under different impingement conditions for the three groups of materials will be reported respectively in this chapter.

5.1 Erosion-corrosion of stainless steels

The total weight loss tests were carried out for the three stainless steels under eight conditions and the results are presented in Figure 5.1. It is shown that the total weight loss of three stainless steels increases as the environment becomes more severe. The significance is clear when a high solid loading level 500 mgl^{-1} is combined with a high velocity level 20 ms^{-1}. Under such severe conditions, the material loss increases as the temperature is elevated. The high alloy stainless steels *Vistar* and *UNS S32760* exhibit better erosion-corrosion resistance compared with *UNS S31603* as expected due to their extents of alloying elements, especially the composition of Chromium, Molybdenum and Nitrogen, which makes the corrosion resistance and hence erosion-corrosion resistance superior as reported in previous works [9, 104] . The total weight loss is under 2 *mg* under most conditions except 18°C, 500 mgl^{-1} sand loading and 20 ms^{-1} velocity and 50°C, 500 mgl^{-1} sand loading and 20 ms^{-1} velocity.

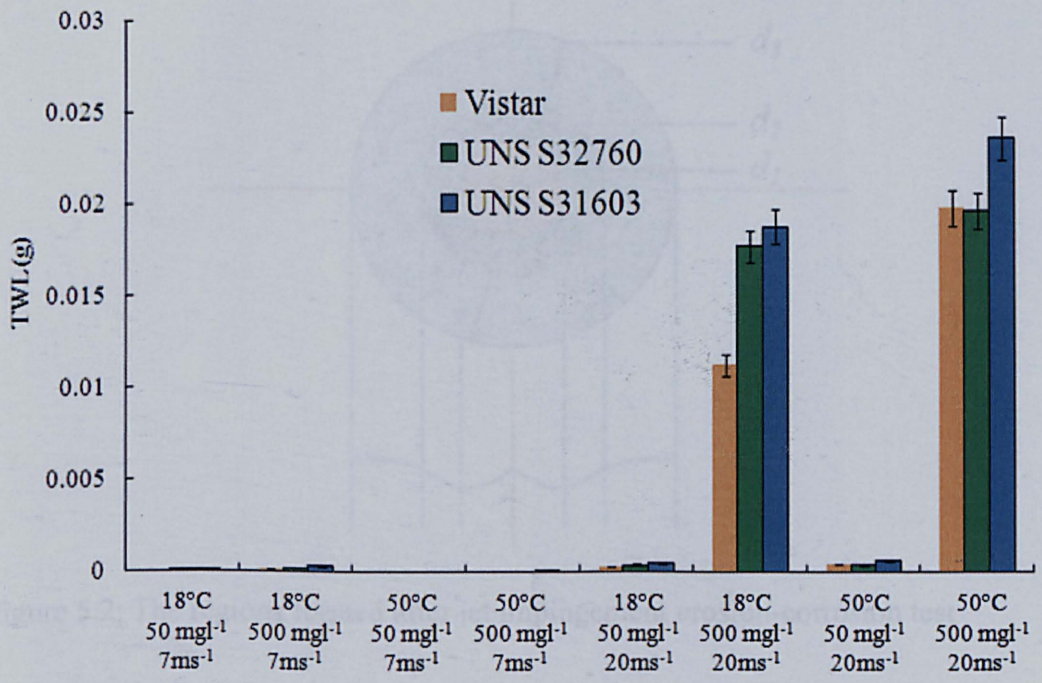

Figure 5.1: Total weight loss for three stainless steels involved in this project

5.1.1 Surface analysis of stainless steels

The *SEM* analyses on the surface after four hours exposure to erosion-corrosion offer a microscopic view of the damaged surface, from which the 'severity' of environmental conditions can be assessed. In this study, the specimen surface under the jet impingement can be divided into three regions [165] as shown in Figure 5.2 and the surface analyses were conducted focusing on:

- Zone 1 – in which the surface is right beneath the water jet experiencing the highest frequency and angle of liquid-solid impacts. The diameter of this zone is $d_1 <$ 5 *mm*;

- Zone 2 – is a relatively low frequency impact zone, named as 'halo' region by Wood [166] (9 $mm < d_2 < 11$ *mm*);

- Zone 3 – where few solid particles impact the surface. It is a "flow-induced" region ($d_3 > 11$ mm).

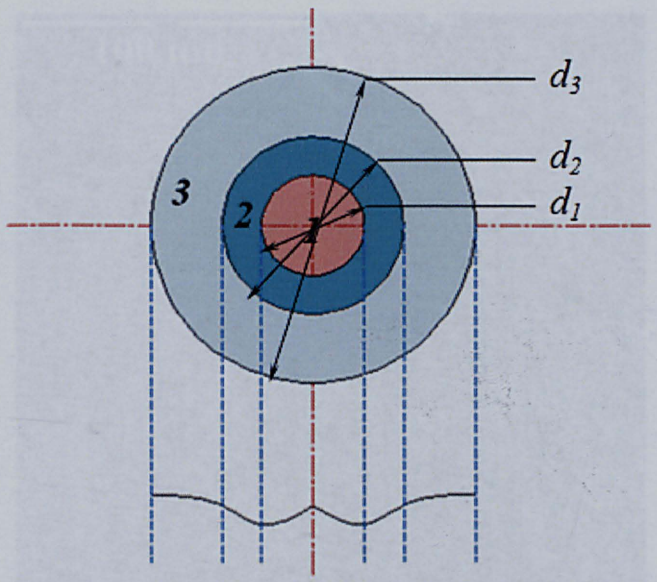

Figure 5.2: The regions formed after jet impingement erosion-corrosion test

From the testing matrix, three conditions are chosen to assess the surface degradation transformations. The severity of the environments is defined as follows:

- Mild: 18 °C, 7 ms^{-1} velocity and 50 mgl^{-1} sand loading
- Moderate:18 °C, 20 ms^{-1} velocity and 50 mgl^{-1} sand loading
- Severe: 50 °C, 20 ms^{-1} velocity and 500 mgl^{-1} sand loading

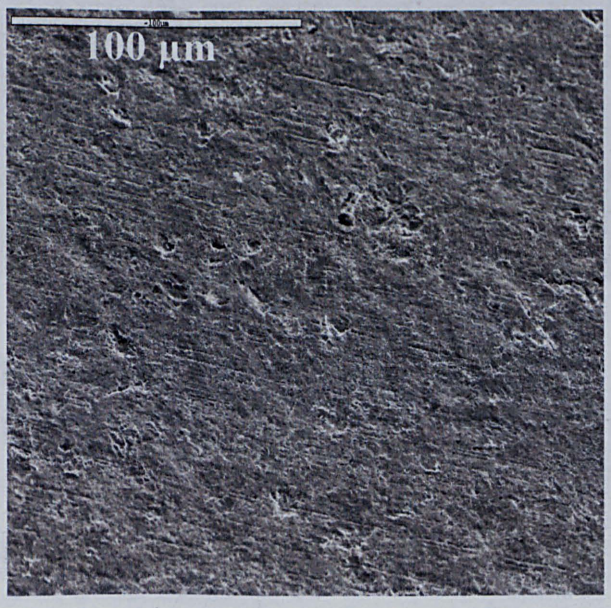

(a)

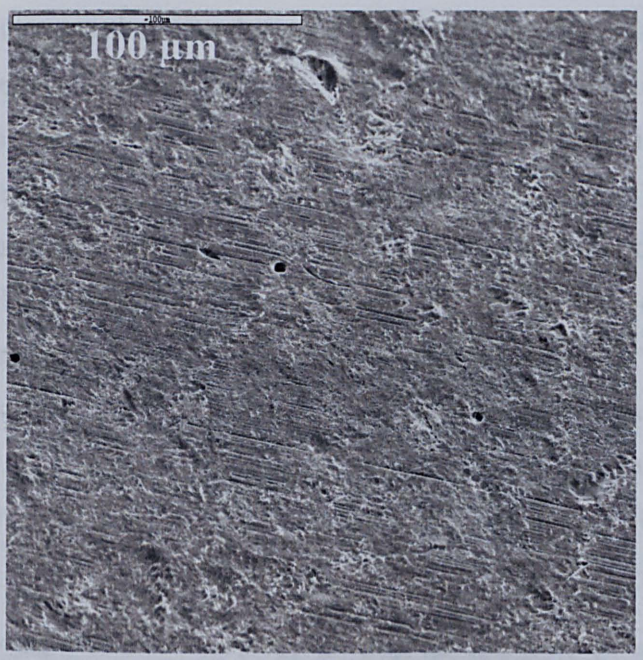

(b)

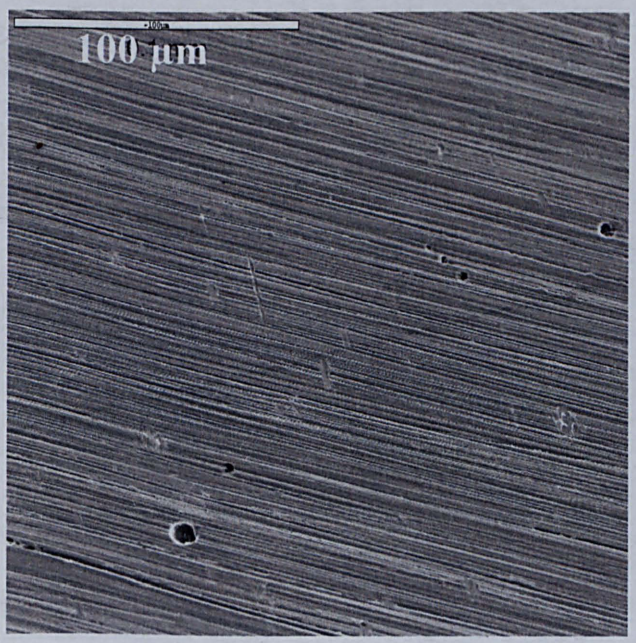

(c)

Figure 5.3: The surface morphology of Vistar at 18 °C, 7 ms^{-1} and 50 mgl^{-1} - mild condition, (a) region one of the specimen; (b) region two of the specimen; (c) region three of the specimen

Figure 5.3 a, b and c show the *SEM* images of *Vistar* in the mild conditions. The material removal is mainly due to ploughing and chipping in region 1 and region 2. No mechanical damage can be found on the surface in region 3. Pitting initiation has been detected in all three inspected areas. As the testing condition

changes from mild to moderate and severe conditions, the degradation on the three stainless steels became more significant. Cutting, ploughing and impact marks are clear as shown Figure 5.4 and Figure 5.5. In region 3 when flow-induced corrosion is dominant, scratches due to low angle cutting mechanism can be observed (Figure 5.6). All three stainless steels experience severe surface degradation at more severe test conditions. High-alloy stainless steel *Vistar* exhibits less erosion-corrosion damages on the surface than standard stainless steel *UNS S31603* when comparing region 1 of the surface exposed to liquid-solid impingement (Figure 5.7). It shows that *UNS S31603* exhibited greater level of material degradation in a form of plastic deformation resulting in a greater material loss than high alloying stainless steels.

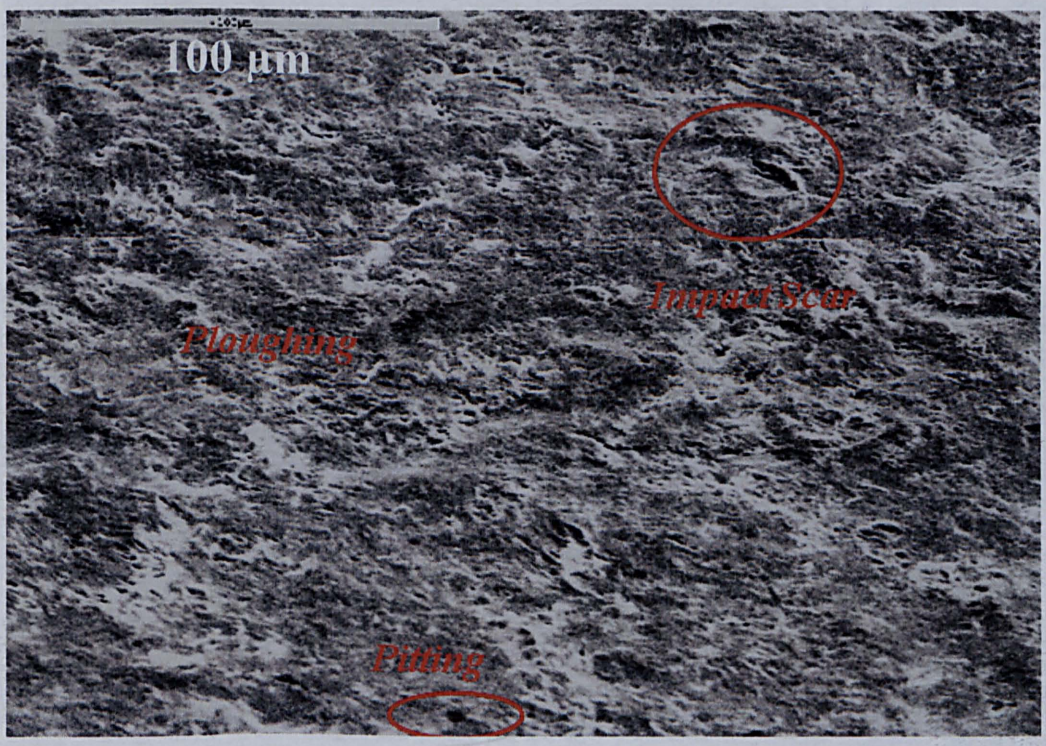

Figure 5.4: The region one of *Vistar* after total weight loss impingement test at moderate condition, 18 °C, 20 ms^{-1} velocity and 50 mgl^{-1} sand loading

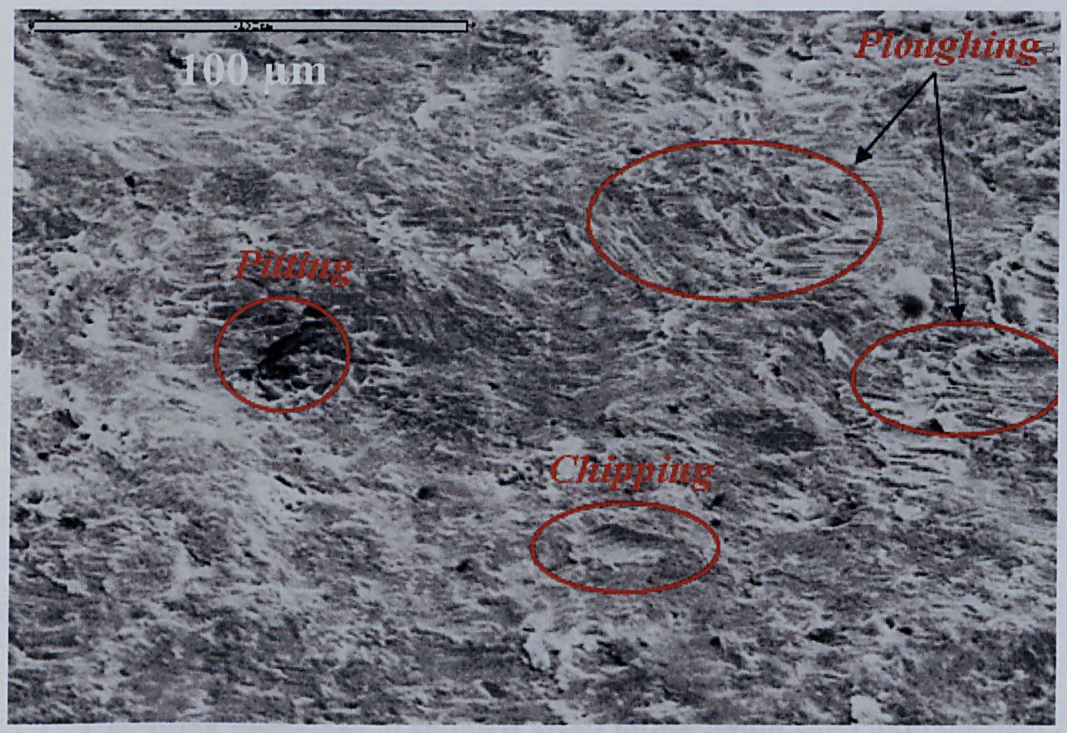

Figure 5.5: Surface in region two of *Vistar* after total weight loss impingement test at moderate condition, 18 °C, 20 ms^{-1} velocity and 50 mgl^{-1} sand loading

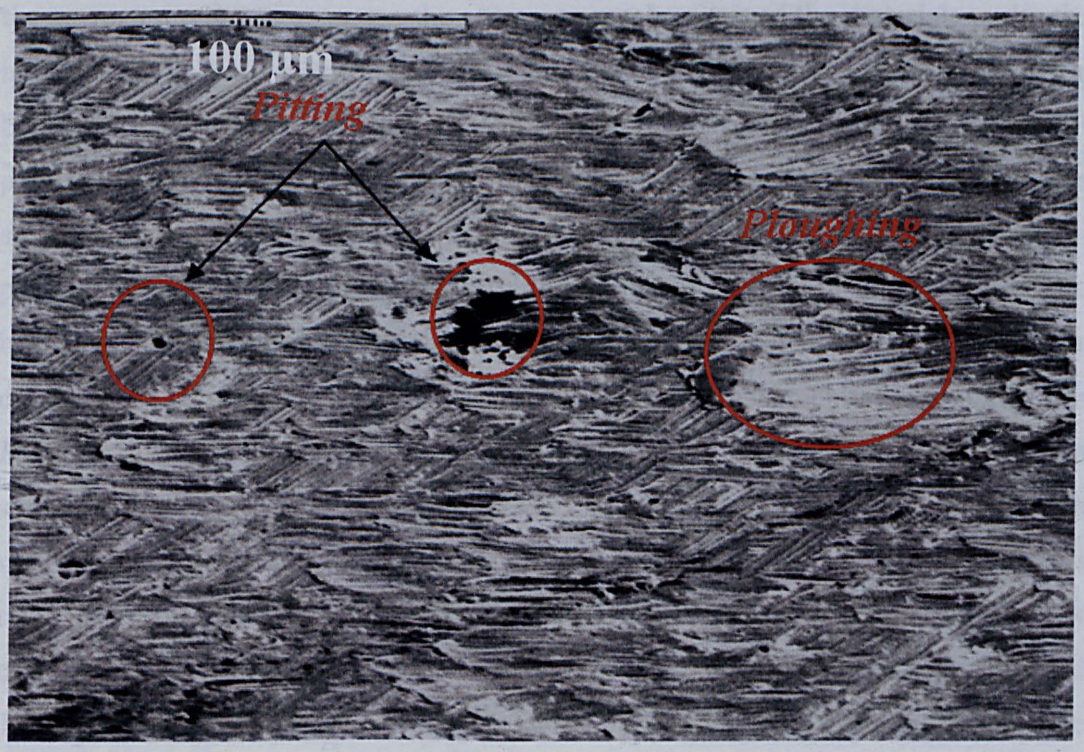

Figure 5.6: Surface in zone 3 of *Vistar* after total weight loss impingement test at moderate condition, 18 °C, 20 ms^{-1} velocity and 50 mgl^{-1} sand loading

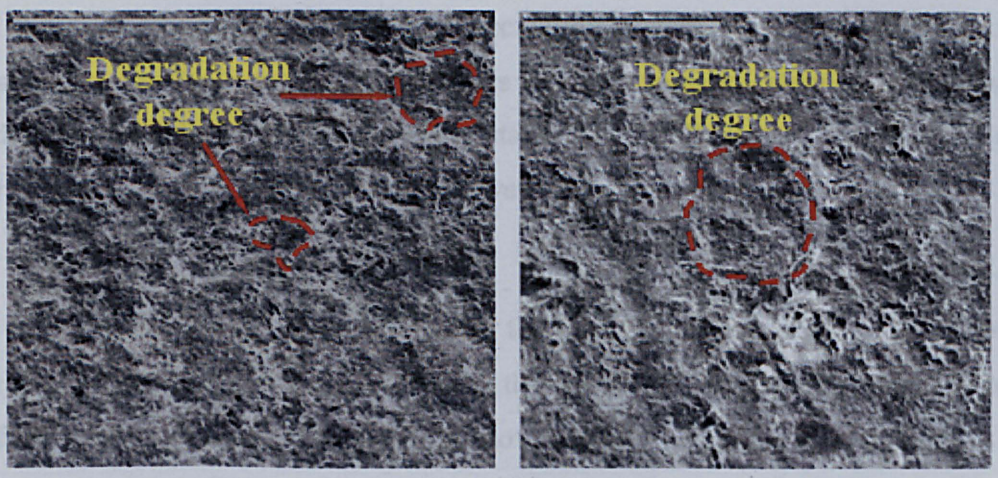

Figure 5.7: The surface morphology comparison between *Vistar* and *UNS S31603* at moderate condition, 18 °C, 20 ms^{-1} velocity and 50 mgl^{-1} sand loading

5.1.2 Corrosion behaviour of stainless steels under liquid-solid impingement

DC Anodic polarisation measurements were carried out *in-situ* to determine the corrosion rate and to assess the corrosion mechanisms of the materials under the influence of a high energy particle-laden flow. Two types of anodic polarisation behaviour can be classified as shown in Figure 5.8: passive behaviour and pseudo-passive behaviour. Passive behaviour indicates that the environment the material is subjected to is not destructive to the passive film on the surface. In terms of pseudo-passive behaviour, at the beginning of the anodic polarisation, under liquid-solid impingement, the anodic polarisation curves showed behaviour akin to active corrosion behaviour with the current rising rapidly as the potential is shifted from E_{corr}. As the potential increased the rate of current increase slowed down and a stabilised current density (i_s) was recorded as shown in Figure 5.8. This stable region was maintained for a large potential range until a breakdown potential, which is represented physically by the passive breakdown on the edge of sample where few or no impacts occurred on the surface, similar to that passive behaviour, was reached. The pseudo-passive behaviour is considered to result from the regional surface electrochemical responses, depassivation and repassivation, to the liquid-solid impingement as described in Figure 5.9 [86]. Similar behaviour has also been found on other corrosion resistant alloys [167]. In this study the high frequency liquid-solid impingement is considered to occur when there is a solid loading of 500 mgl^{-1}

and flow velocity of 20 ms^{-1} in the re-circulating system. According to the anodic polarisation results, corrosion behaviours of three passive stainless steels were studied and the breakdown potentials, stable but oscillating current density and corrosion rate under different conditions were compared.

During the anodic polarisation test, there is a potential when current density increases in a dramatic manner indicating the protective films on the stainless steels surface on the surface collapse or break down. Such a potential is referred to as the breakdown potential (Figure 4.4). Refer to some previous work with Eb [11, 85, 122, 168], different stainless steels show different breakdown potentials in the same environment and breakdown potential can be used to assess the resistance to localised corrosion of the different materials. In the mild condition, breakdown potential represents a localised breakdown of passive film, *e.g.* pitting. This breakdown of passive film could be any area on the surface. As the testing conditions became more severe, the current density increases rapidly when the potential shifts from free corrosion potential. The surface then enters a stable region with relative high stabilised current density, which is followed by a breakdown potential. This breakdown potential suggests that passivity breakdown occurs in regions where the passive film remained on the surface, such as at zone 3 (Figure 5.9). The comparison of the anodic polarisation curves in mild conditions and in severe conditions under liquid-solid impingement is shown in Figure 5.9.

Although the form of anodic polarisation curve exhibit similar manners, the current in the stable region is far in excess of what would be expected to indicate passivity [7, 127]. There are three distinct zones defined as zone 1 (active), zone 2 (pseudo-passive) and zone 3 (passive) [167]. Zone 1 indicates that rapid dissolution occurs in the wear affected zone and again a re-passivation in the wear effected zone. The rate of this reaction taking place in the areas where the passive film is removed initially increases with potential. The current in zone 2 is determined by the level of solid loading, temperature and material characteristics. It represents the steady state charge transfer in the zone activated by the impacting solids. The current value at the pseudo-passive region is defined as the stabilised current (i_s). In zone 3 of the anodic polarisation curve the passive areas break down through initiation of

localised attack. In general [9, 11, 104], high alloy austenitic stainless steel *Vistar* always exhibits the highest break down potential over the range of test conditions followed by super duplex stainless steel UNS S32760 and UNS S31603 (Figure 5.10).

Based on the anodic polarisation results, it has been demonstrated that the environmental parameters not only affect the corrosion rates of all materials, but also the breakdown potential as shown in Figure 5.11 - Figure 5.13 for the three stainless steels. It is clear that the breakdown potential decreases as the environments became more severe. Moreover the environmental factors affect the changes of breakdown potential to a different degree according to the difference between $E_b$max and $E_b$min. The smallest breakdown potential difference for Vistar (0.19 *V*) indicates the least affect on the localised corrosion resistance by change of the environmental parameters (Figure 5.14).

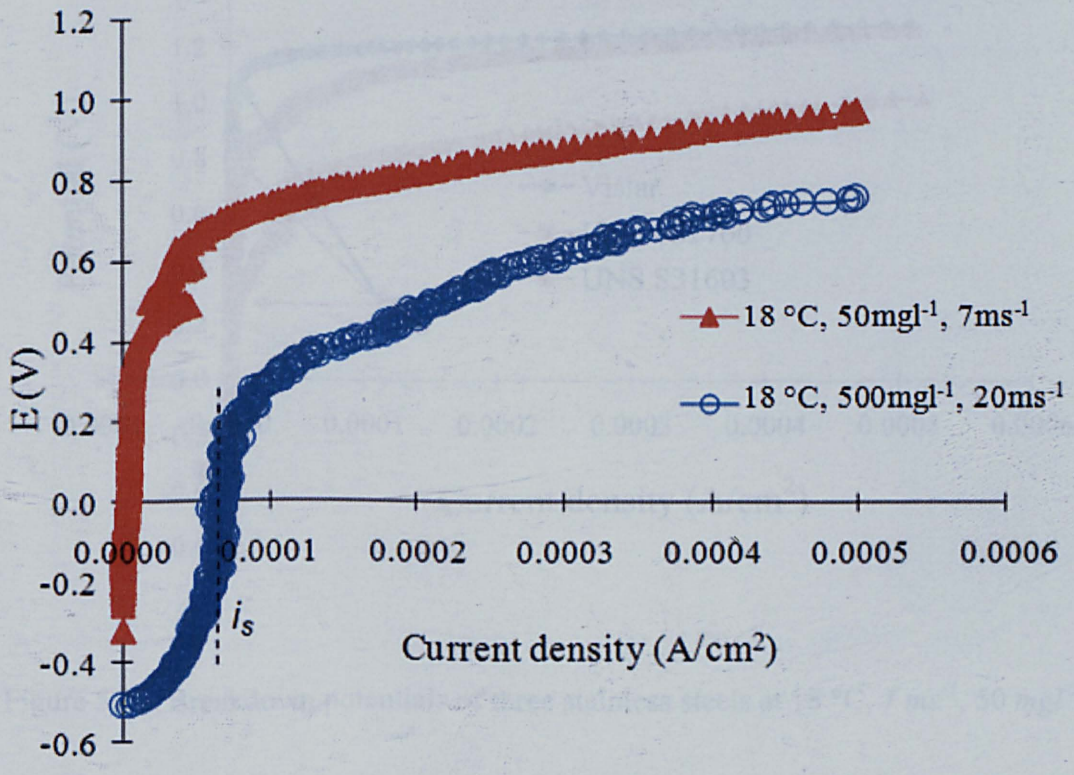

Figure 5.8: Two typical anodic polarization curves of UNS S31603 to compare the passive and pseudo-passive behaviours.

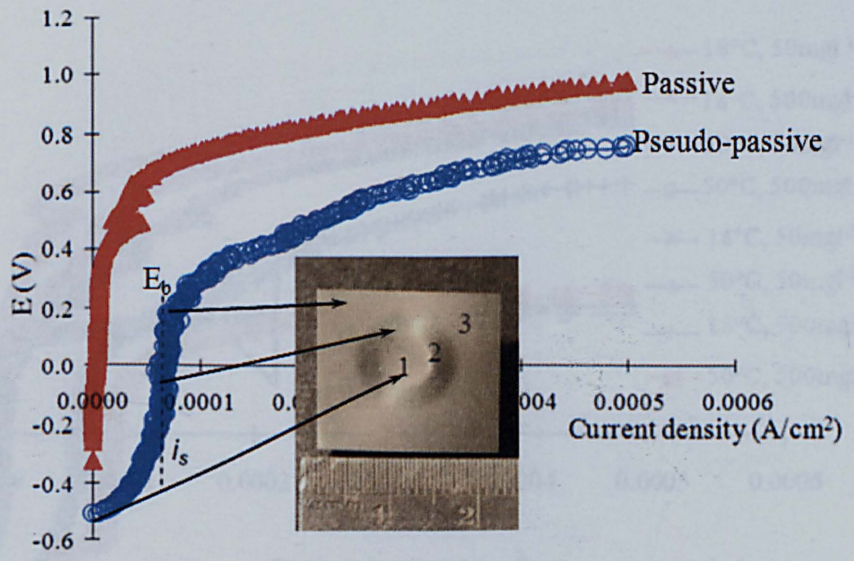

Figure 5.9 Three zones formed on the specimen under liquid-solid jet impingement at severe condition: Region 1 active; region 2 pseudo-passive; region 3 passive (relating to the anodic polarisation)

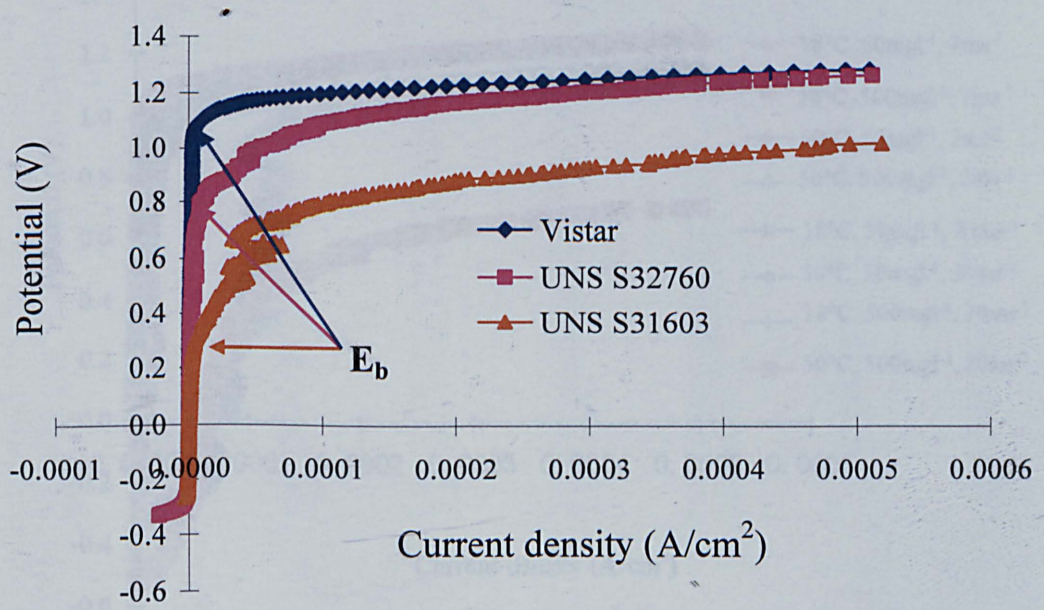

Figure 5.10: Breakdown potentials of three stainless steels at 18 °C, 7 ms^{-1}, 50 mgl^{-1}

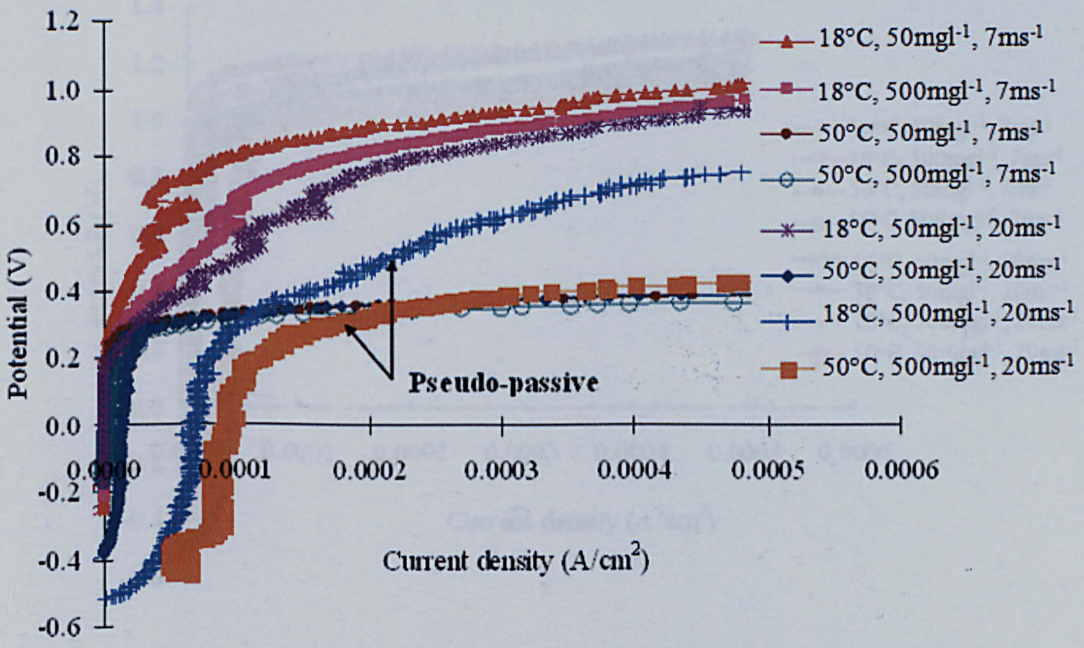

Figure 5.11: Anodic polarization curves for UNS S31603 for the eight conditions

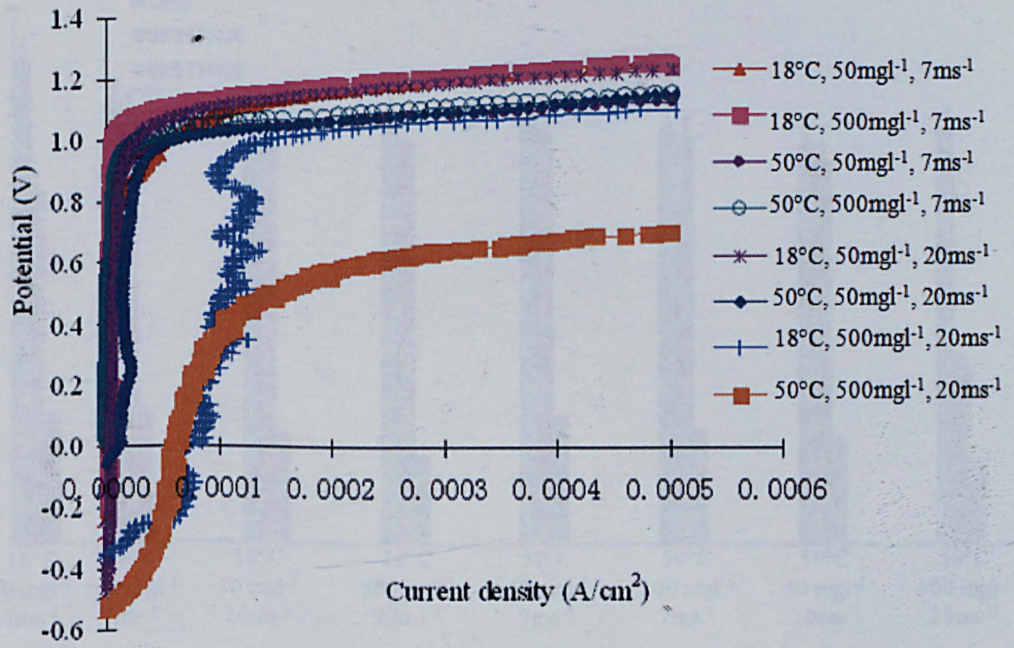

Figure 5.12: Anodic polarization curves for UNS S32760 for the eight conditions

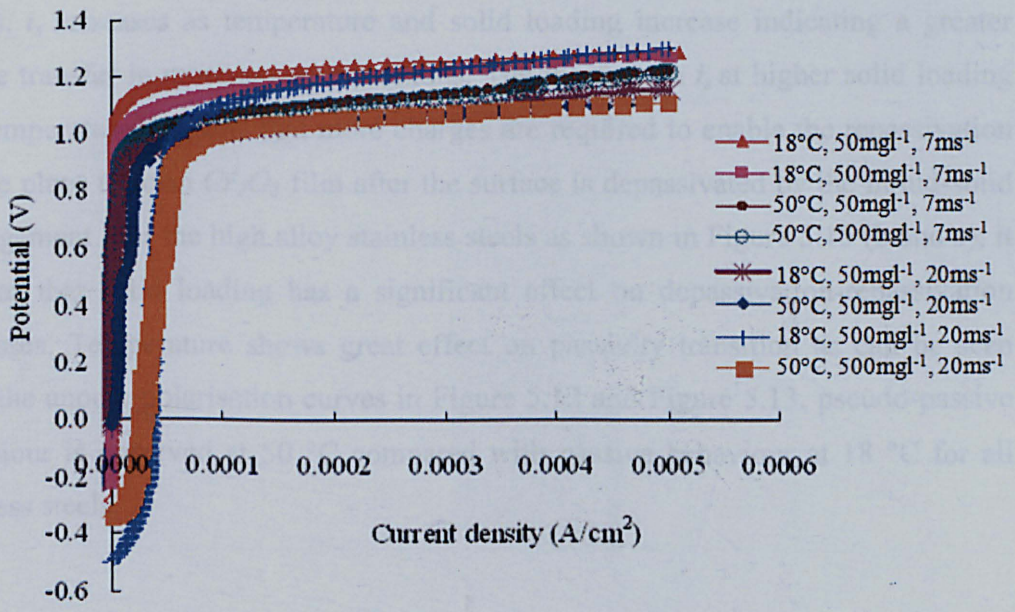

Figure 5.13: Anodic polarization curves for Vistar for the eight conditions

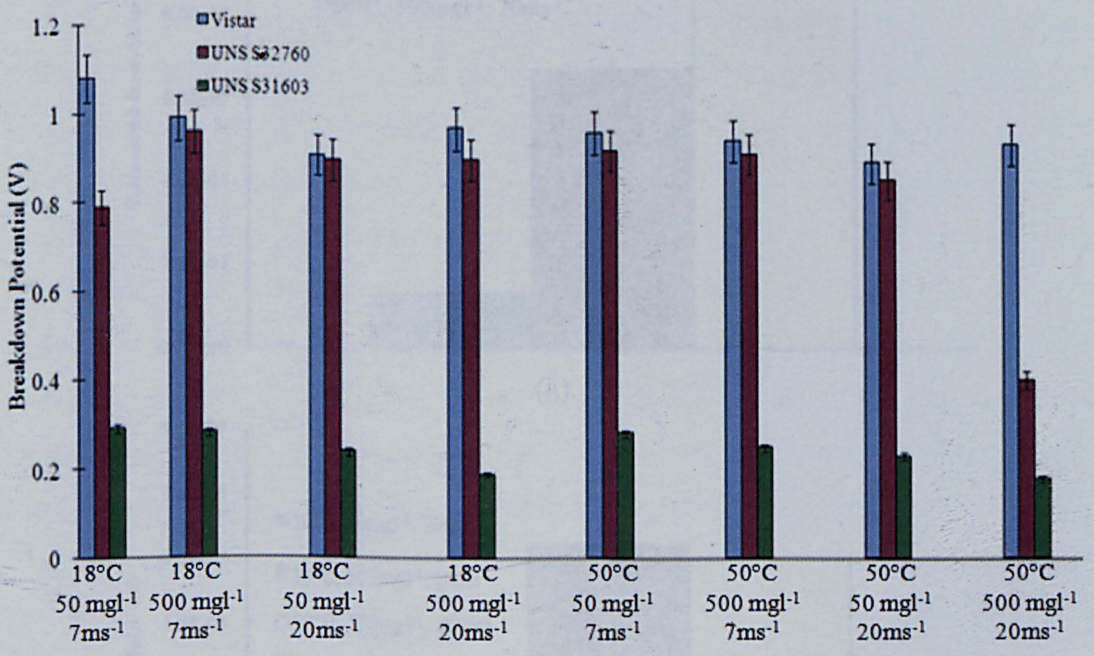

Figure 5.14: Breakdown potential of three studied stainless steels for the eight conditions

The stable current density for the three stainless steels under conditions when pseudo-passive behaviour was observed has been compared to study the effects of environmental parameters on the depassivation and repassivation processes on the surface Figure 5.15 (a, b and c). For standard stainless steel UNS S31603 (Figure

5.15a), i_s increases as temperature and solid loading increase indicating a greater charge transfer in more severe conditions. The increase in i_s at higher solid loading and temperature suggests that more charges are required to enable the repassivation to take place to form Cr_2O_3 film after the surface is depassivated by the liquid-solid impingement. For the high alloy stainless steels as shown in Figure 5.15 (b and c), it is clear that solid loading has a significant effect on depassivation-repassivation processes. Temperature shows great effect on passivity transition as can be seen from the anodic polarisation curves in Figure 5.12 and Figure 5.13, pseudo-passive behaviour is observed at 50 °C compared with passive behaviour at 18 °C for all stainless steels.

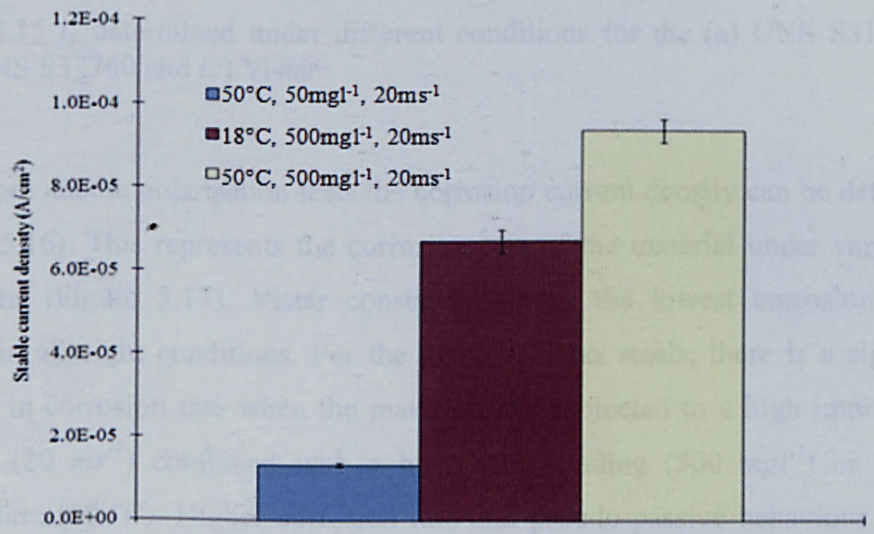

(a)

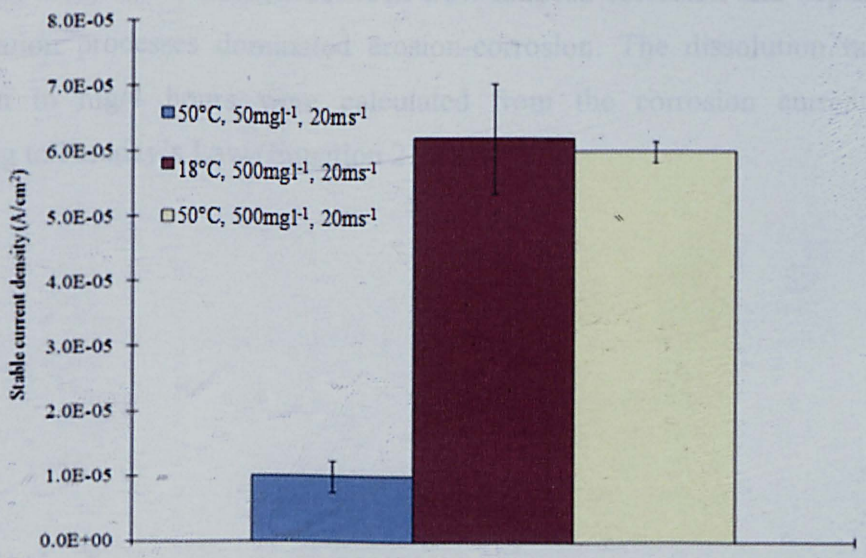

(b)

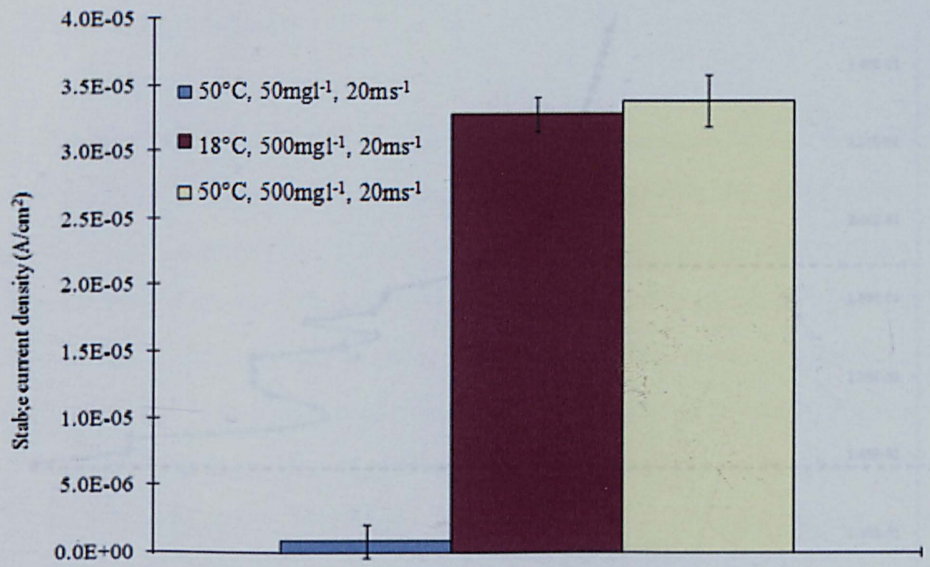

(c)

Figure 5.15 i_s determined under different conditions for the (a) UNS S31603, (b) UNS S32760 and (c) Vistar

From anodic polarisation tests the corrosion current density can be determined (Figure 5.16). This represents the corrosion rate of the material under various test conditions (Figure 5.17). Vistar constantly shows the lowest corrosion current density in all eight conditions. For the three stainless steels, there is a significant increase in corrosion rate when the materials are subjected to a high impingement velocity (20 ms^{-1}) combined with a high solid loading (500 mgl^{-1}) or working temperature (50 °C). Higher corrosion rate and pseudo-passive behaviour in these conditions suggest a transition between flow-induced corrosion and depassivation-repassivation processes dominated erosion-corrosion. The dissolution rates from corrosion in mg/4 hours were calculated from the corrosion current density according to Faraday's Law (Equation 2.14).

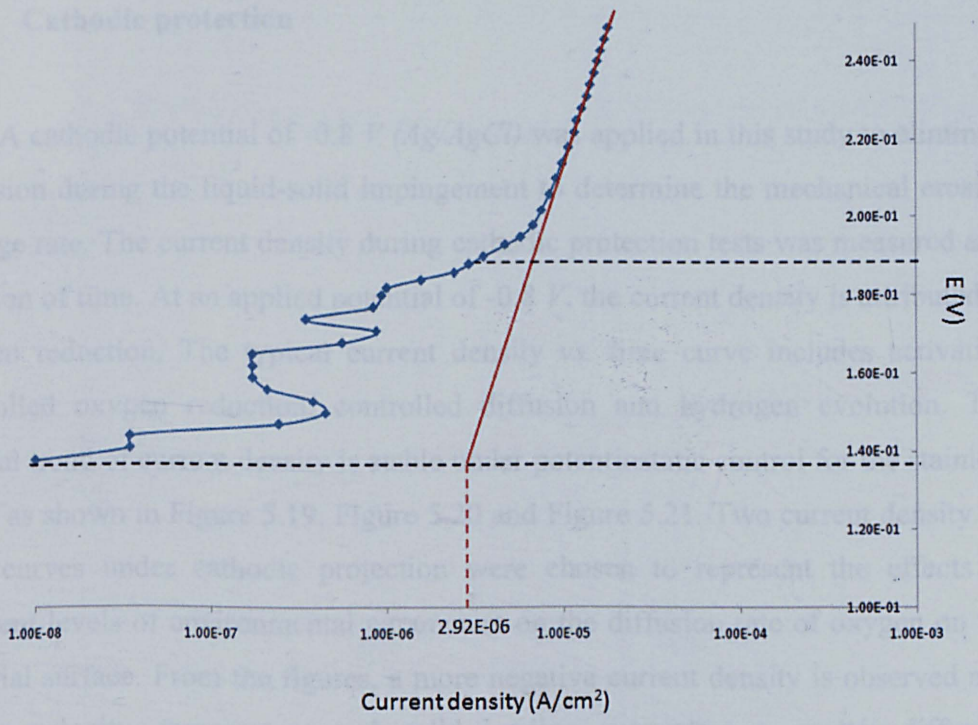

Figure 5.16: Tafel extrapolation to determine corrosion current density for UNS S31603 at 18 °C, 7 ms^{-1} velocity and 50 mgl^{-1} sand loading

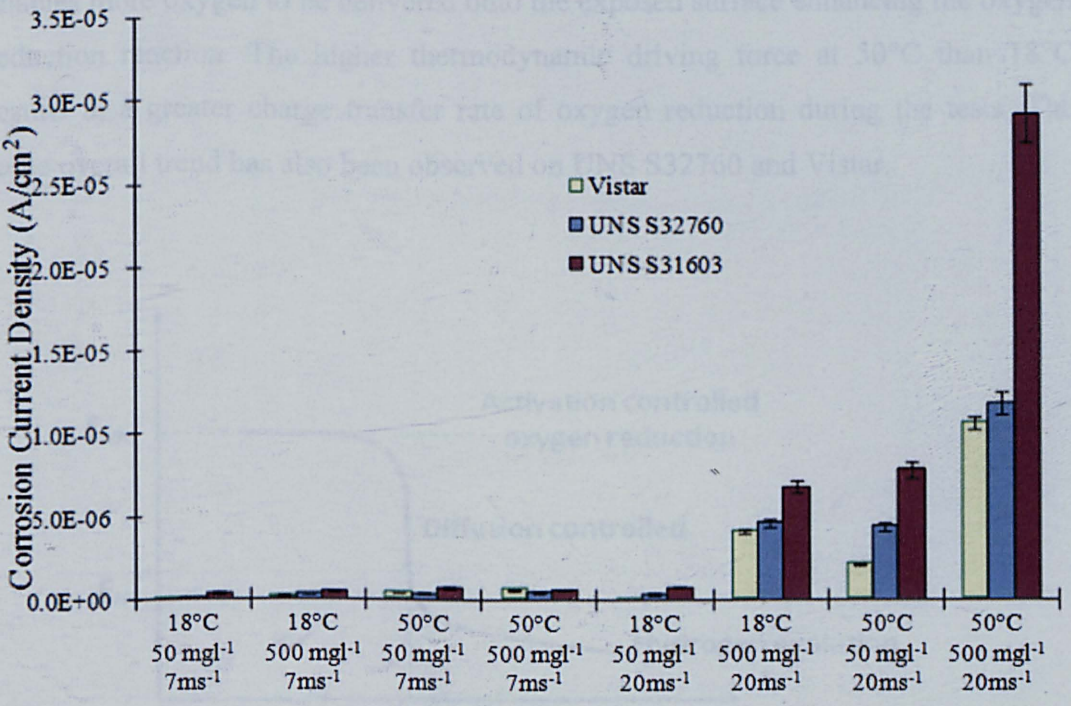

Figure 5.17: Corrosion current density (i_{corr}) in the eight conditions for the stainless steel alloys

5.1.3 Cathodic protection

A cathodic potential of -0.8 *V (Ag/AgCl)* was applied in this study to eliminate corrosion during the liquid-solid impingement to determine the mechanical erosion damage rate. The current density during cathodic protection tests was measured as a function of time. At an applied potential of -0.8 *V*, the current density is attributed to oxygen reduction. The typical current density *vs.* time curve includes activation controlled oxygen reduction, controlled diffusion and hydrogen evolution. The general trend of current density is stable under potentiostatic control for the stainless steels as shown in Figure 5.19, Figure 5.20 and Figure 5.21. Two current density *vs.* time curves under cathodic protection were chosen to represent the effects of different levels of environmental parameters on the diffusion rate of oxygen on the material surface. From the figures, a more negative current density is observed at a higher velocity, temperature and solid loading suggesting a greater diffusion controlled oxygen reduction rate resulting from the great transport rate of oxygen and thermodynamic driving force as environmental parameters are at high level. From a fluid dynamics point of view, the increase in velocity and solid loading enables more oxygen to be delivered onto the exposed surface enhancing the oxygen reduction reaction. The higher thermodynamic driving force at 50°C than 18°C results in a greater charge transfer rate of oxygen reduction during the tests. The same overall trend has also been observed on UNS S32760 and Vistar.

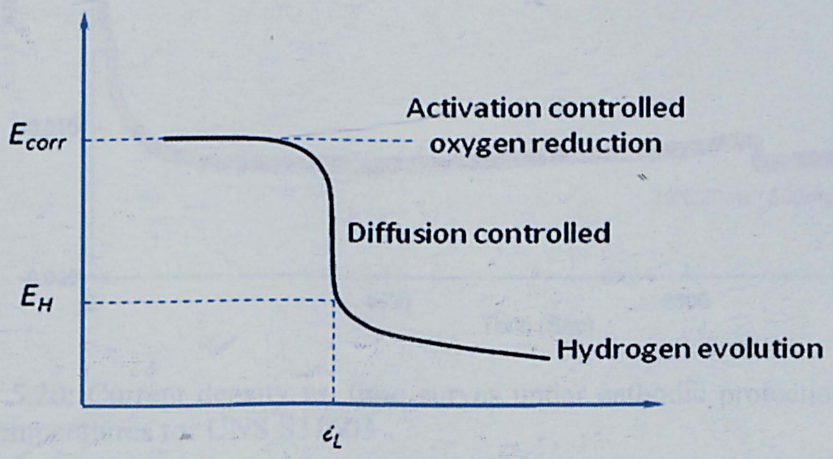

Figure 5.18: Schematic cathodic polarization curve

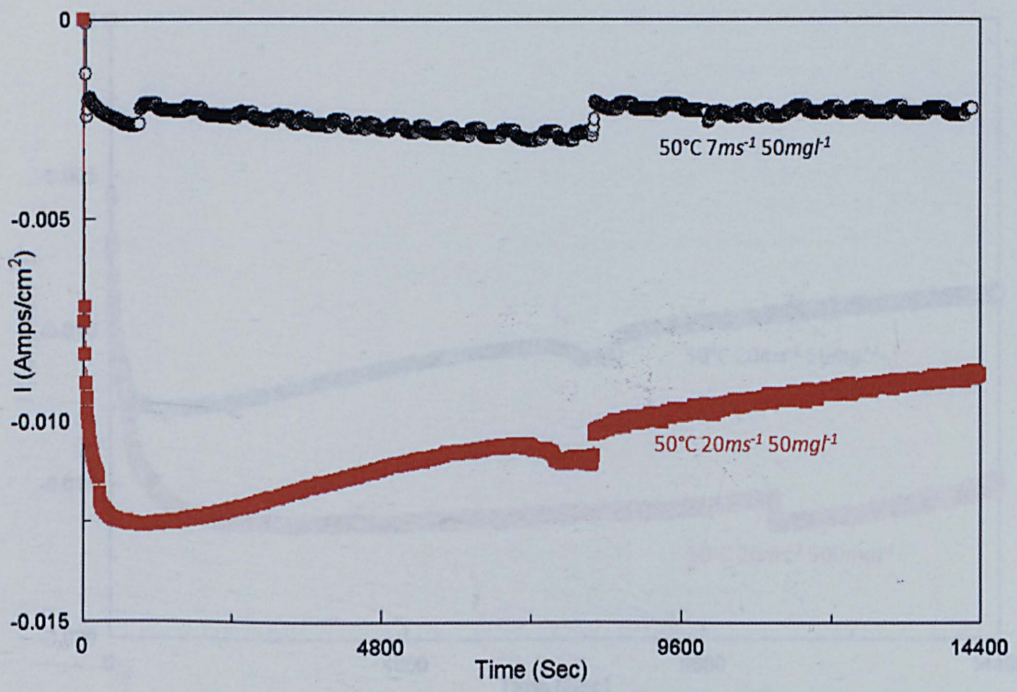

Figure 5.19: Current density *vs.* time curves under cathodic protection at different velocities for UNS S31603

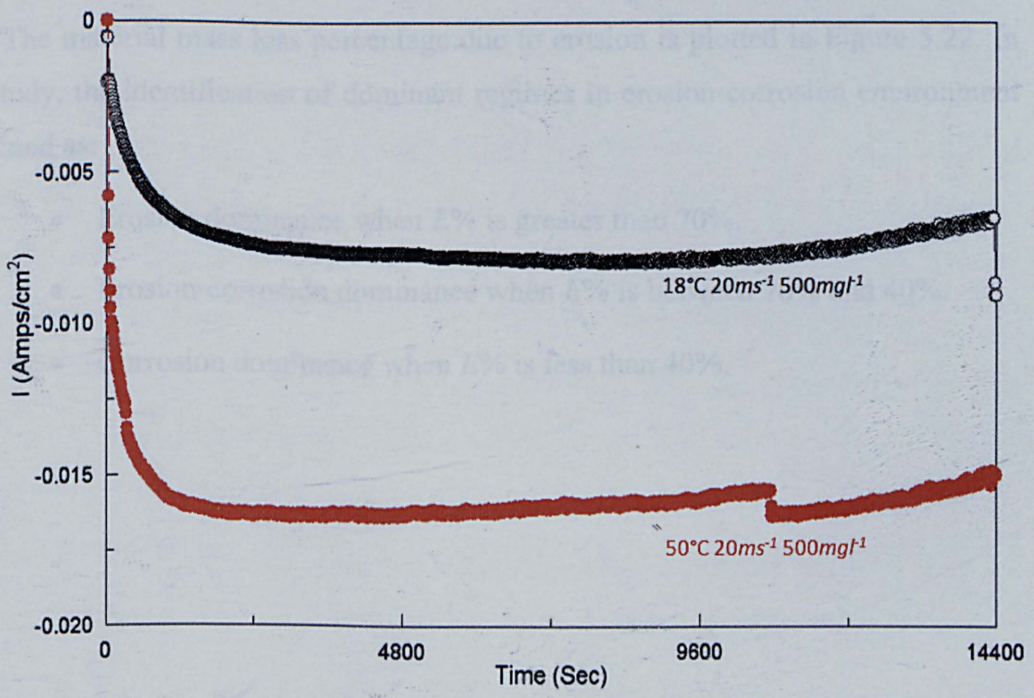

Figure 5.20: Current density *vs.* time curves under cathodic protection at different temperatures for UNS S31603

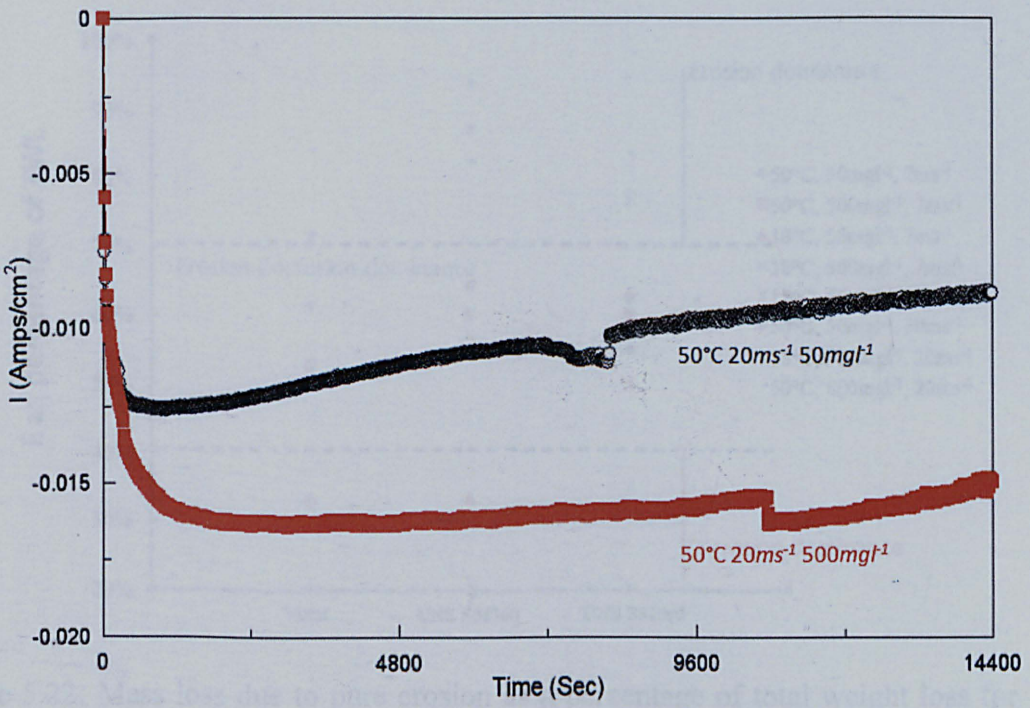

Figure 5.21: Current density *vs.* time curves under cathodic protection at different sand loadings for UNS S31603

The material mass loss percentage due to erosion is plotted in Figure 5.22. In this study, the identification of dominant regimes in erosion-corrosion environment is defined as:

- Erosion dominance when *E*% is greater than 70%.
- Erosion-corrosion dominance when *E*% is between 70% and 40%.
- Corrosion dominance when *E*% is less than 40%.

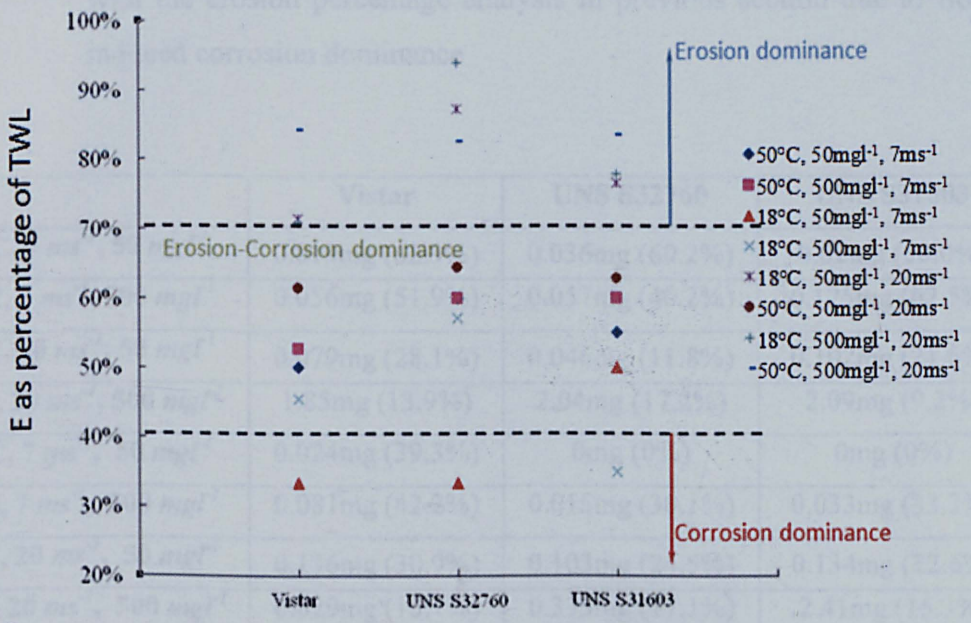

Figure 5.22: Mass loss due to pure erosion as a percentage of total weight loss for three stainless steels at eight conditions

5.1.4 Synergy of stainless steels

As reviewed in the literature review section, synergy is defined as the effect of corrosion on erosion and can be calculated by $S = TWL - E - C$. The percentage of synergy on total weight loss shows the synergistic effect in erosion-corrosion processes of the three stainless steels in Table 5.1 According to the material loss due to the synergistic effect at various conditions, it can be summarised that:

- Kinetic energy plays an important role in enhancing material degradation as high velocity (20 ms^{-1}) and high solid loading (500 mgl^{-1}) result in some weight loss due to synergy.
- Effect of temperature on weight loss due to synergy is less significant at low flow velocity (7 ms^{-1}) compared with high flow velocity (20 ms^{-1})
- Standard stainless steel UNS S31603 exhibits a more prominent weight loss due to synergy compared with the high alloy stainless steels Vistar and UNS S32760
- In the conditions (50 °C, 7 ms^{-1} and 50 mgl^{-1}), it was found that environmental parameters show no effects on synergy as in agreement

with the erosion percentage analysis in previous section due to flow-induced corrosion dominance

	Vistar	UNS S32760	UNS S31603
18 °C, 7 ms^{-1}, 50 mgl^{-1}	0.019mg (62.9%)	0.036mg (60.2%)	0.02mg (50.0%)
18 °C, 7 ms^{-1}, 500 mgl^{-1}	0.056mg (51.9%)	0.057mg (40.2%)	0.125mg (62.5%)
18 °C, 20 ms^{-1}, 50 mgl^{-1}	0.079mg (28.1%)	0.046mg (11.8%)	0.102mg (21.6%)
18 °C, 20 ms^{-1}, 500 mgl^{-1}	1.85mg (13.9%)	2.04mg (17.2%)	2.09mg (9.2%)
50 °C, 7 ms^{-1}, 50 mgl^{-1}	0.024mg (39.3%)	0mg (0%)	0mg (0%)
50 °C, 7 ms^{-1}, 500 mgl^{-1}	0.081mg (42.2%)	0.015mg (30.1%)	0.033mg (33.3%)
50 °C, 20 ms^{-1}, 50 mgl^{-1}	0.136mg (30.9%)	0.103mg (24.5%)	0.134mg (22.6%)
50 °C, 20 ms^{-1}, 500 mgl^{-1}	0.629mg (15.1%)	0.333mg (17.1%)	2.41mg (15.3%)

Table 5.1: Synergy values (g) of stainless steels at eight conditions (% shows the percentage of synergy value on total weight loss)

5.2 Total weight loss of copper-base alloys

The copper-base alloys are widely used as corrosion resistant materials in marine service due to their relatively low corrosion susceptibility. However, the copper-base alloys (Figure 5.23) show higher erosion-corrosion susceptibilities compared with stainless steels (Figure 5.1). This damage is caused by the mechanical disruption of the protective film formed on the copper-base alloys in aqueous environments and the removal of the base material. Such film disruption is commonly caused by excessive fluid flow velocities, and the protective films are more susceptible to be stripped off compared with the tenacious films on stainless steels. There is porosity of the film on copper-base alloys although the nickel addition has enabled the corrosion resistance to be improved by incorporating into the cation vacancies of the protective films [169]. The adhesion ability of the protective film on the material surface is also considered to be weaker than stainless steel and this aspect will be further discussed in Chapter 7. Comparing the erosion-corrosion mass loss magnitude within the copper-base alloys, high strength copper nickel alloys have higher erosion-corrosion resistance compared with other copper-

base alloys. This is due to the increasing mechanical properties of high strength copper nickel alloys.

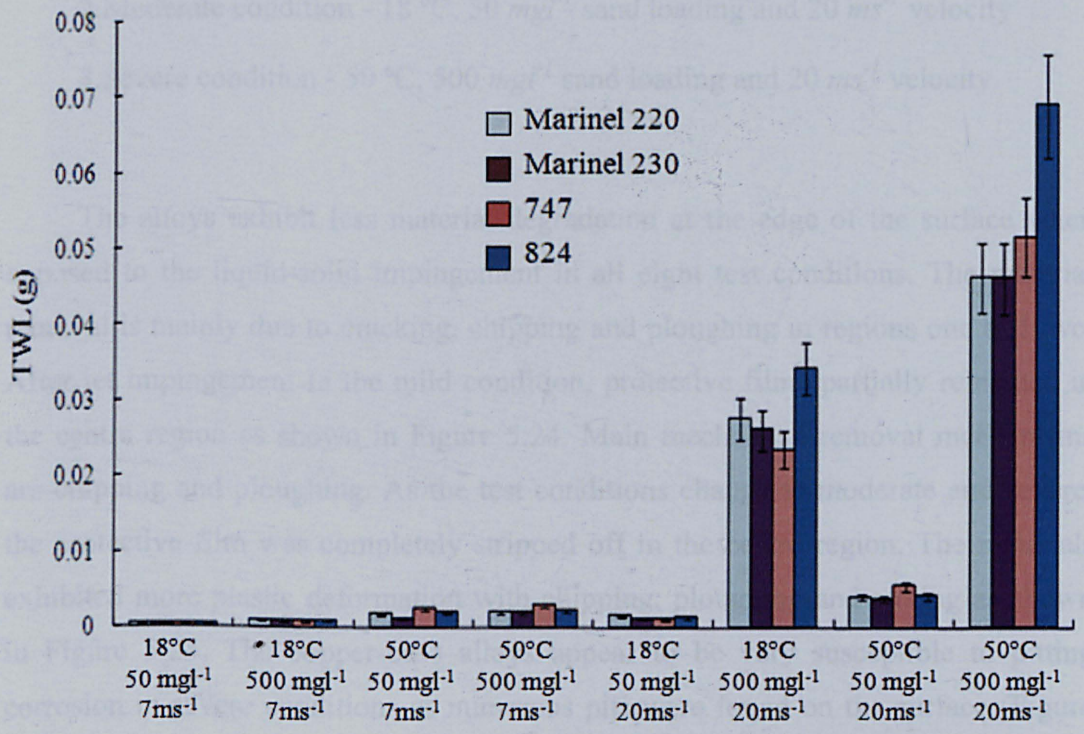

Figure 5.23: Total weight loss of copper based alloys at eight conditions

According to the total weight loss of copper based alloys under eight conditions in this study, the higher total weight loss occurred at high velocity and high sand loading which can result in a high impact energy.

5.2.1 Surface analysis of copper-base alloys

The same surface analysis method to stainless steels was applied to copper-base alloys to study the degradation mechanisms in different zones across the surface after liquid-solid impingement. In addition, film adhesion and surface microhardness analysis were conducted to improve the understanding of the erosion-corrosion characteristics of copper-base alloys. In this study, with consideration of kinetic and thermodynamic aspects, three representative conditions were chosen to

analyse the damaged surface of copper-base alloys after the jet impingement erosion-corrosion tests:

1.Mild condition – 18 °C, 50 mgl^{-1} sand loading and 7 ms^{-1} velocity

2.Moderate condition - 18 °C, 50 mgl^{-1} sand loading and 20 ms^{-1} velocity

3.Severe condition - 50 °C, 500 mgl^{-1} sand loading and 20 ms^{-1} velocity

The alloys exhibit less material degradation at the edge of the surface when exposed to the liquid-solid impingement in all eight test conditions. The material removal is mainly due to cracking, chipping and ploughing in regions one and two. After jet impingement in the mild condition, protective films partially remained in the centre region as shown in Figure 5.24. Main mechanical removal mechanisms are chipping and ploughing. As the test conditions change to moderate and severe, the protective film was completely stripped off in the centre region. The materials exhibited more plastic deformation with chipping, ploughing and cutting as shown in Figure 5.25. The copper-base alloys appear to be very susceptible to pitting corrosion in severe conditions as numerous pits were found on the surface (Figure 5.26).

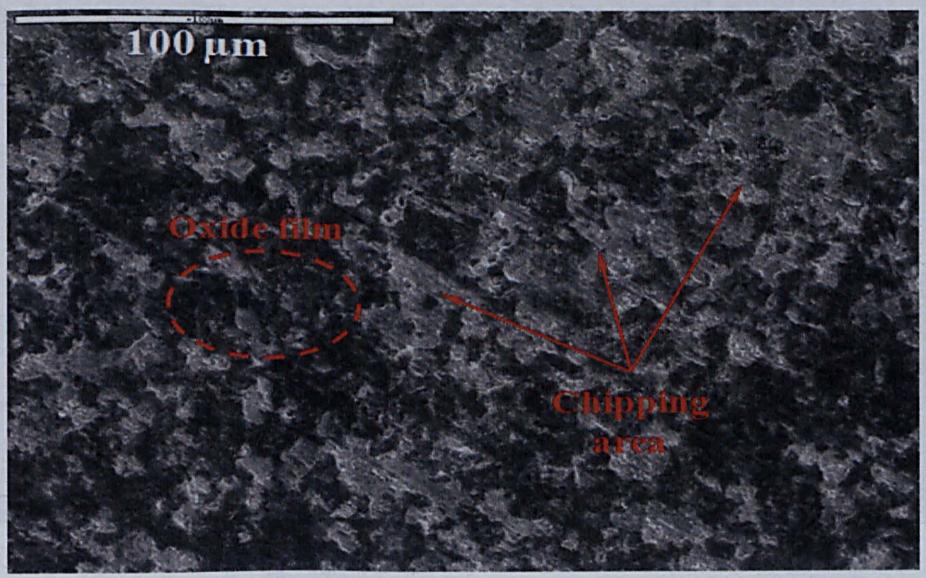

Figure 5.24: The surface morphology in region one of Marinel 230 after jet impingement erosion-corrosion test at 18°C, 7 ms^{-1} and 50 mgl^{-1}

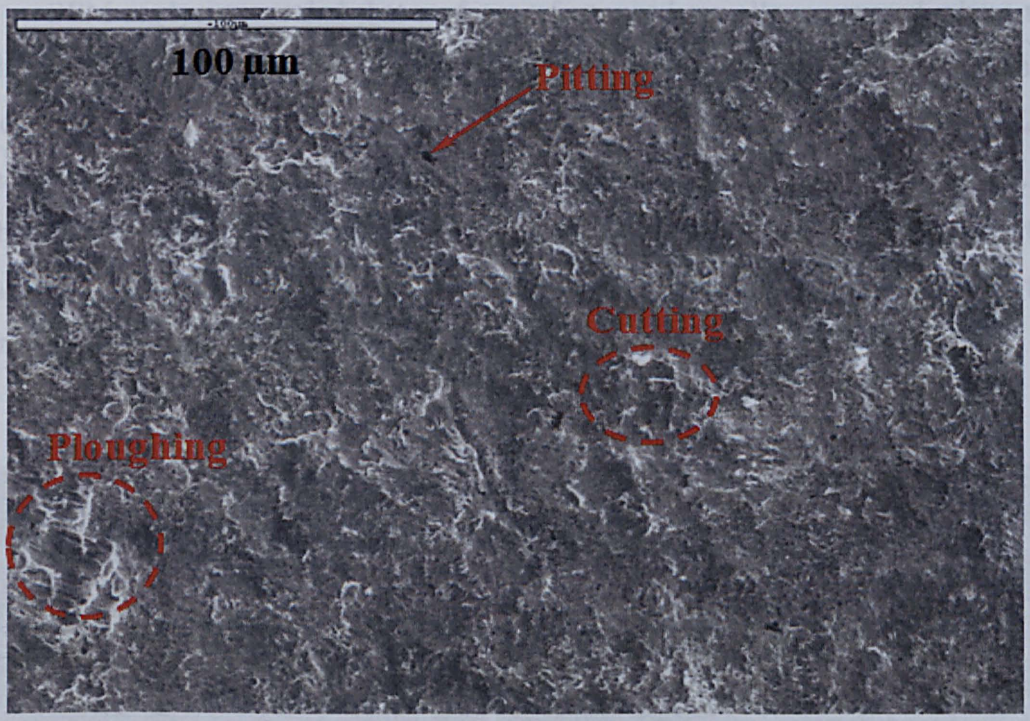

Figure 5.25: The surface morphology in region one of Marinel 230 after jet impingement erosion-corrosion test at 18°C, 20 ms^{-1} and 50 mgl^{-1}

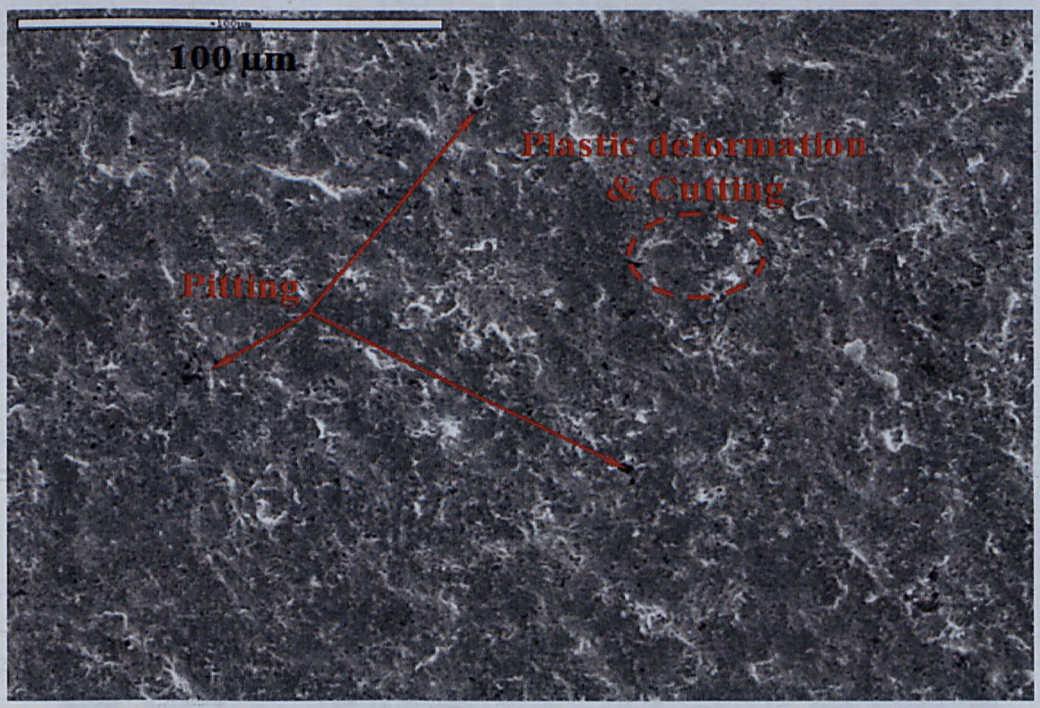

Figure 5.26: The surface morphology in region one of Marinel 230 after erosion-corrosion test at 50 °C, 20 ms^{-1} and 500 mgl^{-1}

SEM analysis revealed that surfaces of copper-base alloys covered where the films remained were distinguished by a darker shade (Figure 5.27). The alloying element composition was determined by EDX analysis (Figure 5.28, Figure 5.29) showing that the films of copper-base alloys are enriched with oxygen (Table 5.2). The film cracking initiation and propagation resulted in a lower adhesion on the surface. Therefore, the unattached protective films can be then chipped off from the surface by liquid solid impingement (Figure 5.27).

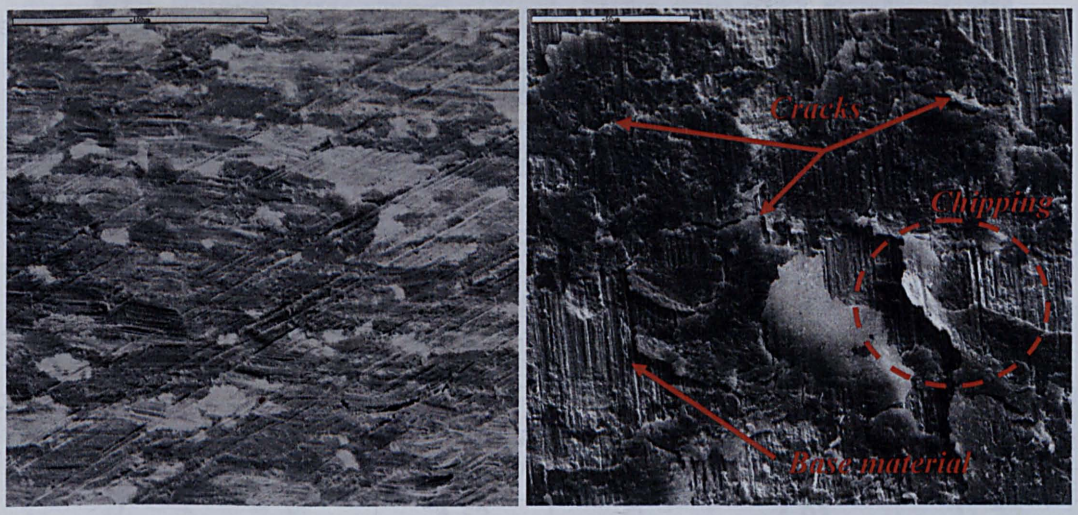

(a) (b)

Figure 5.27: (a) the surface partially covered by the protective films after impingement jet test; (b) removal mechanism of protective film of copper-base alloys

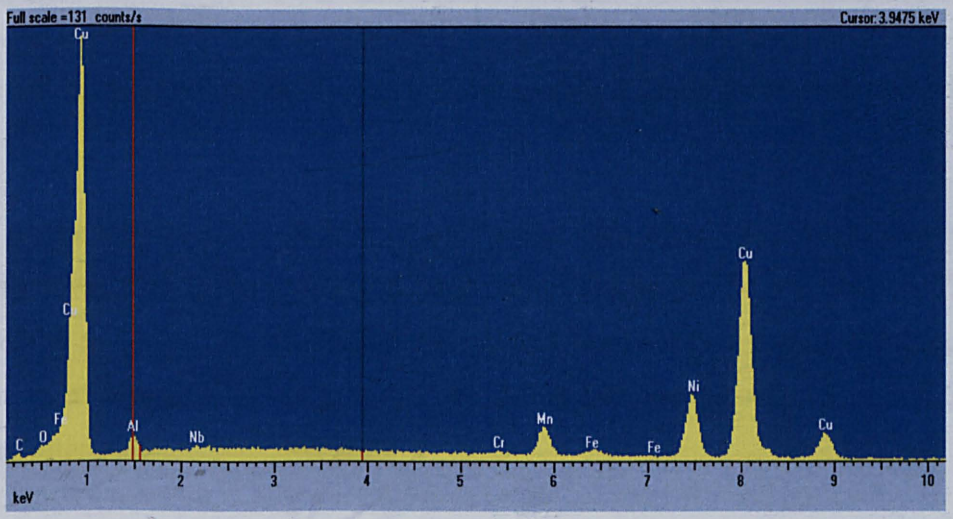

Figure 5.28: The alloying element composition in light area (no protective film) by EDX analysis

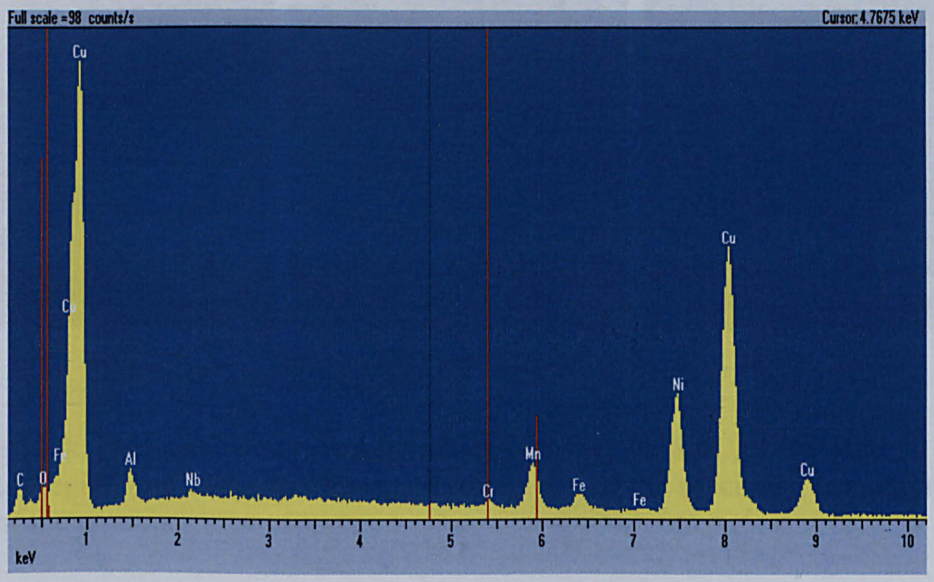

Figure 5.29: The alloying element composition in dark area (protective film) by EDX analysis

Light area			Black area		
Element	Element%	Atomic%	Element	Element%	Atomic%
Al	2.02	4.52	*O*	6.93	21.70
Cr	0.33	0.39	*Al*	2.59	4.81
Mn	4.27	4.70	*Cr*	0.55	0.53
Fe	0.68	0.74	*Mn*	4.16	3.79
Ni	17.74	18.28	*Fe*	1.36	1.22
Cu	74.95	71.36	*Ni*	21.15	18.05
Total	100	100	*Cu*	63.26	49.89
			Total	100	100

Table 5.2: Alloying element and atomic composition in the areas with and without protective films

As the impingement angle decreased away from the centre area of the surface (Figure 5.30), the erosion-corrosion degradation appears to be less severe. This is considered to be due to less impact energy and lower impact angles resulting in a transition of damage from impact to shear. More film can be seen to remain on the surface after erosion-corrosion tests.

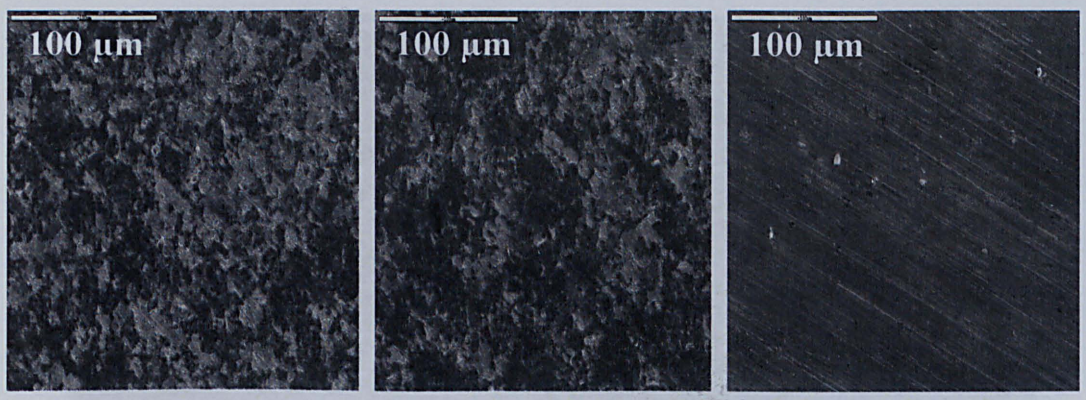

(a) (b) (c)

Figure 5.30: The surface morphology of Marinel 230 at 18 °C, 7 ms^{-1} and 50 mgl^{-1}: (a) region one of the specimen; (b) region two of the specimen; (c) region three of the specimen

The amount of oxide layer remained on the surface (Figure 5.31) after jet impingement was analysed by the surface analysis software Aequitas IA (Figure 5.32). Marinel 230 exhibits the highest adhesion ability at the same condition (Table 5.3).

	18°C 7m/s 50mg/l	
	Protective percentage	Naked metal percentage
Marinel 220	65.9%	34.1%
Marinel 230	70.5%	29.5%
747	63.9%	36.1%
824	37.9%	62.1%

Table 5.3: Remained amount of protective films surface analysis

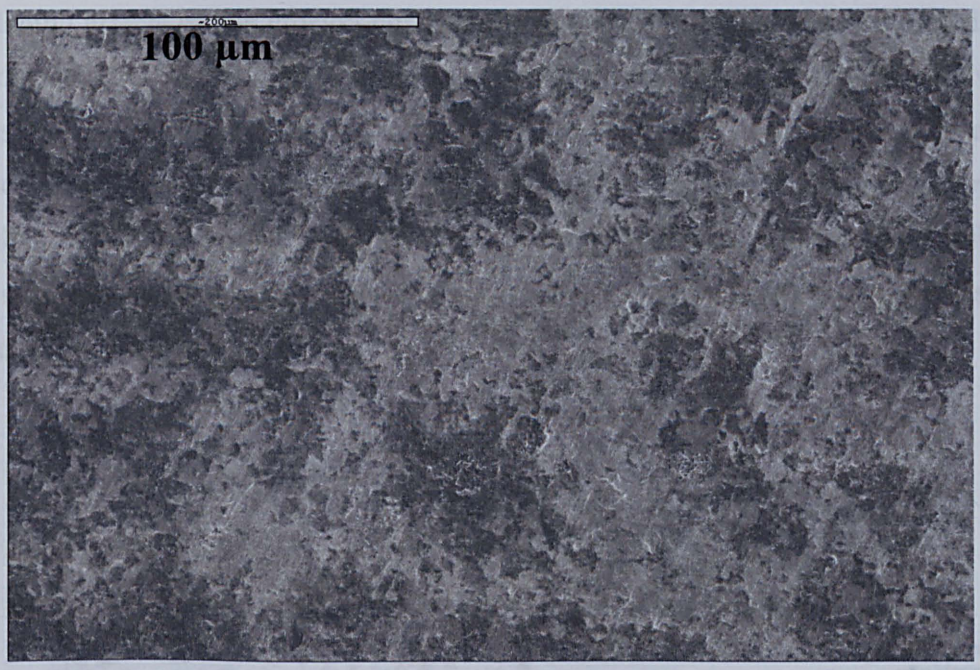

Figure 5.31: The surface morphology in region one of 824 after jet impingement erosion-corrosion test at 18°C, 7 ms^{-1} and 50 mgl^{-1}

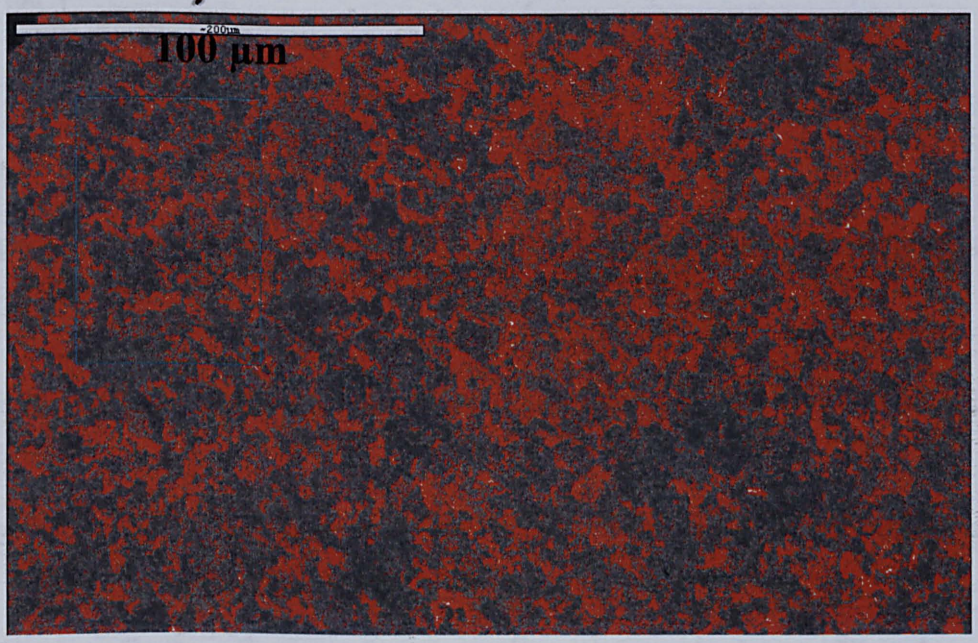

Figure 5.32: The interface of Surface analysis software Aequitas IA

The mechanical properties of materials are often used to determine susceptibility of material removal in an erosion environment. However, the microhardness has not been accepted as a criterion of the erosion-corrosion resistances of different materials. In this study to investigate the surface work

hardening effects on the erosion-corrosion resistance of materials the microhardness distributions across the surfaces after tested in the most severe condition were measured. Figure 5.33 shows that the highest microhardness values are observed in the centre of the specimens due to high frequency impacts of liquid-solid which resulted in greatest surface work hardening. Comparing the microhardness profile of the surface, measured before and after liquid-solid impingement, two interesting features can be found:

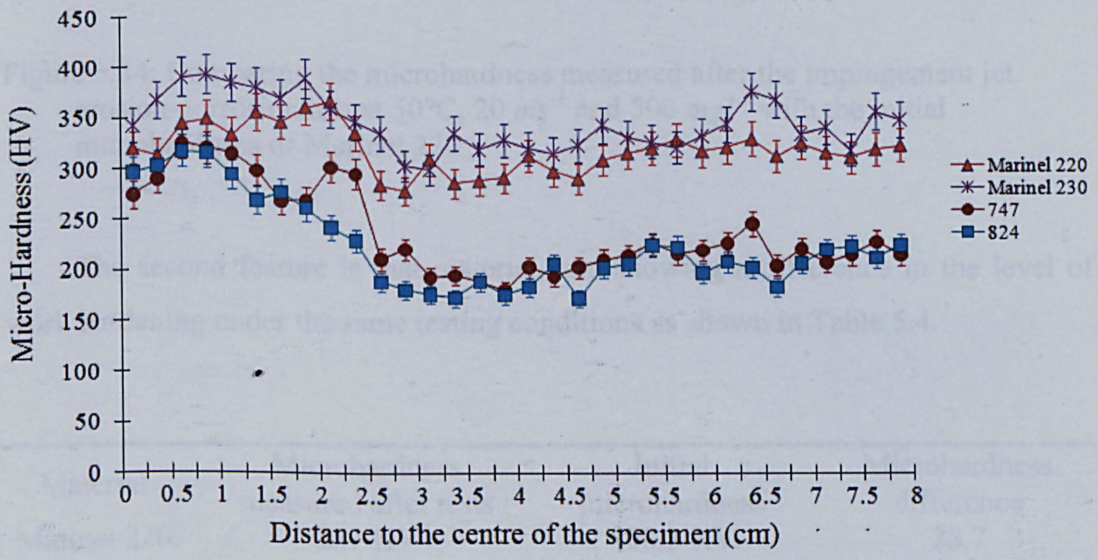

Figure 5.33: Microhardness distributions on the specimens after impingement jet erosion-corrosion test at 50 °C, 20 ms^{-1} and 500 mgl^{-1}

The changes of the microhardness is dependent on the impact angle (Figure 5.34):

a) High angle (zone 1) – great degree of surface work hardening occurs due to most solid particle impacts

b) Acute angle (zone 2) – corrosion dominant region, which reduces the microhardness compared with the initial microhardness.

c) Low angle (zone 3) – covered by the preformed oxide films, which results in a higher microhardness than the initial microhardness.

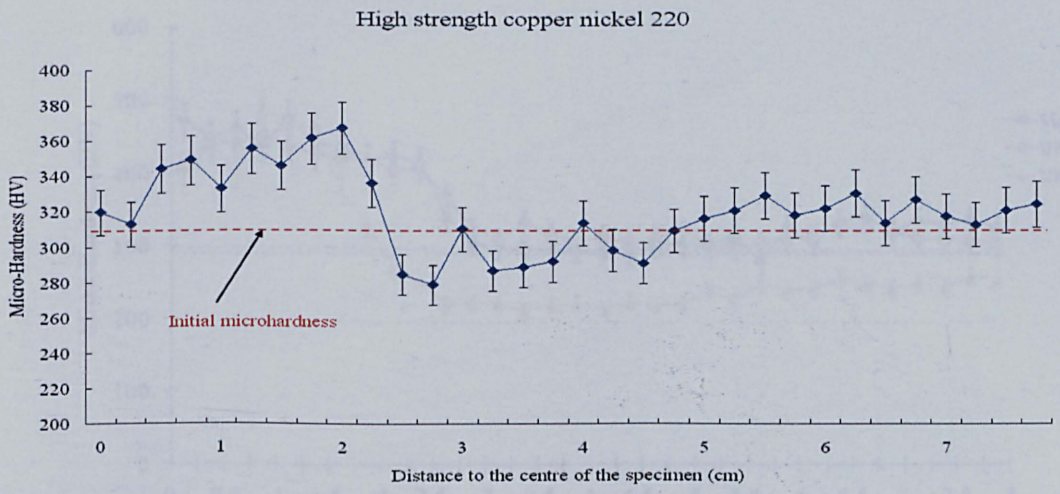

Figure 5.34: Comparing the microhardness measured after the impingement jet erosion-corrosion test at 50°C, 20 ms^{-1} and 500 mgl^{-1} with the initial microhardness of Marinel 220

The second feature is that materials are showing a difference in the level of work hardening under the same testing conditions as shown in Table 5.4.

Material	Microhardness measured after tests	Initial microhardness	Microhardness difference
Marinel 220	337 HV	308.3 HV	28.7
Marinel 230	375 HV	325.6 HV	49.4
747	299 HV	192.7 HV	105.7
824	295 HV	177.7 HV	117.8

Table 5.4: Difference of microhardness measured after the tests from the initial microhardness

Compared with copper based alloys, stainless steel alloys exhibit a similar hardness distribution from the centre region towards the edge of the specimen (Figure 5.35). The electrochemical processes (depassivation-repassivation) in zone 2 show no effect on the material hardness. Compared with Vistar and UNS S32760, UNS S31603 shows a greater hardness increment caused by work hardening. The correlation of hardness and the total weight loss will be discussed in the discussion chapter.

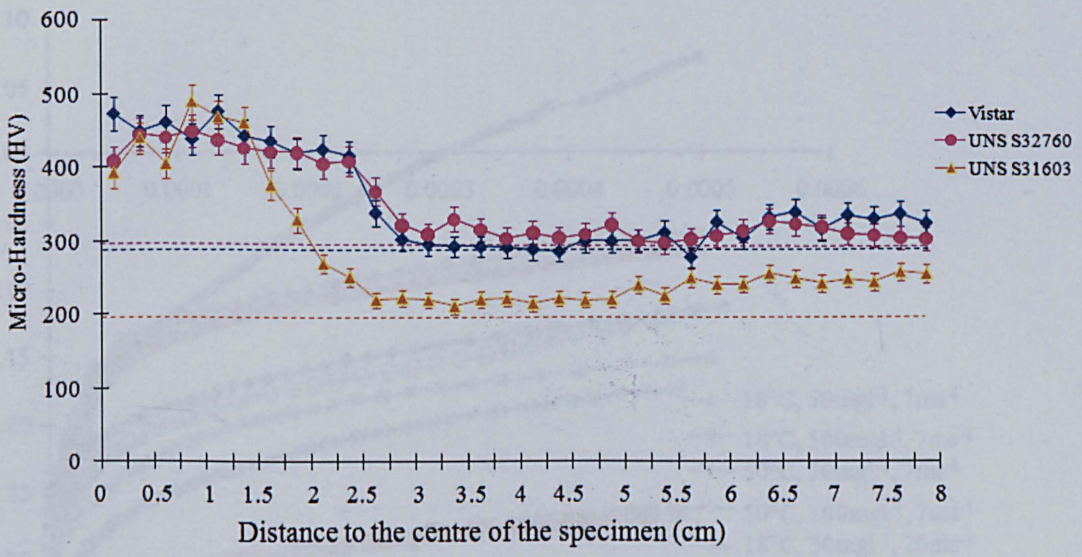

Figure 5.35: Microhardness distributions on the specimens after impingement jet erosion-corrosion test at 50 °C, 20 ms^{-1} and 500 mgl^{-1}

5.2.2 Corrosion behaviour of copper-base alloys under liquid-solid impingement.

A typical set of anodic polarisation curves subjected to impingement are shown from Figure 5.36 to Figure 5.39, from which the copper-base alloys exhibit behaviour which is not classified as "passive" but which is also not what would be referred to as "active" behaviour. Hence in this study, such anodic polarization curve is referred as "low current active" under liquid-solid impingement. Compared with active behaviour which shows an instant increase in current density as potentio increases, low current active exhibits an initial low increment of current density during polarization (*e.g.* $20\mu A/cm^2$ for a range of $150mV$) followed by a rapid increase in current density indicating a general dissolution of material. Materials 220, 230 and 824 exhibit more active behaviour as velocity, sand loading and temperature increase.

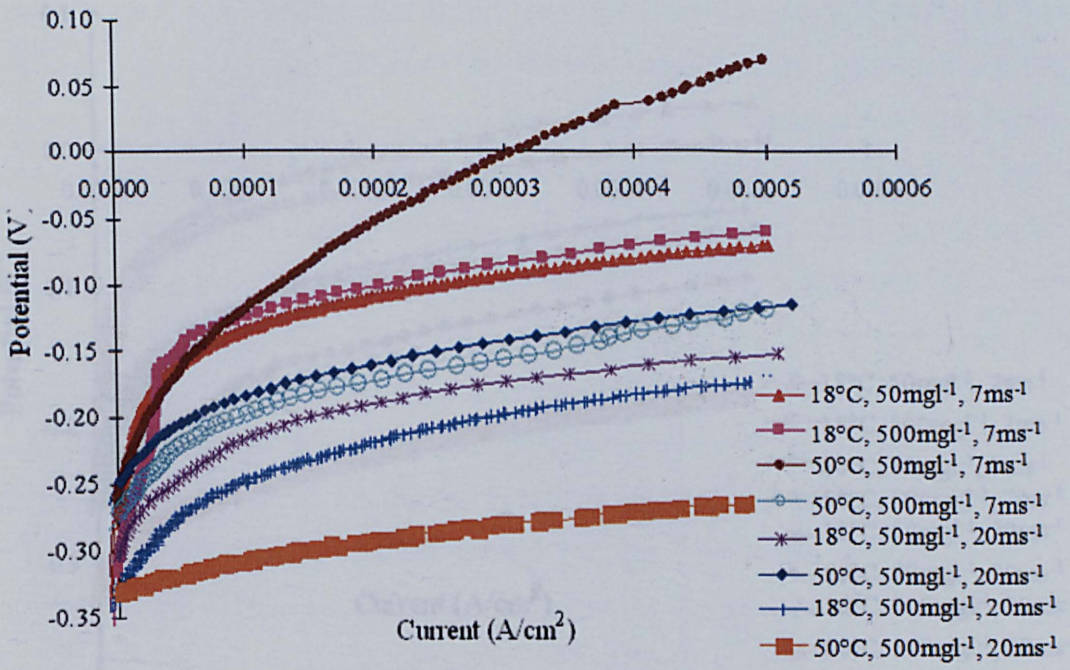

Figure 5.36: Anodic polarization curves for Marinel 220 at eight conditions

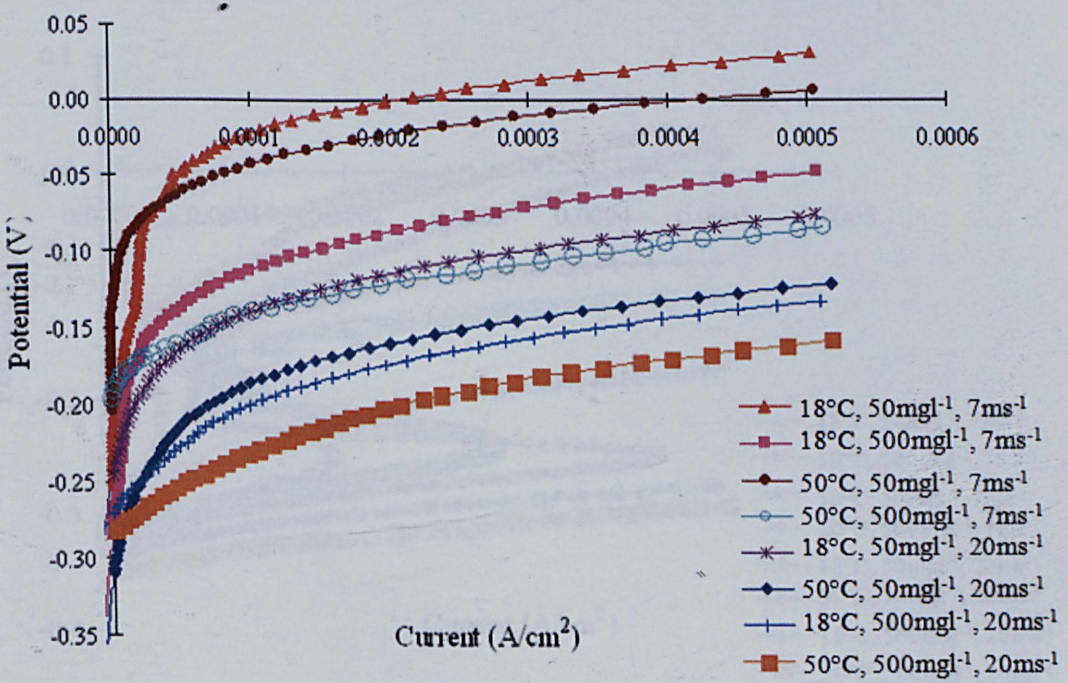

Figure 5.37: Anodic polarization curves for Marinel 230 at eight conditions

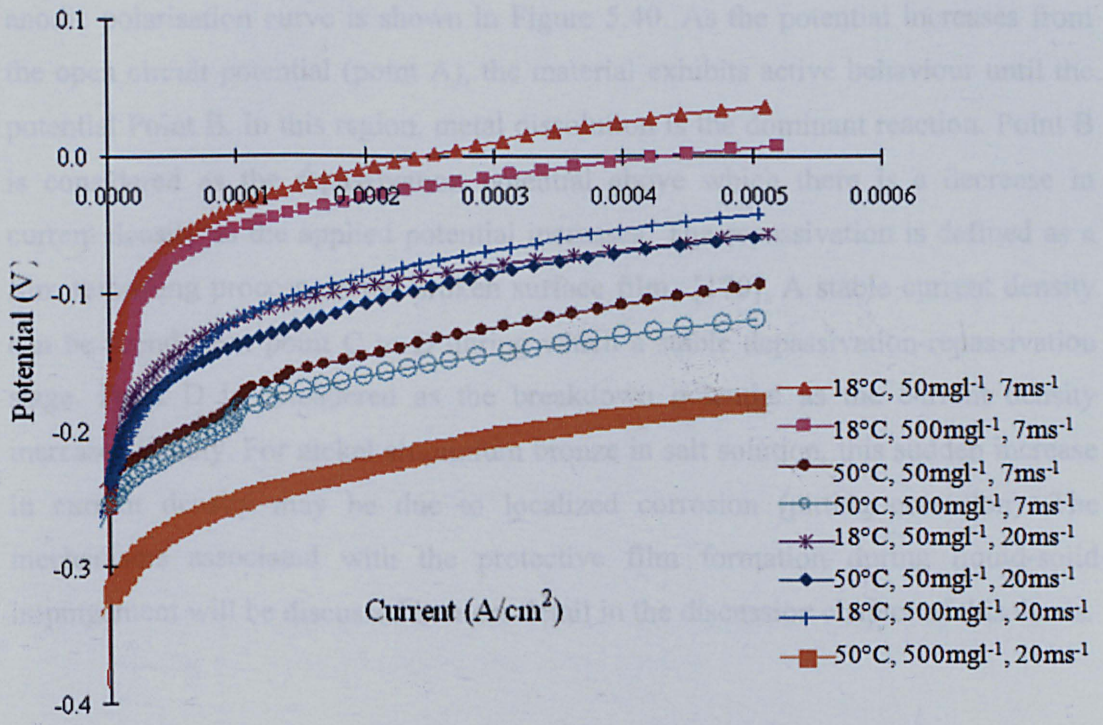

Figure 5.38: Anodic polarization curves for 824 at eight conditions

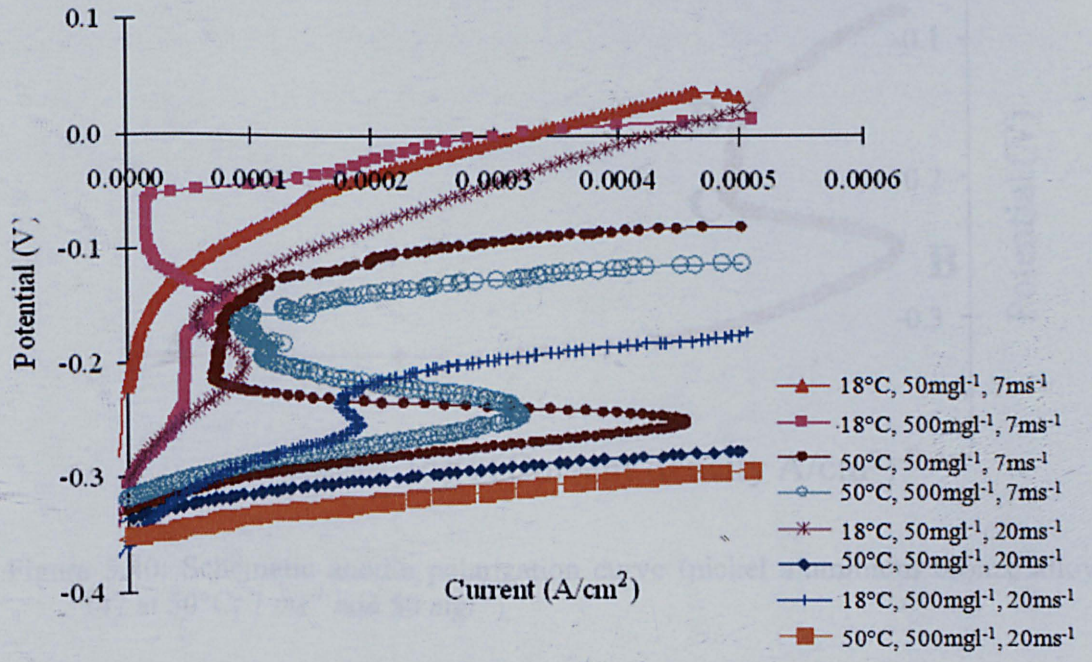

Figure 5.39: Anodic polarization curves for 747 at eight conditions

Nickel aluminium bronze alloy 747 exhibits more complex corrosion behaviour (Figure 5.39) than the other copper-base alloys in this study. A schematic

anodic polarisation curve is shown in Figure 5.40. As the potential increases from the open circuit potential (point A), the material exhibits active behaviour until the potential Point B. In this region, metal dissolution is the dominant reaction. Point B is considered as the repassivation potential above which there is a decrease in current density as the applied potential increases. The repassivation is defined as a film reforming process on the broken surface film [170]. A stable current density can be found from point C to D during which a stable depassivation-repassivation stage. Point D is considered as the breakdown potential as the current density increases rapidly. For nickel aluminium bronze in salt solution, this sudden increase in current density may be due to localized corrosion (pitting corrosion). The mechanisms associated with the protective film formation during liquid-solid impingement will be discussed in more detail in the discussion chapter of this thesis.

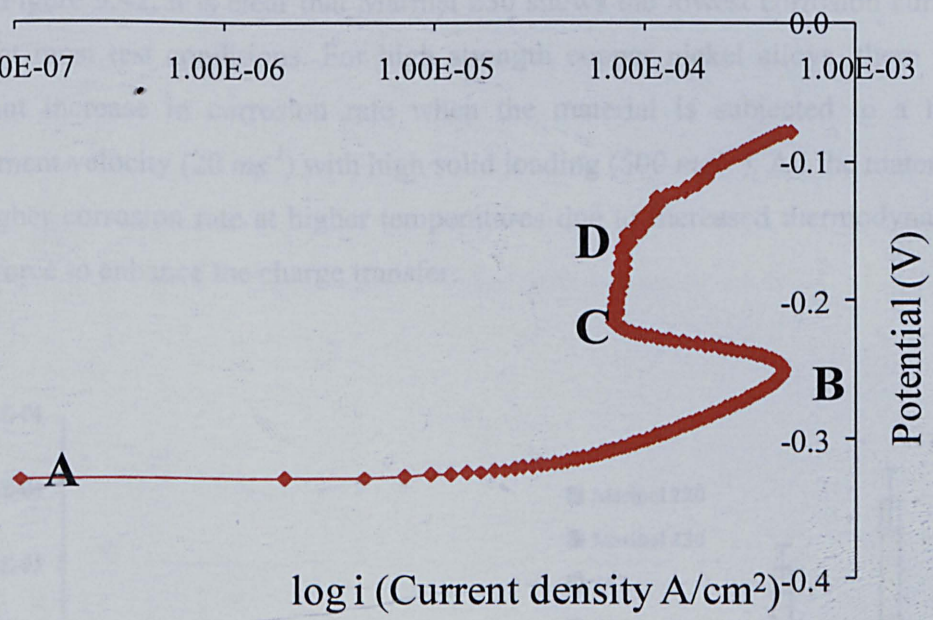

Figure 5.40: Schematic anodic polarization curve (nickel aluminium bronze alloy 747 at 50°C, 7 ms^{-1} and 50 mgl^{-1})

To determine the *in-situ* electrochemical corrosion rate during erosion-corrosion, the conventional Tafel extrapolation method is used to determine the corrosion current density (Figure 5.41) and calculation of corrosion rate is made according to Faraday's law as presented previously.

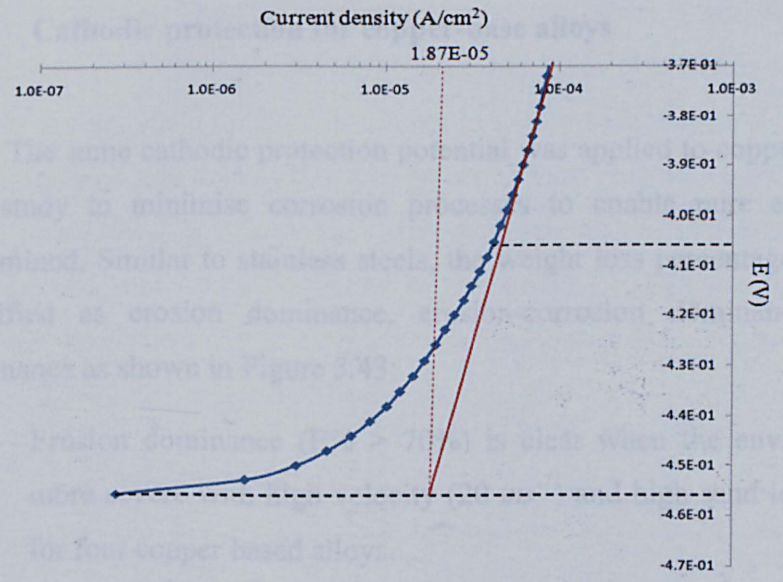

Figure 5.41: Tafel extrapolation to determine corrosion current density for 747 at 18°C, 20 ms^{-1} velocity and 50 mgl^{-1} sand loading

In Figure 5.42, it is clear that Marinel 230 shows the lowest corrosion current density at most test conditions. For high strength copper nickel alloys, there is a significant increase in corrosion rate when the material is subjected to a high impingement velocity (20 ms^{-1}) with high solid loading (500 mgl^{-1}). All the materials show higher corrosion rate at higher temperatures due to increased thermodynamic driving force to enhance the charge transfer.

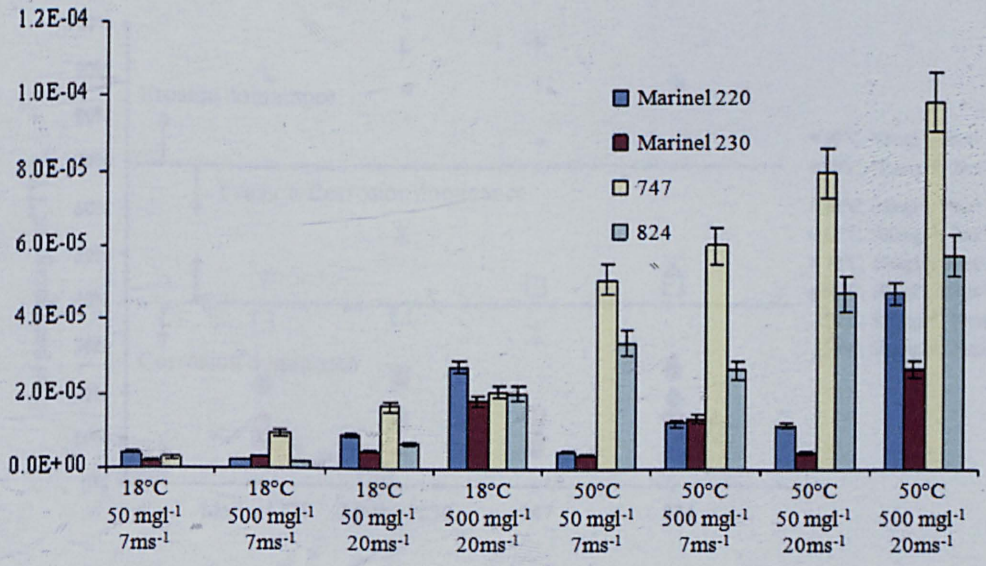

Figure 5.42: Corrosion current densities for copper-base alloys at eight conditions

5.2.3 Cathodic protection for copper-base alloys

The same cathodic protection potential was applied to copper-base alloys to in this study to minimise corrosion processes to enable pure erosion rate to be determined. Similar to stainless steels, the weight loss percentage due to erosion is classified as erosion dominance, erosion-corrosion dominance and corrosion dominance as shown in Figure 5.43:

- Erosion dominance (E% > 70%) is clear when the environment becomes more severe with high velocity (20 ms^{-1}) and high sand loading (500 mgl^{-1}) for four copper based alloys.
- For high strength copper nickel alloys, the transition condition of dominant process between erosion dominant and corrosion dominant is 18 °C with 20 ms^{-1} velocity and 50 mgl^{-1} sand loading.
- The transition conditions of dominant process of copper nickel chrome alloy 824 between erosion dominant and corrosion dominant are located at low temperature with intermediate impact energy.
- Nickel aluminium bronze alloy 747 exhibits corrosion dominant at high temperature with low or intermediate impact energy. At low temperature, erosion of the material is enhanced when sand loading increases.

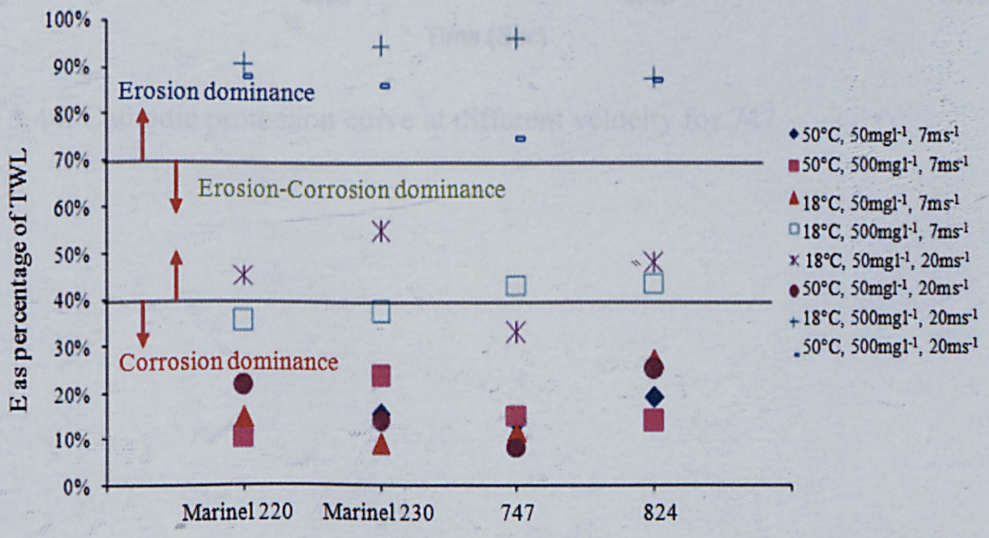

Figure 5.43: Mass loss due to pure erosion as a percentage of total weight loss for four copper based alloys at eight conditions

The current density during cathodic protection tests was measured as a function of time. The general trend of current density is stable under potentiostatic control for copper-base alloys as shown in Figure 5.44, Figure 5.45 and Figure 5.46. From dynamic and thermodynamic points of view, higher velocity and temperature result in higher oxygen diffusion rates. Oxygen will be delivered to more exposed surface with more sand contained in the solution. Therefore, the current density exhibited more negative at a higher velocity, temperature and solid loading, which results in a greater oxygen diffusion rate.

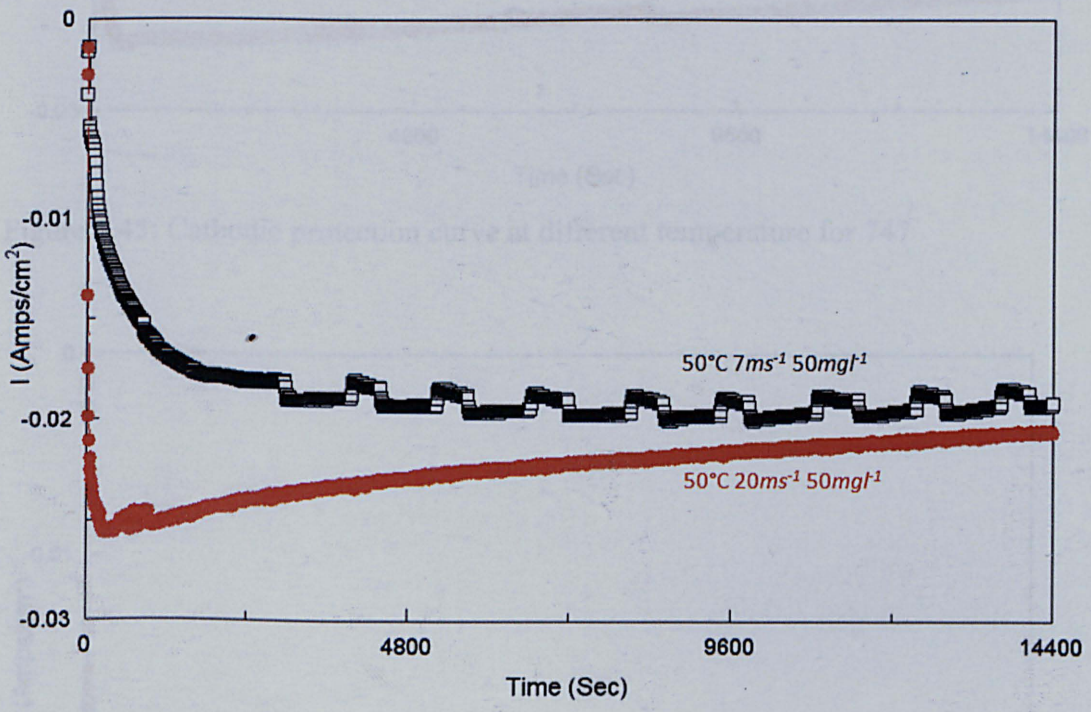

Figure 5.44: Cathodic protection curve at different velocity for 747

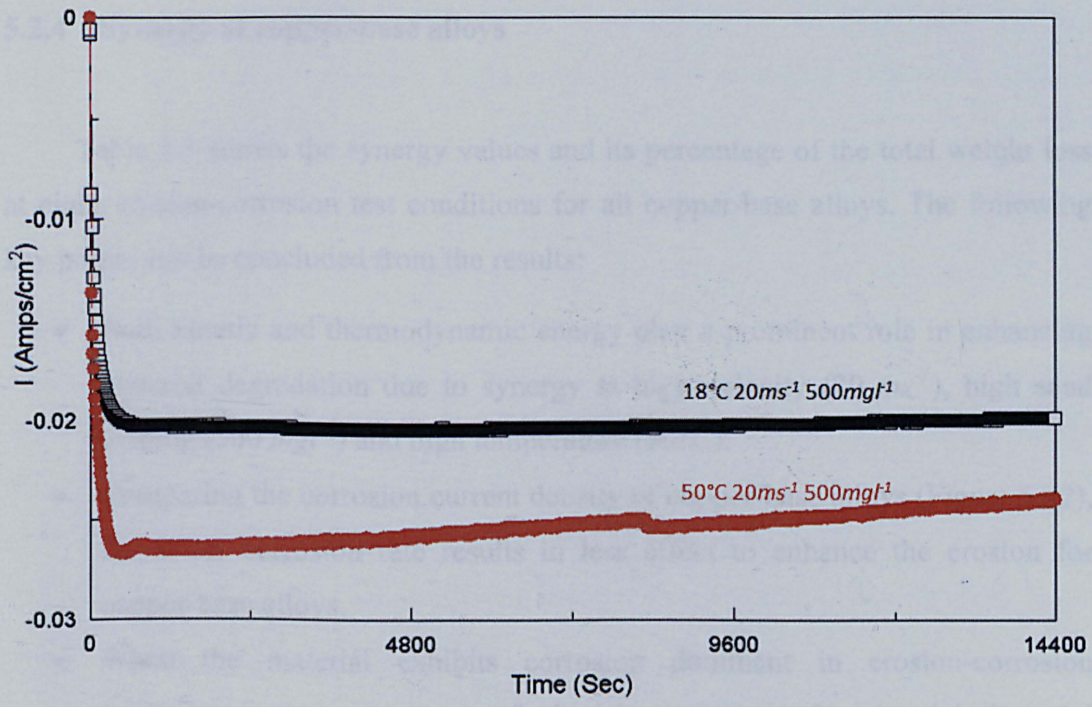

Figure 5.45: Cathodic protection curve at different temperature for 747

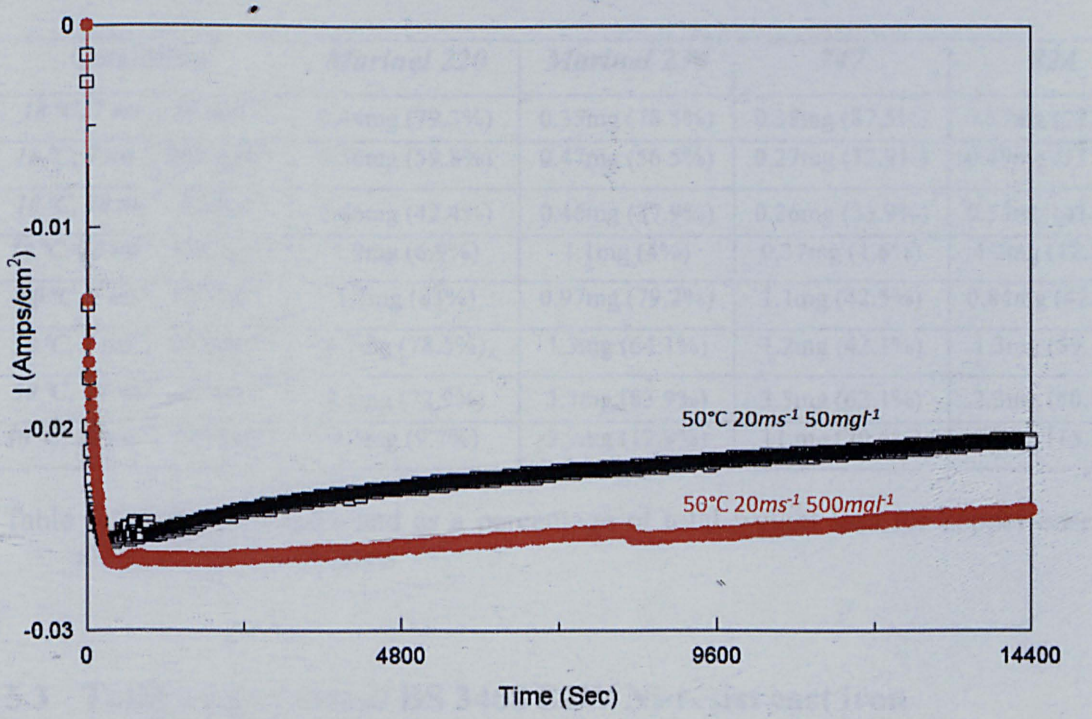

Figure 5.46: Cathodic protection curve at different sand loading for 747

5.2.4 Synergy of copper-base alloys

Table 5.5 shows the synergy values and its percentage of the total weight loss at eight erosion-corrosion test conditions for all copper-base alloys. The following key points can be concluded from the results:

- Both kinetic and thermodynamic energy play a prominent role in enhancing material degradation due to synergy at high velocity (20 ms^{-1}), high sand loading (500 mgl^{-1}) and high temperature (50°C).
- Comparing the corrosion current density of copper-base alloys (Figure 5.42), the lower corrosion rate results in less effect to enhance the erosion for copper-base alloys.
- When the material exhibits corrosion dominant in erosion-corrosion environment, synergy accounts for higher percentage of total weight loss and *vice versa.*

Conditions	*Marinel 220*	*Marinel 230*	*747*	*824*
18 °C, 7 ms^{-1}, 50 mgl^{-1}	0.44mg (79.3%)	0.35mg (78.5%)	0.38mg (87.5%)	0.37mg (72.4%)
18 °C, 7 ms^{-1}, 500 mgl^{-1}	0.56mg (59.8%)	0.47mg (56.5%)	0.27mg (32.9%)	0.49mg (52.5%)
18 °C, 20 ms^{-1}, 50 mgl^{-1}	0.66mg (42.4%)	0.46mg (37.9%)	0.36mg (33.9%)	0.57mg (41.2%)
18 °C, 20 ms^{-1}, 500 mgl^{-1}	1.9mg (6.9%)	1.1mg (4%)	0.37mg (1.6%)	4.2mg (12.3%)
50 °C, 7 ms^{-1}, 50 mgl^{-1}	1.5mg (83%)	0.97mg (79.2%)	1.1mg (42.5%)	0.84mg (42.4%)
50 °C, 7 ms^{-1}, 500 mgl^{-1}	1.7mg (78.5%)	1.3mg (64.1%)	1.2mg (42.1%)	1.3mg (59.1%)
50 °C, 20 ms^{-1}, 50 mgl^{-1}	3.1mg (72.9%)	3.3mg (83.9%)	3.5mg (62.1%)	2.3mg (50.8%)
50 °C, 20 ms^{-1}, 500 mgl^{-1}	4.5mg (9.7%)	5.9mg (12.9%)	11 mg (20.6%)	8.3mg (15.3%)

Table 5.5: Synergy values and as a percentage of total weight loss for copper-base alloys at eight conditions

5.3 Total weight loss of BS 3468 S2W Ni-resist cast iron

A systematic study on erosion-corrosion of Ni-resist cast iron was reported [122]. In this study, Ni-resist cast iron is used to compare the erosion-corrosion resistance with other cast stainless steels and copper-base alloys to enable an integrated material selection envelope to be established. In this section, the total

weight loss, erosion, corrosion and their interactions of Ni-resist cast iron are presented with surface analyses to improve the understanding of the degradation mechanisms.

Results from total weight loss measurements under liquid-solid jet impingement at eight conditions are plotted in Figure 5.47. The highest total weight loss value can be found at the most severe environment with 20 ms^{-1} velocity, 500 mgl^{-1} sand loading and at 50 °C. It is clearly shown that the kinetic energy of the solid particle impact plays a prominent role. The environmental effect on total weight loss in erosion-corrosion environment is also demonstrated in Figure 5.47. The increase in individual environmental parameter results in an acceleration of the mass loss rate under erosion-corrosion.

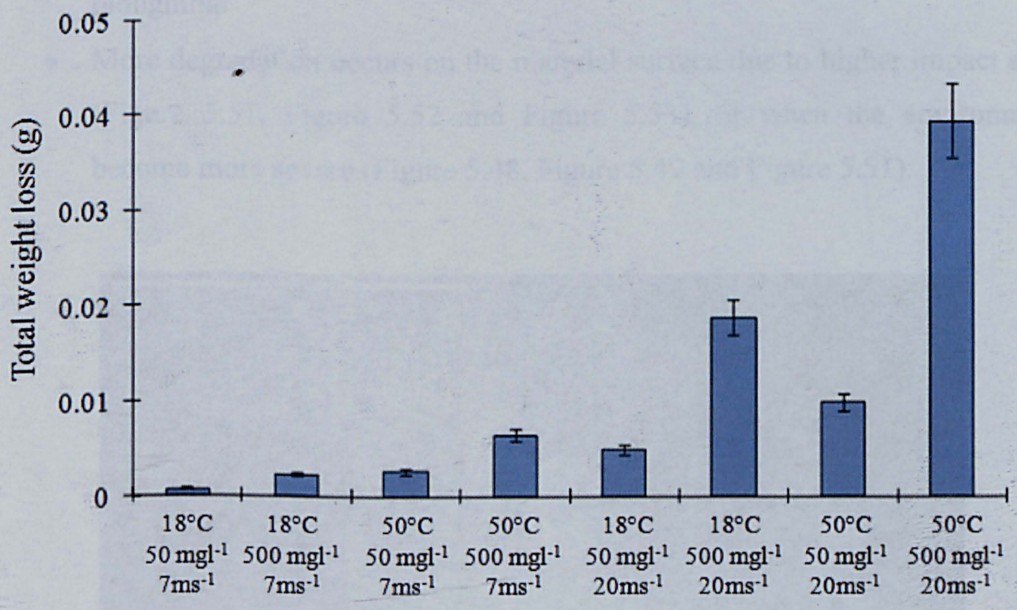

Figure 5.47: Total weight loss for BS 3468 S2W in the eight conditions

5.3.1 Surface analysis of BS 3468 S2W Ni-resist cast iron

The surface morphology analysis has been conducted by SEM for surface exposed to mild, moderate and severe conditions:

- In the mild conditions, the material degradation is caused by the graphite removal, ploughing in the main matrix and corrosion (Figure 5.48). The environment has few mechanical effects on the rest of the matrix in Ni-resist cast iron due to its good mechanical properties. The removal mechanism of graphite results from a consequence of mechanical impact, crack and removal. Corrosion product formed on the surface can also result in the low adhesion of graphite to the metal matrix.
- In moderate conditions, no graphite is left in region 1 due to higher impact energy, the surface shows severe degradation compared with mild condition (Figure 5.49). Higher velocity enhances the turbulence of the flow, which enables more solids impacting on the surface in low angles resulting in more material degradation (Figure 5.50).
- In the severe condition, no graphite is left in region 1 and 2 (Figure 5.51 and Figure 5.52). Surface degradation includes severe cracks and wider range of ploughing.
- More degradation occurs on the material surface due to higher impact angle (Figure 5.51, Figure 5.52 and Figure 5.53), or when the environments become more severe (Figure 5.48, Figure 5.49 and Figure 5.51).

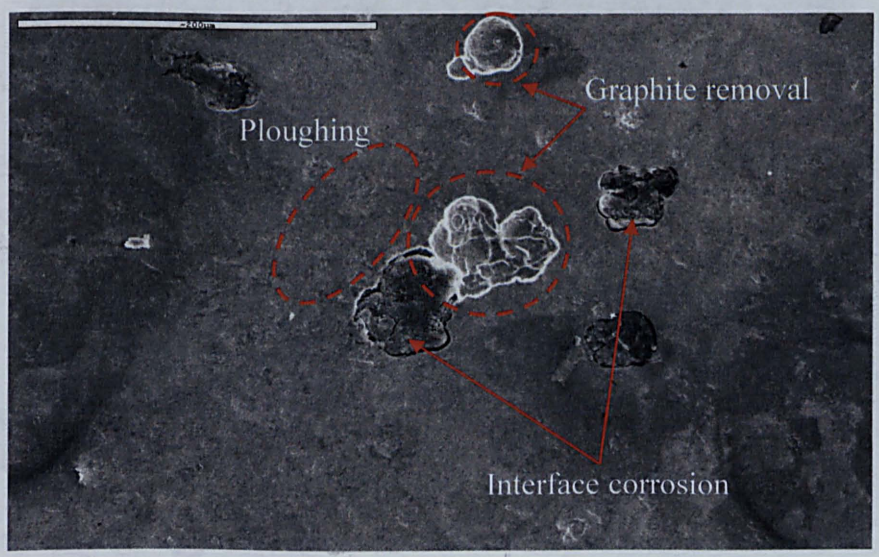

Figure 5.48: Surface morphology of BS 3468 S2W in region one at 18°C, 7 ms^{-1} velocity and 50 mgl^{-1} sand loading

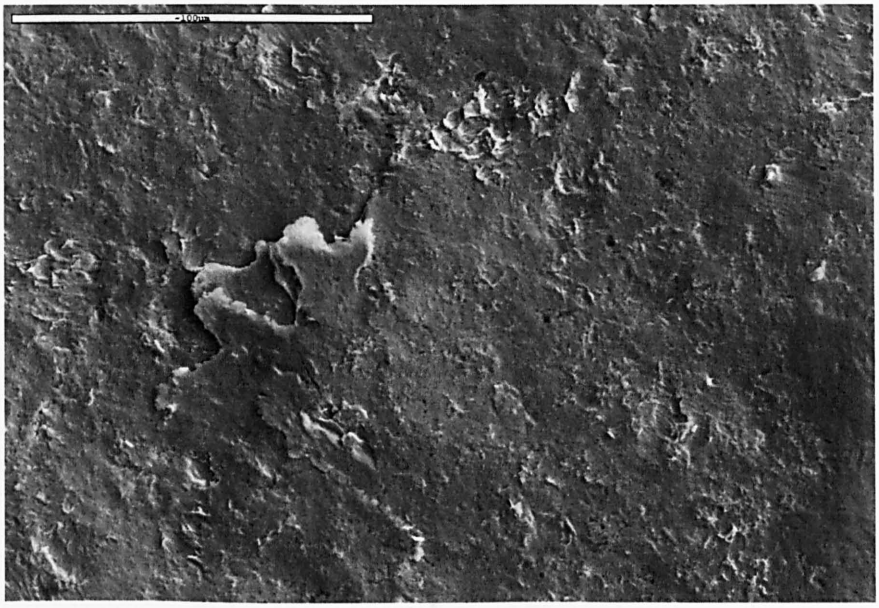

Figure 5.49: Surface morphology of BS 3468 S2W in region one at 18°C, 20 ms^{-1} velocity and 50 mgl^{-1} sand loading

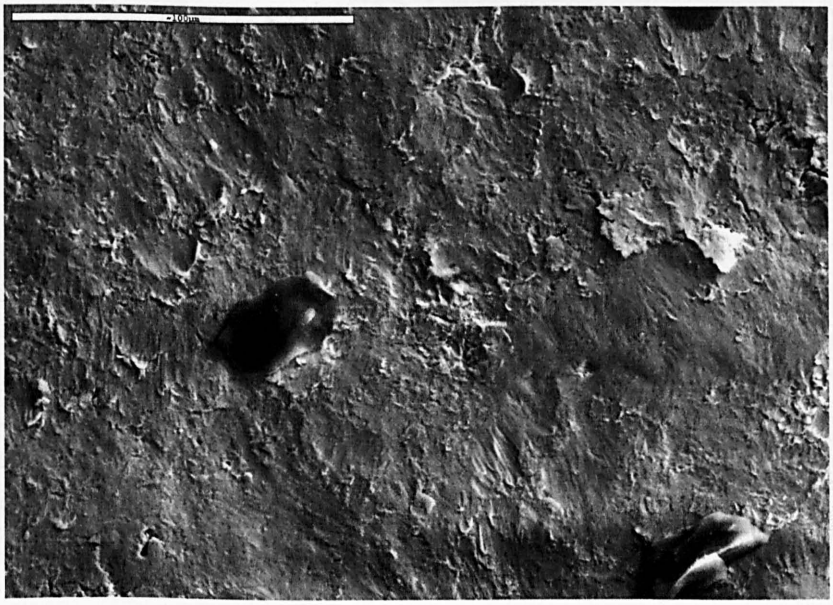

Figure 5.50: Surface morphology of BS 3468 S2W in region two at 18°C, 20 ms^{-1} velocity and 50 mgl^{-1} sand loading

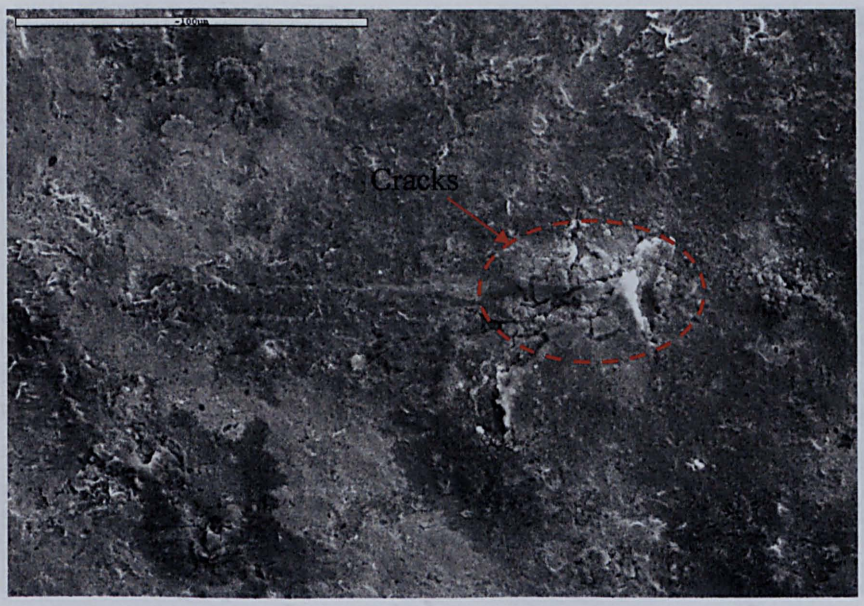

Figure 5.51: Surface morphology of BS 3468 S2W in region one at 50°C, 20 ms^{-1} velocity and 500 mgl^{-1} sand loading

Figure 5.52: Surface morphology of BS 3468 S2W in region two at 50°C, 20 ms^{-1} velocity and 500 mgl^{-1} sand loading

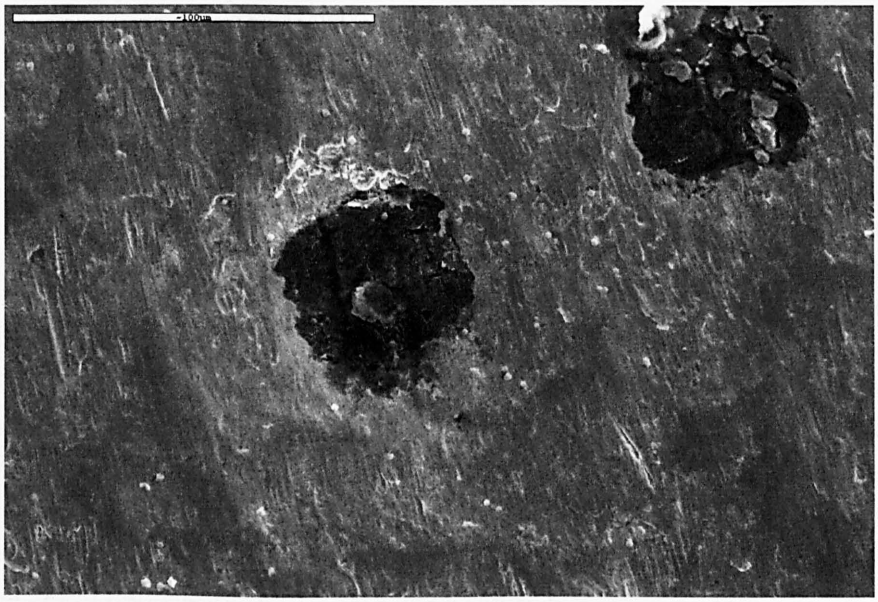

Figure 5.53: Surface morphology of BS 3468 S2W in region three at 50°C, 20 ms^{-1} velocity and 500 mgl^{-1} sand loading

5.3.2 Corrosion behaviour of BS 3468 S2W Ni-resist cast iron under solid-liquid impingement

Anodic polarisation curves are plotted for eight conditions under liquid-solid impingement and BS 3468 S2W shows active behaviour as shown in Figure 5.54. Current density for BS 3468 S2W at eight conditions is then determined from (Figure 5.55). The highest current density is observed when Ni-resist cast iron is exposed to jet impingement with 20 ms^{-1} velocity, 500 mgl^{-1} sand loading and at 50 °C temperature.

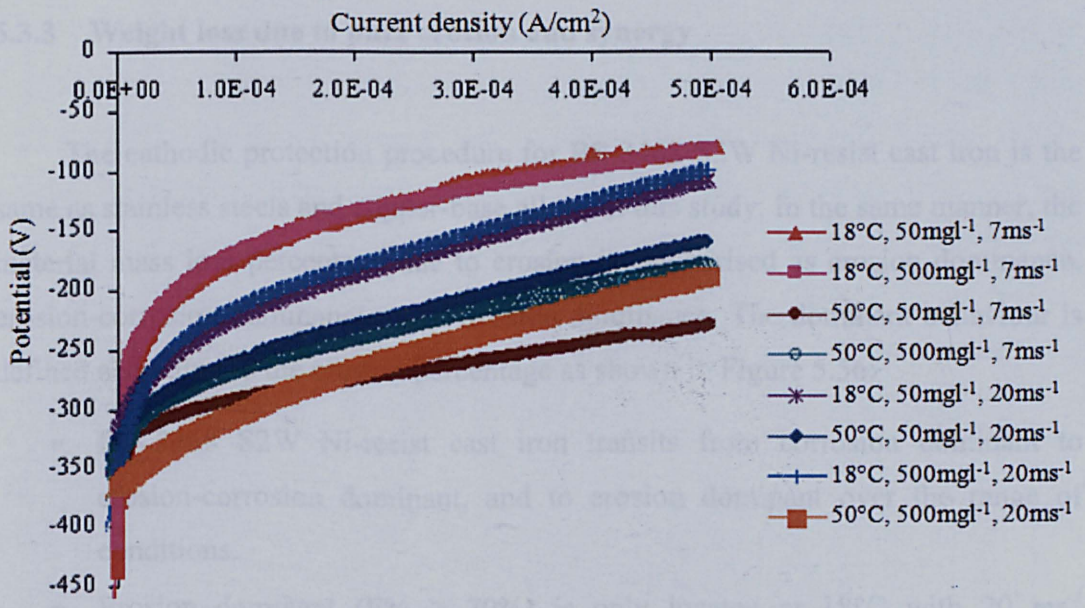

Figure 5.54: Anodic polarization curves for Ni-resist cast iron BS 3468 S2W for the eight conditions

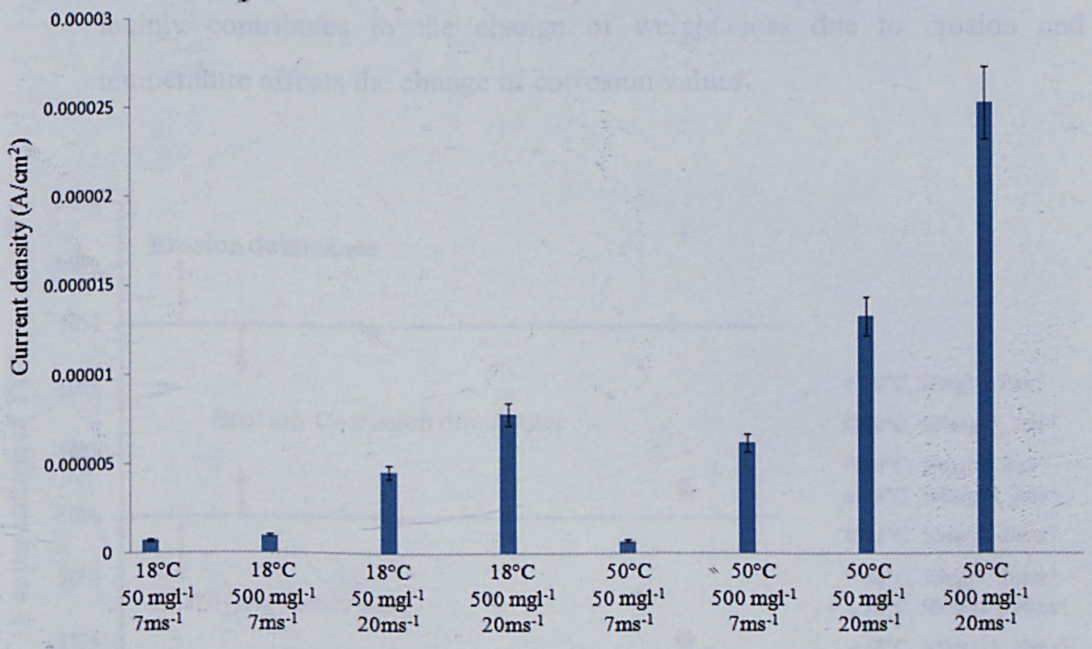

Figure 5.55: Current density for BS 3468 S2W Ni-resist cast iron for the eight conditions

5.3.3 Weight loss due to pure erosion and synergy

The cathodic protection procedure for BS 3468 S2W Ni-resist cast iron is the same as stainless steels and copper-base alloys in this study. In the same manner, the material mass loss percentage due to erosion is categorised as erosion dominance, erosion-corrosion dominance and corrosion dominance. The dominant behaviour is defined according to the erosion percentage as shown in Figure 5.56:

- BS 3468 S2W Ni-resist cast iron transits from corrosion dominant to erosion-corrosion dominant, and to erosion dominant over the range of conditions.
- Erosion dominant (E% > 70%) is only located at 18°C with 20 ms^{-1} impingement velocity and 500 mgl^{-1} sand loading. It is different from stainless steel and copper based alloys. When the condition turned most severe, erosion is not a dominant process.
- This distribution shows that the kinetic energy of flow containing solids mainly contributes to the change of weight loss due to erosion and temperature affects the change of corrosion values.

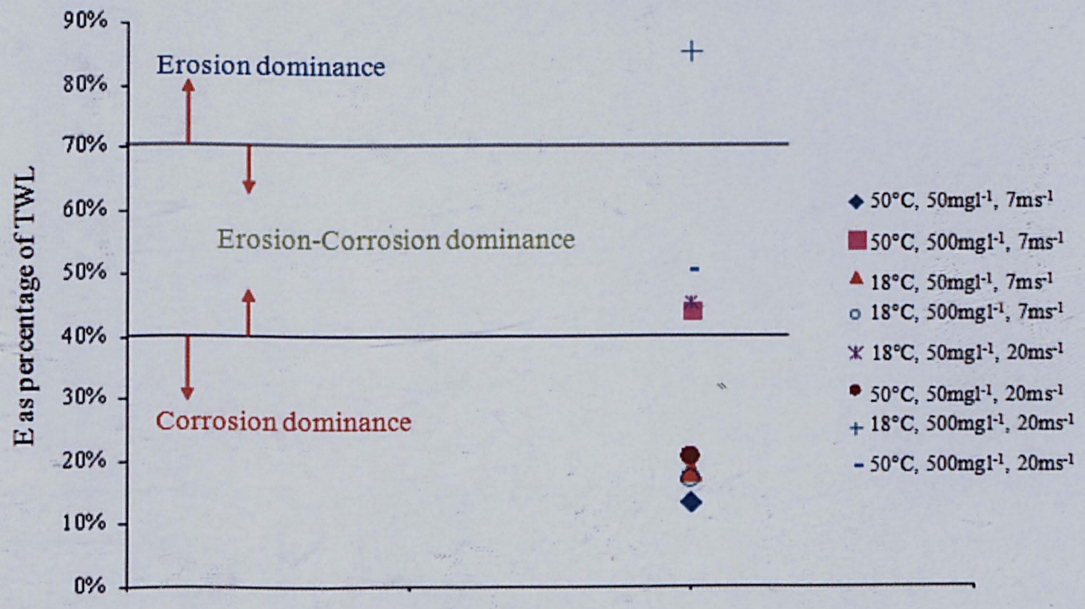

Figure 5.56: Mass loss due to pure erosion as a percentage of total weight loss for BS 3468 S2W Ni-resist cast iron at eight conditions

Table 5.6 summarised the synergy values and its percentage of total weight loss at eight conditions. Synergy accounts for a very small percentage of total weight loss at 18 °C with 20 ms^{-1} impingement velocity and 500 mgl^{-1} sand loading due to erosion dominance. In the most severe condition, BS 3468 S2W Ni-resist cast iron processes more synergy percentage than stainless steel and copper-base alloys as the general corrosion at high temperature enhances the material removal by mechanical erosion suggesting a significant interactive effect between temperature, velocity and solid loading on synergy, which will be quantified in the following chapter.

18 °C 7 ms^{-1} 50 mgl^{-1}	0.57mg (80.3%)
18 °C 7 ms^{-1} 500 mgl^{-1}	1.94mg (82.9%)
18 °C 20 ms^{-1} 50 mgl^{-1}	2.63mg (53.4%)
18 °C 20 ms^{-1} 500 mgl^{-1}	2.66mg (14.1%)
50 °C 7 ms^{-1} 50 mgl^{-1}	2.26mg (86.3%)
50 °C 7 ms^{-1} 500 mgl^{-1}	3.54mg (54.5%)
50 °C 20 ms^{-1} 50 mgl^{-1}	7.62mg (77.5%)
50 °C 20 ms^{-1} 500 mgl^{-1}	19.19mg (48.2%)

Table 5.6: Synergy values and percentage of total weight loss for BS 3468 S2W Ni-resist cast iron at eight conditions

Chapter 6 ANOVA AND PREDICTION MODEL

In the previous chapter the results of total weight loss tests, tests under cathodic protection and electrochemical *in-situ* measurements were presented. The experiments were performed in a matrix of conditions according to *ANOVA* experimental design method and in this chapter the results of this are statistically examined.

After completing the experimental matrix, quantitative assessment of the contributions from individual environmental parameters and their interactions to the total weight loss and its components can be made using the virtue of the power statistical tool, Analysis Of Variance (*ANOVA*). In statistics, analysis of variance is a collection of statistical models and their associated procedures, in which the observed variance is partitioned into components due to different explanatory variables. The experimental design method combined with factorial *ANOVA* can then be used to assess the statistical significance of the effect that a particular factor exerts on the dependent variable of interest, which represent velocity, sand loading, temperature and their interactions in this project.

6.1 Statistical calculation

In order to obtain a systematic analysis on how environmental parameters and their interactions affect total weight loss and its components over a range of concerned conditions, a routine statistical calculation method was applied to all the materials. Some terms such as average effect of the factors for each level, sum of squares and corresponding calculations will be explained in details. The design matrix for velocity, sand loading and temperature with two levels each was shown in Table 4.3, eight conditions have been set for each material in total.

The following represents how the contributing percentage is derived. Using velocity factor as an example, trial conditions 1, 3, 5 and 7 in Table 4.3 are considered to be the low level. Hence the calculation for the average output at the low velocity level can be calculated:

$$W_{lv} = 1/4\left(W_1 + W_3 + W_5 + W_7\right) \qquad \text{Equation 6.1}$$

Where W_1, W_3, W_5 *and* W_7 represent the weight loss outputs in Table 4.3 corresponding to trial conditions 1, 3, 5, and 7. The outputs at high level of velocity can also be calculated using the same method. Table 6.1 demonstrates the average outputs of individual factors at each level.

Factors	Level	
	Low	High
Velocity	W_{lv}	W_{hv}
Sand Loading	W_{ls}	W_{hs}
Temperature	W_{lt}	W_{ht}

Table 6.1: The average outputs of individual factors for each level

Sum of squares is well known as the sum of the squared deviations. In this study, for example, the sum of squares of outputs due to velocity factor can be obtained by using the following formula:

$$SS_V = 2(W_{lv} - W_G)^2 + 2(W_{hv} - W_G)^2 \qquad \text{Equation 6.2}$$

Where;

W_{lv}: the average effect corresponding to the velocity at low level

W_{hv}: the average effect corresponding to the velocity at high level

W_G: the average total weight loss for eight trial conditions

The sums of squares for other factors including possible interactions were computed in the same way. The final part of statistical calculation of ANOVA was finished easily to obtain the percentage contribution, for example the percentage contribution by velocity to the components of total weight loss could be calculated by the following equation:

$$V\% = \frac{SS_V}{SS_V + SS_S + SS_T + SS_{VS} + SS_{VT} + SS_{TS} + SS_{TVS}} \times 100\% \qquad \text{Equation 6.3}$$

The percentage contributions of the environmental parameters and their interactions to the components of the total weight loss could be obtained in the same manner. If the percentage is greater than 10%, it means this factor or interactive factor significantly affect the corresponding interest. If the percentage is less than 1%, it represents the factor has a negligible effect on the corresponding component of the total weight loss.

6.2 Results of ANOVA

In this section, ANOVA results of all eight materials will be presented individually. The common interests in how environmental parameters and their interactions affect the total weight loss and its components over a range of concerned conditions are summarised in different groups as defined previously.

ANOVA results of stainless steel alloys are shown in Table 6.2, Table 6.3 and Table 6.4 which shown that:

- Velocity (V%), sand loading (S%) and their interaction play the most important role on total weight loss and weight loss due to pure erosion over the range of test conditions, which can be explained as the mechanical removal of the materials are determined by the kinetic energy of liquid-solid impingement.

- More affective factors on corrosion for stainless steel alloys are related to velocity, sand loading, temperature, velocity and sand loading interaction, velocity and temperature interaction. All these factors are related to the determination of protective film removal, growth and corrosion rate.
- Sand loading, velocity and their interaction are prominent to synergy of stainless steels over the range of testing conditions.

	V%	*S%*	*T%*	*VS%*	*VT%*	*ST%*	*VST%*
TWL	33%	31%	2%	31%	1%	1%	1%
E	31%	30%	2%	30%	2%	3%	2%
C	26%	17%	18%	15%	13%	5%	6%
S	57%	14%	1%	13%	1%	7%	7%

Table 6.2: *ANOVA* results for stainless steel Vistar over a range of concerned conditions

	V%	*S%*	*T%*	*VS%*	*VT%*	*ST%*	*VST%*
TWL	32%	37%	0%	30%	1%	0%	0%
E	35%	33%	0%	32%	0%	0%	0%
C	41%	16%	14%	13%	13%	1%	2%
S	25%	24%	7%	23%	8%	7%	6%

Table 6.3: *ANOVA* results for stainless steel UNS S32760 over a range of concerned conditions

	V%	*S%*	*T%*	*VS%*	*VT%*	*ST%*	*VST%*
TWL	34.%	32%	0%	32%	1%	0%	1%
E	35%	33%	0%	32%	0%	0%	0%
C	35%	13%	16%	14%	15%	3%	4%
S	35%	33%	0%	32%	0%	0%	0%

Table 6.4: *ANOVA* results for stainless steel UNS S31603 over a range of concerned conditions

Table 6.5 to Table 6.8 summarised the *ANOVA* results of copper-base alloys. Similar to stainless steels, the most affective factors on total weight loss and weight loss due to pure erosion are velocity, sand loading and their interactions. However, in the group of copper-base alloys, effects of individual factors and their interactions on corrosion and synergy are dependent on the alloy itself:

- For high strength copper-base alloys, all the interactions play a significant role (more than 10% contribution) on corrosion behaviour. Additional to high strength copper-base alloys, the corrosion behaviour of nickel aluminium bronze 747 and copper nickel chromium 824 alloys was also affected by temperature, which is in agreement with the analysis reported in the previous chapter.
- All the effects from the interactions between environmental factors exhibit to be most significant on the synergy of copper-base alloys as corrosion dominance accounts for most of the materials degradation over the range of test conditions.

	V%	*S%*	*T%*	*VS%*	*VT%*	*ST%*	*VST%*
TWL	34%	29%	3%	28%	2%	2%	2%
E	32%	30%	2%	30%	2%	2%	2%
C	6%	4%	1%	23%	13%	11%	43%
S	5%	1%	7%	11%	24%	14%	38%

Table 6.5: *ANOVA* result for Marinel 220 over a range of concerned conditions

	V%	*S%*	*T%*	*VS%*	*VT%*	*ST%*	*VST%*
TWL	32%	26%	7%	24%	5%	3%	3%
E	31%	31%	2%	30%	2%	2%	2%
C	4%	7%	1%	23%	10%	16%	39%
S	4%	1%	6%	10%	23%	12%	44%

Table 6.6: *ANOVA* results for Marinel 230 over a range of concerned conditions

	V%	*S%*	*T%*	*VS%*	*VT%*	*ST%*	*VST%*
TWL	31%	28%	5%	27%	3%	3%	3%
E	30%	30%	3%	29%	2%	2%	4%
C	2%	0%	13%	4%	26%	18%	36%
S	3%	1%	5%	9%	19%	12%	51%

Table 6.7: *ANOVA* results for 747 over a range of concerned conditions

	V%	*S%*	*T%*	*VS%*	*VT%*	*ST%*	*VST%*
TWL	30%	28%	5%	27%	4%	3%	3%
E	35%	34%	2%	26%	1%	1%	1%
C	0%	3%	27%	3%	33%	14%	19%
S	5%	4%	2%	21%	14%	11%	44%

Table 6.8: *ANOVA* results for 824 over a range of concerned conditions

Effects of environmental factors on BS 3468 S2W Ni-resist cast iron differ from both stainless steel and copper-base alloys which possess a oxide layer accounting for erosion-corrosion resistance under liquid-solid impingement. The individual environmental parameter does not exhibit to have significant effect on the total weight loss and its components (Table 6.9). Greatest level of effect is shown to be the interactions between velocity, solid loading and temperature due to the active nature of BS 3468 S2W Ni-resist cast iron.

	V%	*S%*	*T%*	*VS%*	*VT%*	*ST%*	*VST%*
TWL	6%	4%	2%	20%	14%	10%	45%
E	3%	2%	0%	12%	4%	3%	76%
C	7%	1%	4%	15%	22%	10%	42%
S	4%	1%	4%	11%	19%	12%	49%

Table 6.9: *ANOVA* result for BS 3468 S2W Ni-resist cast iron over a range of concerned conditions

6.3 Prediction model

Linear regression is one of the most widely used statistical techniques to predict un-sampled values between the known variable levels. It is adopted in this study to develop an empirical material loss prediction model based on the outputs collected under eight testing conditions for the eight materials. Initial framework is established and improved prediction can be made by further experimental work by future studies.

This linear regression model can be expressed as the following empirical equation (Equation 6.4), in which velocity, sand loading and temperature are appointed as X_1, X_2 and X_3 respectively. Based on the outputs (total weight loss and its components) at eight conditions ([Y]: 1*8 matrix), the coefficients of the empirical equation ([a]: 1*8 matrix) can be calculated by the matrix algorithm (Equation 6.5).

Once the coefficients of the empirical equation are obtained, total weight loss and its components can then be calculated for a given testing condition as shown in the excel spreadsheet (Figure 6.1). All the coefficients for eight materials are summarised in Table 6.10 to Table 6.17. In agreement with previous *ANOVA* analysis, the coefficient values of velocity, sand loading and their interactions in the total weight loss and erosion prediction models are greater than others.

$$Y = a_0 + a_1\overline{X_1} + a_2\overline{X_2} + a_3\overline{X_3} + a_{12}\overline{X_1X_2} + a_{23}\overline{X_2X_3} + a_{13}\overline{X_1X_3} + a_{123}\overline{X_1X_2X_3} \quad \text{Equation 6.4}$$

$$[Y] = [a] \times \begin{bmatrix} 1 & 1 & 1 & 1 & 1 & 1 & 1 & 1 \\ -1 & -1 & -1 & -1 & 1 & 1 & 1 & 1 \\ -1 & 1 & -1 & 1 & -1 & 1 & -1 & 1 \\ -1 & -1 & 1 & 1 & -1 & -1 & 1 & 1 \\ 1 & -1 & 1 & -1 & -1 & 1 & -1 & 1 \\ 1 & 1 & -1 & -1 & -1 & -1 & 1 & 1 \\ 1 & -1 & -1 & 1 & 1 & -1 & -1 & 1 \\ -1 & 1 & 1 & -1 & 1 & -1 & -1 & 1 \end{bmatrix} \quad \text{Equation 6.5}$$

	A	B	C	D	E	F	G	H	I	J
1	***Input***									
2	X_1 *(velocity~m/s)*			X_2 *(sand loading~ppm)*			X_3 *(temperature~ ℃)*			
3										
4										
5										
6	***Output (TWL)***									
7										
8	0. 08107906									
9										
10	$Y = a_0 + a_1\overline{X_1} + a_2\overline{X_2} + a_3\overline{X_3} + a_{12}\overline{X_1X_2} + a_{13}\overline{X_1X_3} + a_{23}\overline{X_2X_3} + a_{123}\overline{X_1X_2X_3}$									
11										
12		$\overline{X_1} = \frac{X_1 - 13.5}{6.5}$			$\overline{X_2} = \frac{X_2 - 275}{225}$			$\overline{X_3} = \frac{X_3 - 34}{16}$		
13										
14										
15										
16	a_0	a_1	a_2	a_3	a_{12}	a_{13}	a_{23}	a_{123}		
17	10.704	9.044	8.306	4.731	8.086	3.691	3.079	3.049		

Figure 6.1: One example spread sheet for mass loss prediction

	a_0	a_1	a_2	a_3	a_{12}	a_{13}	a_{23}	a_{123}
TWL	4.0213	3.9238	3.8188	1.1013	3.7663	1.0738	1.0538	1.0413
E	3.3350	3.2875	3.2075	0.9250	3.1800	0.9075	0.9025	0.8950
C	0.0325	0.0274	0.0219	0.0225	0.0204	0.0195	0.0129	0.0128
S	0.6542	0.6094	0.5899	0.1532	0.5664	0.1461	0.1377	0.1329

Table 6.10: The coefficients for the prediction model of stainless steel alloy Vistar

	a_0	a_1	a_2	a_3	a_{12}	a_{13}	a_{23}	a_{123}
TWL	4.2900	4.2400	4.0850	0.7125	4.0400	0.7625	0.7325	0.7275
E	3.4375	3.4050	3.2800	0.6700	3.2575	0.6875	0.6925	0.7000
C	0.0302	0.0268	0.0161	0.0156	0.0154	0.0144	0.0040	0.0044
S	0.8216	0.8082	0.7888	0.0269	0.7664	0.0598	0.0353	0.0230

Table 6.11: The coefficients for the prediction model of stainless steel alloy UNS S32760

	a_0	a_1	a_2	a_3	a_{12}	a_{13}	a_{23}	a_{123}
TWL	4.2188	4.1338	3.9437	1.8487	3.8787	1.8837	1.8287	1.8437
E	3.4275	3.3900	3.2400	1.575	3.2125	1.5825	1.5775	1.575
C	0.0642	0.0583	0.0375	0.0410	0.0375	0.0395	0.0207	0.0213
S	0.712	0.682	0.6625	0.2178	0.6135	0.2602	0.2293	0.2328

Table 6.12: The coefficients for the prediction model of stainless steel alloy UNS S31603

	a_0	a_1	a_2	a_3	a_{12}	a_{13}	a_{23}	a_{123}
TWL	10.6500	9.2975	8.6350	2.9925	8.4425	2.3800	2.0025	2.0000
E	8.5738	8.3637	8.1037	2.0062	8.0388	2.0012	1.9162	1.9762
C	0.2963	0.1812	0.1488	0.0837	0.1187	0.0287	0.0662	0.0163
S	0.0018	0.0008	0.0004	0.0009	0.0003	0.0004	0.00002	0.00001

Table 6.13: The coefficients for the prediction model of Marinel 220

	a_0	a_1	a_2	a_3	a_{12}	a_{13}	a_{23}	a_{123}
TWL	10.2813	9.1462	8.5538	3.0937	8.2587	2.5987	2.2012	2.0962
E	8.3613	8.1062	7.9962	1.8912	7.8563	1.8113	1.8813	1.8763
C	0.1762	0.0763	0.1088	0.0487	0.0588	-0.0113	0.0413	0.0012
S	0.0017	0.001	0.0004	0.0012	0.0003	0.0008	0.0003	0.0002

Table 6.14: The coefficients for the prediction model of Marinel 230

	a_0	a_1	a_2	a_3	a_{12}	a_{13}	a_{23}	a_{123}
TWL	10.704	9.044	8.306	4.731	8.086	3.691	3.079	3.049
E	7.5900	7.3025	7.2875	2.2150	7.1950	2.1075	2.1125	2.1500
C	0.8887	0.2412	0.1012	0.6287	0.0187	0.1113	0.0462	0.0337
S	0.0022	0.0015	0.0009	0.0019	0.0009	0.0015	0.0009	0.0009

Table 6.15: The coefficients for the prediction model of 747

	a_0	a_1	a_2	a_3	a_{12}	a_{13}	a_{23}	a_{123}
TWL	14.3612	12.9462	12.2887	5.0513	12.1187	4.3613	3.9238	3.9688
E	11.6875	11.3775	11.1125	3.8500	11.0625	3.8150	3.6750	3.7600
C	0.38	0.03	-0.11	0.3225	-0.08	-0.0075	-0.0925	-0.0425
S	0.0023	0.0015	0.0013	0.0009	0.0011	0.0006	0.0003	0.0003

Table 6.16: The coefficients for the prediction model of 824

	a_0	a_1	a_2	a_3	a_{12}	a_{13}	a_{23}	a_{123}
TWL	10.6713	7.6288	6.1463	3.9513	4.7687	2.4338	2.2463	1.6838
E	5.5150	4.5775	4.3300	0.7925	3.6325	0.1200	0.7875	0.2250
C	0.1043	0.077	0.0358	0.0575	0.0185	0.0358	0.0265	0.0047
S	0.0051	0.003	0.0018	0.0031	0.0011	0.0023	0.0014	0.0015

Table 6.17: The coefficients for the prediction model of BS 3468 S2W Ni-resist cast iron

6.4 Prediction model validation

Validation of the initial prediction model developed in this study is carried out by conducting erosion-corrosion tests on UNS S31603 and 747 in 10 sets of conditions which are either within (eight conditions) or outside (two conditions) of testing matrix from experimental design as shown in Figure 6.2. More extensive validation of the model for other materials could be done in the future but due to time restrictions one passive stainless steel and one copper-base alloy were chosen.

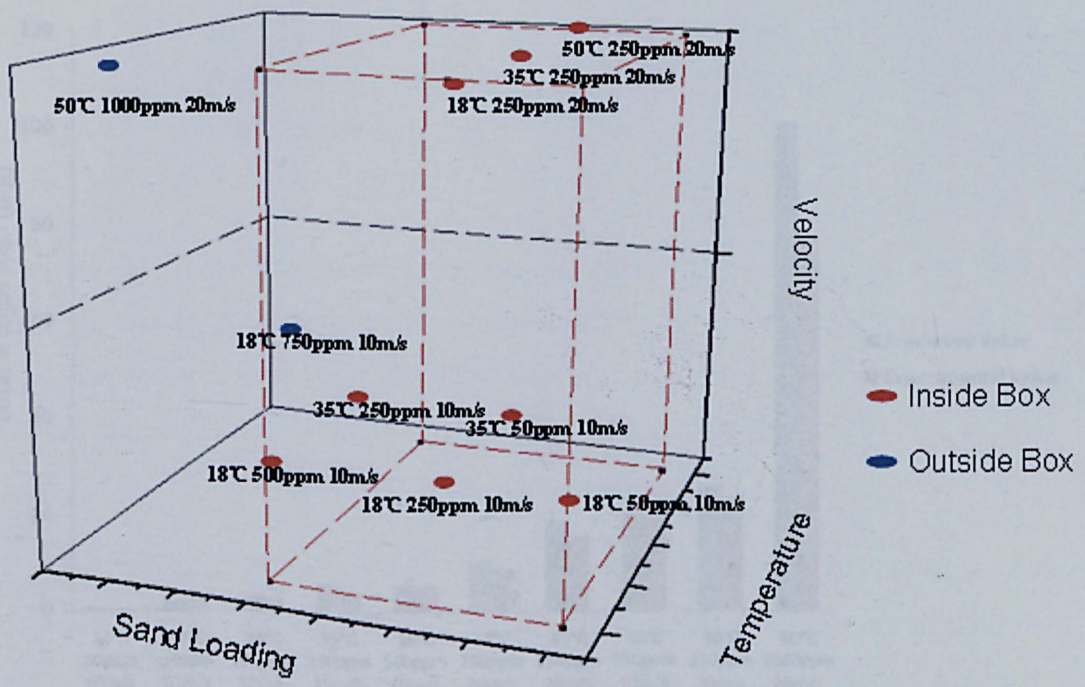

Figure 6.2 Ten sets of test conditions for the prediction modelling validation

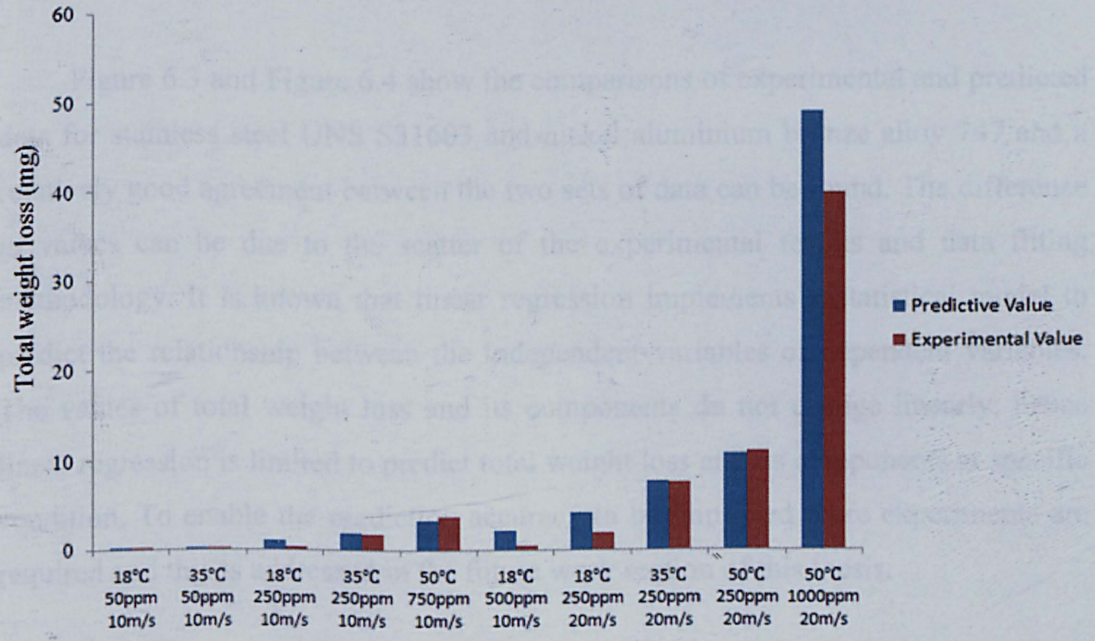

Figure 6.3: The validation between the predictive and experimental values for stainless steel alloy UNS S31603

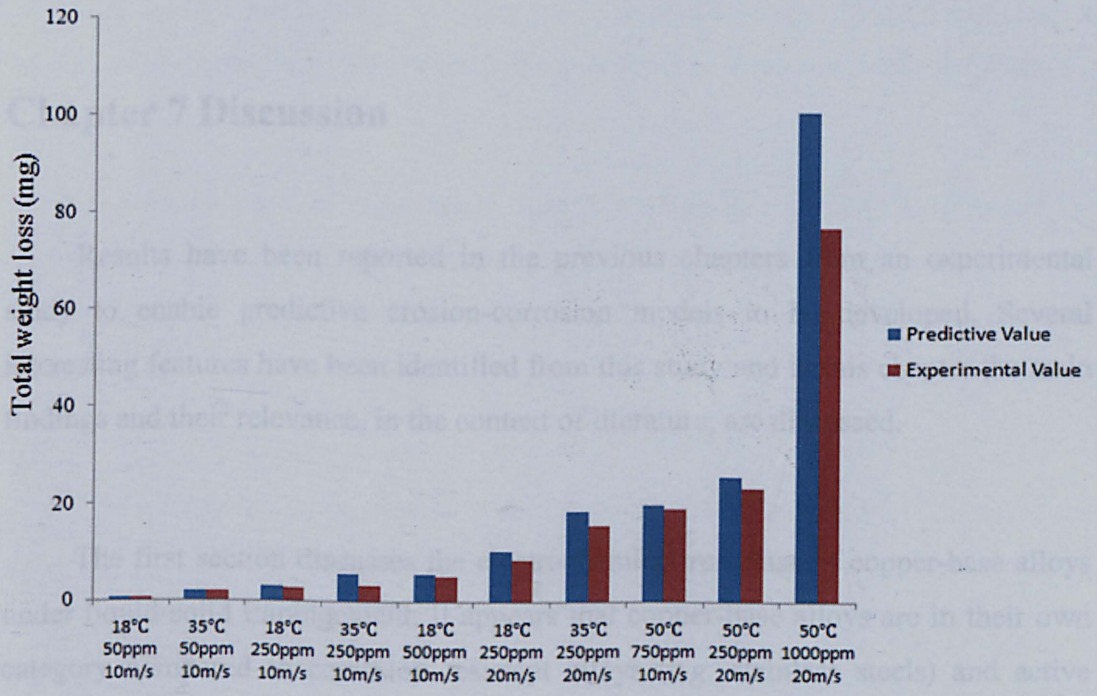

Figure 6.4: The validation between the predictive and experimental values for nickel aluminium bronze alloy 747

Figure 6.3 and Figure 6.4 show the comparisons of experimental and predicted data for stainless steel UNS S31603 and nickel aluminium bronze alloy 747 and a relatively good agreement between the two sets of data can be found. The difference in values can be due to the scatter of the experimental results and data fitting methodology. It is known that linear regression implements a statistical model to predict the relationship between the independent variables or dependent variables. The values of total weight loss and its components do not change linearly; hence linear regression is limited to predict total weight loss and its components at specific condition. To enable the prediction accuracy to be improved more experiments are required and this is addressed in the future work section of this thesis.

Chapter 7 Discussion

Results have been reported in the previous chapters from an experimental study to enable predictive erosion-corrosion models to be developed. Several interesting features have been identified from this study and in this chapter the main findings and their relevance, in the context of literature, are discussed.

The first section discusses the electrochemical response of copper-base alloys under liquid-solid impingement. It appears that copper-base alloys are in their own category compared to corrosion resistant alloys (*e.g.* stainless steels) and active materials (*e.g.* cast iron). Extensive discussion is presented in this chapter to describe the corrosion mechanisms in detail. The role of corrosion in dominating the total material degradation is also discussed.

The effect of hardness of materials is always considered to be essential when studying erosion and erosion-corrosion. However, the surface work hardening on material under liquid-solid impingement is rarely taken into account. In this study, a good correlation between surface work hardening and total weight loss is found and the mechanisms are discussed in the second section.

The third section compares the materials performance as volume loss values under all conditions applied in this study. Distinctive differences in erosion-corrosion degradation rate of materials can be determined and this is discussed from various aspects such as degradation mechanisms, film tenacity, mechanical properties and surface work hardening effects *etc.*

In the following sections in addition to the dominant processes (electrochemical, mechanical and synergistic), the contribution of environmental parameters to the total weight loss and its components is discussed. Using the

ANOVA method has enabled not only the individual environmental parameters to be studied, but also their interactions which were not reported by published works.

The final section of this chapter discusses the model developed to predict the damage of marine alloys when exposed to the erosion-corrosion environments. The significance of the model is discussed from both methodological and practical aspects.

The integration of the results from this work with related work throughout the discussion provides the basis for the recognition and advancement in understanding of erosion-corrosion and prediction.

7.1 Corrosion behaviour under erosion-corrosion conditions

In contrast to passive behaviour, the anodic polarisation curves of three stainless steels demonstrate a pseudo-passive behaviour as the conditions become more severe. Similar corrosion behaviour has been well reported and discussed by Reyes [85] and Hu [122]. The additions of alloying elements *N*, *Cr*, *Mo* and *Ni* have greatly improved the corrosion resistance of the high alloy stainless steels compared with standard stainless steel UNS S31603. The reduction in the corrosion current density suggests an improvement of resistance to the charge transfer when the protective layer is removed by the liquid-solid impingement. As the stabilised current density (i_s) is an indication of repassivation property. It is clear from Figure 5.15 that super austenitic stainless steel Vistar possesses the best resistance to the depassivation, and followed by super duplex stainless steel UNS S32760 and standard stainless steel UNS S31603 [122].

Compared to stainless steels which show passive and pseudo-passive behaviour, anodic polarisation curves of copper-base alloys in erosion-corrosion conditions exhibit low current active behaviour. This suggests the less tenacity of the film with less dense microstructure formed on the surface of copper-base alloys

in contrast to stainless steels. The materials were immersed in the 3.5% *NaCl* solution for 24 hours before commencing to the liquid-solid impingement. The electrochemical behaviour of copper-containing alloys exposed to natural seawater was markedly different from that previously reported by the authors for stainless steels and titanium exposed under identical conditions [70, 171, 172]. Impedance spectra for stainless steels and titanium did not change as a function of exposure time. In contrast, spectra for the copper-containing alloys varied as a function of exposure time. Moreover, it has been reported that up to thirty days of immersion time is required to enable an integrated protective film to be formed on the copper-base alloys.

For nickel aluminium bronze 747, an interesting feature is discovered during anodic polarisation when exposed to erosion-corrosion conditions of moderate severity as shown schematically in Figure 7.1. Such behaviour is considered to be related to the film removal and reformation during the liquid-solid impingement processes. As shown in Figure 7.2(a), under mild conditions there is a semi-protective film formed on the material surface. Unlike the tenacious passive films of stainless steels, dissolution charge transfer is allowed due to the existence of the pores within the film. General low current active behaviour is clear from the results. Under severe conditions, high frequency liquid-solid impacts result in severe degradation of the surface. Film formation is unlikely to occur and active dissolution is considered to be the corrosion degradation mechanism (Figure 7.2(b)). According to the anodic polarisation curve under moderate conditions, there is a region where current density reduces and stabilises followed by 'breakdown' behaviour as the potential increases. The increase in applied potential enhances the formation of the film on the surface accounting for the current reduction. However, the values are greater than mild conditions due to (1) partial removal of the film under liquid-solid impingement and (2) less resistance to dissolution charge transfer as the thickness and tenacity are smaller compared with films under mild conditions as illustrated in Figure 7.2 (c). Further increase in potential enables general corrosion to occur resulting in a rapid increase in current density which appears similar to the localised breakdown behaviour of stainless steels.

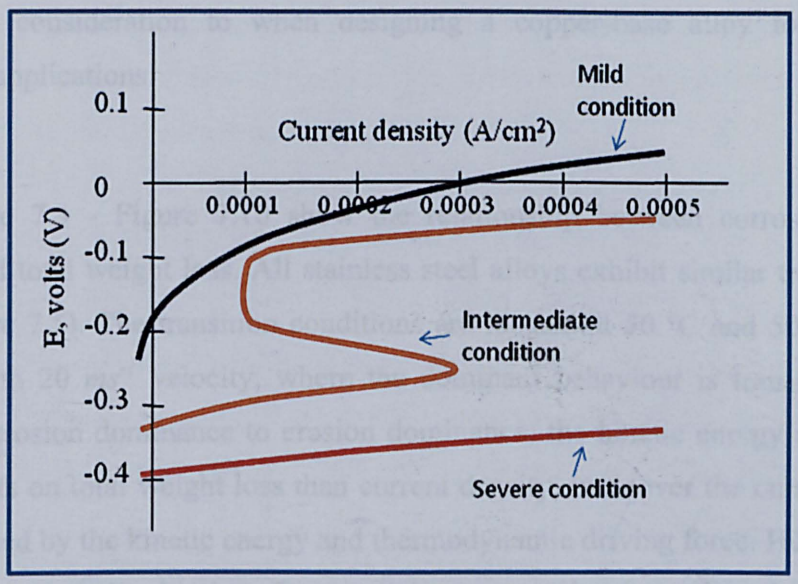

Figure 7.1 Schematic anodic polarisation curve for nickel aluminium bronze 747

(a) (b) (c)

Figure 7.2 Schematic diagrams demonstrating the surface characteristics of nickel aluminium bronze 747 during anodic polarization in (a) mild conditions, (b) moderate conditions and (c) severe conditions

Figure 5.42 shows that high strength copper nickel alloy Marinel 230 exhibits the lowest corrosion rate over a range of conditions followed by high strength copper nickel alloy Marinel 220, copper nickel chromium alloy 824 and nickel aluminium bronze alloy 747. As discussed in the literature, corrosion and erosion-corrosion resistance of copper-base alloys benefits from a number of alloying elements such as *Fe*, *Mn*, *Cr* and *Ni* [55, 59]. However, by only improving the content of chromium and nickel does not seem to be the most effective solution when comparing the corrosion performance of 824 with Marinel 220 and 230 in erosion-corrosion conditions. For nickel aluminium bronze 747, although strength and scaling resistance are increased by aluminium [77], the corrosion resistance is clearly reduced according to the greatest corrosion current density under most of the testing conditions. Hence, the synergistic effects of the alloying elements need to be

taken into consideration to when designing a copper-base alloy for corrosion resistance applications.

Figure 7.3 - Figure 7.10 show the relationship between corrosion current density and total weight loss. All stainless steel alloys exhibit similar trend (Figure 7.3 - Figure 7.5). The transition conditions are located at 50 °C and 50 mgl^{-1} sand loading with 20 ms^{-1} velocity, where the dominant behaviour is transferred from erosion-corrosion dominance to erosion dominance, the kinetic energy of fluid has more effects on total weight loss than current density; moreover the current density is determined by the kinetic energy and thermodynamic driving force. Hu [122] *et al.* found a linear relationship between corrosion current density and total weight loss, which proved the link between the number of impacts and the electrochemical charge transfer when the sand loading is increased. It was also noted that in saline solutions containing liquid-solid impingement, higher solid loading enables more particles impacts on the specimen surface and the removal of the passive films results in a higher metal dissolution rate. Continuous impacts may prevent repassivation from occurring, and also the higher corrosion current is due to the higher thermodynamic driving force making corrosion occur at a higher rate during the depassivation period. In this study, some more points need to be taken account:

- When the dominance behaviour is located in the range of corrosion dominance or erosion-corrosion dominance, the linear relationship between corrosion current density and total weight loss could be detected.
- The effects of the interactions between environmental parameters on this correlation need taking more accounts.
- When the condition was changed from 50 °C, 20 ms^{-1} and 50 mgl^{-1} to 18 °C, 20 ms^{-1} and 500 mgl^{-1}, the environmental parameters played more effects on depassivation rather than repassivation.

The copper-base alloys exhibit two linear trends between the current density and total weight loss.

- Linear relationship with sharp slope - When the materials exhibited corrosion dominant and erosion-corrosion dominant behaviours under impingement jet erosion-corrosion tests at 18 °C, 7 ms^{-1} and 50 mgl^{-1}; 18 °C, 7 ms^{-1} and 500 mgl^{-1}; 50°C, 7 ms^{-1} and 50 mgl^{-1}; 50°C, 7 ms^{-1} and 500 mgl^{-1}; 18 °C, 20 ms^{-1} and 50 mgl^{-1}, the environmental parameters played more effects on corrosion then erosion.
- Linear relationship with slower slope - When the conditions turned to be more severe (50 °C, 20 ms^{-1} and 50 mgl^{-1}; 18 °C, 20 ms^{-1} and 500 mgl^{-1}; 50 °C, 20 ms^{-1} and 500 mgl^{-1}), the kinetic energy is the crucial factor to the total weight loss. That is, the environmental severity results in more erosion than corrosion.

However, BS 3468 S2W Ni-resist cast iron shows nearly linear relationship between corrosion current density and total weight loss. That is, the severity of the environment affects current density at the same degree as the total weight loss.

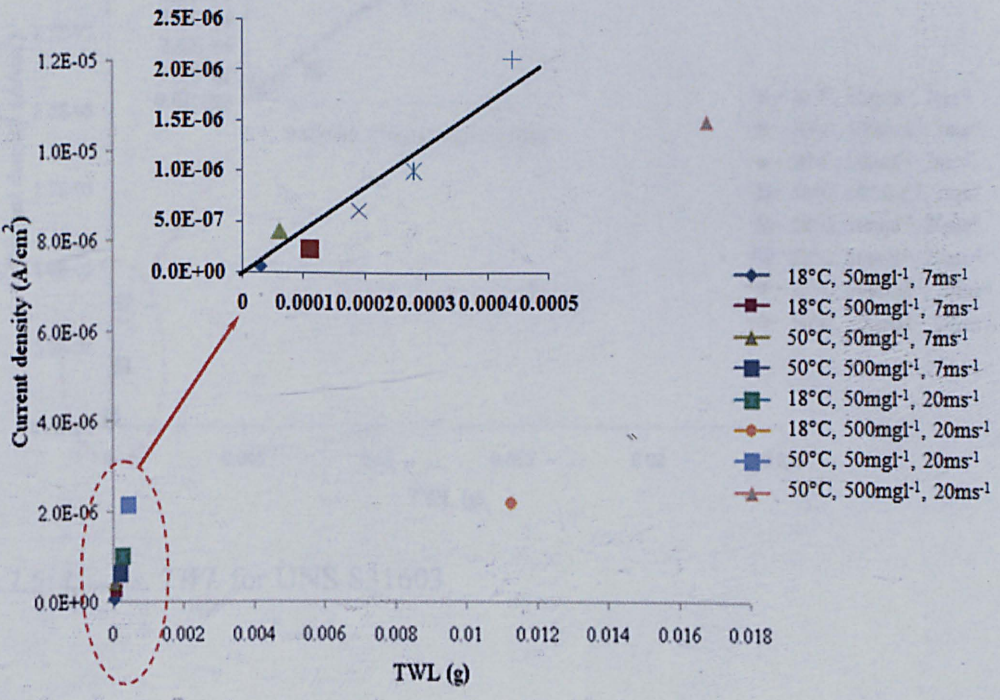

Figure 7.3: i_{corr} *vs. TWL* for stainless steel Vistar

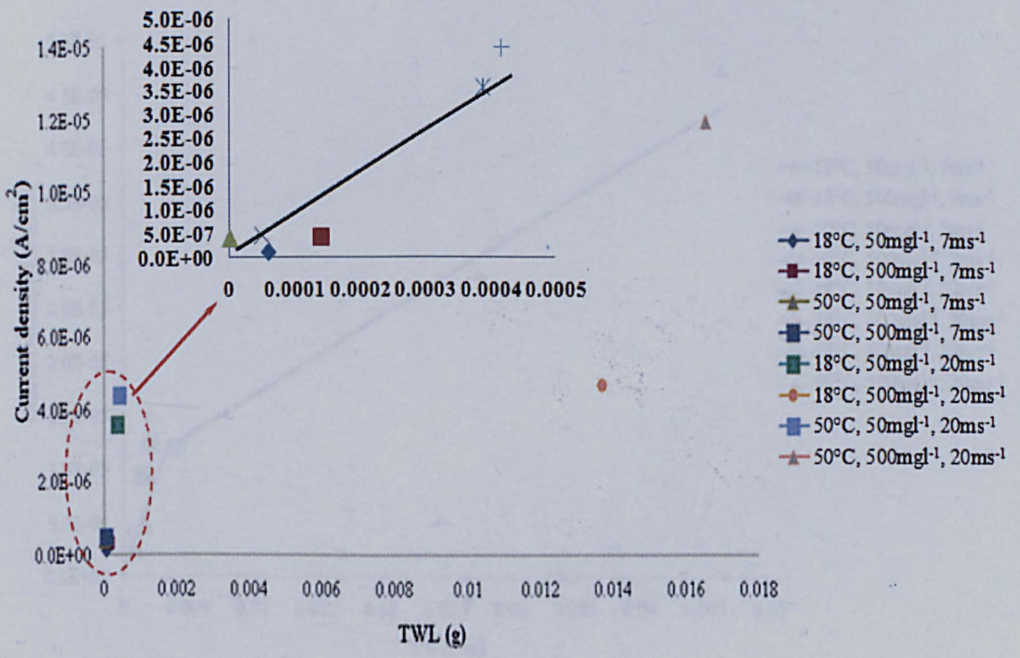

Figure 7.4: i_{corr} *vs. TWL* for UNS S32760

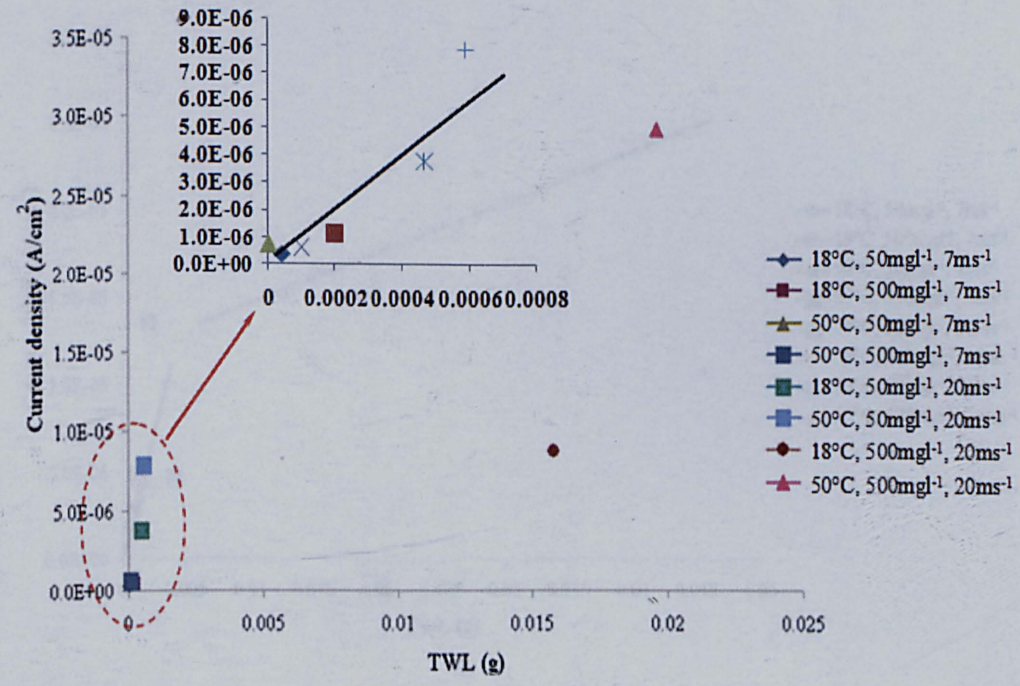

Figure 7.5: i_{corr} *vs. TWL* for UNS S31603

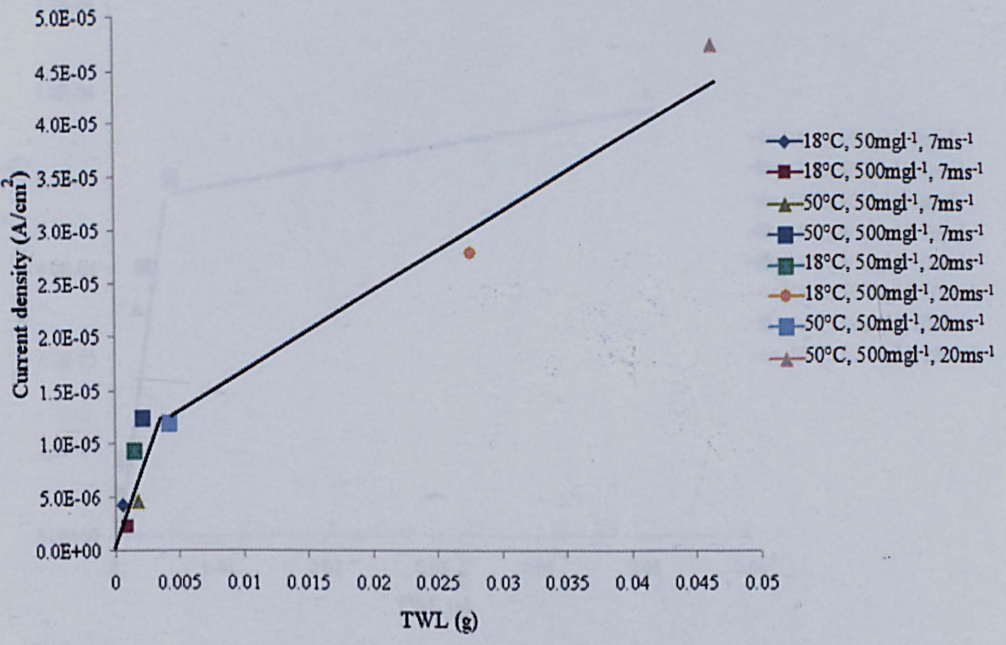

Figure 7.6: i_{corr} *vs. TWL* for high strength copper nickel alloy Marinel 220

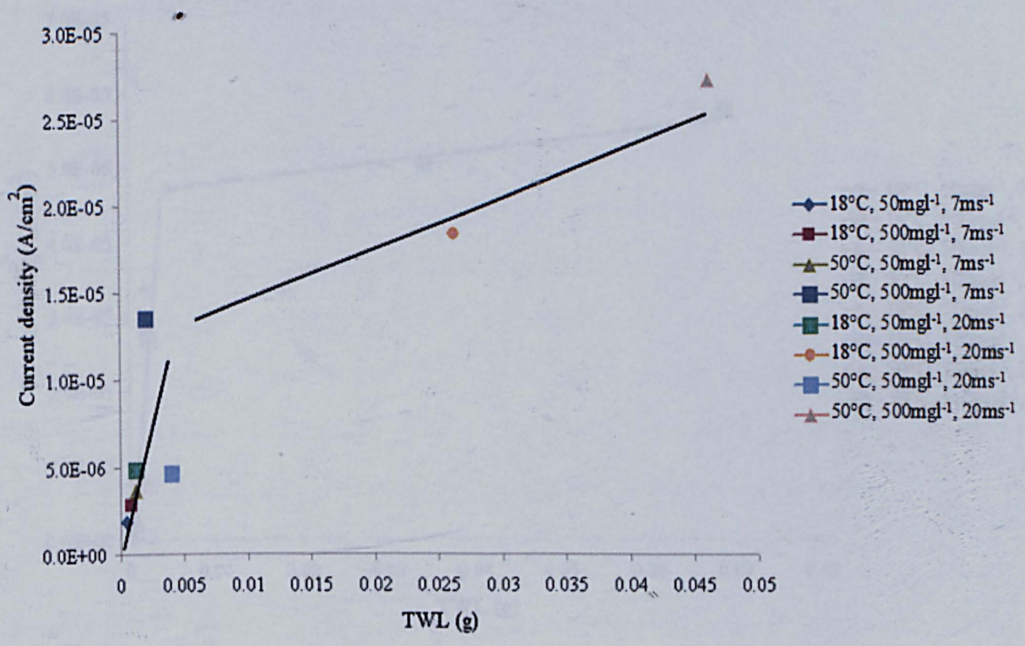

Figure 7.7: i_{corr} *vs. TWL* for high strength copper nickel alloy Marinel 230

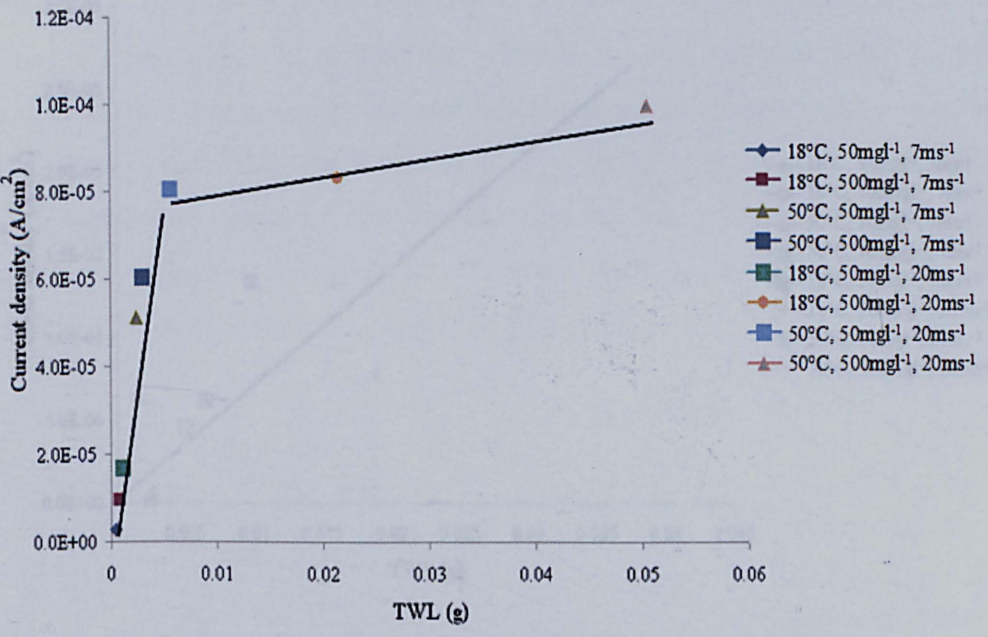

Figure 7.8: i_{corr} *vs. TWL* for nickel aluminium bronze alloy 747

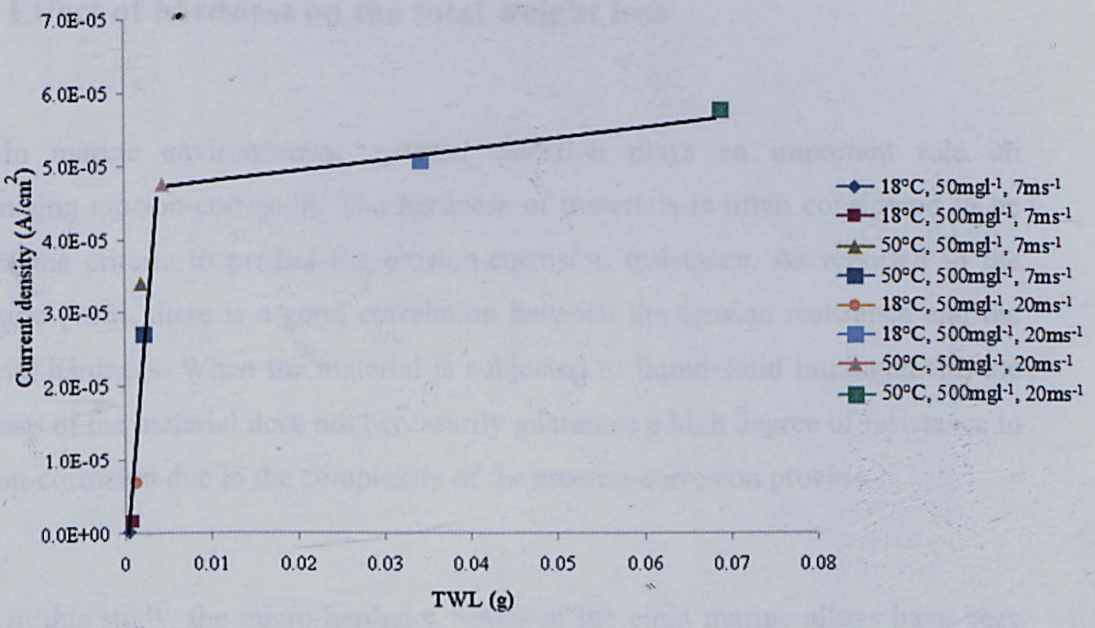

Figure 7.9: i_{corr} *vs. TWL* for copper nickel chromium alloy 824

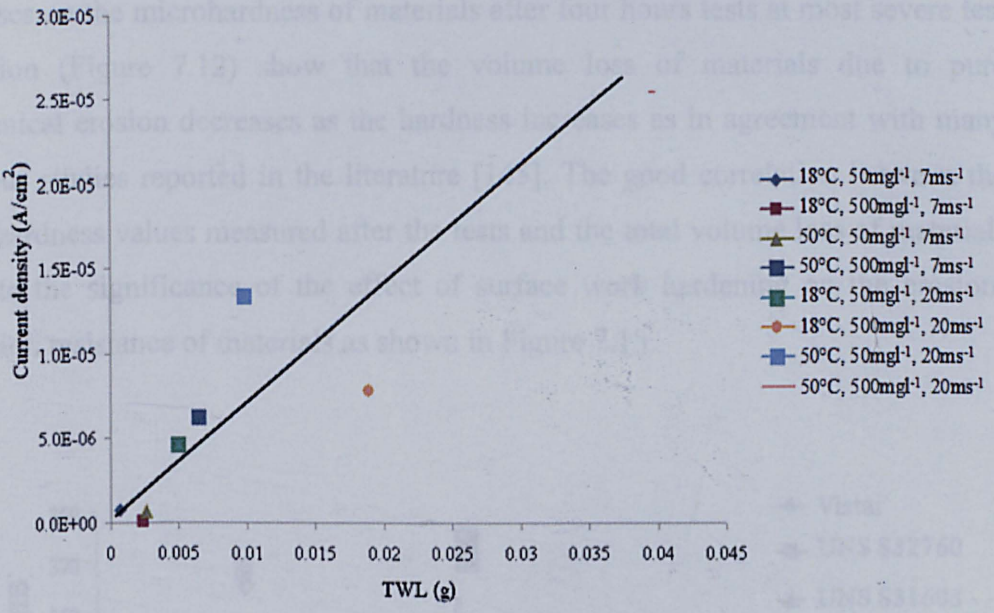

Figure 7.10: i_{corr} *vs. TWL* for BS 3468 S2W Ni-resist cast iron

7.2 Effect of hardness on the total weight loss

In marine environments, material selection plays an important role on minimizing erosion-corrosion. The hardness of materials is often considered to be one of the criteria to predict the erosion-corrosion resistance. As reported in the literature [145], there is a good correlation between the erosion resistance and the material hardness. When the material is subjected to liquid-solid impingement, the hardness of the material does not necessarily guarantee a high degree of resistance to erosion-corrosion due to the complexity of the erosion-corrosion process.

In this study, the micro-hardness values of the eight marine alloys have been plotted versus the total volume loss under the severe erosion-corrosion condition. It is clear in Figure 7.11 that there is on universal relationship between the initial microhardness and erosion-corrosion resistance as also reported by Hu *et al.* [122] due to the significant contribution to the total material degradation resulting from corrosion related processes. As presented in Chapter 5, under such a severe erosion-corrosion condition, the weight loss is dominated by erosion process. Surface work hardening is often considered to be one important feature of erosion mechanisms.

Analyses on the microhardness of materials after four hours tests at most severe test condition (Figure 7.12) show that the volume loss of materials due to pure mechanical erosion decreases as the hardness increases as in agreement with many previous studies reported in the literature [145]. The good correlation between the microhardness values measured after the tests and the total volume loss of materials indicate the significance of the effect of surface work hardening on the erosion-corrosion resistance of materials as shown in Figure 7.13.

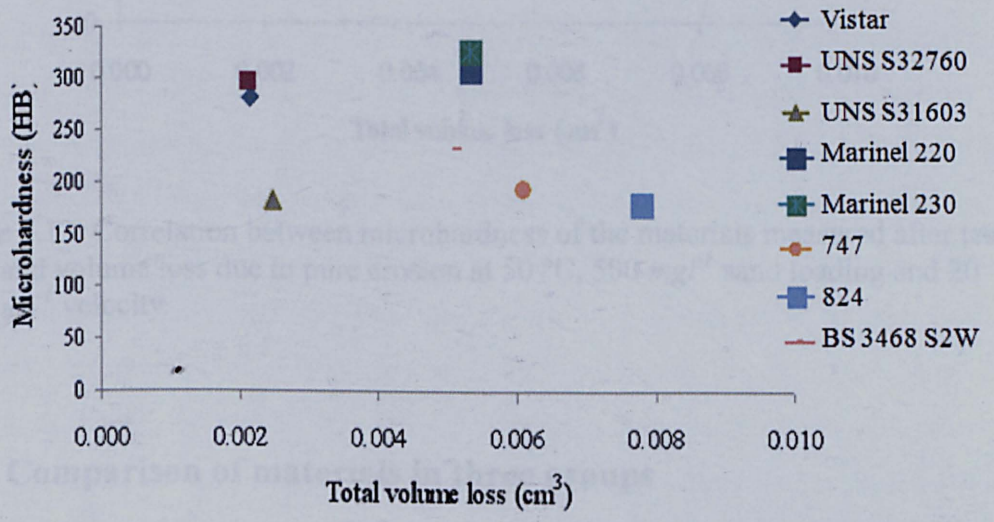

Figure 7.11: Correlation between initial microhardness of the materials and total volume loss at 50 °C, 500 mgl^{-1} sand loading and 20 ms^{-1} velocity.

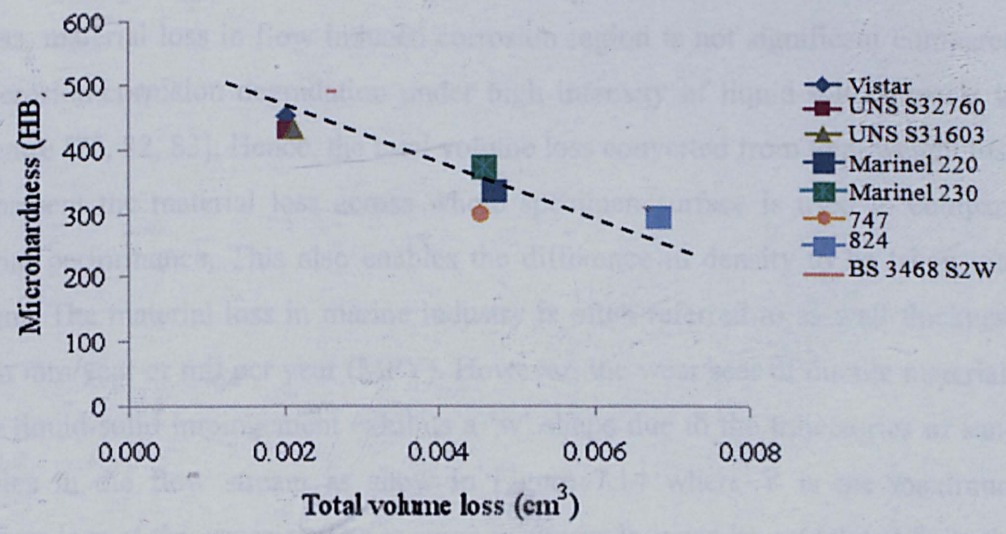

Figure 7.12: Correlation between microhardness of the materials measured after test and total volume loss at 50 °C, 500 mgl^{-1} sand loading and 20 ms^{-1} velocity.

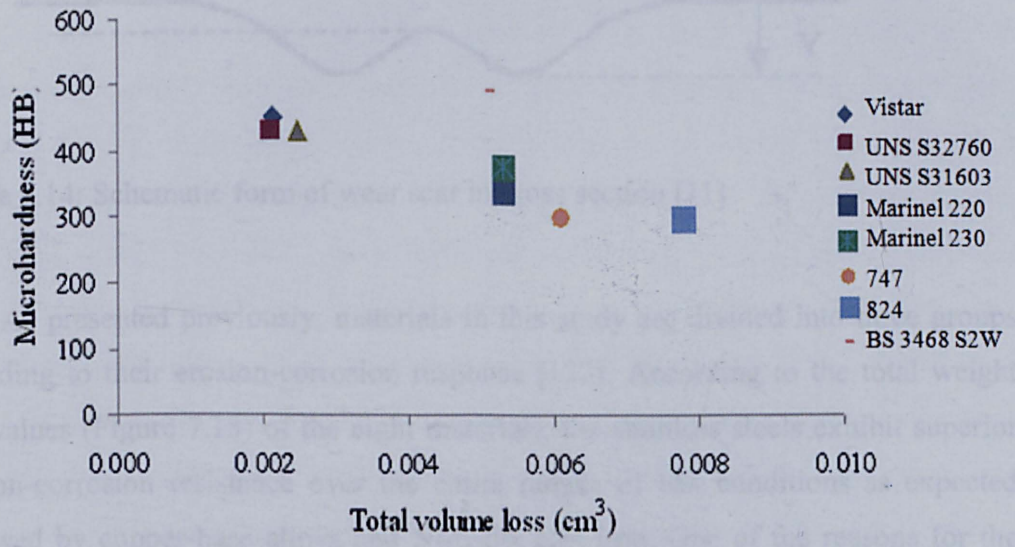

Figure 7.13: Correlation between microhardness of the materials measured after test and volume loss due to pure erosion at 50 °C, 500 mgl^{-1} sand loading and 20 ms^{-1} velocity.

7.3 Comparison of materials in three groups

In this study, for stainless steels it is considered to be due to only the degradation to form the wear scar as flow-induced corrosion on the edge is very small. For copper-base alloys, although flow can result in enhanced corrosion process, material loss in flow induced corrosion region is not significant compared with erosion-corrosion degradation under high intensity of liquid-solid impacts in the centre [75, 82, 83]. Hence, the total volume loss converted from total weight loss to represent the material loss across whole specimen surface is used to compare material performance. This also enables the difference in density to be taken into account. The material loss in marine industry is often referred to as wall thickness loss in mm/year or mil per year (MPY). However, the wear scar of ductile materials under liquid-solid impingement exhibits a 'w' shape due to the trajectories of sand particles in the flow stream as show in Figure 7.14 where Y is the maximum thickness loss of the material. The average thickness loss can be calculated from the total weight loss or total volume loss obtained from this study.

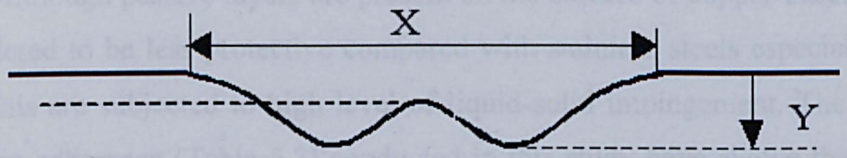

Figure 7.14: Schematic form of wear scar in cross section [11]

As presented previously, materials in this study are divided into three groups according to their erosion-corrosion response [132]. According to the total weight loss values (Figure 7.15) of the eight materials, the stainless steels exhibit superior erosion-corrosion resistance over the entire ranges of test conditions as expected followed by copper-base alloys and Ni-resist cast iron. One of the reasons for the superiority of stainless steels has been due to the tenacious passive film to protect the materials from corrosion in a marine environment as discussed previously. Another contribution results from the surface work hardening effect. A great deal of increment of hardness values is clear after the liquid-solid impingement especially for standard stainless steel UNS S31603 The improvement in the overall erosion-corrosion resistance of the high alloy stainless steels is mainly due to their alloying additions to improve their corrosion resistance as discussed by Neville [104].

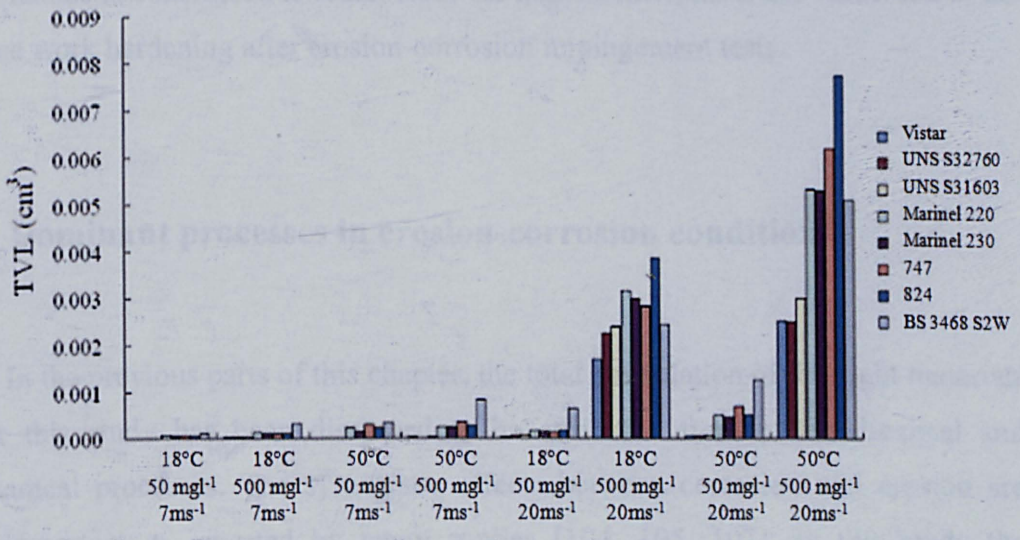

Figure 7.15: Total volume loss of eight test materials at eight conditions

Although passive layers are present on the surface of copper based alloys, it is considered to be less protective compared with stainless steels especially when the materials are subjected to high level of liquid-solid impingement. The analyses on the film adherence (Table 5.3) conducted in this study have shown the lowest film coverage for copper nickel chromium alloy 824 after the severe impingement attack in erosion-corrosion environments. The adhesion ability is followed by nickel aluminium bronze alloy 747, high strength copper nickel alloy Marinel 220 and high strength copper nickel alloy Marinel 230. It is in agreement with the ranking of total weight loss results suggesting the erosion-corrosion resistance of the copper-base alloys is greatly affected by the films formed on the material surface. Another contribution is considered to be the surface work hardening as discussed previously showing the lowest microhardness value after the measurements on copper nickel chromium alloy 824.

For the Ni-resist cast iron, a general high weight loss rate under erosion-corrosion conditions is observed due to its least corrosion resistance. However, it is not always the case that BS 3468 S2W Ni-resist cast iron exhibits the lowest erosion-corrosion resistance. As shown in Figure 7.15, when the material is subject to a high level of liquid-solid impingement (20 ms^{-1} velocity and 500 mgl^{-1} sand loading) the total weight loss values are less than the copper based alloys. Such performance is considered to result from the highest microhardness value due to the surface work hardening after erosion-corrosion impingement tests.

7.4 Dominant processes in erosion-corrosion conditions

In the previous parts of this chapter, the total degradation of the eight materials under this study has been discussed to be attributed from electrochemical and mechanical processes. The synergistic effects between corrosion and erosion are also important as reported by many studies [104, 105, 107]. In this study the components and the percentage contribution of the total weight loss of the eight materials under eight testing conditions has been determined as shown in Figure 5.22, Figure 5.43, Figure 5.56, Table 5.1, Table 5.5 and Table 5.6. The considerable

efforts have been made to develop diagrams separating the dominant processes for materials under erosion-corrosion conditions as it can be useful tool of material selection and performance prediction for marine industry [107]. In this study, the percentage due to erosion has been plotted for the three groups of materials under all the conditions assessed (Figure 5.22, Figure 5.43 and Figure 5.56). Such a diagram enables the erosion and corrosion related processes (C+S) to be compared to determine the dominant processes across a range of conditions. In comparison with Hu's [11] work which only separated the processes into only corrosion dominance and erosion dominance, three regime: corrosion dominance (E% ‹ 40%), erosion-corrosion dominance (40% ‹ E% ‹ 70%) and erosion dominance (E% › 70%) have been defined in this study. As presented in the results chapter, the shift of regime is dependent on the change of the environment: kinetic energy of the impacts on the surface per unit of time and the temperature which affect the mechanical and electrochemical processes of the material degradation respectively. Hence it is necessary to study effect of the environmental parameters on the erosion-corrosion behaviour of the materials as discussed in the following section of this chapter. The transitions from corrosion dominance to erosion-corrosion dominance and then to erosion dominance are determined by the electrochemical and mechanical effects on material degradations. Both stainless steel alloys and copper based alloys exhibit ductile behaviour, and mechanical effect plays more important role on dominance transition. For BS 3468 S2W Ni-resist cast iron, it exhibits brittle behaviour, and the dominance transition depends on both electrochemical and mechanical effects over the range of test conditions.

7.5 Effect of environmental parameters

Many studies have proved that environmental parameters affect erosion-corrosion behaviour [4, 8-10, 22], with which this thesis provided verification. The individual effects of increased velocity, sand loading and temperature positively contribute to enhance the overall material degradation, but also this later analyses show that the interaction between environmental parameters can accelerate weight loss during the erosion-corrosion process. If a predictive model is to be constructed

for erosion-corrosion it is necessary to be able to quantify the effects of these interactions in the total damage but also on the components of total weight loss.

7.5.1 Contribution to total weight loss and weight loss due to pure erosion

Table 6.2 - Table 6.8 show the contributions of environmental parameters and their interactions to the total weight loss and the weight loss due to pure erosion and over the range of conditions considered for the stainless steels and copper-base alloys assessed in this study. In term of percentage contributions shown, they are the percentage values of the sum of squares for that term relative to the total sum of squares for all terms, while sum of squares can be considered as the amount of information in the design that is attributed to that term. Higher sums of squares correlate to higher effects, which are the changes in the responses as the parameters are varied from its high level. Obviously, larger effects are going to be more significant, for example a two-level factor contributes 30%, then that term accounts for one third the total information in the data generated.

The prominent contributions to the total weight loss and weight loss resulting from pure mechanical erosion are due to velocity, sand loading and their interaction. It is clear that more kinetic energy needs to be dissipated by the materials at higher velocity to produce the deformations, cracks and even cuttings. The kinetic energy of the impact per second has been calculated in this work as shown in Table 7.1. It has been concluded that at higher impingement velocity, the particle impact velocities increase and more energy was provided to the moving particles, thus causing more severe degradation on the specimen surface [11, 107]. Moreover Ruff *et al.* [32] summarised some other parameters which affect the erosion rate of metals. This main parameter that controls the rate of erosion of materials is the particle velocity, the erosion rate is found to increase as v^2 to v^3 in most cases, therefore the rate of material erosion is proportional to v^2 in Bitter's model [33]. In terms of sand loading, as the sand loading increases, the protective film on the surface of the materials will be stripped off, and the naked metal will be exposed to the severe erosion-corrosion environment, which will enhance degradation. This analysis agrees with that velocity and sand loading play very important roles, but also the

results show that the interaction between velocity and sand loading is another key factor in erosion-corrosion environment.

Velocity (ms^{-1})	Sand loading (mgl^{-1})	No. of impacts	impact energy/second (J/s)
7	50	3	1.00E-04
7	500	30	1.00E-03
20	50	9	2.50E-03
20	500	90	2.50E-02

Table 7.1: Different levels of kinetic energy over the range of concerned conditions

In contrast to the passive materials, the interactive effect from velocity, sand loading and temperature exhibits to be most contributive to the total degradation and mechanical process for BS 3468 S2W Ni-resist cast iron. This is considered to be due to it active corrosion behaviour. Although the kinetic energy is playing an important role during erosion-corrosion, the increase in temperature to enhance the corrosion charge transfer is also very significant for BS 3468 S2W Ni-resist cast iron.

7.5.2 Contribution to the weight loss due to pure corrosion

For the contributions of the environmental parameters to the weight loss of stainless steels due to pure corrosion, the most influent parameter is velocity, but the effects from sand loading, temperature, the interaction between velocity and sand loading and the interaction between velocity and temperature also play a relatively important role in corrosion. As a result of the high velocity and sand loading, the protective film on the surface will be removed easily, which leads to reactive surface from the part of view of corrosion. It should be noted that the velocity plays a positive role on corrosion, which means higher frequency transfer of chloride ion on the surface at higher velocity. In terms of the effect of temperature, higher thermodynamic driving force occurs at higher temperature. As mentioned previously, the corrosion rate in static condition (C_0) and the erosion enhanced corrosion (ΔC_E). In defining the dynamic erosion enhanced corrosion is the key component of the corrosion correlating with environmental factors and their interactions. It could be

explained recursively that velocity, sand loading and their interaction have been approved to accelerate erosion, which will enhance corrosion further. In term of temperature effect on corrosion the higher thermodynamic driving force accelerates corrosion at higher temperatures. So it could be concluded that the environmental parameters and their interactions apply more or less effects on corrosion behaviour over the defined range of erosion-corrosion conditions for stainless steel alloys.

For the contributions of environmental parameters to the weight loss of high strength copper nickel alloys due to pure corrosion in erosion-corrosion environments, the prominent factors are all the interactions with velocity. Even though high strength cooper nickel alloys have high impingement resistance [74], the protective films on the surface are easily stripped off by the impingement with solid content. Moreover the mass transfer is assumed to be the rate of movement of a cuprous chloride complex away from the electrode surface to the bulk of the electrolyte [68]. At higher velocity and temperature, the velocity provides the greater amount of chloride ion transferring on the surface, and also the temperature produces greater thermodynamic driving force to accelerate corrosion in erosion-corrosion environment. But for nickel aluminium bronze alloy 747 and copper nickel chromium alloy 824, temperature and its interaction with other environmental parameters exhibit more effect on the weight loss due to pure corrosion in erosion-corrosion environment. At higher temperature, the solution has higher oxide content and higher thermodynamic driving force, which enhance the thermal oxidation of aluminium in nickel aluminium bronze alloy and chromium in copper nickel chromium alloy. Ni-resist cast iron shows similar contributions of environmental parameters to corrosion.

7.5.3 Contribution to the synergy

For the contributions of environmental parameters to the synergy for the stainless steels, it is clear that the most contributions to the synergy are due to velocity, sand loading and their interaction consistent with what was found for total weight loss and weight loss due to pure erosion in erosion-corrosion environments. The detailed magnitudes of synergy effects under impingement tests are shown in

Table 5.1. Even though the prominent factors to synergy are velocity, sand loading and their interaction, the relatively high synergy occurs as both high velocity and high sand loading are applied. It could be concluded that the synergy cannot be affected by either velocity or sand loading individually over the range of test conditions, because the brittle roughened surface can be removed under inadequate impact kinetic energy. But there is still sudden increase of synergy magnitude; the crucial impact energy could be reached as both velocity and sand loading increase. So it is hypothesized that the sudden increase of synergy magnitude could be determined by the critical impact kinetic energy. The synergy is defined as the corrosion enhanced erosion, and also reduction of mechanical properties occurred. They are made the materials erode easily. But the interactions between the environmental parameters are the key factors to affect the synergy of total weight loss for copper-base alloys and Ni-resist cast iron. The definition of synergy is the corrosion enhanced erosion in erosion-corrosion environment. All these interactions are the prominent factors to roughen the material surface, which resulted that the materials are easily to the eroded in eroded in erosion-corrosion environment.

7.6 Prediction model

The significance of the laboratory simulation experiments not only contributes to the detailed analysis for the specific cases, but it intangibly has built up a huge database to develop the prediction model for future material selection. If any physical or chemical phenomenon and processes can be explained, the rest of the modelling process is usually a mathematical exercise or numerical mapping. As mentioned in Chapter 5, the methodology for modelling is a linear regression method. It is not a final ideal model, but is the basis or initial skeleton to which more and more experimental points can be added, and hence the accuracy of the model could be improved. The current empirical model now forms the basis of the prediction model for erosion-corrosion which can now be refined by improving the data range and addressing more non-linear mathematical exercise, but actually the components of total weight loss changed non-linearly over the range of concerned

conditions. That is the reason for the difference between the experimental value and the predictive value produced by the model.

One function of this prediction model is to map the distribution of the components of total weight loss over a range of concerned conditions, which improve the scientific and technological understanding of the erosion-corrosion in varied conditions. The function was realised by the programming in MatLab which is a technical computing environment for high performance numeric computation and visualization. It integrates numerical analysis, matrix computation, signal processing and graphics in an easy-to-use environment. The components of total weight loss at eight conditions are defined as a matrix following to define the mesh distance to obtain high smoothness. Finally the distribution of the component of the total weight loss is interpolated by linear method. The rationale behind this interpolation is on average values of the attribute are more likely to be similar at points close together than at those further apart. It could be adopted to predict the values of attributes at un-sampled site from measurements made at point locations within the same area or region. More points we input into this model, the higher accuracy we obtained by this method. The general programming text is shown below:

Clear;

$V = zero\ (2,2,2)$; %make V a three-dimension matrix

$V(1,1,1) = W_1$; % initialise (W_i represents any components of the total weight loss)

$V(1,1,2) = W_2$;

$V(1,2,1) = W_3$;

$V(1,2,2) = W_4$;

$V(2,1,1) = W_5$;

$V(2,1,2) = W_6$;

$V(2,2,1) = W_7$;

$V(2,2,2) = W_8$;

$[x_i,y_i,z_i] = mashgrid$ (1:0.1:2, 1:01:2, 1:0.1:2)

VI = *interp3* (v,x_i,y_i,z_i)

After interpolation, the solid model of the distribution of the components of total weight loss could be visualized, from which more material damages occurred as the environmental parameters changed towards higher level (2 in Figure 7.16). Moreover, the distribution of any component of total weight loss at any concerned condition could be picked out this solid model (Figure 7.17), also it provides a way to compare the magnitude of the components of total weight loss between the materials at a specific condition (Figure 7.18). The variation tendency could be predicted at any specific test condition, for example the total weight loss will be increased as velocity increased at 50 °C and 500 mgl^{-1} sand loading (b in Figure 7.18). And also the total weight loss value could be compared by prediction at any condition (b and d in Figure 7.18, for example total weight loss value are predicted 0.008 g for UNS S31603 and 0.019g for NAB 747 at selected condition.

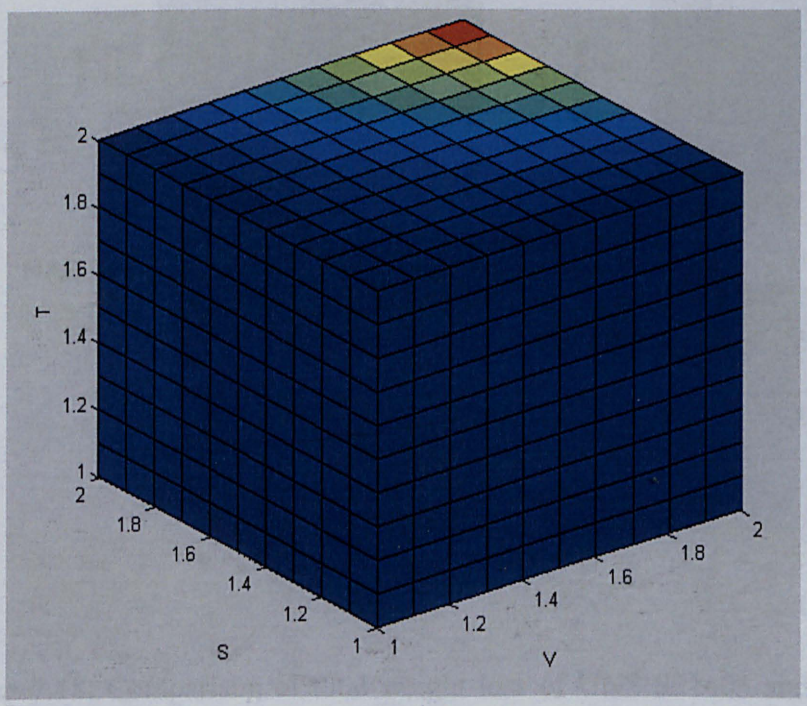

Figure 7.16: UNS S31603 the distribution model of total weight loss (T-temperature; V-velocity; S-sand loading)

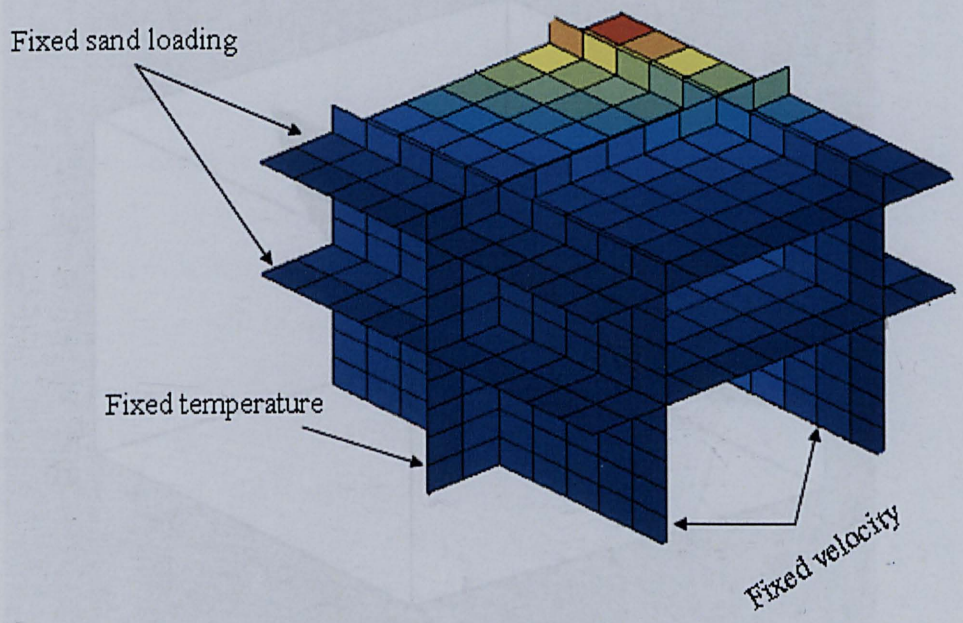

Figure 7.17: The distribution of total weight loss of UNS S31603 at fixed velocity, sand loading and temperature.

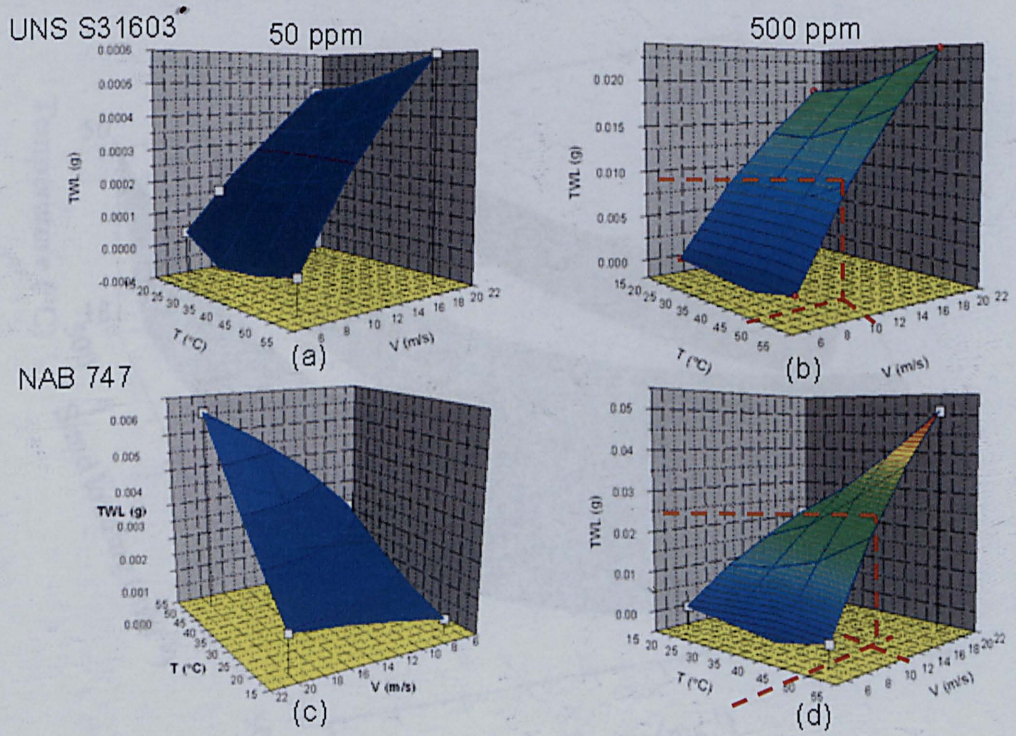

Figure 7.18: Comparison of total weight loss of UNS S31603 and NAB 747 at 50 and 500 mgl^{-1} predicted by modeling.

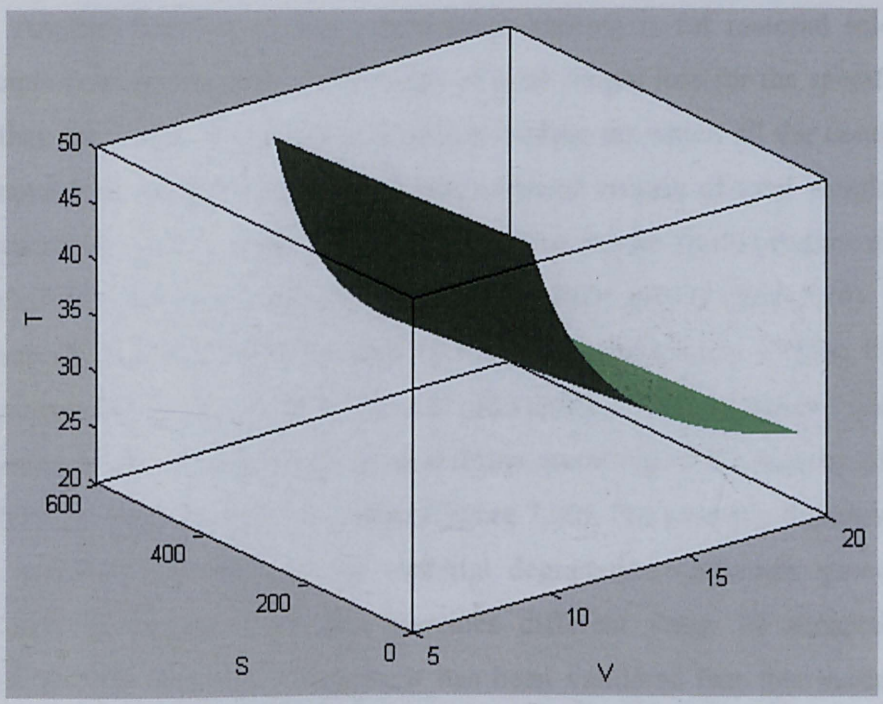

Figure 7.19: Example total weight loss limit for UNS S31603

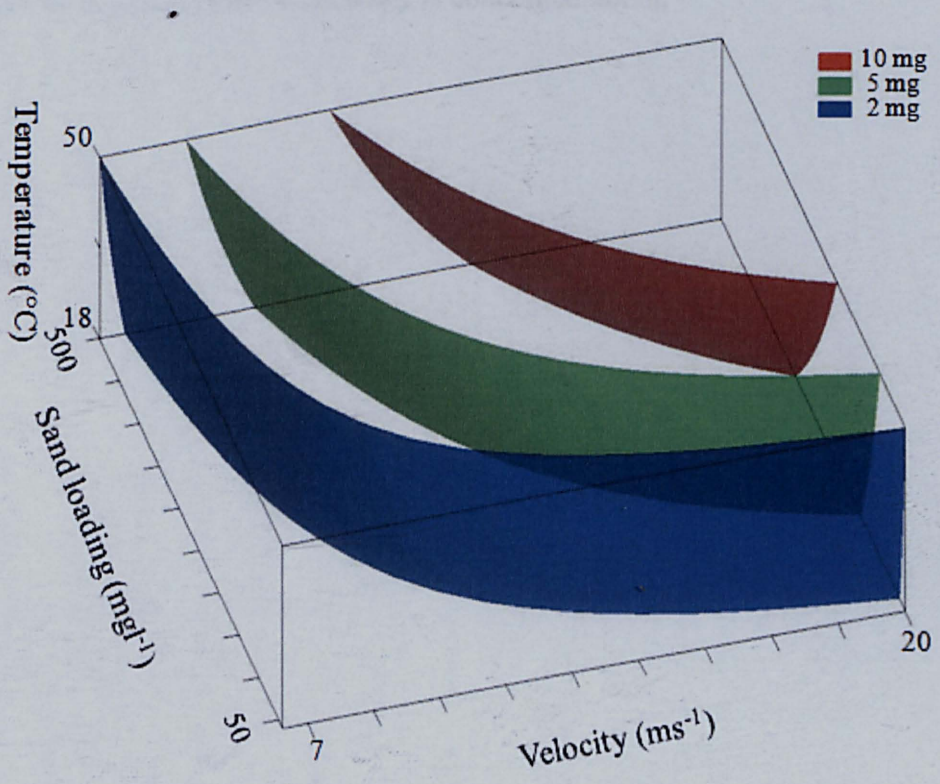

Figure 7.20: Three defined total weight loss limit (severe, moderate and mild)

Another function of this prediction modelling is for material selection. The principle is to set the critical allowance of total weight loss for the specific material, and then the model will produce a critical surface on which all the conditions have the same total weight loss value. Three assumed criteria of total weight loss were chosen as 10 *mg*, 5 *mg* and 2 *mg*. The prediction model could produce three critical surfaces for these assumed criteria of total weight loss (Figure 7.20). Finally the concerned condition will be located over or below this critical surface. If it is below the critical surface, it will be acceptable. Reversely, it will be denied. Moreover this prediction model could provide several limits according to the severity of conditions in which the material will be applied (Figure 7.20). For example different customers have different allowance of the material degradation (red-high; green-moderate; blue-mild in Figure 7.20), this provides different range of acceptable service conditions for the same materials. It has been validated that this model has good predictability not only inside the box, but also out of the range of conditions in Chapter 6. Hence the range of environmental conditions for this function could be extended to any condition the industry is concerned about.

Chapter 8 Conclusions

In this thesis, an experimental design method was adopted to study the erosion-corrosion behaviour of eight marine alloys under jet impingement using liquid containing solids. The erosion-corrosion mechanisms, the properties of the protective films and the correlation with the mechanical properties have been identified, analysed and quantified over a range of conditions of relevance across marine industry. It has been proved that the erosion-corrosion resistance of the selected materials is dependent on a series of factors such as properties of the protective films on the material surface, alloying elements and severity of the environmental conditions.

For erosion-corrosion tests carried out under liquid-solid impingement to determine the erosion-corrosion resistance of eight marine alloys, the following conclusions can be made:

- The eight marine alloys can be divided into three groups according to their total weight loss values:

    1. **First group**: Stainless steels form greatest protective surface films exhibits best erosion-corrosion resistance at all test conditions compared with other materials in this study.

    2. **Second group**: Copper-base alloys show relatively good erosion-corrosion resistance at low velocity due to their porous protective surface films. However, when the materials are subjected to severe erosion-corrosion, high grade of degradation occurs as the protective films can be stripped from the metal surface due to intermediate or high energy impact.

    3. **Third group**: Ni-resist cast iron shows active behaviour in all environmental conditions. Although low corrosion resistance is observed over the range of conditions, better erosion-corrosion resistance than copper-base alloys can be found conditions with

high energy impact due to its better mechanical properties such as hardness than copper-base alloys.

- Within the stainless steel alloys group, Vistar exhibits the best erosion-corrosion resistance followed by UNS S32760 and UNS S31603, which is as expected due to the extent of alloying elements, especially the composition of Chromium, Molybdenum and Nitrogen. These alloying elements improve the corrosion resistance of the alloys and hence the superior erosion-corrosion resistance.

- Within the group of copper-base alloys, high strength copper nickel Marinel 230 shows better erosion-corrosion resistance due to enhanced mechanical properties and optimum elemental compositions.

- The materials exhibit the different corrosion behaviour as the environmental conditions change:

    1. For stainless steels, there is a transition of corrosion behaviour from passive to pseudo-passive dependent on the severity of the erosion-corrosion environment.

    2. Copper-base alloys exhibit low current active behaviour in mild conditions. There is a film reformation process in the moderate condition during anodic polarisation. Finally the materials show active behaviour in the most severe conditions.

    3. Ni-resist cast iron always shows active behaviour in all conditions.

- The protective films on the surface of copper-base alloys have been identified. The amount of protective films remaining on the surface after erosion-corrosion tests depends on the impact angle and impact energy. The protective film on high strength copper nickel Marinel 230 exhibits better adhesion ability.

- The erosion-corrosion resistance of the range of materials has been correlated with the hardness of the materials. There is no correlation between the erosion-corrosion resistance and the initial hardness of the materials. However, a linear relationship can be found between the erosion-corrosion resistance and the hardness measured after the tests

carried out under the most severe conditions suggesting the significance of the surface work hardening process during erosion-corrosion.

- Kinetic energy plays an important role in enhancing material degradation of stainless steels as high velocity (20 ms^{-1}) and high sand loading (500 mgl^{-1}) result in greater than 15% weight loss due to synergy.
- Standard stainless steel UNS S31603 exhibits a more prominent weight loss due to synergy compared with the high alloy stainless steels Vistar and UNS S32760.
- In the conditions of 50 °C, velocity 7 ms^{-1} and sand loading 50 mgl^{-1}, it was found that there is no effect on synergy of stainless steels as in agreement with the erosion percentage analysis due to flow-induced corrosion dominance.
- Erosion dominance (E% > 70%) is clear when the environment becomes more severe with high velocity (20 ms^{-1}) and high sand loading (500 mgl^{-1}) for the copper-base alloys.
- For high strength copper nickel alloys, the transition condition between corrosion dominance and erosion dominance is 18 °C with 20 ms^{-1} velocity and 50 mgl^{-1} sand loading due to the high intensity of liquid-solid impacts resulting in the significant surface work hardening and removal of protective film and base metal.
- The transition conditions of copper nickel chromium alloy 824 between erosion dominance and corrosion dominance are located at low temperature with moderate impact energy.
- Nickel aluminium bronze alloy 747 exhibits corrosion dominance at high temperature with low or moderate impact energy. At low temperature, erosion of the material is enhanced when sand loading increases.
- When the material exhibits corrosion dominance in erosion-corrosion environment, synergy accounts for higher percentage of total weight loss and *vice versa*.

An experimental design method was adopted to study the corrosion resistance, erosion resistance and erosion-corrosion resistance of different materials at a range of conditions. It is also applied to identify the effects of environmental parameters on erosion-corrosion. The contributions of environmental parameters to the erosion-corrosion resistance can quantified by ANOVA analysis. From the results the following conclusions can be made:

- The values of the total weight loss components increase as any environmental parameter changed from the low level to the high level. The erosion-corrosion resistance of different materials show great dependence on the environmental severities.
- The sand loading and velocity exhibit greater effects than temperature on corrosion behaviour of the materials.
- Effect of temperature on weight loss due to synergy is less significant at low flow velocity (7 ms^{-1}) compared with high flow velocity (20 ms^{-1})
- Both kinetic and thermodynamic energy play an important role in enhancing material degradation due to synergy at high velocity (20 ms^{-1}), high sand loading (500 mgl^{-1}) and high temperature (50 °C).
- According to ANOVA analysis, effects of velocity, sand loading and their interaction are more significant on total weight loss and weight loss due to pure erosion for both stainless steels and copper-base alloys over the range of test conditions as mechanical removal of the materials are determined by the kinetic energy of liquid-solid impingement.
- Affective factors on corrosion for stainless steel alloys are velocity, sand loading, temperature, interaction between velocity and sand loading, and interaction between velocity and temperature. All these factors are relevant to the removal of protective film, film growth and corrosion rate.
- All the interactions between the environmental parameters play an important role on corrosion behaviour of high strength copper nickel alloys. The corrosion behaviour of nickel aluminium bronze and copper nickel chromium alloys are affected by temperature.

- Sand loading, velocity and their interaction are prominent to synergy for stainless steels over the range of testing conditions.
- All the effects from the interactions between environmental factors exhibited to be the most significant on the synergy for copper-base alloys as corrosion dominance accounts for most of the materials degradation over the range of testing conditions.
- Effects of environmental factors on Ni-resist cast iron differ from both stainless steel and copper-base alloys which possess an oxide layer accounting for erosion-corrosion resistance under liquid-solid impingement. The individual environmental parameter does not exhibit to have significant effect on the total weight loss and its components. The interactions between velocity, sand loading and temperature produced the greater effects.

From the study, the erosion-corrosion resistance have been assessed over a range of test conditions, based on which the industry could have overall comparison with different materials.

- This study assessed the erosion-corrosion resistance of the materials over a range of test conditions, which built up the database for future material selection relating to their material and maintenance costs in the service.
- The analysis of dominance process in erosion-corrosion environment could help the industry to understand the material degradation, but also it helps the manufacturers to improve the overall erosion-corrosion resistance and longevity by adding alloying elements and enhancing the mechanical properties.
- This study enabled the effects of the environmental parameters on erosion-corrosion resistance of the materials to be assessed. The overall erosion-corrosion degradation and its components were quantified in a range of test conditions. Such information can assist the future corrosion management in mass loss prediction, future material selection and erosion-corrosion prevention methods *etc.*

- The linear regression model could be used to develop commercial software, which can provide general criteria for the material selections at different levels of environmental severities.

Chapter 9 Future work

The overall erosion-corrosion and its components of eight marine alloys used in marine applications have been systematically studied. The environmental parameters were set two levels. Velocity and sand loading exhibited more important effects on overall erosion-corrosion degradation for eight materials. In future work, more levels of sand loading and velocity could be taken into account according to experimental design method, for example velocity could extend to 3 and 30 ms^{-1}, and 1000 mgl^{-1} sand loading can be considered. 3.5% sodium chloride was used to simulate seawater, but 15% H_2S or CO_2 is a popular environmental problem in oil and gas industry. In the future work, erosion-corrosion resistance of the selected materials can be assessed in 3.5% sodium chloride solution with H_2S or CO_2 dissolution. As severity of the conditions is defined in this study, more work needs to determine the environmental effects on the transition of the dominance process in erosion-corrosion.

In this study, all the specimens were immersed in 3.5% solution for 24 hours before erosion-corrosion tests which is to grow the passive or protective film on the surface of the materials. The growth of protective films for copper-base alloys is time dependent. In the future work, longer immersion time could be considered to assess the effect of immersion time on erosion-corrosion resistance of copper-base alloys. Moreover different adhesion abilities of protective films on the copper-base alloys were found, so the reasons for different adhesion abilities need to be carried out, but also the film characterisation in relation to corrosion and erosion-corrosion performance could be considered.

The prediction model was initialised by using linear regression method in this study. In order to develop the mass loss prediction and material selection model for the end users from the industry, a mature computational program need to be adopted in the future work. It is also necessary to apply a wider range of the practical conditions to enable the predictability of the model to be improved. Validation of the

model with field data is also recommended to relate the laboratory work to meet the industrial requirements.

References

1. Evans, U.R., *An introduction to metallic corrosion.* 1963, London: Arnold.
2. Limited, C., *Review of corrosion management for offshore oil and gas processing.* Health & Safety Executive, 2001.
3. Wood, R.J.K., *Erosion-corrosion interactions and their effect on marine and offshore materials.* Wear, 2006. **261**(9): p. 1012-1023.
4. M.U.S.O., C., *Personal Communication.* October 1999.
5. Johnson, J.T., *Ships.* CC Technologies Laboratories, Inc., Dublin, Ohio.
6. Heitz, E., *Mechanical based prevention strategies of flow-induced corrosion.* Electrochimica Acta, 1995. **41**(4): p. 503-509.
7. Scully, J.C., *The fundamentalsof corrosion.* 1990.
8. A. Neville, M.R., H. Xu, *Examining corrosion effects and corrosion/erosion interactions on metallic materials in aqueous slurries.* Tribology International, 2002. **35**: p. 643-650.
9. A. Neville, T.H., *An Assessment of The Corrosion Behaviour of High-grade Alloys in Seawater at Elevated Temperature and Under a High Velocity Impinging Flow.* Corrosion Science, 1996. **38**(6): p. 927-956.
10. M. M. Stack, N.C., S. Zhou, *A methodology for the construction of the erosion-corrosion maps in aqueous environments.* Wear, 1997. **203-204**: p. 447-488.
11. Xinming, H., *The corrosion and erosion-corrosion behaviour of high alloy stainless steels*, in *School of Mechanical Engineering.* 2002, University of Leeds.
12. Kean, R.L., *Cathodic protection.* DTI, 1981.
13. B. R. Pearson, P.A.B., R. B. Waterhouse, *Influnece of electrochemical potential on the wear of metals, particularly nickel.* Tribology International, 1988. **21**: p. 191-197.
14. Y. Li, G.T.B., I. M. Hutchings, *Influence of environmental composition and electrochemical potential on the slurry erosion-corrosion of aluminium.* Wear, 1995. **181-183**: p. 70-79.
15. Y. Naerheim, M.W.K., *The influence of electrochemical potential on wear.* Wear, 1985. **104**: p. 139-150.
16. Z. Yao, Y.Z., W. Ke, *The influence of applied potential on the erosion corrosion behaviour of AISI321 stainless steel in acidic slurry medium.* Wear, 1995. **186-187**: p. 568-572.
17. V. A. de Souza, A.N., *Corrosion and erosion damage mechanisms during erosion-corrosion of WC-Co-Cr cermet coatings.* Wear, 2003. **255**: p. 146-156.
18. Pourbaix, M., *Applications of electrochemistry in corrosion science and in practice.* Corrosion Science, 1974. **14**: p. 25-82.
19. *Corrosion ASTM Handbook.* 2005. **13B**.
20. Uhlig, H.H., *Corrosion Handbook.* John Wiley & Sons, 1948.
21. LaQue, F.L., *Localized Corrosion.* National Association of Corrosion Engineers, 1974: p. 47.
22. T. S. Lee, R.M.K., J. W. Oldfield, *Factor Influencing the Crevice Corrosion Behaviour of Stainless Steels.* Corrosion, 1983: p. 69.
23. G. J. Schafer, P.K.F., J. Electrochem. Soc., 1959. **106**: p. 468.

24. Freiman, T.A.M.a.S.W., *A molecular interpretation of stress corrosion in silica.* Nature, 1982. **295**: p. 511.
25. Andrews, E.H., *Developments in Polymer Science.* 1979, London: Applied Science.
26. McIntyre, P. *Corrosion problems and costs in the UK offshore and chemical industries.* in *Proceedings of EUROCORR 2000.* 2000.
27. Campbell, H.S., *The compromise between mechnical properties and corrosion resistance in copper and aluminium alloys for marine applications.* Ocean Engng, 1969. **1**: p. 387-393.
28. R. J. K. Wood, A.J.S., *Erosion-corrosion of candidate HVOF aluminium based marine alloys.* Wear, 2004. **256**: p. 545-556.
29. *Specification for ductile iron.* Http://www.keytosteel.com, 2003.
30. Yongxin Zhou, Z.L., Min Zhan, *An investigation of the erosion-corrosion characteristics of ductile cast iron.* Materials and Design, 2007. **28**: p. 260-265.
31. Nabil Fatahalla, A.A., Moenes Semeida, *C, Si and Ni as Alloying Elements to Vary Carbon Equivalent of Austenitic Ductile Cast Iron: Microstructure and Mechanical Properties.* Materials Science and Engineering, 2008.
32. Rafael A. Gonzaga, J.F.C., *Influence of an appropriate balance of the alloying elements on microstruture and on mechanical properties of nodular cast iron.* Material Processing Technology, 2005. **162-163**: p. 293-297.
33. Brown, J.R., *Ductile iron.* Foseco Ferrous Foundryman's Handbook, 2000: p. 70-89.
34. Xu, H., *Art assessment of corrosion and erosion-corrosion behaviour of austenitic cast iron and surface coatings for pump application.* 2002, Heriot Watt Univeristy.
35. J. O. Bello, R.J.K.W., J. A. Wharton, *Synergistic effects of micro-abrasion-corrosion of UNS S30403, S31603 and S32760 stainless steels.* Wear, 2007. **263**: p. 149-159.
36. Alfonsson, E., *Corrosion of stainless steels, general introduction,* in *Corrosion handbook for stainless steel.* 1994, Avesta Sheffield AB.
37. Wallen, B., *Some factors affecting stainless steel corrosion in seawater,* in *Corrosion handbook for stainless steels.* 1994, Avesta Sheffield AB.
38. Brigham, R.J., *Temperatuer as a pitting criterion.* Corrosion, 1974. **30**: p. 396-398.
39. S. Jin, A.A., Appl. Phys, 1988. **A 46**(51).
40. C. O. A. Olsson, S.E.H., *An AES and XPS study of the high alloy austenitic stainless steel 254 SMO tested in a ferritic chloride solution.* Corrosion Science, 1994. **36**(1): p. 141-151.
41. Diana Lopez, N.A.F., Andre Paulo Tschiptschin, *Corrosion-erosion behaviour of austenitic and martensitic high nitrogen stainless steels.* Wear, 2007. **263**: p. 347-354.
42. Hanninen, H., *Applications and performance of high nitrogen steels.* Proceedings of HNS 2004, 2004: p. 371-380.
43. R. M. Davison, T.R.L., J. D. Redmond, H. Watanabe, M. Semchyshen, *A review of worldwide developments in stainless steels.* Materials & Design, 1986. **7**(3).
44. M. B. Ives, Y.C.L., J. L. Luo, *Cathodic reactions involved in metallic corrosion in chlorinated saline environments.* Corrosion Science, 1991. **32**(1): p. 91-102.

45. R. D. Villenbruch, C.R.C., M. oversluizen, D. Kim, Y. Lu, *An XPS and electrochemical study of the influence of molybdenum and nitrogen on the passivity of austenitic stainless steel.* Corrosion Science, 1990. **31**: p. 179-190.
46. A. R. Troiano, R.F.H., *Sulfide stress cracking of high strength modified Cr-Mo steels.* Mater. Performance, 1979. **18**: p. 31-39.
47. Moller, G.E., *Successful use of austenitic stainless steels in seawater.* Society of Petroleum Engineering, 1977.
48. A. Neville, T.H., J. T. Dallas, *A study of the erosion-corrosion behaviour of engineering steels for marine pumping applications.* Wear, 2001. **251**: p. 1257-1264.
49. D. Lopez, C.S., A. Toro, *Corrosion-erosion behaviour of TiN-coated stainless steels in aqueous slurries.* Wear, 2005. **258**: p. 684-692.
50. M. A. Quraishi, F.A.A., D. Jamal, *Thiourea derivatives as corrosion inhibitors for mild steel in formic acid.* Materials Chemistry and Physics, 2003. **77**(3): p. 687-690.
51. Sedriks, A.J., *Corrosion of Stainless Steels.* Wiley, 1996(2nd edition): p. 88.
52. Arnvig, P.-E., *Stainless steels in oil and gas production*, in *Corrosion handbook for stainless steels*. 1994, Avesta Sheffield AB.
53. Ralph M. Davison, J.D.R., *Practical guide to using duplex stainless steels.* Material Performance, 1990. **29**(1): p. 57-62.
54. G. Kear, B.D.B., F. C. Walsh, *Electrochemical study of UNS S32550 super duplex stainless steel corrosion in turbulent seawater using the rotating cylinder electrode.* Corrosion, 2004. **60**.
55. C. A. Powell, H.T.M., *Copper-Nickel for Seawater Corrosion Resistance and Antifouling - A State of the Art Review.* NACE Corrosion, 2000.
56. R. J. Ferrara, J.P.G., *Corrosion behaviour of copper base alloys with respect to seawater velocity.* Naval ship R&D Centre, 1972(NSRDC-28-108).
57. Syrett, B.C., *Erosion-corrosion of copper nickel alloys in seawater and other aqueous enviroments - a literature review.* 1976.
58. Pearson, C., *Role of iron in the inhibition of corrosion of marine heat exchangers - a review.* Brit. Corros, 1972. **7**(3).
59. R. F. North, M.J.P., *Influence of corrosion product structure on the corrosion rate of Cu-Ni alloys.* Corrosion Science, 1970. **10**: p. 297-311.
60. Waheed A. Badawy, K.M.I., Ahlam M. Fathi, *Effect of Ni content on the corrosion behaviour of Cu-Ni alloys in neutral chloride solutions.* Electrochimica Acta, 2005. **50**(18): p. 3603-3608.
61. *Summary of experimental data-copper-nickel alloys IN-828 and IN-848.* Trade literature of international nickel Co. Inc, 1970.
62. Institute, G.C., *DKI German copper institute booklet: Copper nickel alloys: Properties, Processing, Application.*
63. Rogers, T.H., *Marine Corrosion.* George Newnes Ltd.,, 1968.
64. S. D. Cramer, B.S.C., *ASM Handbook - Corrosion: Materials.* 2005. **13B**.
65. Efird, K.D., *The international of corrosion and fouling of metals in seawater.* Material Performance, 1976. **15**(4): p. 16-25.
66. C. Kato, H.W.P., Electrochem Soc., 1984. **131**.
67. W. C. Stewart, F.L.L., Corrosion, 1952. **8**: p. 259.
68. G. Kear, B.D.B., K. Stokes, F. C. Walsh, *Electrochemical corrosion behaviour of 90/10 Cu-Ni alloy in chloride-based electrolytes.* Journal of Applied Electrochemistry, 2004.

69. C. A. Powell, H.T.M., *Marine applications of Cu-Ni alloys, Section 1: Cu-Ni alloy - resistance to corrosion and biofouling.* 1998.
70. F. Mansfeld, B.L., *Microbiologically influenced corrosion of copper-based materials exposed to natural seawater.* Electrochimica Acta, 1992. **37**(12): p. 2291-2297.
71. J. E. Castle, M.S.P., *Corrosion Prevention and Control.* 1986.
72. Y. Z. Wang, A.M.B., G. Poggi, *The effect of temperature on the corrosion behaviour of a 70/30 Cu-Ni commercial alloy in seawater.* corrosion Science, 1994. **36**(8): p. 1277-1288.
73. S. A. Campbell, G.J.W.R., C. D. S. Tuck, B. D. Barker, *Corrosion and Galvanic Compatibility Studies of a High-Strength Copper-Nickel Alloy.* NACE Corrosion, 2002.
74. Tuck, C.D.S., *High Strength Copper Nickels.* 2004.
75. Tuthill, A.H., *Guidelines for the use of copper alloys in seawater.* Material Performance, 1987. **26**(9): p. 12-22.
76. Meigh, H.I., *Cast and wrought aluminium bronzes - properties, processes and structure.* Institute of Material, 2000.
77. Callcut, V., *Aluminium Bronze.* www.copper.org, 2002.
78. Harold T. Michels, R.M.K., *Effect of composition and microstructure on the seawater corrosion resistance of nickel aluminium bronze.*
79. Howell, P.R., *On the Phases Micro constituents in Nickel-Aluminium-Bronze.* 2000.
80. A. Schussler, H.E.E., *The corrosion of nickel-aluminium-bronzes in seawater - I. Protective layer formation and the passivation mechanism.* Corrosion Science, 1993. **34**(11): p. 1793-1802.
81. S. M. Sayed, E.A.A., B. G. Ateya, *Inhibitive effects of benzotriazole on the stress corrosion cracking of α-brass in nitrite solution.* Corrosion Science, 1994. **36**(2): p. 221-225.
82. J. A. Wharton, R.C.B., G. Kear, R. J. K. Wood, K. R. Stokes, F. C. Walsh, *The corrosion of nickel aluminium bronze in seawater.* Corrosion Science, 2005. **47**(12): p. 3336-3367.
83. Ault, J.P., *Erosion-Corrosion of nickel aluminium bronze in flowing seawater.* Corrosion, 1995.
84. *http://corrosion-doctors.org/Forms-Erosion/erosion.htm.* [cited.
85. Villarreal, M.E.R.d., *Examining mechanical and electrochemical degradation mechanisms on materials used in sub-sea drilling.* 2002, Heriot Watt University.
86. Xinming, H., *The corrosion and erosion-corrosion behaviour of high alloy stainless steels, PhD thesis.*
87. S. Das, Y.L.S., D. P. Mondal, *Erosive-corrosive wear of aluminium alloy composites: Influence of slurry composition and speed.* Wear, 2006. **261**: p. 180-190.
88. *Annual Book of ASTM Standards 2002.* Vol. 03. 2002.
89. K. S. Tan, J.A.W., R. J. K. Wood, *Solid particle erosion-corrosion behaviour of a novel HVOF nickel aluminium bronze coating for marine applications - correlation between mass loss and electrochemical measurements.* Wear, 2005. **258**(1-4): p. 629-640.
90. Madsen, B.W., *Measurement of erosion-corrosion synergism with a slurry wear test apparatus.* Wear, 1988. **123**: p. 127-142.
91. A. W. Batchelor, G.E.S., *Predicting synergism between corrosion and abrasive wear.* Wear, 1988. **123**: p. 281-291.

92. D. C. Kotlyar, C.H.P., M. E. Wadsworth, *Simultaneous corrosion and abrasion measurements under grinding conditions.* Corrosion, 1988. **44**: p. 221-228.
93. A. Neville, T.H., T. Dallas, *A study of the erosion-corrosion behaviour of engineering steels for marine pumping applications.* Wear, 1995. **186-187**: p. 497-507.
94. A. Neville, T.H., *Electrochemical and mechanical erosion-corrosion of high-velocity oxy-fuel (HVOF) coatings.* Wear, 1999. **235**: p. 623-634.
95. J. Perry, A.N., T. Hodgkiess, V. A. Wilson, *Erosion-corrosion of WC-Co thermal sprayed cermet coatings in saline environments.* Surf. Coat. Technol., 2001. **137**: p. 43-51.
96. J. Yang, J.H.S., *Erosion-corrosion behaviour and cathodic protection of alloys in seawater - sand slurries.* Mater. Eng. Perform., 1993. **2**: p. 843-50.
97. F. H. Stott, J.E.B., R. C. Newman, *The corrosion wear of cast iron under potentiostatically-controlled conditions in sulphuric acid solutions.* Corrosion Science, 1990. **30**: p. 813-830.
98. K. Y. Kim, S.B., V. Agarwala, *An electrochemical polarisation technique for evaluation of wear-corrosion in moving components under stress.* Wear, 1981: p. 772-778.
99. X. X. Jiang, S.Z.L., D. D. Tao, J. X. Yang, *Accelerative effect of wear on corrosion of high-alloy stainless steel.* Corrosion, 1993. **49**: p. 836-841.
100. A. Neville, M.R., T. Hodgkiess, A. Gledhill, *Mechanisms of wear on a Co-base alloy in liquid-solid slurries.* Wear, 2000. **238**: p. 138-150.
101. M. Reyes, A.N., *Degradation mechanisms of Co-based alloy and WC metal-matrix composites for drilling tools offshore.* Wear, 2003. **255**: p. 1143-1156.
102. V. A. de Souza, A.N., *Aspects of microstructure on the synergy and overall material loss of thermal spray coatings in erosion-corrosion environments.* Wear, 2007. **263**: p. 339-346.
103. A. Neville, T.H., *A study of the effect of liquid corrosivity in liquid-solid impingement of a cast iron and austenitic stainless steel.* British Corrosion, 1997. **32**(3): p. 197-205.
104. A. Neville, X.H., *Mechanical and electrochemical interactions during liquid-solid impingement on high-alloy stainless steels.* Wear, 2001. **251**: p. 1284-1294.
105. R. J. K. Wood, S.P.H., *The synergistic effect of erosion and corrosion: trends in published results.* Wear, 1990. **140**: p. 387-394.
106. Wood, R.J.K., *Erosion-corrosion interactions and their effect on marine and offshore materials.* Wear, 2006. **261**: p. 1012-1023.
107. M. M. Stack, S.Z., R. C. Newman, *Identification of transitions in erosion-corrosion regimes in aqueous environments.* Wear, 1995. **186-187**: p. 523-532.
108. M. M. Stack, S.L., F. H. Stott, *Erosion-corrosion regimes: number, nomenclature and justification.* Tribology International, 1995. **28**(7): p. 445-451.
109. Nesic, S., *Key issues related to modelling of internal corrosion of a oil and gas pipelines - A review.* Corrosion Science, 2007. **49**: p. 4308-4338.
110. Poulson, B., *Complexities in predicting erosion-corrosion.* Wear, 1999. **233-235**: p. 497-504.
111. Finnie, I., *The mechanism of erosion of ductile metals.* Proc. 3rd U. S. Natl. Congr. Appl. Mech, 1958: p. 527-532.

112. G. L. Sheldon, A.K., *An investigation of impingement erosion using single particle.* Wear, 1972. **21**: p. 195-209.
113. G. Sundararajan, P.G.S., *A new model for the erosion of metals at normal incidence.* Wear, 1983. **84**: p. 237-258.
114. Hutchings, I.M., *A model for the erosion of metals by spherical particles at normal incidence.* Wear, 1981(70): p. 269-281.
115. B. K. Gandhi, S.N.S., V. Seshadri, *Study of the parametric dependence of erosion wear for the parallel flow of solid-liquid mixtures.* Tribology International, 1999. **32**(275-282).
116. Elkholy, A., *Prediction of abrasion wear for slurry pump materials.* Wear, 1983. **84**: p. 39-49.
117. Girish R. Desale, B.K.G., S. C. Jain, *Slurry erosion of ductile materials under normal impact condition.* Wear, 2008. **264**: p. 322-330.
118. R. Gupta, S.N.S., V. Seshadri, *Prediction of uneven wear in a slurry pipeline on the basis of measurements in a pot tester.* Wear, 1995. **184**: p. 169-178.
119. HMcI, C., *The influence of flow field in slurry erosion.* Wear, 1992. **152**: p. 223-240.
120. A. Neville, F.R., S. Chiovelli, T. Revega, *Erosion-corrosion behaviour of WC-based MMCs in liquid-solid slurries.* Wear, 2005. **259**: p. 181-195.
121. M. G. S. Ferreira, N.E.H., G. Goodlet, S. Faty, A. M. P. Simose, M. DaCunha Belo, *Influence of the temperature of film formation on the electronic structure of oxide films formed on 304 stainless steel.* Electrochimica Acta, 2001. **46**(24-25): p. 3767-3776.
122. X. Hu, A.N., *The electrochemical response of stainless steels in liquid-solid impingement.* Wear, 2005. **258**: p. 641-648.
123. Fanaiming, L., Taoziyun, *An investigation of the corrosive wear of stainless steels in aqueous slurries.* Wear, 1996. **193**: p. 73-77.
124. D. H. Mesa, A.T., A. Sinatora, A. P. Tschiptschin, *The effect of testing temperature on corrosion-erosion resistance of martensitic stainless steels.* Wear, 2003. **255**: p. 139-145.
125. H. C. Behrens, F.D.M., O. Osborn, L. Rice, W. B. Russell, C. F. Schrieber, J. A. Hunter, W. S. Gilman, F. H. Coley, *Seawater corrosion test program, Research and Development progress report.* 1969.
126. Anderson, D.B., *Factors affecting corrosion of copper and copper alloys in hot seawater.* Meeting of the national association of corrosion engineers, 1971.
127. Fontana, M.G., *Corrosion Engineering.* 3rd ed. 1987, Singapore: McGraw-Hill.
128. J. A. Wharton, R.J.K.W., *Influence of flow conditions on the corrosion of AISI 304L stainless steel.* Wear, 2004. **256**: p. 525-536.
129. LaQue, F.L., *Marine Corrosion.* 1975, New York: Wiley.
130. Weber, J., *Flow induced corrosion: 25 years of industrial research.* British Corrosion, 1992. **27**(3): p. 193-199.
131. D. Lopez, J.P.C., J. R Cano, A. Toro, A. P. Tschiptschin, *Effect of particle velocity and impact angle on the corrosion-erosion of AISI 304 and AISI 420 stainless steels.* Wear, 2005. **259**: p. 118-124.
132. Danek, G.J., *The effect of seawater velocity on the corrosion behaviour of metals.* Naval Engineers, 1966. **78**(5): p. 763-769.
133. Y. G. Zheng, Z.M.Y., W. Ke, *Erosion-corrosion resistant alloys development for aggressive slurry flows.* Material Letters, 2000. **46**(6): p. 362-368.

134. T. R. Beck, S.G.C., *Experimental observations and analysis of hydrodynamic effects on growth of small pits.* Corrosion, 1981. **37**: p. 665-671.
135. K. Anand, H.C., *Microstructure effects in the erosion of cemented carbides.* Wear, 1989. **1**: p. 136-142.
136. HMcl. Clark, K.K.W., *Impact angle, particle energy and mass loss in erosion by dilute slurries.* Wear, 1995. **186-187**: p. 454-464.
137. P. Novak, A.M., *Erosion-corrosion of passive metals by solid particles.* Corrosion Sceince, 1993. **35**: p. 635-640.
138. Finnie, I., *Erosion of surfaces by solid particle.* Wear, 1960. **3**: p. 87-103.
139. Courtney, T.H., *Mechanical Behavior of Materials.* 1990, New York: McGraw-Hill.
140. M. Liebhard, A.L., *The effect of erodent particle characteristics on the erosion of metals.* Wear, 1991. **151**: p. 381-390.
141. S. Bahadur, R.B., *Erodent particle characterization and the effect of particle size and shape on erosion.* Wear, 1990. **138**: p. 189-208.
142. Z. Feng, A.B., *The erosion of four materials using seven erodents - towards an understanding.* Wear, 1999. **233-235**: p. 674-684.
143. A. V. Levy, P.C., *Teh effects of erodent composition and shape on the erosion of steel.* Wear, 1983. **89**: p. 151-162.
144. F. Y. Lin, H.S.S., *Effect of impact velocity on slurry erosion and a new design of a slurry erosion tester.* Wear, 1991. **143**: p. 231-240.
145. F. G. Hammitt, F.J.H., *Liquid-erosion failures.* ASM Metal Handbook, 1975. **10**: p. 160-167.
146. K. C. Barker, A.B., *Synergistic abrasive-corrosive wear of chromium containng steels.* British Corrosion, 1989. **24**(3): p. 222-228.
147. J. G. Chacon Nava, F.H.S., M. M. Stack, *The effect of substrate hardness on the erosion-corrosion resistance of materials in low-velocity conditions.* Corrosion Science, 1993. **35**: p. 1045-1051.
148. Preece, C.M., *Treatise on materials science and technology.* Erosion, 1979. **16**.
149. Hutchings, I.M., *Tribology: Friction and wear of engineering materials.* 1992: p. 179-197.
150. Kelton, W.D., *Experimental design for simulation.* 2000.
151. K. Hinkelmann, O.K., *Design and Analysis of Experiments.* Advanced Experimental Design. Vol. 2. 2005: John Wiley & Sons.
152. M. Abdel Aziz, T.S.M., A. Abdel Aal, *Modeling and optimizing the factors affecting erosion-corrosion of AA6063-(TiC/Al2O3) hybrid composites by experimental design method.* Material Science and Engineering, 2008. **486**: p. 313-320.
153. Jonas V. Bilenas, J.P.M.C., Design for quality - An introduction to experimental design using SAS.
154. Tai Yue Wang, C.Y.H., Improving forecasting performance by emplying the Taguchi method, European Journal of operational research, 2005.
155. Callcut, V., *Aluminium Bronze.* www.copper.com.
156. *Standard Practice for Preparing, Cleaning, and Evaluating Corrosion Test Specimens.* Designation: G 1-90, 1999.
157. A. U. Malik, N.A.S., A. Ahamad, I. N. Andijani, *The effect of dominant alloy additions on the corrosion behaviour of some conventional and high alloy stainless steels in seawater.* Corrosion Science, 1995. **37**(10): p. 1521-1535.

158. Ahmad, Z., *Principles of corrosion engineering and corrosion control.* 2006: Butterworth-Heinemann.
159. http://engnet.anu.edu.au/DEcourses/engn4520/Pourbaix.pdf.
160. DeHoff, R., *Thermodynamics in materials science.* 2006: CRC Presser.
161. Revie, R.W., *Corrosion and Corrosion Control.* 2008: Wiliy.
162. R. A. Flinn, P.K.T., *Engineering Materials and Their Application.* 4th Edition, Houghton Mifflin Company, 1990.
163. http://en.wikipedia.org/wiki/Analysis_of_variance.
164. http://www.mathworks.com/products/matlab/.
165. R. S. Lynn, K.K.W., HMcI Clark, *On the particle size effect in slurry erosion.* Wear, 1991. **149**: p. 55-71.
166. Wood, F.W., *Erosion by solid-particle impacts - a testing update.* J. Test. Eval., 1986. **14**: p. 23-27.
167. Ugur Malayoglu, A.N., *Mo and W as alloying elements in Co-based alloys - their effects on erosion-corrosion resistance.* Wear, 2005. **259**: p. 219-229.
168. V. A. de Souza, A.N., *Corrosion and synergy in a WC-Co-Cr HVOF thermal spray coating - understanding their role in erosion-corrosion degradation.* Wear, 2005. **259**: p. 171-180.
169. R. G. Blundy, M.J.P., *The potential dependence of reaction product composition on copper-nickel alloys.* Corrosion Science, 1972. **12**: p. 65-75.
170. C. J. Park, H.S.K., *Comparison of repassivation kinetics of stainless steels in chloride solution.* Metals and Materials International, 2005. **11**: p. 309-312.
171. F. Mansfeld, B.L., *A technical review of electrochemical techniques applied to microbiologically influenced corrosion.* Corrosion Sceince, 1991. **32**(3): p. 247-272.
172. F. Mansfeld, R.T., Hong Shih, B. Little, R. Ray, P. Wagner, *An electrochemical and surface analytical study of stainless steels and titanium exposed to natural seawater.* Corrosion Science, 1992. **33**(3): p. 445-456.

Appendix – Publications

1. H. Meng, X. Hu and A. Neville, A systematic erosion-corrosion study of two stainless steels in marine conditions via experimental design, Wear, 263 (2007) 355-362

2. H. Meng, X.Hu and A. Neville, Study of corrosion in erosion-corrosion of two stainless steels in simulated marine conditions via experimental design, Paper No. 07254, NACE CORROSION, 2007

Available online at www.sciencedirect.com
ScienceDirect
Wear 263 (2007) 355–362
WEAR
www.elsevier.com/locate/wear

A systematic erosion–corrosion study of two stainless steels in marine conditions via experimental design

H. Meng*, X. Hu, A. Neville

Corrosion and Surface Engineering Research Group, School of Mechanical Engineering, University of Leeds, Leeds LS2 9JT, UK

Received 25 August 2006; received in revised form 13 December 2006; accepted 18 December 2006
Available online 26 March 2007

Abstract

Erosion–corrosion performance of two stainless steels (UNS S32760 and UNS S31603) for marine applications has been assessed under liquid–solid impingement conditions in 3.5% NaCl. The total material loss rate and the components of mechanical erosion, electrochemical corrosion and their synergistic *interactions* have been determined under various conditions. The major environmental parameters considered are solid loading, flow velocity and fluid temperature. For the two stainless steels, a quantitative analysis of the damage showed mechanical erosion to be the dominant process under erosion–corrosion over the range of conditions considered. A full two-level factorial experimental design method was applied to study the individual effects of each parameter as well as their interactive contributions to the overall material degradation. The analysis shows that the *interactions* between environmental factors all accelerate mass loss during the erosion–corrosion process and the interactive effect between velocity and sand loading is the greatest. Fluid temperature has the smallest effect of the three parameters. Some guidelines to assist in material selection for erosion–corrosion and progress towards prediction of erosion–corrosion in marine applications are discussed in this paper.

Keywords: Stainless steels; Marine; Erosion–corrosion; Experimental design

1. Introduction

It is well known that the industries that transport slurries and other particle-laden liquids in pipes for sectors such as offshore and marine technologies spend millions of pounds every year to repair material damage. The typical examples of this kind of material destruction are erosion–corrosion damage to pumps, impellers, propellers, valves, heat exchanger tubes and other fluid handling equipment. In a recent survey, erosion–corrosion was rated in the top five most prevalent forms of corrosion damage in the oil and gas industry [1,2]. A lot of work has been carried out to characterise and classify the materials related to mining and marine industries.

Erosion–corrosion in aqueous systems is dominated by two major mechanisms: electrochemical corrosion and mechanical erosion [3]. On account of the greater material loss than the sum of their individual components, the *interaction* between electrochemical and mechanical processes has been recognised in many works, and they have been referred to as 'Synergistic' and 'Additive' effects [3–5]. The so-called synergistic effect is normally used to describe the way in which corrosion can enhance erosion, while the so-called additive effect refers to the mechanism by which erosion can enhance corrosion. In defining the erosion–corrosion behaviour the regimes are often defined to be erosion-dominated, corrosion-dominated or erosion corrosion-dominated with the regime depending on the specific working environments and the material type [6].

There have been numerous studies by the authors and others which have focused on assessing material durability in erosion–corrosion environments as a function of several parameters including velocity, sand loading, temperature or pH [7–15]. Though the studies show how environmental factors affect erosion–corrosion behaviour, it has been difficult to predict quantitatively how the damage will be affected by factors and their *interactions*. In an attempt to extend understanding of how factors affect the extent of damage in erosion–corrosion and constitution of that damage (i.e. corrosion, erosion or synergy); an experimental design method has been used. The primary goal of experimental design in scientific research is usually to show

* Corresponding author.
E-mail address: menhme@leeds.ac.uk (H. Meng).

0043-1648/$ – see front matter © 2007 Elsevier B.V. All rights reserved.
doi:10.1016/j.wear.2006.12.007

Table 1
Nominal compositions and macrohardness of UNS S32760 and UNS S31603

	Cr	Ni	Mo	Mn	C	N	Macro
UNS S32760	24.9	8.4	3.65	0.94	0.026	0.21	222 HB
UNS S31603	18.5	10.3	2.2	1.18	0.048		153 HB

the statistical significance of the effect that a particular factor exerts on the dependent variable of interest. Experimental design provides a well-defined framework for data collection, analysis and interpretation. The process can help to answer the questions relating to a hypothesis and interpret how different factors influence an interesting variable [16].

In this study, a full two-level factorial experimental design method is presented, which was applied to study the individual effects of each parameter as well as their interactive contributions to the overall material degradation. In addition, the components of the total weight loss of two stainless steels (UNS S32760 and UNS S31603) under the conditions are presented. Based on the experimental design analysis, the correlation between the material hardness and the test results enables some contributions to the detailed understanding of the erosion–corrosion resistance of the two stainless steels to be made.

2. Materials under study and experimental methods

2.1. Materials under study

The two types of materials selected for this study were stainless steels UNS S32760 and UNS S31603, which represent a super duplex and a standard austenitic grade respectively. It is appreciated that the performance of UNS S32760 in every respect will be superior to UNS S31603, but in this study the main focus is to assess the effect on erosion–corrosion of the parameters specified and quantify the effects for the two materials. The information of the chemical composition of the two materials and their average Brinell macrohardness is shown in Table 1. The average hardness values were obtained from five measurements on each sample surface of the raw material after specified heat treatments.

2.2. Experimental methods

The sample specimens were cut from the square bar. The surface of the test specimen was polished by SiC papers up to 1200 grit, followed by washing in acetone and high pressure air drying. Immediately after weighing in a high precision balance, the specimen was exposed to an impinging jet of liquid containing solids generating by the recirculating liquid–solid impingement rig which will be described later. The liquid brine used in the tests was 3.5% sodium chloride solution and the liquid was continuously recirculated via a speed controlled pump.

The impingement apparatus (Fig. 1) comprised a submerged liquid–solid jet generated using a recirculating rig and the electrochemical apparatus used for *in-situ* monitoring as described in [17]. The rig comprised a dual nozzle system with each nozzle diameter being 4 mm. The distance between the nozzle and the specimen was kept constant at 5 mm. The area of the specimen was 2.89 cm^2. For all tests the angle of impingement was 90°. The size of silica sand as erodent is in a range of 150–350 μm in this study. Tests were typically conducted for four hours and repeated for three times, and the specimens were weighed before and after the experiments to determine the components of the total weight loss using a Mettler At201 high precision digital balance (0.01 mg). Electrochemical tests were carried out to determine the contribution to the total weight loss due to the pure electrochemical corrosion processes. For the anodic polarisation and cathodic protection tests, samples were used with electrical connecting wires attached to the back face of the samples. Anodic and cathodic polarisation potentiodynamic scans were undertaken during impingement at a scan rate of 0.25 mV/s using a computer-driven potentiostat. A Ag/AgCl reference electrode and a platinum counter electrode were used in the 3-electrode cell. The material weight loss due to the pure mechanical erosion (E) was obtained by applying cathodic protection on the test sample followed by weight measurement. The cathodic protection potential for all the tests for both materials was −0.8 V.

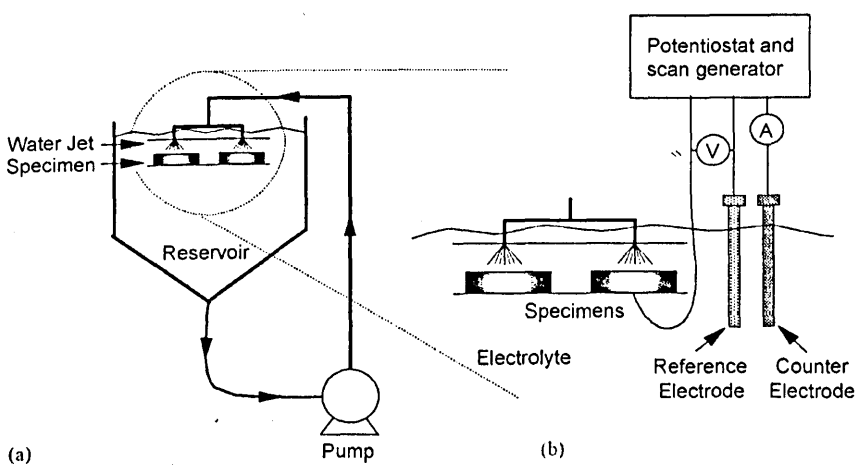

Fig. 1. (a) Re-circulating rig used to generate impinging jet of liquid–solid slurry for erosion–corrosion test. (b) *In-situ* electrochemical monitoring apparatus.

Table 2
Design matrix for a three-parameter, eight-run experiment for each material

TRIAL	VARIABLES			OUTPUTS		
	Temperature	Sand content	Velocity	Weight loss	Corrosion rate	Erosion rate
1	*1*	*1*	*1*	W_1	C_1	E_1
2	*1*	*1*	2	W_2	C_2	E_2
3	*1*	2	*1*	W_3	C_3	E_3
4	*1*	2	2	W_4	C_4	E_4
5	2	*1*	*1*	W_5	C_5	E_5
6	2	*1*	2	W_6	C_6	E_6
7	2	2	*1*	W_7	C_7	E_7
8	2	2	2	W_8	C_8	E_8

2 in this matrix represents high level of all parameters, while 1 represents low level.

The experimental tests in this study focused on three environmental parameters: temperature, sand loading and velocity. Each parameter was set at two levels, thus there were $2 \times 2 \times 2 = 8$ trials for each type of the material. The temperature was set at 20 °C and 50 °C; sand loadings were 50 ppm and 500 ppm, and velocities were set at 7 m/s and 20 m/s. For each condition at least three tests were carried out to determine the reproducibility of results. The test matrix is shown in Table 2.

This test matrix gives the following information:

(a) how weight loss, corrosion rate under erosion–corrosion, and the *interaction* between erosion and corrosion are affected by temperature, sand loading and velocity and their *interactions*;
(b) identifies the key factors and *interactions* and quantifies their effects.

3. Results and discussion

3.1. Component of the material total weight loss (TWL)

3.1.1. TWL under eight experimental conditions

From the total weight loss measurements under eight conditions in Fig. 2, it is clear that the total weight loss of both materials increases as the environment becomes more severe. It is also demonstrated that UNS S32760 has higher erosion–corrosion resistance than UNS S31603 over all the range of conditions. As expected, the 'severity' is assumed to increase as either sand loading, velocity or temperature increase as validated in previous work [3,18]. However, the extent of these effects is unknown. The main reason for the different relative erosion–corrosion resistances of the two materials is the extent of alloying elements, especially the composition of chromium, molybdenum and nitrogen, which makes the corrosion resistance and hence erosion–corrosion resistance superior as reported in previous work [3].

3.1.2. Erosion as a percentage of total weight loss

From Fig. 3 both materials show mechanical erosion (E) to be the dominant process under erosion–corrosion impingement over the range of conditions considered. This will be discussed further in due course.

3.1.3. Weight loss due to pure corrosion

In-situ electrochemical monitoring using DC anodic polarisation enables the corrosion characteristics under the impinging jet test system to be determined. The *in-situ* corrosion current (i_{corr}) can be obtained via the Tafel extrapolation technique [19], and then the weight loss due to pure corrosion is determined by Faraday's law (Eq. (1)).

$$C = \frac{i \times W \times A \times T}{F \times n} \tag{1}$$

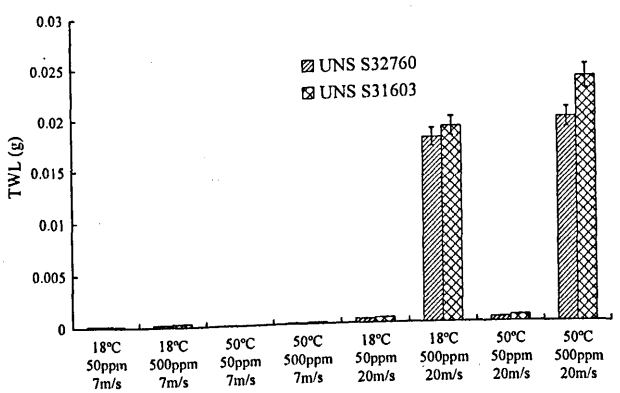

Fig. 2. Total weight loss of UNS S32760 and UNS S31603 under the eight conditions defined by the factorial design methods.

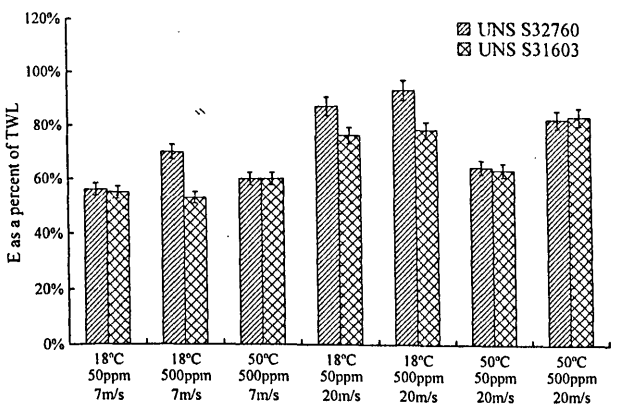

Fig. 3. Weight loss due to pure mechanical erosion as a percent of total weight loss.

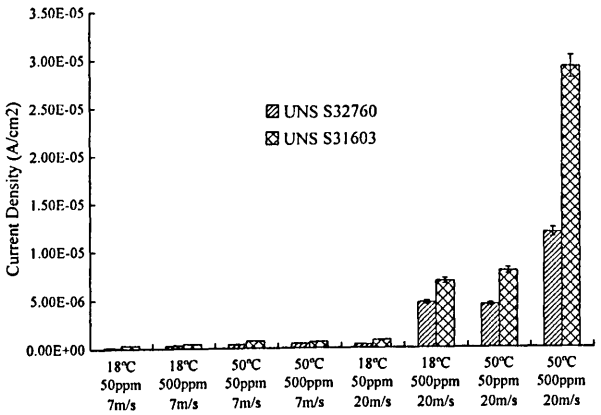

Fig. 4. Corrosion current densities (i_{corr}) obtained under eight test conditions defined by the factorial design methods.

where C is the weight loss due to pure corrosion (g), i the current density (A/cm^2), W the atomic weight (g/mol), A the specimen area (cm^2), T the time (s), F the Faraday constant, n the number of ions.

Fig. 4 shows that i_{corr} of both materials also increases as the environment becomes more severe. Although the stainless steels are depassivated under erosion–corrosion, it is clear that the corrosion rate is still lower on UNS S32760 than UNS S31603 in line with other work [3]. The current densities of both materials increase suddenly as specific test conditions are reached indicating a critical level of severity. This suggests that the corrosion behaviour of both materials transfers from passive to pseudo-passive behaviour. This is validated from the anodic polarisation curve (Fig. 5), there the charge transfer is clearly increased when the sample is exposed to the impinging jet.

Hu and Neville [3,18] have focused on the corrosion transition behaviour of stainless steels from passive behaviour to pseudo-passive behaviour, and they have proved the existence of a critical sand loading and a critical flow velocity. It is well known that the environmental parameters affect the corrosion behaviour of the materials, but in this project (Table 5) it has been proved that the *interactions* between certain parameters are very important, which will be discussed later in this paper.

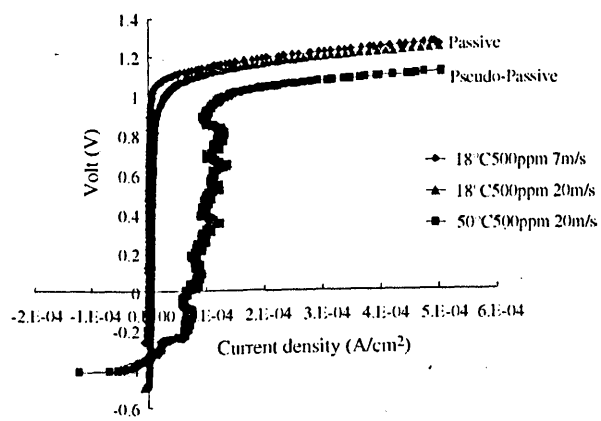

Fig. 5. Example corrosion behaviour from passive to pseudo passive.

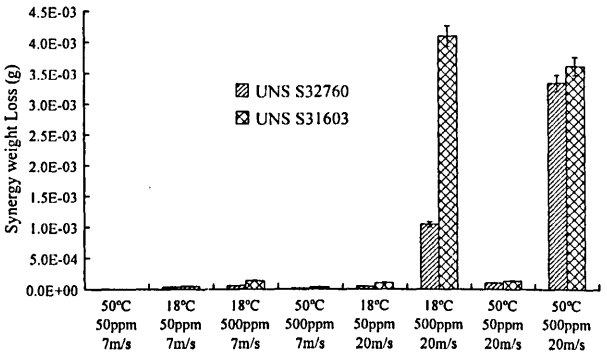

Fig. 6. Synergistic weight loss of both materials under eight conditions defined by the factorial design methods.

So, it can be hypothesized that there might be a corrosion transition behaviour of stainless steels determined by not only the individual environmental parameters but also the *interactions* between parameters.

3.1.4. Synergy

The components of weight loss under erosion–corrosion are often represented by either of the two Eqs. in (2) [3] and (3) [5] as follows:

$$\mathrm{TWL} = E + C + S \tag{2}$$

where E is the weight loss due to pure mechanical erosion obtained from the cathodic protection tests. C in this equation is the weight loss due to pure electrochemical process determined by anodic polarisation tests. Because this is a corrosion rate measured under erosion–corrosion conditions the effects of flow increasing the mass transfer, and impacts of sand are accounted for in the corrosion rate. S is then defined as the effect of corrosion on erosion and this is often referred to as the synergistic effect, which is defined previously.

$$\mathrm{TWL} = E + C_0 + \Delta C_E + \Delta E_C \tag{3}$$

where E is as described in Eq. (2); C_0 is the corrosion rate in static condition; ΔC_E is the additive effect, which is defined in introduction; ΔE_C is the synergistic effect. Therefore, $C_0 + \Delta C_E$ is in Eq. (3) is equivalent to C in Eq. (2). Fig. 6 shows the synergistic effect in erosion–corrosion processes of both materials; it is clear that the synergy increases significantly at high velocity *and* sand loading, and also the synergistic process on UNS S31603 are more prevalent than UNS S32760.

3.2. Experimental design analysis of the influence of the parameters (V, S, T) on erosion–corrosion resistance

Many studies have proved that environmental parameters affect erosion–corrosion behaviour [3,7–15], for which this paper provides verification. The individual effects of increased velocity, sand loading and temperature positively contribute to enhance the overall material degradation, but also this latter analysis shows that the *interactions* between environmental parameters can accelerate weight loss during the

Table 3
The contributions of environmental parameters to the total weight loss (*TWL*)

	V (%)	*S* (%)	*T* (%)	*V* and *S* (%)	*V* and *T* (%)	*S* and *T* (%)	*V*, *S* and *T* (%)
UNS S32760	32.4	37.02	0	29.85	0.41	0	0.32
UNS S31603	34.32	32.34	0.38	31.5	0.54	0.42	0.41

Table 4
The contributions of environmental parameters to the weight loss due to pure erosion (*E*)

	V (%)	*S* (%)	*T* (%)	*V* and *S* (%)	*V* and *T* (%)	*S* and *T* (%)	*V*, *S* and *T* (%)
UNS S32760	34.67	32.77	0.02	32.53	0	0.007	0
UNS S31603	34.41	32.53	0.2	32.13	0.27	0.23	0.23

Table 5
The contributions of environmental parameters to the weight loss due to pure corrosion (*C*)

	V (%)	*S* (%)	*T* (%)	*V* and *S* (%)	*V* and *T* (%)	*S* and *T* (%)	*V*, *S* and *T* (%)
UNS S32760	40.98	16.35	14.04	13.35	13.28	0.82	1.18
UNS S31603	34.93	13.04	16.32	13.56	14.77	3.37	4.01

Table 6
The contributions of environmental parameters to the synergy effect (*S*)

	V (%)	*S* (%)	*T* (%)	*V* and *S* (%)	*V* and *T* (%)	*S* and *T* (%)	*V*, *S* and *T* (%)
UNS S32760	25.32	23.93	6.84	23.03	7.69	6.77	6.42
UNS S31603	34.48	33.37	0.22	31.57	0.05	0.17	0.14

erosion–corrosion process. If a predictive model is to be constructed for erosion–corrosion it is necessary to be able to quantify the effects of these *interactions* on the total damage but also on the components of total weight loss.

3.2.1. Contribution to total weight loss and weight loss due to pure erosion

Tables 3 and 4 show the quantitive effects of environmental parameters and their *interactions* on the total weight loss and the weight loss due to pure erosion using the analysis of variance (ANOVA) approach over the range of conditions considered. The percentages shown in Tables 3–6 are the values of the sum of squares for that variable relative to the total sum of squares for all variables. Higher percentage values correlate to that parameter having a greater effect.

In order to obtain a good understanding of ANOVA, the average effect of factors for each level, the sum of squares and corresponding calculations need detailed explanation. The following calculation is applied to obtain the final contribution percentage.

The average effects of the factors for each level are shown in Table 7. The velocity factor is at the low level for trial conditions 1, 3, 5 and 7 in Table 2. Hence the calculation for the average effect of velocity at the low level is shown below:

$$W_{lv} = \tfrac{1}{4}(W_1 + W_3 + W_5 + W_7). \quad (4)$$

where W_1, W_3, W_5 and W_7 are the total weight losses in Table 2 corresponding to trial conditions 1, 3, 5 and 7 respectively. The others including all interactions could be computed in the same manner as W_{lv}.

In the ANOVA method the sum of squares is defined. For example, the sum of squares due to velocity factor is calculated using the following formula:

$$SS_V = 2(W_{lv} - W_G)^2 + 2(W_{hv} - W_G)^2. \quad (5)$$

where W_{lv} and W_{hv} refer to the average effects corresponding to the velocity factor for low and high levels and W_G is the average total weight loss for eight trial conditions. The sums of squares for other factors including possible interactions were computed in the same way and are tabulated in Table 8. The final part of the ANOVA was finished easily to obtain the percentage contribution with the following equation:

$$V(\%) = \frac{SS_V}{SS_V + SS_S + SS_T + SS_{VS} + SS_{VT} + SS_{TS} + SS_{TVS}} \times 100\% \quad (6)$$

Table 7
The average effects of individual factor for each level

Column	Factors	Level	
		Low	High
1	Velocity	W_{lv}	W_{hv}
2	Sand loading	W_{ls}	W_{hs}
3	Temperature	W_{lt}	W_{ht}

Table 8
Sum of squares of factors and interactions

Column	Factors	Sum of squares	Percentage contribution (%)
1	Velocity	SS_V	V
2	Sand loading	SS_S	S
3	Temperature	SS_T	T
4	Velocity and temperature	SS_{VT}	VT
5	Velocity and sand loading	SS_{VS}	VS
6	Temperature and sand loading	SS_{TS}	TS
7	Velocity, temperature and sand loading	SSV_{TS}	VTS

Table 3 shows that for UNS S31603, velocity contributed the highest percentage to total weight loss; followed by sand loading and their interaction. The rest of the variable effect contribution percentages were all less than 10%, and in this case are considered insignificant. The prominent contributions to the total weight loss and weight loss resulting from pure mechanical erosion are due to velocity, sand loading and their *interaction*. This is the same for both materials so whilst there are differences in the extent of degradation, it appears that the effects of velocity, sand loading, temperature and their *interactions* on total weight loss and erosion are remarkably similar under erosion–corrosion conditions and differences exist only in the effect on synergy (Table 6). It is common that more kinetic energy needs to be dissipated by materials at higher velocity to produce deformation, cracks and even cuttings. It has been concluded that at higher impingement velocity, the particle impact velocities increase and more energy was provided to the moving particles, thus causing more severe degradation on the specimen surface [9,10]. Moreover, Ruff et al. [20] summarised some other parameters which affect the erosion rate of metals. The main parameter that controls the rate of erosion of materials is the particle velocity; the erosion rate is found to increase as v^2 to v^3 in most cases. The rate of material erosion is proportional to v^2 in Bitter's model [21]. In terms of sand loading, as the sand loading increases, the protective film on the surface of the materials will be stripped off, and the bare metal will be exposed to the severe erosion–corrosion environment, which will enhance degradation. This analysis confirms that velocity and sand loading play very important roles, but also the results show that the *interaction* between velocity and sand loading is another key factor in the erosion–corrosion environment.

3.2.2. Contribution to the weight loss due to pure corrosion

Table 5 shows the contributions of the environmental parameters to the weight loss due to pure corrosion. The most influential parameter is velocity, but the effects from sand loading, temperature, the *interaction* between velocity and sand loading and the *interaction* between velocity and temperature also play a relatively important role in corrosion. As a result of the high velocity and sand loading, the protective film on the surface will be removed easily, which leads to creation of a reactive surface from the point of view of corrosion. It should be noted that the velocity plays a role in increasing corrosion; one effect being the increased mass transfer and transport of aggressive chloride ions to the surface in particular. In terms of the effect of temperature, a higher thermodynamic driving force exists at higher temperature. As mentioned in the previous part, the corrosion rate in erosion-corrosion environments is composed of two parts; the corrosion rate in static conditions (C_0) and the erosion enhanced corrosion (ΔC_E). The *dynamic* corrosion rate (ΔC_E) is the most affected component of the corrosion by environmental parameters and their interactions. It could be explained recursively that velocity, sand loading and their *interaction* have been approved to accelerate erosion, which will enhances corrosion further; but the static corrosion rate will keep invariable (C_0), which will be affected by temperature due to the different thermodynamic driving force. So it could be concluded that the environmental parameters and their *interactions* apply more or less effects on corrosion behaviour over the defined range of erosion–corrosion conditions.

3.2.3. Contribution to the synergy

Table 6 shows the importance of environmental parameters to the synergy, and it is clear that the greatest factors in determining the synergy are velocity, sand loading and their *interaction*, consistent with what was found for TWL and E in erosion–corrosion environments. The detailed magnitudes of synergy effects under impinging jet tests are shown in Fig. 6. Even though the prominent factors in the synergy material loss defined from statistical analysis are velocity, sand loading and their *interaction*, the relatively high synergy weight loss occurs when high velocity *and* high sand loading are applied. It could therefore be concluded that the synergy is not largely affected by *either* velocity *or* sand loading individually over the range of test conditions, because the brittle roughened surface cannot be removed when there is inadequate impact kinetic energy. So, it is hypothesized that the sudden increase of synergy magnitude is affected primarily by a critical impact kinetic energy. The synergy is defined as corrosion enhanced erosion, but still describes a kind of erosion. The analysis in [17] provides a good understanding of synergy. The anodic polarisation curve can be sub-divided into three potential regions as described below (Fig. 7):

- Region I: the magnitude of current measured in the anodic potential region immediately adjacent to E_{corr} rises to reach a stable value.
- Region II: for a potential range spanning several hundred millivolts (depending on the temperature) the current shows an oscillating response.

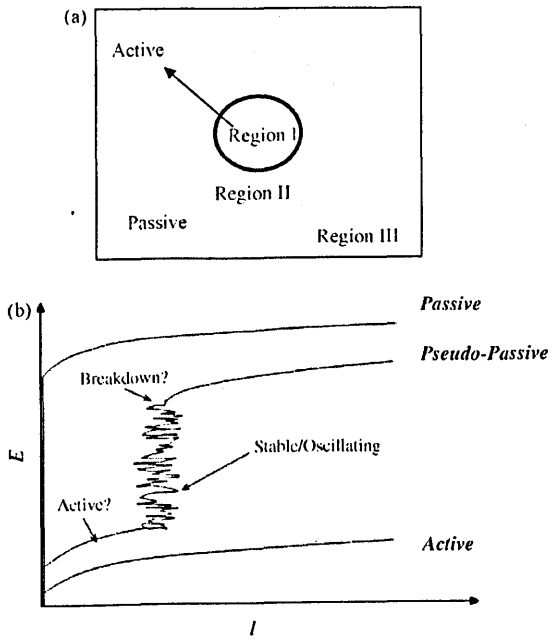

Fig. 7. (a) Schematic representation of the erosion–corrosion surface exposed to the impinging jet. (b) Electrochemical response associated with the impinged surface.

- Region III: a breakdown potential similar to that seen during anodic polarisation in mild conditions is observed.

According to the above analysis the corrosion enhanced erosion (synergy) is mainly from region I, where the surface was roughened due to corrosion, and also reduction of mechanical properties occurred making materials more susceptible to erosion.

3.3. Future predictive erosion–corrosion modelling

Statistical analysis from experimental design enables a systematic database to be constructed in which the data can be analysed using statistical methods and provides directions for future predictive erosion–corrosion modelling to be established. The future predictive erosion–corrosion modelling can be simplified as the components of total weight loss and how they are affected by sand loading, velocity and temperature are more clearly understood. As a next step, the conversion of the 3D interpolating model to the expected functions will enable the predictive capability to be derived. 3D interpolation is valuable computational method to build the model based on the known data collected from the tests defined by experimental design methods, and moreover to predict any unknown points in this model.

As a result of statistical analysis, the significant factors in determining the components of total weight loss are defined for future predictive erosion–corrosion modelling; while the minor factors can be appropriately ignored. This work has demonstrated certain parameters and their interactions (under this regime and this range of conditions) e.g. temperature, do not significantly affect material loss. Predictive modelling of material loss can therefore be simplified and be represented as a function of velocity, sand loading and their interaction.

4. Conclusions

The erosion corrosion behaviour of two stainless steels has been examined over the range of conditions considered. UNS S32760 stainless steel exhibits better erosion corrosion resistance than UNS S31603 by 6 to 50%, and both respond to changes in test conditions in the same way. The importance of all variables was analysed using the methods of statistical experiment design and it can be summarised that:

1. Erosion is the dominant weight loss process over corrosion, under all test conditions. The overall material loss and it erosion component are significantly affected by sand loading and velocity, with strong interaction between.
2. Weight loss by corrosion is also affected by sand loading and velocity, and in addition is affected by temperature.
3. Improving the understanding of the controlling parameters in all components of the damage enables progress to be made towards predictive models for erosion–corrosion damage.

Acknowledgements

This research work was sponsored by Weir Materials & Foundries, Noel Village Ltd., Lloyds Register, Sea Technology Group, Weir Pumps, Weir Engineering Services, DSTL and Langley Alloys Meighs Ltd.

References

[1] P. McIntyre, Marine Corrosion Club Meeting, Aberdeen, April 1999.
[2] R. J. K. Wood, Review Erosion-Corrosion interactions and their effect on marine and offshore materials, Wear (2006), in press.
[3] X. Hu, A. Neville, The electrochemical response of stainless steels in liquid–solid impingement, Wear 258 (2005) 641–648.
[4] M.M. Stack, B.D. Jana, Modelling particulate erosion–corrosion in aqueous slurries: some views on the construction of erosion–corrosion maps for a range of pure metals, Wear 256 (2004) 986–1004.
[5] M.M. Stack, S. Zhou, R.C. Newman, Identification of transitions in erosion–corrosion regimes in aqueous environments, Wear 186-187 (1995) 523–532.
[6] B.D. Jana, M.M. Stack, Modelling impact angle effects on erosion–corrosion of pure metals: construction of materials performance maps, Wear 259 (2005) 243–255.
[7] M.G.S. Ferreira, N.E. Hakiki, G. Goodlet, S. Faty, A.M.P. Simões, M. Da Cunha Belo, Influence of the temperature of film formation on the electronic structure of oxide films formed on 304 stainless steel, Electrochim. Acta 46 (2001) 3767–3776.
[8] G.J. Danek, Naval Engineers J. 78 (1966) 763.
[9] H.McI. Clark, The influence of the flow field in slurry erosion, Wear 152 (1992) 223–240.
[10] G.L. Sheldon, A. Kanhere, An investigation of impingement erosion using single particles, Wear 21 (1972) 195–209.
[11] H.M. Shalaby, S. Attari, W.T. Riad, V.K. Gouda, Erosion–corrosion behaviour of some cast alloys in seawater, Corrosion 48 (1992) 206–217.
[12] E.W. Madsen, Measurement of erosion–corrosion synergism with a slurry wear test apparatus, Wear 123 (1988) 127–142.

[13] A. Neville, M. Reyes, T. Hodgkiess, A. Gledghill, Mechanisms of wear on a Co-base alloy in liquid–solid slurries, Wear 238 (2000) 138–150.
[14] A. Neville, T. Hodgkiess, H. Xu, An electrochemical and microstructural assessment of erosion–corrosion of cast iron, Wear 233-235 (1999) 523–534.
[15] A. Neville, X. Hu, Mechanical and electrochemical *interactions* during liquid–solid impingement on high-alloy stainless steels, Wear 251 (2001) 1284–1294.
[16] J.V. Bilenas, J.P. Morgan Chase, D.E. Wilmington, An Introduction to Experimental Design using SAS.
[17] A. Neville, M. Reyes, H. Xu, Examining corrosion effects and corrosion/erosion *interactions* on metallic materials in aqueous slurries, Tribol. Int. 35 (2002) 643–650.
[18] X. Hu, A. Neville, An examination of the electrochemical characteristics of two stainless steels (UNS S32654 and UNS S31603) under liquid–solid impingement, Wear 256 (2004);
X. Hu, A. Neville, An examination of the electrochemical characteristics of two stainless steels (UNS S32654 and UNS S31603) under liquid–solid impingement, Wear 256 (2004) 537–544.
[19] M. Stem, A.L. Geary, J. Electrochem. Soc. 104 (1) (1957) 56–63.
[20] A.W. Ruff, S.M. Wiederhorn, Erosion by solid particle impact, Mater. Sci. Technol. 16 (1979) 69–124.
[21] J.G.A. Bitter, A study of erosion phenomena, Part II, Wear 6 (1963) 169–190.

Study of corrosion in erosion-corrosion of two stainless steels in simulated marine conditions via experimental design

H. Meng, X. Hu*, A. Neville

Corrosion and Surface Engineering Research Group, School of Mechanical Engineering, University of Leeds, Leeds, LS2 9JT, U.K.

* Corresponding author

ABSTRACT

The corrosion behavior of two stainless steels (UNS S32760 and UNS S31603) for marine applications has been assessed under liquid-solid impingement conditions in 3.5% NaCl. The corrosion rate and the amount of material degradation due to corrosion and corrosion effects on erosion have been determined under various conditions. The three environmental parameters considered in this study are solid loading, flow velocity and temperature. A full two-level factorial experimental design method was applied to study the individual effects of each parameter as well as their interactive contributions to corrosion and the effect of corrosion in erosion-corrosion. From the analysis, velocity shows the greatest effect on the corrosion rate of both materials, followed by solid loading, temperature, and interactive effects of temperature-velocity and solid loading-velocity. However, the most effective contributions to the corrosion effect on erosion, often denoted synergy, are mainly from velocity, solid loading and the interactive effect of solid loading and velocity. In this paper, the corrosion behavior of two stainless steels and the mechanisms of material degradation under different experimental conditions will be discussed.

Keywords: stainless steels, marine, corrosion, experimental design.

INTRODUCTION

Year year year corrosion causes rapid material degradation in marine environments, and millions of dollars are spent to repair material damage in marine industries every year. Marine corrosion continues to cause mundane failures everyday, which lead to downtime of sub-sea systems, material wastage, energy inefficiency and large costs to industry. In the oil and gas sector it is condition for corrosion to occur in partnership with erosion as large flow velocities and solid-laden fluids are encountered. This makes long term material performance even more challenging.

In 1912 English metallurgist Harry Brearley invented stainless steels in his search for an alloy to protect cannon bores from erosion; stainless steels still play a very important role in industry and still offer good resistance to erosion-corrosion. It is well known that stainless steel is one of the prominent corrosion resistant alloys due to a tightly adherent, stable and self-healing film on the surface to provide a barrier to charge transfer between the relatively active bulk material and the corrosive environment. But solid particles are entrained, the protective film can be removed by mechanical wear or bubble collapse during the impingement process. Where the films are mechanically removed, charge transfer can occur at the steel/water interface without retardation from the barrier film[1]. Technical developments over the decades have improved the standard grades invented in the 1920s with higher strength, higher corrosion resistance and lower maintenance. A wealth of recorded data contributes to the excellent understanding of stainless steels' corrosion behavior and corrosion mechanisms.

Erosion-corrosion in aqueous systems is dominated by two major mechanisms: electrochemical corrosion and mechanical erosion[2]. On account of the greater material loss from erosion-corrosion than the sum of their individual contributing components, the *interaction* between electrochemical and mechanical processes has been recognized in many works, and they have been referred to as 'Synergistic' and 'Additive' effects[2,3]. The so-called synergistic effect is normally used to describe the way in which corrosion can enhance erosion, while the so-called additive effect refers to the mechanism by which erosion can enhance corrosion. The corrosion rate measured *in-situ* in any erosion-corrosion system consists of the pure corrosion component in the absence of erosion plus and the additive effect.

There have been numerous studies by authors and others which have focused on assessing corrosion behavior and corrosion mechanisms of stainless steels in erosion-corrosion environments[4,5], and also some analyzing the corrosion behavior in erosion-corrosion environments as a function of several parameters including velocity, sand loading or temperature[2,6-8]. Though the studies show how the environmental factors affect corrosion rate and the degree of synergy in an erosion-corrosion environment, it has been difficult to predict quantitatively how the damage will be affected by various individual factors and their combined, synergistic interactions. In an attempt to extend understanding of how each factor affects the extent of corrosion and the synergy in erosion-corrosion, an experimental design method has been used. The primary goal of experimental design in scientific research is usually to show the statistical significance of the effect that a particular factor exerts on the dependent variable of interest. Experimental design provides a well-defined framework for data collection, analysis and interpretation. The process can help to answer the questions relating to hypothesis and interpretation of how different factors influence an interesting variable[9]

In this study the corrosion rate and synergistic effect of two stainless steels (UNS S32760 and UNS S31603) measured over the range of the conditions considered are presented, and in addition a full two-level factorial experimental design method is presented, which was applied to study the individual effects of each parameter as well as their interactive contributions to the corrosion rate and degree of synergy in an erosion-corrosion impingement system.

MATERIALS STUDIED AND EXPERIMENTAL METHODS

Materials Under Study

The two of materials selected for this study were stainless steels UNS S32760 and UNS S31603, which represent a super duplex and a standard austenitic grade respectively. The localised corrosion behaviors of super duplex and UNS S31603 have been comprehensively analysed and compared in conditions simulating those in real seawater systems, in particular marine pumping systems by Neville *et al*[4], and has been shown that the corrosion resistance of UNS S32760 is better than UNS S31603. However, in this study the main focus is to assess the environmental parameters' effect on corrosion rate and synergy and quantify these effects for the two materials. The information of the chemical composition of the two materials is shown in Table 1.

Experimental Methods

The sample specimens were cut from a cast square bar. The surface of the test specimen was polished by SiC papers up to 1200 grit, followed by washing in acetone and high pressure air drying. Immediately after weighing by a high precision balance, the specimen was placed in a liquid-solid impingement rig which will be described later. The liquid brine used in the tests was 3.5% sodium chloride solution and the liquid was continuously recirculated via a speed controlled pump.

The impingement apparatus (Fig. 1) comprised a submerged liquid-solid jet generated using a recirculating rig and the electrochemical apparatus used for *in situ* monitoring as described in [10]. The rig comprised a dual nozzle system with each nozzle diameter being 4 mm. The distance between the nozzle and the specimen was kept constant at 5 mm. The area of the specimen was 2.89 cm^2. For all tests the angle of impingement was 90°. Tests were typically conducted for four hours and repeated three times, and the specimens were weighed before and after the experiments to determine the total weight loss of each specimen. The total weight loss (TWL) of the material tested was obtained from total weight loss test; electrochemical tests were carried out to determine the contribution to the total weight loss due to the pure electrochemical corrosion processes (C). The material weight loss due to the pure mechanical erosion (E) was obtained by applying cathodic protection on the sample specimens tested. The cathodic protection potential for all the tests for both materials was -0.8 V. The potential was controlled by a potentiostat. For both anodic polarization and cathodic protection tests, electrical connecting wires were attached to the back face of the samples, and anodic and cathodic polarization potentiodynamic scans were undertaken during impingement at a scan rate of 0.25 mV/s using a computer driven potentiostat, and employing a Ag/AgCl reference electrode and a platinum counter electrode.

The experimental tests in this study focused on three environmental parameters: temperature, sand loading and velocity. Each parameter was set at two levels, thus there were 2*2*2=8 trials for each type of the materials. The temperature was set at 20°C and 50°C; sand loading were 50ppm and 500ppm, and velocities were set at 7m/s and 20m/s. The test matrix is shown in Table 2.

The test matrix gives the following information: a) How corrosion rate and synergy under erosion-corrosion are affected by temperature, sand loading and velocity and their relative

interactions with one and another and b) identifies the key factors and *interactions* and quantifies their effects.

EXPERIMENTAL RESULTS

Corrosion Behavior of Two Stainless Steels

In-situ electrochemical monitoring using DC anodic polarization enables the corrosion characteristics under the impingement test system to be determined. The *in-situ* corrosion current (i_{corr}) can be obtained via the Tafel extrapolation technique, and then the weight loss due to pure corrosion is determined by Faraday's law (Eq. 1).

$$C = \frac{i \cdot W \cdot A \cdot T}{F \cdot n} \qquad \text{(Eq. 1)}$$

where

C: weight loss due to pure corrosion (g)

i: current density (A/cm^2)

W: atomic weight (g/mol)

A: specimen area (cm^2)

T: time (s)

F: Faraday Constant

n: number of ions

Figure 2 shows i_{corr} of both materials at various conditions assessed in this work. It is clear that corrosion rate of the two stainless steels increases as the environment becomes more severe. From a specific test condition (18°C, 500ppm, 20m/s), increasing both temperature and solid content results in a dramatic increase in the corrosion rate indicating a critical level of severity. The reason for this has been discussed by Hu and Neville[2,11]. There is a transition behavior of stainless steels from passive to pseudo-passive, and the existence of critical sand loading and critical flow velocity were proved in their study. In this present work the results from the anodic polarization diagrams plotted in Figure 3 for standard stainless steel UNS S31603, demonstrates that the current density as a function of potential is under the most severe conditions when velocity is 20m/s, sand loading is 500 mg/l and temperature is 50°C. The same behavior has been found on the superduplex stainless steel UNS S32760. Although the stainless steels are depassivated under erosion-corrosion conditions, UNS S32760 exhibits lower corrosion rate and current density during anodic polarization than UNS

S31603 as shown in Figure 4. This is believed to be due to the alloying additions for improving the *corrosion* resistance and resistance to charge transfer is lower in liquid-solid impingement conditions as repassivation occurs faster in agreement with other work[2].

It is well known that environmental parameters affect the corrosion behavior of the materials under erosion-corrosion conditions, but in this project it has been proved that the *interactions* among certain parameters are very important by experimental design analysis method and this will be discussed in a later section in this paper. So it can be hypothesized that there might be a corrosion transition behavior of stainless steels determined by not only the individual environmental parameters but also the *interactions* between selected parameters.

As breakdown potential (E_b) is representative of the material resistance to localized corrosion[4], in this work it has been determined for both materials according to the anodic polarization curves under impingement and is defined as the point where current density starts to deviate from stabilization (as highlighted in Figure 4). Figure 5 shows the plot of E_b for the two stainless steels. There is a decrease in E_b for both stainless steels under severe erosion-corrosion conditions and this indicates that the interaction between the jet velocity and solid content is playing an important role in affecting the localized corrosion resistance and the corresponding presence of or lack of an oxide layer. Figure 5 also confirms the vulnerability to localized corrosion of the lower-alloyed stainless steel (UNS S31603), in contrast the higher-alloyed stainless steel (UNS S32760) possesses considerably superior resistance to localized corrosion, which is in line with the statement made by Khalid *et al.*[12]. For UNS S31603 from the anodic polarization curves, although E_b values are not greatly affected by the change of conditions, it is noticed that for all curves at 50°C the current density increase in a much greater rate after E_b is reached compared with 18°C. This suggests that the material is more susceptible to corrosion propagation under erosion-corrosion conditions.

Synergy

The components of weight loss under erosion-corrosion are often represented by the equation as follows [2]:

$$TWL = E + C + S \qquad \text{(Eq. 2)}$$

where E is the weight loss due to pure mechanical erosion obtained from cathodic protection tests. C

in this equation is the weight loss due to pure electrochemical processes determined by anodic polarization tests. S is then defined as the effect of corrosion on erosion and this is often referred to as the synergistic effect. Figure 4 shows the synergistic effect in erosion-corrosion processes of both materials; it is clear that the synergy increases significantly with increasing at high velocities and with increasing sand loading The synergistic process on UNS S31603 are more prevalent than UNS S32760.

Experimental Design Analysis of the Effect of V, S, and T on the Corrosion Rate and Synergy

Contribution to mass loss due to pure corrosion. Figure 6 shows the quantitive effects of environmental parameters and their interactions on the mass loss due to pure corrosion using the **AN**alysis **O**f **VA**riance (ANOVA) approach over the range of conditions considered. The percentages shown in Figures 6 and 7 are the values of the sum of squares for that variable relative to the total sum of squares for all variables. Higher percentage values correlate to that parameter having a greater effect.

In order to obtain a good understanding of ANOVA, the average effect of factors for each level, the sum of squares and corresponding calculations need detailed explanation. The following calculation is applied to obtain the final contribution percentage.

The averages of the factors for each level were shown in Table 3. The velocity factor was at the low level for trial conditions 1, 3, 5 and 7 in Table 2. Hence the calculation for the average effect of velocity at the low level is shown below:

$$C_{lv} = \frac{1}{4}(C_1 + C_3 + C_5 + C_7) \qquad \text{(Eq. 3)}$$

where C_1, C_3, C_5 and C_7 were the corrosion rates in Table 2 corresponding to trial conditions 1, 3, 5 and 7 respectively. The others include all interactions that could be computed in the same manner as C_{lv}.

In the ANOVA method the sum of squares is defined. For example, the sum of squares due to velocity factor is calculated using the following formula:

$$SS_V = 2(C_{lv} - C_G)^2 + 2(C_{hv} - C_G)^2 \qquad \text{(Eq. 4)}$$

where C_{lv} and C_{hv} refer to the average effects corresponding to the velocity factor for low and high levels and C_G is the average mass loss due to pure corrosion for eight trial conditions. The sums of squares for other factors including possible interactions were computed in the same way and are tabulated in Table 4. The final part of the ANOVA was finished easily to obtain the percentage contribution with the following equation:

$$V\% = \frac{SS_V}{SS_V + SS_S + SS_T + SS_{VS} + SS_{VT} + SS_{TS} + SS_{TVS}} \times 100\% \qquad \text{(Eq. 5)}$$

Figure 6 shows that the contribution percentages of last two interactions for both materials were all less than 10%, and in this case they are considered insignificant. The most influential parameter is velocity, but the effects from sand loading, temperature, the interaction between velocity and sand loading and the interaction between velocity and temperature also play relatively important roles in corrosion. As a result of the high velocity and sand loading, the protective film on the surface will be removed easily, which leads to creation of a reactive surface from the point of view of corrosion. It should be noted that the velocity plays a role in increasing corrosion; one effect being the increased mass transfer and transport of aggressive chloride ions to the surface in particular. In terms of the effect the temperature, a higher thermodynamic driving force exists at higher temperature. As mentioned in the previous part, the corrosion rate in erosion-corrosion environments is composed of two parts; the corrosion rate in static conditions (C_0) and the erosion enhanced corrosion (ΔC_E). The *dynamic* corrosion rate (ΔC_E) is the most affected component of the corrosion by environmental parameters and their *interactions*. It could be explained that velocity, sand loading and their *interaction* accelerate erosion, which will also enhances corrosion further. The static corrosion rate will remain invariable, which will be affected by temperature due to the different thermodynamic driving force. So it could be concluded that the environmental parameters and their *interactions* influence on the corrosion behavior over the defined range of erosion-corrosion conditions.

Contribution to the synergy. Figure 7 shows the importance of environmental parameters to synergy, and it is clear that the greatest factors in determining the synergy are velocity, sand loading and their *interaction*. As defined previously, synergy is *corrosion enhanced erosion*. Synergy is still a type of erosion even though its origin can be due to a corrosion process. It is common that more kinetic energy needs to be dissipated by materials at higher velocities to produce deformation, cracks

and cuttings due to acute angle impacts by sharp particles. It has been concluded that at a higher impingement velocity, the particle impact velocities increase and more energy was provided to the moving particles, thus causing more severe degradation on the specimen surface. In terms of sand loading, as the sand loading increases, the surface protective film on the surface of the materials will be more effectively stripped off, and the bare metal will be exposed to the severe erosion-corrosion environment, which will enhance material degradation. However, the function of corrosion cannot be negligible. Impact processes include roughening of the surface and even reduction of the mechanical properties of surface materials by fatigue and thus erosion is assisted by mechanically-based processes. Even though the prominent factors in the synergy material loss defined from statistical analysis are velocity, sand loading and their *interaction*, the relatively high synergy weight loss occurs when high velocity *and* high sand loading are applied. It could therefore be concluded that the synergy is not largely affected by *either* velocity *or* sand loading individually over the range of test conditions, because the brittle roughened surface can not be removed when there is inadequate impact kinetic energy. So it is hypothesized that the sudden increase of synergy magnitude is affected primarily by a critical impact kinetic energy or described as the critical shear velocity of Efird[13].

CONCLUSIONS

The corrosion behavior of two stainless steels has been examined over a range of conditions considered under impingement system. The following summarizing comments can be made.

1. UNS S32760 has better corrosion resistance than UNS S31603 over the range of conditions. Moreover, UNS S32760 has wider range of passive state than UNS S31603 when both of them show passive behavior.
2. Weight loss due to pure corrosion is affected not only by velocity, sand loading and their interaction but also by temperature, and the interaction of velocity and temperature.
3. The contributions of environmental parameters to synergy could be correlated with how parameters affect erosion behavior of the materials. The prominent parameters on synergy are velocity, sand loading and their interaction.
4. The important factors for the different aspects of damage are the same for the two types of stainless steels. The magnitude of the effects differs slightly, so there are differences in the

extent of degradation.

ACKNOWLEDGEMENTS

This research work was sponsored by Weir Materials & Foundries, Noel Village Ltd, Lloyds Register, Sea Technology Group, Weir Pumps, Weir Engineering Services, DSTL and Langley Alloys Meighs Ltd.

REFERENCES

1. M. Stemp, S.M., D. Landolt, *The effect of mechanical and electrochemical parameters on the tribocorrosion rate of stainless steel in sulphuric acid.* Wear, 2003. **255**: p. 466-475.
2. X. Hu, A.N., *The electrochemical response of stainless steels in liquid-solid impingement.* Wear, 2005. **258**: p. 641-648.
3. M. M. Stack, B.D.J., *Modelling particulate erosion-corrosion in aqueous slurries: some views on the construction of erosion-corrosion maps for a range of pure metals.* Wear, 2005. **256**: p. 986-1004.
4. A. Neville, T.H., *An assessment of the corrosion behaviour of high-grade alloys in seawater at elevated temperature and under a high velocity impinging flow.* Corrosion Science, 1996. **38**(6): p. 927-956.
5. H. Dong, P.-Y.Q., X. Y. Li, R. J. Llewellyn, *Improving the erosion-corrosion resistance of AISI 316 austenitic stainless steel by low temperature plasma surface alloying with N and C.* Material Science and Engineering 2006. **431**(A): p. 137-145.
6. Silverman, D.C., *The Rotating Cylinder Electrode for Examining Velocity-Sensitive Corrosion --- A review.* Corrosion, 2004. **Vol. 60, No. 11**(0010-9312/04/000173): p. 1003-1023.
7. T. Hodgkiess, A.N., S. Shrestha, *Electrochemical and mechanical interactions during erosion-corrosion of a high-velocity oxy-fuel coating and a stainless steel.* Wear, 1999. **233-235**: p. 623-634.
8. Weber, J., *Flow induced corrosion: 25 years of industrial research.* British Corrosion Journal, 1992. **27**(3): p. 193-199.
9. Jonas V. Bilenas, J.P.M.C., Wilmington, *An introduction to experimental design using SAS.*
10. A. Neville, M.R., H. Xu, *Examining corrosion effects and corrosion/erosion interactions on metallic materials in aqueous slurries.* Tribology International, 2002. **35**: p. 643-650.
11. X. Hu, A.N., *An examination of the electrochemical characteristics of two stainless steels (UNS S32654 and UNS S31603) under liquid-solid impingement.* Wear, 2004. **256**: p. 537-544.
12. Khalid S. E. Al-Malahy, T.H., *Comparative studies of the seawater corrosion behaviour of a range of materials.* Desalination, 2003. **158**: p. 35-42.
13. K. D. Efird. *Effect of Fluid Dynamics on the Corrosion of Copper Base Alloys.* Corrosion-NACE. Vol. 33, No. 1, January 1977.

TABLE 1

NOMINAL COMPOSITIONS OF UNS S32760 AND UNS S31603

	Cr	Ni	Mo	Mn	C	N
UNS S32760	24.9	8.4	3.65	0.94	0.026	0.21
UNS S31603	18.5	10.3	2.2	1.18	0.048	

TABLE 2

DESIGN MATRIX FOR A THREE-PARAMETER, EIGHT-RUN EXPERIMENT FOR EACH MATERIAL. 2 IN THIS MATRIX REPRESENTS HIGH LEVEL OF ALL PARAMETERS, WHILE 1 REPRESENTS LOW LEVEL

TRIAL	***VARIABLES***			***OUTPUTS***		
	Temperature	*Sand Content*	*Velocity*	*Weight Loss*	*Corrosion Rate*	*Erosion Rate*
1	*1*	*1*	*1*	W_1	C_1	E_1
2	*1*	*1*	*2*	W_2	C_2	E_2
3	*1*	*2*	*1*	W_3	C_3	E_3
4	*1*	*2*	*2*	W_4	C_4	E_4
5	*2*	*1*	*1*	W_5	C_5	E_5
6	*2*	*1*	*2*	W_6	C_6	E_6
7	*2*	*2*	*1*	W_7	C_7	E_7
8	*2*	*2*	*2*	W_8	C_8	E_8

TABLE 3

THE AVERAGE EFFECTS OF INDIVIDUAL FACTOR FOR EACH LEVEL

Column	Factors	Level	
		Low	High
1	*Velocity*	C_{lv}	C_{hv}
2	*Sand Loading*	C_{ls}	C_{hs}
3	*Temperature*	C_{lt}	C_{ht}

TABLE 4

SUM OF SQUARES OF FACTORS AND INTERACTIONS.

Col.	Factors	Sum of Squares	Percentage Contribution
1	Velocity	SS_V	$V\%$
2	Sand Loading	SS_S	$S\%$
3	Temperature	SS_T	$T\%$
4	Velocity & Temperature	SS_{VT}	$VT\%$
5	Velocity & Sand Loading	SS_{VS}	$VS\%$
6	Temperature & Sand Loading	SS_{TS}	$TS\%$
7	Velocity, Temperature & Sand loading	SSV_{TS}	$VTS\%$

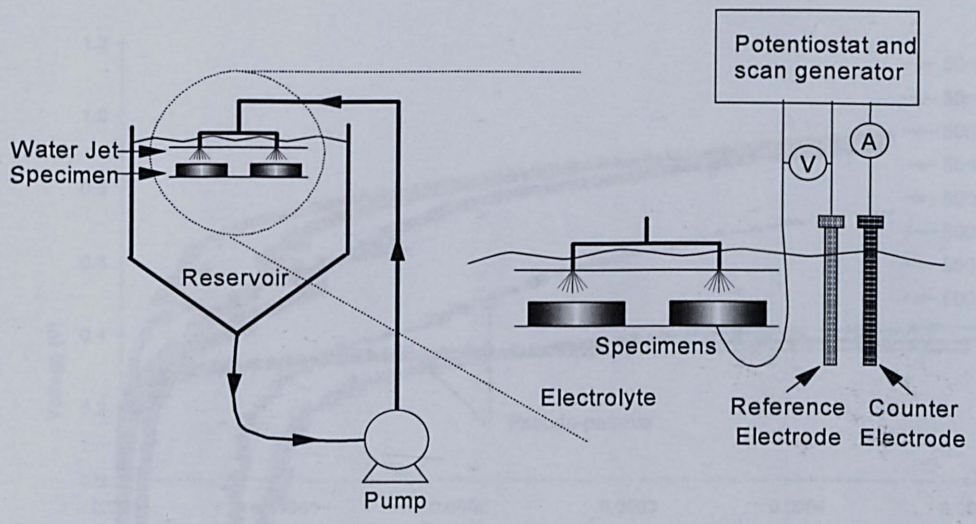

(a) (b)

FIGURE 1 - (a) Recirculating rig used to generate impinging jet of liquid-solid slurry for erosion-corrosion test.

(b) *In-situ* electrochemical monitoring apparatus

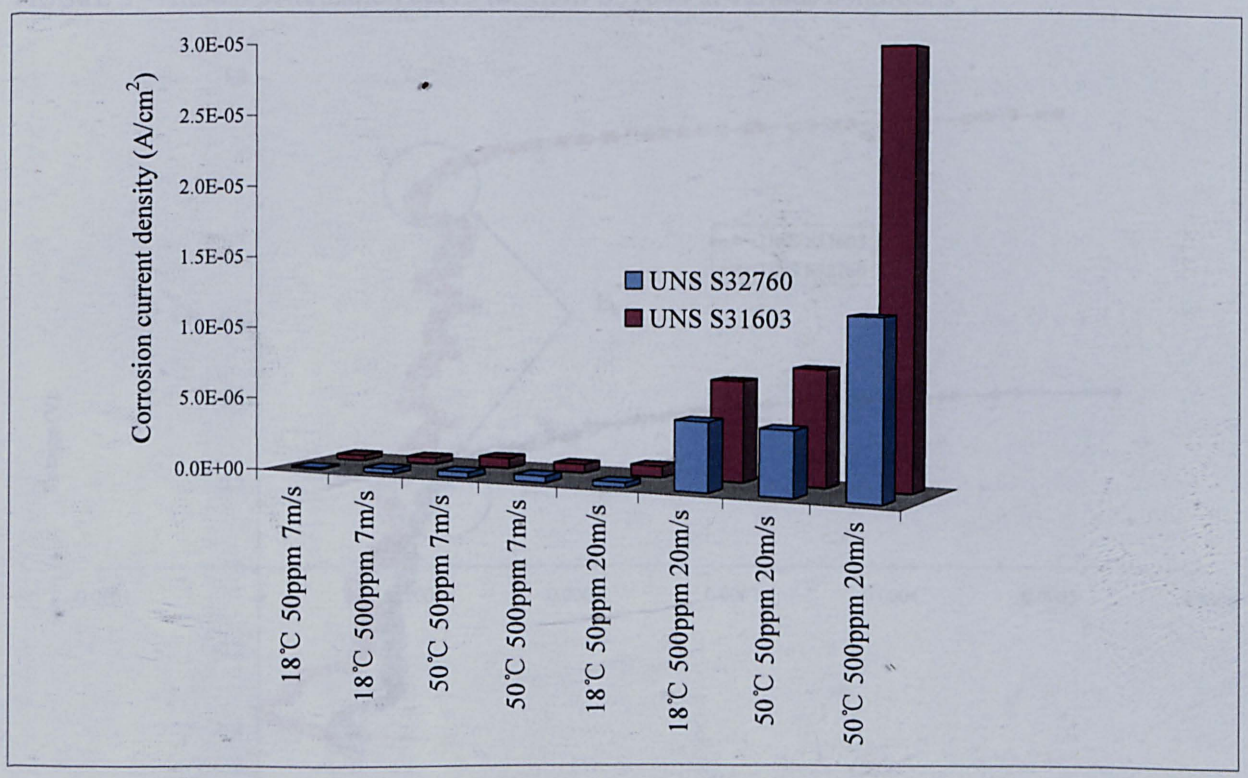

FIGURE 2 - Corrosion current densities (i_{corr}) obtained under eight test conditions defined by the factorial design methods

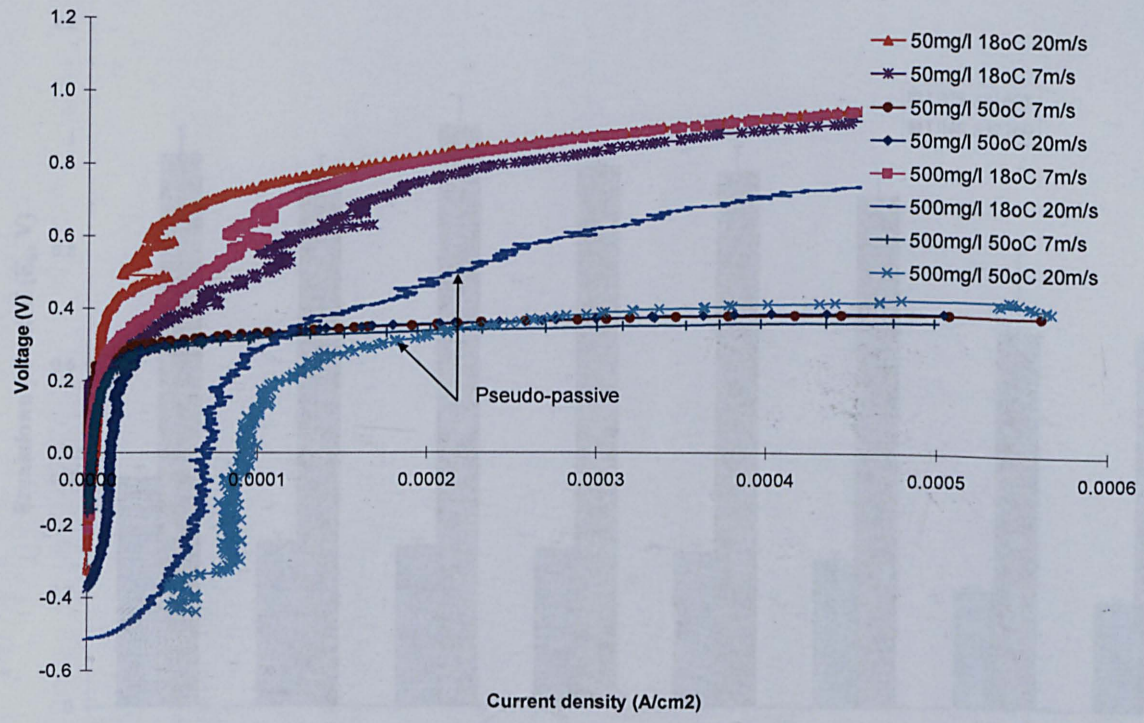

FIGURE 3 - Anodic polarization curve for UNS S31603 at various conditions

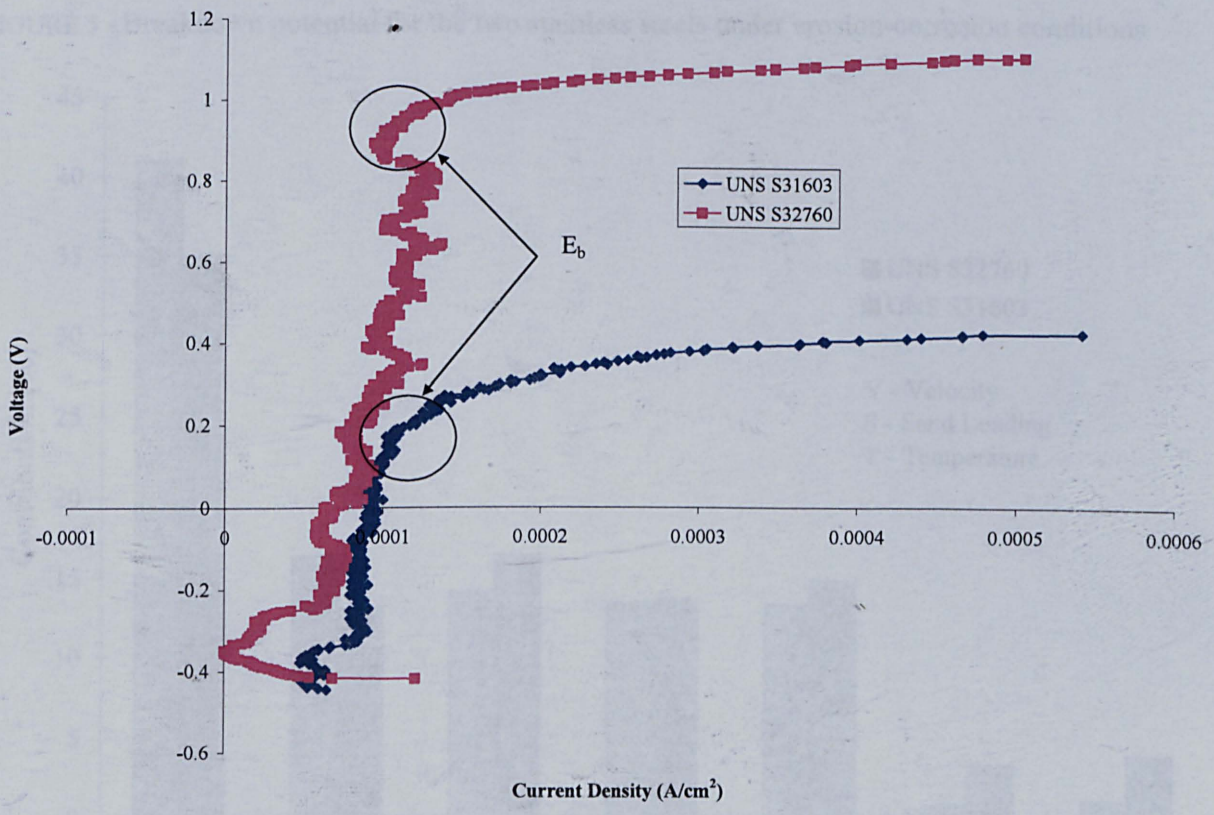

FIGURE 4 - Anodic polarization curve for the stainless steels at 50°C, 20 m/s and 500 mg/l solid loading

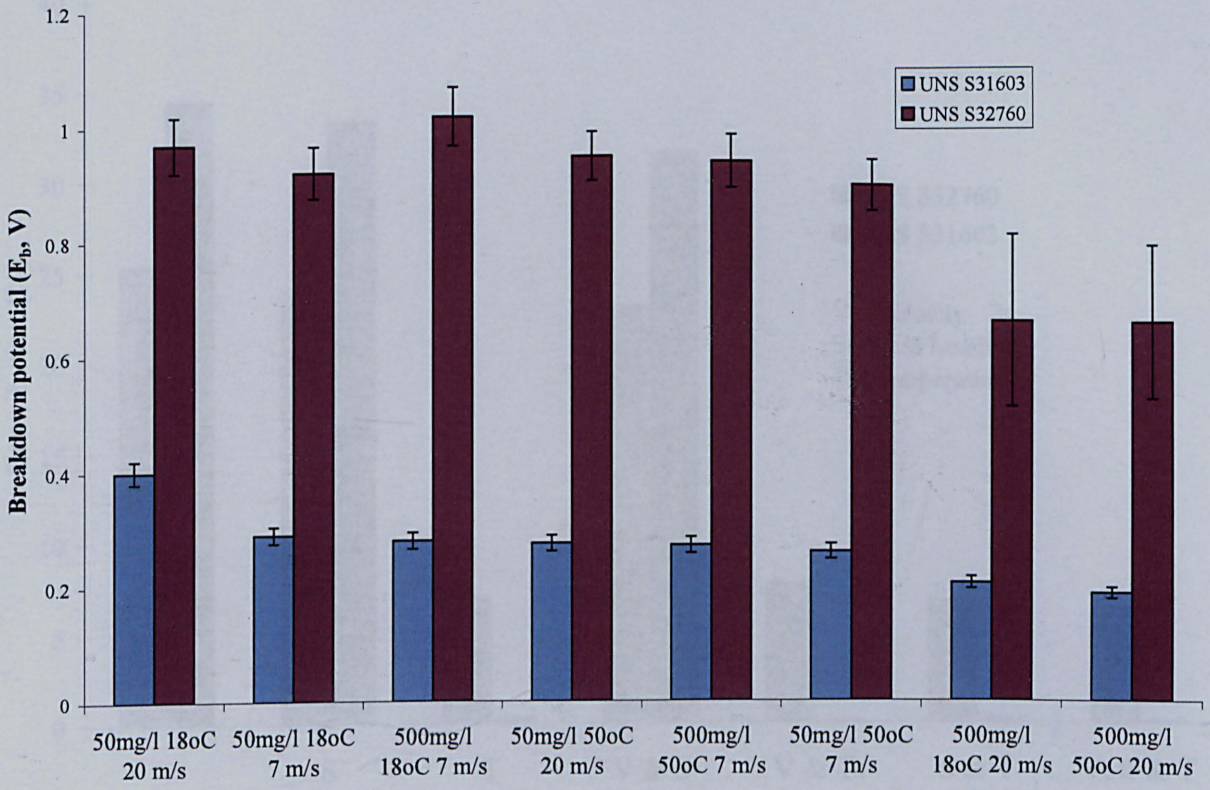

FIGURE 5 - Breakdown potential for the two stainless steels under erosion-corrosion conditions

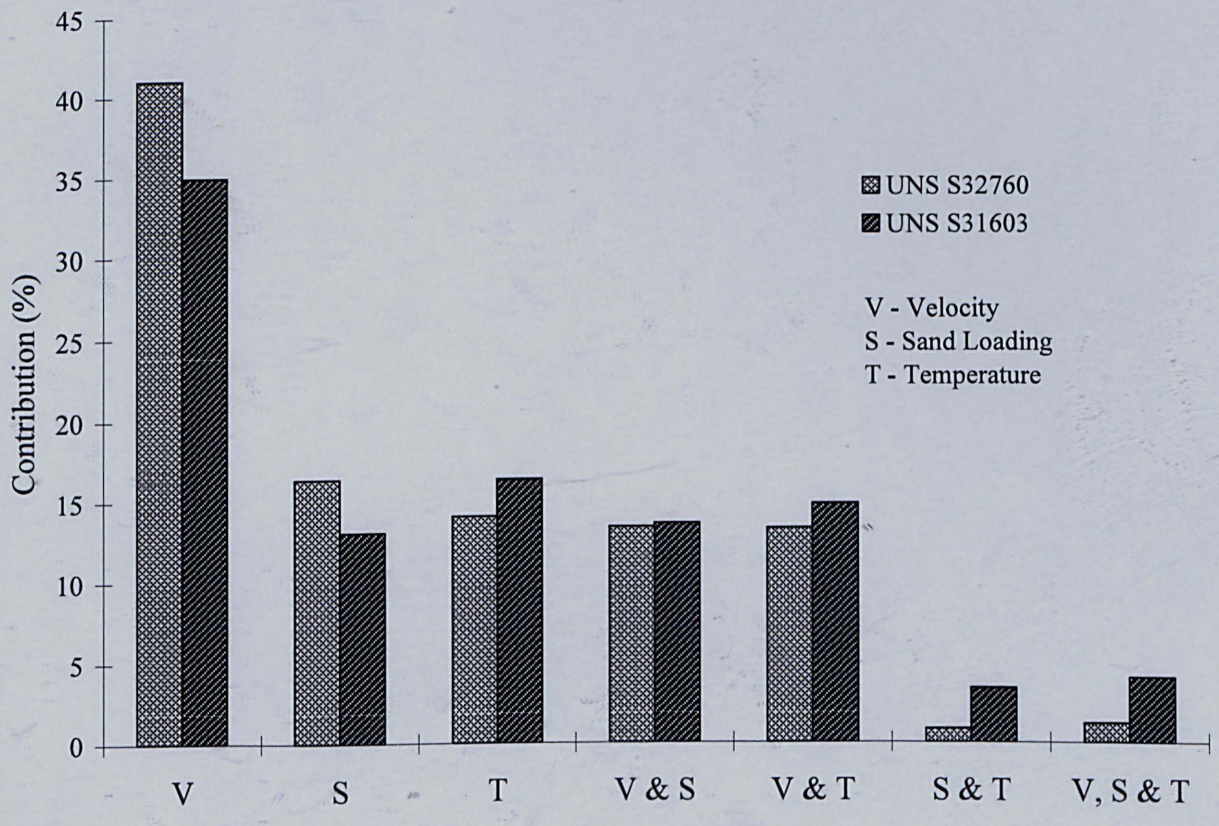

FIGURE 6 - The contributions of environmental parameters to the mass loss due to pure corrosion

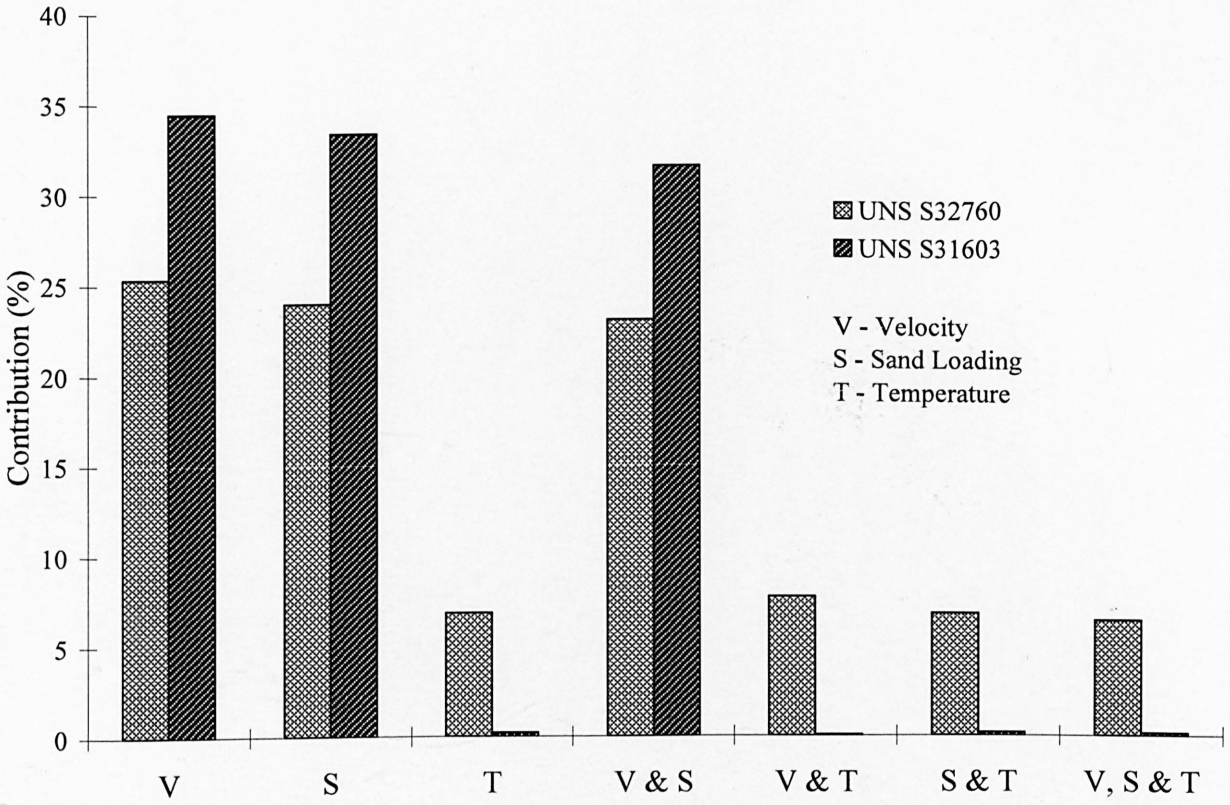

FIGURE 7 - The contributions of environmental parameters to the mass loss due to pure synergy